

Advances in Printing Science and Technology

Proceedings of the 31st International **iarigai** Research Conference

Acta Graphica Publishers
Zagreb MMIV

Advances in Printing Science and Technology

Proceedings of the 31st International IARIGAI Research Conference

Copenhagen, Denmark
September 2004

Published by Acta Graphica Publishers, Zagreb, Croatia
for the International Association of Research Organisations
for the Printing, Information and Communication Industries

The facts published in this volume are obtained from sources believed
to be reliable. However, publishers can accept no legal liability for the
contents of papers, nor for any information contained therein, nor for
conclusions drawn by any party from it.

Post-conference edition

ISBN 953-96276-9-9

Selected by the Program committee of IARIGAI

Nils Enlund, Stockholm, Sweden
Helmut Kipphan, Heidelberg, Germany
Svend Lawaetz, Copenhagen, Denmark
Mladen Lovreček, Zagreb, Croatia
Renke Wilken, Munich, Germany

Edited by Mladen Lovreček

CIP - Katalogizacija u publikaciji
Nacionalna i sveučilišna knjižnica - Zagreb

UDK 655:004.91>(063)
004.91:655>(063)

INTERNATIONAL Association of Research Organisations
for the Printing, Information and Communication Industries.
International Research Conference (31 ; 2004 ; Copenhagen)

Advances in printing science and technology : proceedings
of the 31st International IARIGAI Research Conference ,
<Copenhagen, 5 - 8 September, 2004> /
<edited by Mladen Lovreček>. - Zagreb :
Acta Graphica Publishers for the
International Association of Research
Organisations for the Printing ,
Information and Communication Industries , 2006.

Bibliografija iza svakog rada . - Kazalo.

ISBN 953-96276-9-9

I. Tiskarstvo. - - Zbornik

460201137

Cover design: Acta Graphica

Printed in Croatia by Narodne Novine, Zagreb - February 2006

Contents

Preface	v
1. Non-impact printing	1
Interaction characteristics in different applications of ink-jet printing <i>U. Lindqvist, L. Hakola, B. Zhmud, E. Wallström</i>	3
Detail rendering in digital dry toner electrophotography <i>H. Al-Rubaiey, P. Räsänen, P. Oittinen</i>	13
CIEDE2000 - a tool for determination of colour differences in inkjet? <i>M. Klamann, P.-Å. Johansson, A. Häggglund</i>	27
2. Prepress and color	41
Testing colour accuracy of PDF files <i>L. Mandić, D. Agić, D. Žvorc</i>	43
Online and automatic RGB to CMYK colour conversion <i>J. Gervasoni, R. Catusse</i>	49
3. Conventional, master based printing	59
Emulsifying of dampening solution in offset ink in short inking units <i>W. Beier, A. Hübner, G. Marx, C. Klinger, N. Meyer</i>	61
The effect of speed on image transfer in rotogravure printing <i>G. R. Davies, T. C. Claypole</i>	75
Tone gain due to deformation of the flexographic plate <i>D. C. Bould, T. C. Claypole, M. F. J. Bohan, D. T. Gethin</i>	83
4. Printing inks	95
Drying of water based inks by use of microwaves <i>A. A. R. Elsaid, J. M. Rodriguez Giles</i>	97
Extensional viscosity of lithographic inks <i>A. Blayo</i>	105
Examining the mechanism of ink transfer <i>I. Naito, Y. Nitta, S. Fujiki, S. Shibata, K. Koga</i>	113

Objective print quality assessment of complex images <i>C. Antoine, O. Diserud, O. Solheim, E. Berli</i>	123
An innovative tool to ensure printing ink performances consistency <i>C. Canet</i>	145
5. Color and image quality	149
Effect of screen ruling on color of printed matter <i>I. Naito, S. Lee, A. Kinoshita</i>	151
Halftone characterisation by image processing <i>J. Gervasoni, R. Passas, S. Lebris</i>	163
Colorimetric description of tolerances in newspaper production <i>J. Gemeinhardt</i>	173
RGB color spaces for optimal reproduction in newsprint <i>M. Werfel, W. Steiger, B. Münch</i>	181
Print quality evaluation for governmental purchase decisions <i>P. Nussbaum, J. Y. Hardeberg, S. E. Skarsbø</i>	189
6. Packaging and labeling	201
Grooving quality research on packing cardboard <i>D. Babić, V. Kropar Vančina, B. Lajić</i>	203
Holography on packaging material and an estimate on the rising trend of its application <i>I. Žiljak</i>	209
Activity-based costing of on demand package production <i>P. Lahtinen</i>	217
7. Current topics	225
Environmental data on gravure and offset printing <i>M. Enroth, M. Johansson</i>	227
Printing process simulation based on data for standards taken from actual production <i>V. Žiljak, K. Pap, Z. Nježić, I. Žiljak</i>	237
Electronic business processes in book production - applicability of JDF/PrintTalk and Papinet/XBITS <i>H. Antikainen, A. Bäck</i>	245
Index of authors	253

Preface

The 31st International Research Conference of *iarigai*, the International Association of Research Organisations for the Printing, Information and Communication Industries, was held in Copenhagen, Denmark, 5-8 September, 2004. The conference was hosted by The Graphic Arts Institute of Denmark.

This volume contains 24 scientific and technical papers presented at the conference. The contributions accepted for presentation were selected by the *iarigai* Program Committee after reviewing all submissions. The papers included here have been subjected only to slight technical editing and the responsibility for the contents lies with the authors. Conference presentations that were not based on full written papers have not been included in these proceedings.

The theme of the conference was Advances in Printing Science and Technology, and these proceedings contain papers on, among other topics, non-impact printing, conventional printing, prepress and colour, printing inks and packaging. The reader will surely find interesting information on advances and current status in these different fields.

In addition to the presentations and the published papers, *iarigai* conferences also provide the participants with excellent opportunities for discussions and networking. In this respect, the Copenhagen conference was also a success, thanks to the meeting facilities and the inspiring and lavish social program. *iarigai* thanks the organizers and all assisting staff for their effort in arranging a truly memorable event.

Nils Enlund

Chairman of the Program Committee





1

Non-impact printing



Interaction characteristics in different applications of ink-jet printing

Ulf Lindqvist¹, Liisa Hakola¹, Boris Zhmud², Eva Wallström³

¹ VTT Information Technology
Metallimiehenkuja 10, P. O. Box 1204
FIN-02044 VTT, Finland
E-mail: forname.surname@vtt.fi

² YKI, Ytkemiska Institute for Surface Chemistry
P. O. Box 5607
SE-144 86 Stockholm, Sweden
E-mail: boris.zhmud@surfchem.kth.se

³ EnPro ApS
Lersø Parkallé 42
DK- 2100 Copenhagen Ø, Denmark
E-mail: ew@enpro.dk

Abstract

The focus of this Nordic R&D project on "Innovative development of ink-jet technology" funded by Nordic Industrial Fund was on developing a normative specification and documentation of adequate measuring techniques for materials and process parameters for different applications of the ink-jet technology. Special attention was paid to the influence of paper and ink properties on formation of print quality during impact, spreading and penetration, and hence, on final print quality. Print quality was seen in terms of image analytical factors.

The first step included an inventory of Nordic and international research results on ink-jet printing and a documentation of measuring methods, especially methods for drop formation, spreading and absorption when printing with different ink-jet printheads and substrates. The further work focused on practical material characterisation and interaction mechanisms in ink-jet printing. In these tests a representative selection of substrates and inks were further analysed on a laboratory scale and ink-jet printing trials were done with them.

By using high-resolution measuring equipment, the spreading and penetration of inkjet drops were monitored. The printing substrates were characterized with respect to surface energy and roughness. The impact, spreading, absorption and drying of the ink droplets on the samples were observed and analysed in a testing environment on a time scale of milliseconds up to several minutes. The final print quality was further analysed with optical density, uniformity of the print and overall visual quality.

Based on the results recommendations for material properties and process conditions, as well as measuring methods have been developed, and reported. The paper also discusses still remaining problem areas in the ink-jet method, where improvement can be achieved through a continued co-operation between scientists, material suppliers, equipment manufacturers and end-users.

1. Introduction

During the last decade the ink-jet printing technology has developed rapidly. New applications have been directed to produce both documents, publications, personalised advertisements, security documents, textiles, packages and cartonage. The ink-jet printing method is suitable for both a wide variety of materials, for frequently updated information and for multicolour high-quality products. The method is

strategically important for the Nordic industry, since the Nordic countries are important suppliers of paper and board for ink-jet printing, digital printing is taking an increasing share of the print market, Nordic SMEs deliver printed products to a global market, ink-jet inks are basically imported an extremely expensive, and the Nordic countries also produce and export advanced printheads.

Ink-jet printing is the only non-contact printing method which makes it the most ideal of all the printing methods. Ink-jet technologies are usually divided into continuous and drop-on-demand printing methods (Figure 1). Continuous printing methods are used in high-speed and low resolution applications whereas drop-on-demand is used in lower speed and higher resolution applications such as wide format printing, office printing, package printing and other industrial applications. Continuous ink-jet printing uses a continuous generation of drops. Printing drops are selected by charging them and directing them to the paper while non-printing drops are re-circulated. In drop-on-demand technology inks are produced only when they are needed. Drop-on-demand ink-jet is usually further divided into piezoelectric and thermal ink-jet. In thermal ink-jet the drop formation is based on transformation of a heater element whereas in piezoelectric ink-jet on transformation of a piezoceramic element.

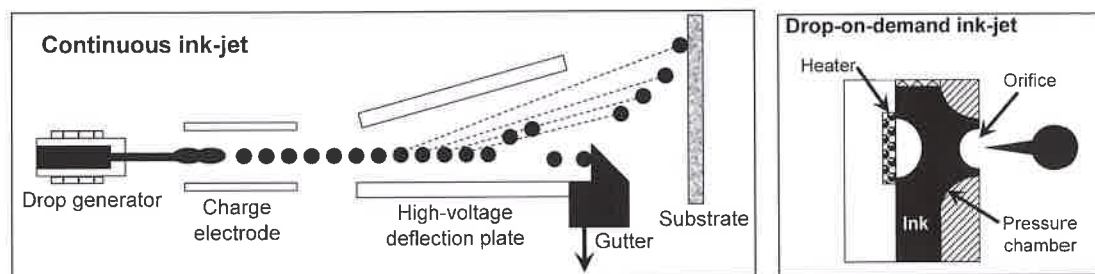


Figure 1: Continuous and drop-on-demand (thermal) ink-jet technologies

Ink-jet systems consist of three parts: printhead, ink and printing substrate, and all of these elements must be taken into account when the system is developed. The printhead affects the drop formation and jet stability. Some of the most common printhead problems are foaming, depriming nozzles, drying and starvation. Important ink parameters are viscosity, surface tension and stability. In addition the ink has to be very fluid and not have particles to pass through the fine nozzles. The most common inks in ink-jet printing are water- and solvent-based inks including oil-based inks, hot-melt inks and UV curable inks. Surface energy and roughness of the printing substrate determine the ink setting profile, ink adhesion as well as scuff- and rub-resistance of the print. Also dynamic ink-substrate interactions such as impact, spreading and penetration as well as coalescence of the ink on the substrate affect the final print quality.

This Nordic R&D project on “Innovative development of ink-jet technology” utilised the outcome of the national research programmes and established a Nordic network of research institutes, material suppliers, printer manufacturers and end users of the ink-jet technology. The scope of the project was to present a normative specification and documentation for materials and process parameters for different applications of the ink-jet technology. Special attention was paid to the influence of paper and ink properties on spreading and penetration, and hence, on print quality.

The project consisted of an inventory of Nordic and international research results on ink-jet printing and its most important parameters in different applications. This step also provided a documentation of measuring methods and routines developed by research partners. The experimental work of the project included laboratory scale and full scale printing trials with different inks and substrates. The materials were selected to give maximum information about the impact of material properties on printing behavior and quality formation. Based on the results from the experimental work recommendations for material properties, process conditions and measuring methods were developed.

VTT Information Technology was responsible for the parts dealing with the ink-jet technology itself, measuring methods for print quality and dynamic ink-substrate interactions, including measuring results. YKI was responsible for the parts dealing with contact angles and flow property measurements, and EnPro for the parts dealing with ink composition and flow properties. Also the industrial partners – Big Image Systems Sweden AB, Sweden, Stora Enso Research Centre, Finland, Sun Chemicals A/S, Denmark and Xaar Jet AB, Sweden – had an active role in the performance of the practical research work.

2. Methods

The first task of the experimental work was to choose the best inks for printing tests from the total of nine inks listed in Table I. One of the inks was a dye-sublimation ink, but the rest were pigmented. The solvent-based inks had some differences in flash point, which indicated that the evaporation profile was differing. The oil-based inks were included because they evaporated even more slowly than solvent-based inks. One UV-curable ink was included to get an indication of if there were any major differences with regard to physical properties compared to solvent-based inks. Measurements for viscosity, surface tension, particle size distribution and thermogravimetric behavior were implemented. The measurements were done only for magenta inks, but each ink set included all four CMYK (cyan, magenta, yellow and black) inks.

*Table I:
Inks for ink
properties
measurements*

Ink code	Ink type	Flash point °C
SB-M1	Solvent-based ink	47
SB-M2	Solvent-based ink	63
SB-M3	Solvent-based ink	63
SB-M4	Solvent-based ink	63,5
SB-M5	Solvent-based ink	68
DS-SB-M6	Dye-sublimation ink	63-85
OB-M7	Oil-based ink	> 120
OB-M8	Oil-based ink	> 134
UV-M9	UV-curable ink	N/A

The ink viscosity was measured on a Bohlin VOR Rheometer according to ISO 3219-93. The surface tension was measured at 23°C on a Krüss Tensiometer according to ISO 304-85. The particle size distribution was measured with a Malven Mastersizer microPlus. Thermogravimetric measurements can be used to determine the solvent/aqueous content (<250°C), the dry matter (approximately rest at 250°C) and the amount of inorganic material (>600°C).

Five substrates that included cloth, polyester, vinyl, two-sided PE-coated carton (Ensocup) and one-sided coated carton (Ensocoat) were chosen for tests. Two sides of Ensocup differed from each other and the different sides are referred as glossy side and matt side. The different sides of Ensocoat are referred as coated and uncoated side.

The wetting ability of a liquid with respect to solid surface can be characterized by measuring the contact angle between the liquid meniscus and the surface. A contact angle less than 90° indicates that the substrate is readily wetted by the test liquid, while an angle greater than 90° shows that the substrate will resist wetting. Differing from other measurements one commercial piezoelectric ink-jet ink (PIJ ink) and one commercial thermal ink-jet ink (TIJ ink) on Ensocup and Ensocoat were used for wetting measurements.

To investigate specific aspects of ink-paper interactions physico-chemical methods were used: XPS (X-Ray Photoelectron Spectroscopy) analysis, profilometry, dynamic contact angle, surface energy decomposition and critical surface tension measurements. XPS analysis was used to analyze elemental composition of a

thin surface layer of printing substrates and to identify chemical elements present in the surface layer. ESCA AXIS-HS instrument from Kratos Analytical was used for these measurements. Surface topography of printing substrates was studied by interferometric profilometry with state-of-the-art ZYGO NewView 5010 profilometer. This instrument allows one to reconstruct a digital image of the surface profile by using the principle of white light interferometry. Drop absorption and dynamic contact angle measurements were done by using the Dynamic contact angle and Absorption Testers, models 1100 and 1129 DAT, from Fibro Systems AB as seen in Figure 2. These devices give dynamic measures of the drop base, volume and height, as well as contact angle with a time resolution of 10 ms.

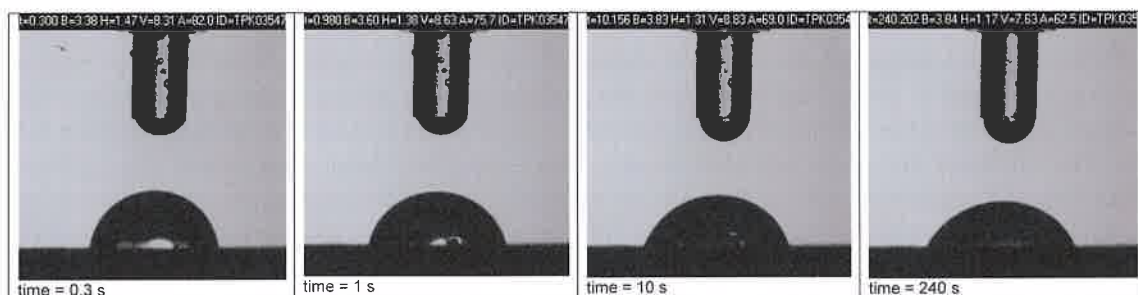


Figure 2: Penetration of a water drop into AKD/rosin-sized packaging board

A better knowledge of the basic mechanisms of the dynamic interactions between ink and paper were needed to produce more reliable and appropriate quality specifications for printing surfaces. A unique approach to this problem was the laboratory-scale testing environment developed by VTT Information Technology for the high-speed imaging of ink-jet drops. The impact, spreading, absorption and drying of the ink droplets can be observed and analyzed in this testing environment on a time-scale of milliseconds up to several minutes. The system is pictured in Figure 3 and both continuous as well as drop-on-demand printheads can be used. Only solvent- and oil-based inks were used for dynamic interaction tests, because the high absorption and spreading tendency of dye-sublimation ink on tested substrates made it impossible to detect the ink by optical means.



Figure 3:
Testing environment for dynamic interactions in ink-jet printing

Ink-jet printability of chosen materials was tested with Agfa testrig and standard piezoelectric 360 dpi printheads from Xaar were used for printing. Dot images were printed with one colour in each series and average dot sizes were measured from these images. Colour stripes were printed at fixed resolution with constant print angle and firing frequency. Based on measured average dot sizes the resolution of samples to achieve full coverage was calculated. Print angle and firing frequency were also calculated. During printing drying time was evaluated visually. Bleeding behavior could be seen in printed samples where two colour stripes were overlapping each other. Optical density values were also measured.

The full-scale printing trials were carried out in Big Image Systems in Sweden with ink-jet presses. Solvent-based inks were printed with Hitachi-Koki ink-jet printheads and oil-based inks with Xaar XJ500 ink-jet printheads. The test points are listed in Table II. With solvent-based inks printings with Ensocup were somewhat problematic as the press put too much ink on these substrates. No print mode was found optimal for these substrates. The oil-based ink didn't adhere on vinyl and Ensocup substrates so these samples weren't printed.

Table II:

*Test points for
full-scale
printing trials*

Test point	Substrate	Ink
1	Cloth	Solvent-based, SB-M1
2	Polyester	Solvent-based, SB-M1
3	Vinyl	Solvent-based, SB-M1
4	Ensocup, matt side	Solvent-based, SB-M1
5	Ensocup, glossy side	Solvent-based, SB-M1
6	Ensocoat, coated side	Solvent-based, SB-M1
7	Cloth	Oil-based, OB-M7
8	Polyester	Oil-based, OB-M7
9	Ensocoat, coated side	Oil-based, OB-M7

From the full-scale printing trials print quality of printed samples was evaluated with optical density measurements and visual comparison tests.

3. Results and discussion

From the ink properties measurements it was observed that the variations between different inks were generally small. Three inks were chosen for printing tests according to ink measurements summarized in Table III. The intention was that as large a span as possible was achieved with regard to viscosity, phase angle and surface tension. From the evaluation of thermogravimetric data it was seen that there were some composition differences also between solvent-based products. It was also seen that the oil-based inks had a dry matter of about 80 wt-%, while the solvent-based inks had about 10 wt-%. The dye-sublimation ink had a dry matter of approximately 50 wt-%.

*Table III: Summary of data from ink measurements. The inks chosen for printing tests are marked with *.
The measurements marked with ? were problematic*

Ink code	ρ Density (g/ml)	η Viscosity (mPa s)	ΔE Phase angle	γ Surface tension (mN/m)	Particle size distribution peak μm	Particle size range μm	Particle size 90 % μm
*SB-M1	0,9783	17,6	87,2	29,8	0,36	0,17-0,78	< 0,49
SB-M2	0,9331	11,3	87,8	28,1	0,36	0,15-0,78	< 0,67
SB-M3	0,9382	13,1	88,1	27,9	0,36	0,17-0,67	< 0,58
SB-M4	0,9908	22,8	69,5	29,4	0,23	0,05-0,58	< 0,42
SB-M5	0,9903	15,9	87,8	27,0	0,36	0,13-0,78	< 0,58
*DS-SB-M6	0,8721	13,4	87,9	33,4	0,07	0,05-0,49	< 0,31
*OB-M7	0,8643	11,9	87,3	28,0	?	?	?
OB-M8	0,8645	10,2	86,7	30,7	0,36 ?	0,11-0,8 ?	?
UV-M9	0,9369	13,8	84,9	28,7	0,27	0,05-0,67 ?	?

From the dynamic wetting tests it was concluded that PIJ ink spread faster than TIJ ink. It was also found that Ensocup demonstrated good wettability, and hence, printability with respect to both inks. This resulted in higher surface energy for Ensocup than for Ensocoat. In Figure 4 and Figure 5 surface profiles for Ensocoat and Ensocup are pictured. It should be noted that the surface of Ensocup seemed to contain a significant amount of small holes. Wettability of the fabric substrates with respect to the solvent-based ink (SB-M1) was similar. Since the fabric surfaces were utterly rough, a significant

scattering of the results was observed. Once absorbed, the ink was rather quickly set by drying and the print demonstrated outstanding water-resistance.

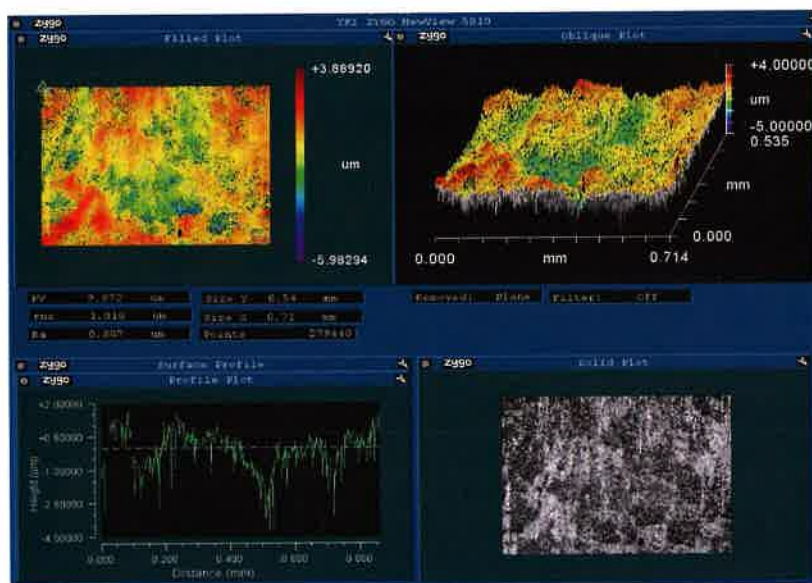


Figure 4: Surface profile of Ensocoat on the coated side

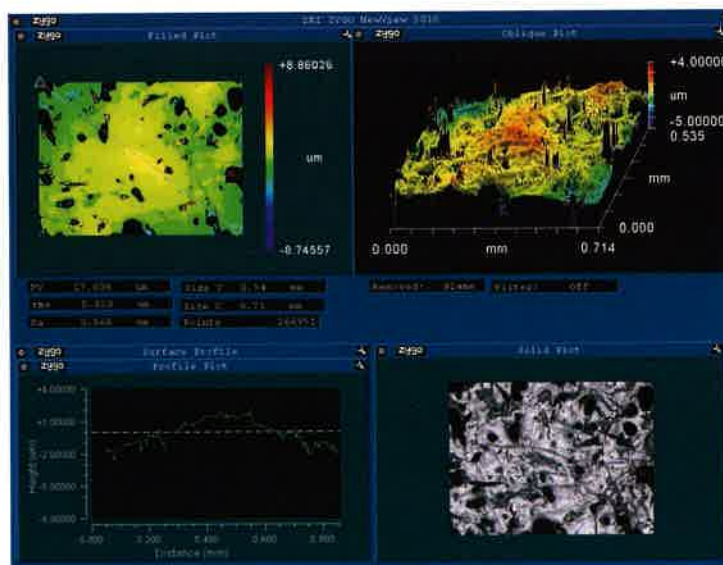


Figure 5: Surface profile of Ensocup on the glossy side

Because the deviation between different test points in dynamic interaction tests were large, proper statistical analysis was impossible to do in these test series. Instead a visual examination of the time series of the selected test points was made based on the long-time experience in the behavior of liquids on various surfaces. The reason for the high deviation was very rough and sometimes very oriented surface structure of the samples in comparison with the drop size. Also the very strong spreading tendency of the inks that depended on the ink viscosity and surface energetic factors, made dots uneven and large, even on relatively flat surfaces. The behavior of different inks on different substrates is pictured in Figure 6.

From dynamic interactions tests it was noticed that each paper-ink combination had its distinctive finger print, even different sides of paper were easily identified. This resulted in different ink behavior for different sides of cartons. Also different inks were distinguished and the spreading was more controlled with oil-based inks. It was also noted that the solvent frontier of the oil-based ink spread to a wider area than the colour itself. With Ensocoat the inks formed more uniform dots on the coated side than on the uncoated side. On Ensocup the ink behavior was first very controlled, but after a while the spreading became non-uniform.

The ink behavior on fabric substrates was very characteristic. The long fiber network of polyester absorbed ink very rapidly thus creating long and narrow dots. Because of this very dominant mechanism the differences between inks were hard to see. Cotton repelled ink, but the furry surface structure dominated the hitting and spreading phase thus creating polymorphous dots. Vinyl behaved like a common, smooth plastic. If the hitting speed of the drop on plastic is high the dot spreads during the mechanical phase strongly. If the speed is low the dot spreads by means of surface energetic powers little by little during the spreading phase. Adhesion is, however, always a problem with smooth and dense material like plastic.

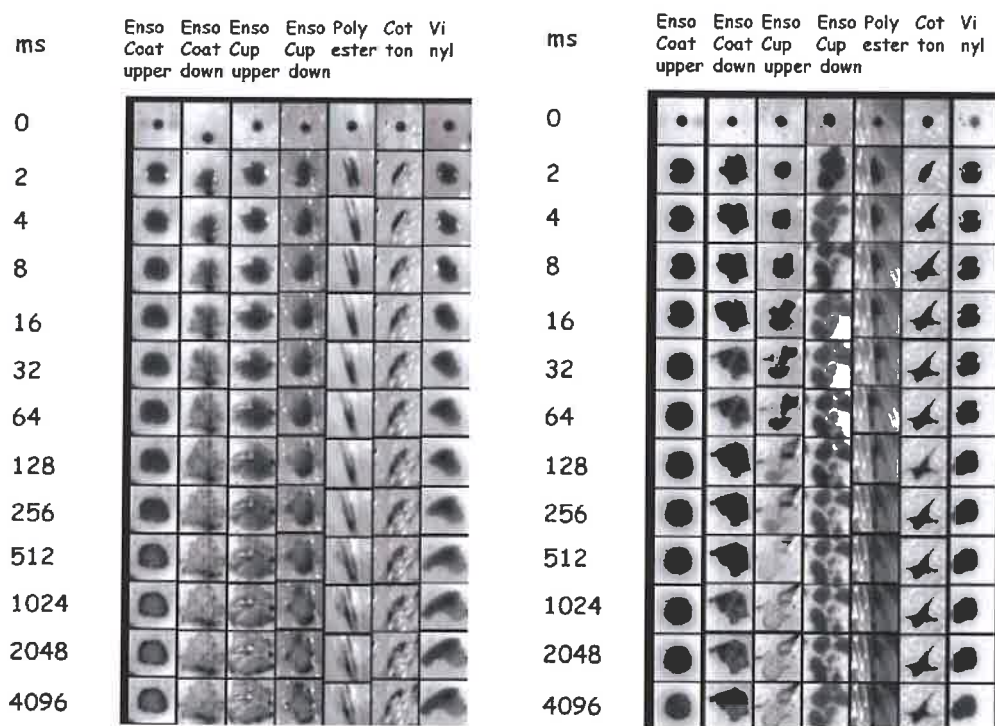


Figure 6: Ink droplet behavior on different substrates for the solvent-based ink (SB-M1, left) and oil-based ink (OB-M7, right) under a time span of 0...4096 ms after the contact.

Ensocoat upper side is the coated side and down side the uncoated side.

Ensocup upper side is the glossy side and down side is the matt side

Samples from the full-scale printing trials are pictured in Figure 7 and Figure 8. The results from optical density measurements and visual comparison tests are given in Table IV. With optical density measurements and visual observations it was concluded that solvent-based ink gave darker colours and better overall print quality than oil-based ink. This had a clear connection with dynamic interaction tests that indicated more spreading with oil-based inks. Solvent-based inks, however, tended to spread uncontrollably on Ensocup as could also be seen from dynamic interactions tests. This resulted in pictures with no outlines and rotten print quality. On Ensocoat both inks produced banded images.



Figure 7: Printed samples (from left to right) on glossy and matt side of Ensocup with solvent-based ink (SB-M1), on coated side of Ensocoat with solvent-based (SB-M1) and with oil-based ink (OB-M7)



Figure 8: Printed samples (from left to right) on cloth with solvent-based (SB-M1) and oil-based (OB-M7) ink, on polyester with solvent-based ink (SB-M1) and on vinyl with solvent-based ink (SB-M1)

With fabric substrates the surface textures were clearly seen under the ink layer, especially with vinyl. The colours were, however, very bright and had high optical density on vinyl although some banding could be seen. The colours on cloth looked dirty and light as can also be seen from the optical density values that were for cloth the lowest ones. With fabric substrates banding was clearly visible with samples printed with oil-based ink which indicated that banding was characteristic for the combination of oil-based ink and printhead used. Based on visual examination vinyl had the best contrast and cloth the worst.

Table IV: Results from ink-jet print quality measurements.

In visual comparison prints on Ensocup and Ensocoat were ranked with each other and prints on other substrates were ranked with each other

Test point	Substrate	Ink	Visual comparison ranking	Optical density
1	Cloth	Solvent-based, SB-M1	3	0,64
2	Polyester	Solvent-based, SB-M1	1	1,30
3	Vinyl	Solvent-based, SB-M1	2	1,71
7	Cloth	Oil-based, OB-M7	5	0,56
8	Polyester	Oil-based, OB-M7	4	0,63
4	Ensocup, matt side	Solvent-based, SB-M1	3	1,49
5	Ensocup, glossy side	Solvent-based, SB-M1	4	1,68
6	Ensocoat, coated side	Solvent-based, SB-M1	1	2,02
9	Ensocoat, coated side	Oil-based, OB-M7	2	1,07

When talking about high-resolution printing the phenomena present in dynamic interaction tests destroyed the print quality as was confirmed with visual tests. But if resolution is low, which is often the case in billboard printing, the strong spreading tendency doesn't necessarily impede as much. This

requires that sufficient amount of ink is added to a substrate to reach the desired tone value, which can, of course, lead to bleeding problems.

4. Conclusions

Ink-jet print quality strongly depends on ink, substrate and printhead and interactions between these three elements. Especially dynamic ink-substrate interactions such as impact, spreading and penetration play an important role. The challenges in industrial ink-jet printing include finding the proper ink-substrate combinations that give optimal print quality, the proper inks for particular printheads, substrates that produce good print quality with various inks as well as proper materials and technologies for inks, substrates and printheads that together give optimal print quality.

Acknowledgements

The authors are greatly indebted to the Nordic Industrial Fund for financing the project and to the industrial partners i.e. Big Image Systems Sweden AB, Stora Enso Research Centre, Sun Chemicals A/S and Xaar Jet AB as well as to the members of the project Steering Group for their support, good co-operation and worthy comments. The authors would also like to thank all members of the project group for good research work and co-operation as well as laboratory personnel for skilled work and assistance in measurements.

Literature

Andersen, Kirsten; Daicic, John; Hakola, Liisa; Heilmann, Jali; Lindqvist, Ulf; Wallström, Eva; Zhmud, Boris. *Innovations in ink-jet technology: survey on the technology and measuring methods. Nordisk Industrifond, NATTKLINIK part 1 report (2002). 30 p*

Heilmann, J. *Measuring dynamic interactions between paper and microscale ink drops. IS&T/NIP17 Conference on Digital Printing, Fort Lauderdale, USA (2002)*

Lindqvist, Ulf; Andersen, Kirsten; Fogden, Andrew; Hakola, Liisa; Hallstensson, Karin; Heilmann, Jali; Wallström, Eva; Zhmud, Boris. *Innovations in ink-jet technology. Nordisk Industrifond, NATTKLINIK final report (2003). 64 p*

Lindqvist, U.; Heilmann, J. *The Paper Dependence of the Print Quality in Drop-on-Demand Ink-Jet Printing. 26th IARIGAI, Munich, Germany (1999). 10 p*

von Bahr, M.; Kizling, J.; Zhmud, B.; Tiberg, F. *Spreading and Penetration of Aqueous Solutions and Water-Borne Inks in Contact with Paper and Model Substrates. Advances in Printing Science and Technology, vol 27 (J.A.Bristow, Ed.). Pira, Surrey (2001). p. 87*

von Bahr, M.; Seppänen, F.; Tiberg, F.; Zhmud, B. *Dynamic Wetting of AKD-sized Paper. J. Pulp Pap Sci, 30(2004)74*

Zhmud, B. *Dynamic Aspects of Ink-Paper Interaction in Relation to Inkjet Printing. Ink on Paper, Proceedings of Pira International Printing Conference, Brussels, Belgium (2003)*

Zhmud, B.; Tiberg, F. *Surfactants in Inkjet Inks. Surfactants in Polymers, Coatings, Inks and Adhesives (D.R. Karsa, Ed). Blackwell Publishing, England (2003).Chapter 8*

Zhmud, B.V.; Tiberg, F.; Hallstensson, K. *Dynamics of capillary rise. Journal of Colloid and Interface Science (2000)228. p. 263-269*

Zhmud, B.V.; Tiberg, F.; Kizling, J. *Dynamic surface tension in concentrated solutions of CnEm surfactants. A comparison between theory and experiment. Langmuir (2000). p. 2557-2565*



Detail rendering in digital dry toner electrophotography

Hussain AL-Rubaiey, Pia Räsänen, Pirkko Oittinen

Helsinki University of Technology, Laboratory of Media Technology

P. O. Box 5500, FIN-02015-HUT, Finland

E-mail: hussain@media.hut.fi; pia.rasanen@hut.fi; pirkko.oittinen@hut.fi

Abstract

Detail rendering is one of the traditional measures used in evaluation of printed image quality. This study explores and compares traditional detail rendering measurement methods from the standpoint of their usefulness when print quality needs to have many different definitions, such as electrical conductivity or visual sharpness. The main objective is to understand the relation between image quality measures as detail reproduction and the specifications and features of each process stage in different electrophotographic machines, such as speed ranges, applications etc. Therefore, process analysis of different dry toner technologies was used to determine the image quality from different perspectives. Also the experiments were designed to contribute to understanding image quality factors from the standpoint of different applications. The study involves measurements on a wide range of dry toner electrophotographic printers with a focus on the performance of each technology at different stages of the printing process such as exposure, development, toner transfer and fusing.

The test image was designed to contain the basic elements; dots, lines and solid prints. A microdensitometer was used to measure the optical density profiles of printed line bar patterns. The dynamic range, contrast transfer function (CTF), signal-to-noise ratio (SNR) and smallest pixel size were calculated. Edge noise, raggedness and sharpness percentage were determined from the lines analysed by special image analysis software and macros. Edge noise was also calculated from 25% halftone dots. Sharpness was additionally evaluated visually using pair comparison.

The results showed that currently detail rendering is better controlled in B/W printers than colour printers, especially at the high speed range. The results also indicated that not only CTF-based measures but also edge noise and raggedness are frequency dependent. The correlation coefficients calculated between the different image quality measures indicate that the data results given by different measuring methods were in accordance with each other.

Keywords

Electrophotography, Detail rendering, Dry toner, Functional quality

1. Introduction

During the last decade, electrophotography has solidified its position as the method of short-run black and white as well as colour digital printing in commercial and office environments. Competition with other methods is, however, becoming continuously tighter. The question is not only about the most suitable method for current applications but the potential of the methods to meet the needs of emerging new applications. These include for instance security-printing, photo printing or finishing and printing of functional structures such as microelectronics components. These new areas of applications require understanding of detail rendering from different perspectives. In the early years of digital printing, resolution was the parameter with highest priority when the quality potential was assessed. This was so in spite of the fact that it was well known that nominal resolution or addressability are not good indicators of the detail rendering capability of a method. Moreover, printing speed is also relevant in

specification of printer performance. The search for higher performance has brought a proliferation of technological implementations.

These aspects were the motivating factors for this study. Its objective was on one hand to provide characterization of the current level of detail rendering in electrophotographic printing. Second, the objective was to create understanding of the role which different technological choices have in determining the appearance of printed images. Parameters which in previous studies have been used to depict detail rendering are numerous. This study focused primarily on parameters in the spatial frequency domain but also included spatial xy-domain parameters and subjective assessments. In photo printing, the visual impression of quality is of course the most important factor, whereas it is insignificant in security and functional printing applications.

At each of the stages of electrophotography, there are several factors and parameters which cause image quality limitations. For instance, the electrostatic and thermal systems in the transfer and fusing stages, the exposing wavelength and photoconductor sensitivity, the charge-to-mass ratio “q/m”, and the size and uniformity of toner particles, the surface properties of print media, and the interactions between these factors and parameters are all influencing the final printed image. In photo finishing small toner particle size is required and just enough fusing energy to avoid high dot gain especially in the halftone area so that small details can be reproduced (AL-Rubaiey & Oittinen, 2001). In printing microelectronic components the issues are somehow different. Continuity and uniformity of printed lines is required to achieve the desired functionality. The requirements for security print can be something else, such as a recognizability of the interaction pattern of the print and paper structures, a kind of fingerprint. This study explores and compares traditional detail rendering measurement methods from the standpoint of their use in cases where print quality needs to have many different definitions, such as electrical conductivity or visual sharpness.

2. Technological framework

To review the dry toner technology, process analysis is likely to be a useful approach from the perspective of the determinants quality. The objective is to understand the relation between image quality measures as detail reproduction and the specifications and features of each process stage in different machines, such as speed ranges, applications and many other features.

The speed is the first identity relevant to any colour or black and white printer. It is usually measured by “ppm” -number of printed pages per time (min). The speed has a clear effect on the image quality. For instance, it was found that the noise of the edge measured from 250 μm lines is increased as the printing speed is increased (Schein et al, 1993). This result is understandable because increasing the speed means increasing the rate of each parameter at each stage of the process to compensate the short time available for image printing. When the charging rates of the toner and photoconductor are increased, it is important to ensure that they are made of materials modified and designed to act at acceptable level of sensitivity with high rate of charging. As the speed is increased, the transfer voltage should also be increased to produce high enough electric field to transfer the developed toner image from photoconductor to paper surface. At certain humidity condition, the resistivity and other electrical properties of paper, which are the indicator of bulk properties and surface treatment, play important roles in determining the development rate and the level of the electric field in the transfer zone (AL-Rubaiey & Oittinen, 2001). High electric field causes toner satellite formation when a high electric force attracts and transfers some toner particles before reaching the transfer zone. The scattered toner particles can cause loss in image sharpness and resolution (Rushing et al, 2001). Even though the toner particle size is the ultimate limiting factor in determining the image resolution (Kipphan, 2001), (Johnson, 1986) and has a large influence on edge raggedness, in such a way that smaller toner particles result in lower edge raggedness (Schleusener et al, 1994), it has been found that

scattering of toner particles in the outlines of the printed area has a more dominant effect on image quality than toner particle size (Majava, 1994). This is obvious when most probably toner particles are scattered over a distance bigger than their size.

Also, the pressure and heating rates at the fusing stage have to be increased and optimised to avoid cold set and heat set offset, and to provide the optimum energy for good image fixing quality in a shorter time (AL-Rubaiey et al, 2002). Fusing is extremely important in giving the final touch to the image printed by dry toner printing technology. All the quality factors produced by the process stages before fusing are subject to be changed during the fusing stage. In general, fusing affects detail rendering through dot spreading and the edge noise or the raggedness characteristic of dry toner based electrophotography (Oittinen & Saarelma, 1994). Under the pressure of the fusing roller, melt toner will spread and cover a larger area than originally, and connect the neighbouring toner particles to the original image with lower raggedness as the result (Schleusener et al, 1994). This might be good for functionality which requires a continuous slab of printed layer such as conductive structures (Vallenius, 2001), but this effect is not appreciated when small detail reproduction is desired as in photo finishing and similar applications. Reducing the pressure by applying a soft roller or belt fusing technologies may give higher edge noise, but some other quality factors are improved such as reduction in gloss variation, which means better print evenness (AL-Rubaiey & Oittinen, 2004).

Dual toner development and monocomponent toner development are further indicators of differences between industrial and desk top printers. In monocomponent development "toner particles" as in desk top printers accept the charge mainly from a development roller surface (Tsunemi et al, 1997). The development roller receives the charge in contact with another roller installed inside the toner cartridge called "toner charging roller". Charging is supplied either directly from the power supply of the printer by a suitable AC-voltage in terms of polarity and magnitude, or indirectly by corona injection "non-contact charging". Conversely the toner charging process in a dual component development takes place by triboelectric charging "contact and friction charging" between dissimilar surfaces of toner particles and carrier particles through the equilibrium charge exchange, where one surface develops a positive charge and the other a negative one (Christy, 1997). In some industrial printers, the carrier particles are fed by a separate special cartridge, and they are mixed with the toner inside the printer just before the development stage. In some other technology, toner and carrier particles are ready mixed inside the toner cartridge.

The differences in toner charging technologies means that different parameters produce and control the final charge to mass ratio " q/m " of the toner particle, which is essential for further electrostatic and mass transfer phenomena in latent image development and toner transfer to paper. Therefore, the description of the electrophotographic process based on six stages is not a complete definition, because toner charging which determines " q/m " is ignored, or considered as a part of development stage (Kipphan, 2004). The importance of this parameter can be predicted from the fact that small toner particles will get a higher charge than large particles under the same charging conditions (Anderson, 1997). This will lead to the opposite and multiple fluctuation of the " q/m " ratio; high " q/m " values for small particles and less for large particles. This means that the smaller toner particles develop the latent image faster and therefore earlier than the larger particles.

Aside from development process, toner must be optimized simultaneously with the parameters of the other process stages like toner transfer, cleaning and fusing. The matching of the toner functionality to each process step makes it difficult to design a toner, because certain optimisation to one process stage does not necessarily mean optimisation with respect to the others. The chemical toner recipe might be the same in different printers; in this case, the charging rate, charging level and charge distribution are strongly influenced by the process engineering factors (Hayashi & Shimizu, 1997). Of course, a lot of physics and chemistry modifications are involved when considering different toner components such as the binder polymers, the colorants, charge control agents "CCA" and the type of carrier beads (Nash

et al, 1997). According to this understanding, the “q/m” is the factor which fractionates the toner particles by consuming the fine particles in printing better image quality at the beginning of the life time of a toner cartridge, and the degradation in image quality resulting from large toner particles is highest at the end of the cartridge’s life time.

After this short introduction of the toner charging stage and its role in electrophotography, this paper suggests completion of the definition of electrophotographic process by considering the ‘Toner Charging’ as a separate stage: the process is redefined as a process of “seven stages”, instead of “six stages”. The seven stages are; 1st photoconductor charging, 2nd exposing the latent image, 3rd toner the paper. charging, 4th development of charged toner into the latent image on the photoconductor surface, 5th transferring the developed image from photoconductor to paper, 6th erasing the remaining charges and stage is fusing the image to be fixed and penetrated into cleaning the residual toner, and finally the 7th.

Another set of differences between the technologies is related to four colours versus black and white “B/W” printing. For example, in tandem transfer technology, the printer usually consists of four printing units, one for each colour. Regardless of the fusing process, “the 7th stage”, which is designed in the same way for all the colours, each unit has its own six process stages and elements with different parameters to fit its toner and the sequence of its colour. Light Emitting Diode “LED” is widely used in this technology to reduce the cost of having four laser exposing units. If the printer consists of one printing unit, then this unit must operate four times with four different sets of parameters adjustable to the four colours and their sequences. With the help of advance automation system, the optimisation of single unit parameters and the synchronisation between the four colours’ operational sequences are achievable, but the problem still remains with the fusing stage which applies same rate of pressure and thermal energy to four different toner materials. B/W printers have no such complexity, so in general B/W image printed by a printer designed only for B/W prints is better than the same B/W image printed by a four-colour printer.

As we have mentioned earlier, the exposing process is accomplished by controlling the wavelength range of the light source such as a laser or LED. The exposing direction of a laser source is along with the cylinder axis of the photoconductor, whereas the LED exposure is perpendicular to the roller axes. So far, the known exposing process technologies are far better than the rest of the electrophotographic process stages in terms of detail reproduction. Therefore, the exposing direction itself cannot make a significant difference as long as the wavelength of the light source is controlled to reproduce a similar spot on a sensitive and uniform photoconductor which rotates at a constant speed and consists of homogeneous layers. The moving directions of the rest of process stages “from image development to the fusing stage” have a clear influence on image quality. With the recent technologies of optical systems and photoconductor materials and their sensitivity levels, the exposing details of high optical resolution can be achieved by using shorter wavelengths, particularly blue laser emitting near 400 nm (Melnyk, 2002).

3. Experimental

Detail rendering is one of the traditional measures used in evaluation of printed image quality. In this paper, the experiments were designed (Räsänen, 2004) so as to contribute to understanding the image quality factors from the standpoint of different applications. The approach of the study involves measurements on a wide range of dry toner electrophotographic printers with a focus on the performance of each technology at different stages of the printing process such as exposing, developing, toner transfer and fusing stages. Previous experience obtained by several studies on digital electrophotography was helpful in the design of the experiments such as selecting the printers and designing the test image. Understanding of the influence of surface treatment of the paper, such as coating and calendering, is also significant; this was considered in the selection the paper grade suitable to the experiments. Also it is known that detail rendering of printed lines in the parallel direction with fibre orientation differs from

lines printed perpendicular to the fibre orientation. The printed lines perpendicular to each other are affected by the directions of exposing, transferring and fusing as well as by the fibre orientation.

3.1 The printers

Five out of eight different printers used in this study were industrial presses “IP”, and three others were desk top office printers “DP”. They are all dry toner based printing machines, but with many differences. Some differences are associated with being industrial presses or desk top printers, such as the speed, the range of suitable paper grammages and dual or single toner development process.

According to the differences in dry toner technologies outlined in the technological framework, the printers were chosen, and the experiments were designed. The eight printers used in this experiment and some of their different features are presented in Table I. Since different printers’ trade marks and brands can have exactly the same engine configuration, therefore there is no sense to mention them in the table. Also, the aim is to look at different technologies and the influence of their process parameters on print quality regardless of printer’s name. For instance, “IP1” and “IP2” are made by the same manufacturer and they have exactly the same engine, but “IP2” is faster than “IP1” and accordingly, the fusing temperature were designed to be higher in “IP2” to complete the fixing of the image in shorter fusing time (dwell time).

Table I: Printers in the experiments. The specifications are from the data sheets of the manufacturers

Printer	(IP1)	(IP2)	(IP3)	(IP4)	(IP5)	(DP1)	(DP2)	(DP3)
Age	1996	2001	2001	2000	1990	2002	1995	1996
dpi	400	800x400	600	600	600	600	600	600
Exposing	laser	laser	LED	LED	laser	laser	laser	laser
Toner size, type	8-9 μm , dual	8-9 μm , dual	5-6 μm , dual	6 μm , dual	6 μm , dual	8 μm , single	8 μm , single	8 μm , single
Toner transfer method	transfer blade	transfer blade	transfer belt	corona & belt	corona	transfer belt	transfer drum	corona
Fusing method	2 hot rollers	2 hot rollers	hot/press rollers	belt/roller nip	hot/press roller	fusing belt	2 hot rollers	1 hot roller
Fusing $^{\circ}\text{C}$	175 $^{\circ}\text{C}$	180 $^{\circ}\text{C}$	140 $^{\circ}\text{C}$	160 $^{\circ}\text{C}$	198 $^{\circ}\text{C}$	170 $^{\circ}$ to 185 $^{\circ}\text{C}$	162 $^{\circ}\text{C}$	200 $^{\circ}\text{C}$
Papers weight (GSM) or (gm^{-2})	65-220	65-270	80-300	60-280	60-250	60-163	60-105	60-200
Speed (ppm), colour	31 A4 colour	50 A4 colour	70 A4 colour	60 A4 colour		5 A4 colour	3 A4 colour	
Speed (ppm), B/W					135 A4 (B/W)	20 A4 (B/W)	12 A4 (B/W)	24 A4 (B/W)

3.2 The paper

The paper used in this study was selected from many grades by a simple pre-test in which the Contrast Transfer Functions “CTF” were measured from many samples printed by the same printer. The desk top printer named “DP2” was used in this pre-test. Six paper grades were examined. One was a commercial uncoated grade 80 gm^{-2} , which is commonly used in dry toner printing. Other five coated paper grades had been made for research purposes. All of these five grades were made of the same base paper, coated by two different coating colour formulations coded as C1 and C2. By using coating colour C1, two grades were produced; (100 gm^{-2} , C1) double layer coating and (135 gm^{-2} , C1) triple layer coating. And by using coating colour C2, three grades were optioned; (90 gm^{-2} , C2) a single layer coating, (100 gm^{-2} , C2) double layer coating and (135 gm^{-2} , C2) triple layer coating.

Figure 1 shows the CTF curves resulted from the printed samples on these six paper grades. The result delivers good judgement to select the paper with the best CTF curve. It is clear from Figure 1 that the best choice was the commercial uncoated grade 80 gm⁻². This result does not mean that this grade is absolutely better than the others, but its bulk, electrical and thermal properties as well as its surface treatment are in good compatible agreement with the process parameters of the desk top printer DP2. The optimisation of the electrical properties with the thermal properties and surface energy is essential in designing the paper to be used in dry toner technology. Some coated paper can have efficient transfer feature through its electrical properties, but later the image quality may be destroyed in the fusing stage due to incompatible paper surface energy with that of the melt toner at melting temperature (AL-Rubaiey et al, 2002). The best solution is to design the required paper properties together with printing process parameters, but this is not a feasible approach because paper making is a mass production process and the small percentage made for digital printing is quite difficult to be optimised for a large number of different printers. Then, printing machines manufacturers may concentrate on further technological development in the aspect of eliminating the effect of paper on print quality (Weigert, 2003).

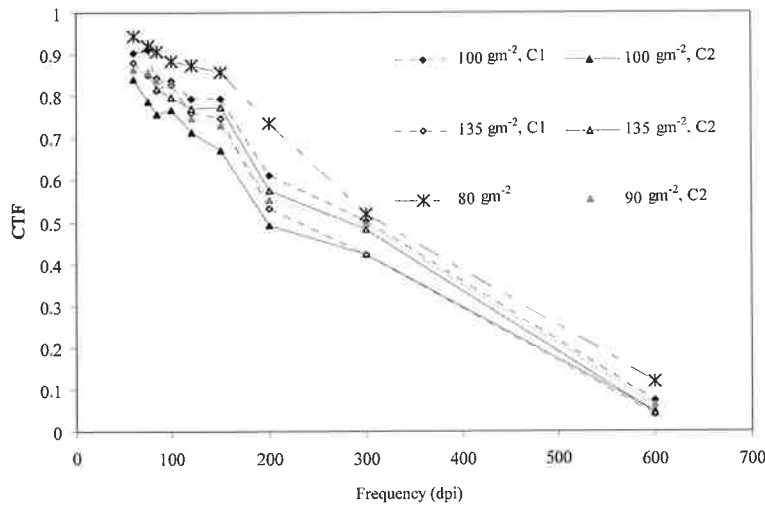


Figure 1:
CTF curves of different
paper grades

3.3 Test image and quantitative measurements

The test image was designed to contain the basic elements of any black and white image; dots, vertical and horizontal lines in ten different frequencies, and twenty grey scale percentages between zero and solid image. A microdensitometer was used to measure the optical density profiles of printed line bar patterns. The dynamic range, contrast transfer function (CTF) and signal-to-noise ratio (SNR) were calculated from the maximum average density of printed area (D_{max}) and minimum average density (D_{min}) of non-printed area as following:

$$\text{Dynamic range} = D_{max} - D_{min} \quad (1)$$

$$\text{CTF} = [(D_{max} - D_{min}) / (D_{max} + D_{min})] \quad (2)$$

$$\text{SNR} = [(D_{max} - D_{min}) / \text{rms noise}] \quad (3)$$

Smallest reproducible pixel size can be calculated from equation 4 by using the frequency at the half of the CTF curve. This is to compare the reproducible pixel size of each printer with the theoretical values, which are 64 μm and 42 μm for 400 dpi and 600 dpi printers respectively.

$$\text{Pixel size } (\mu\text{m}) = \frac{25400 \mu\text{m} / \text{inch}}{\text{frequency (dpi)}_{0.5}} \quad (4)$$

The printed line bar patterns at different frequencies and halftone dots were captured by a digital camera mounted on top of a microscope. Special image analysis software and macros were used to analyse the images. Edge noise, raggedness and sharpness percentage were determined from the lines.

Edge noise was also calculated from the 25% halftone dots. Figures 2 and 3, display the microscopic images of captured lines and dots, and the software processing procedures.

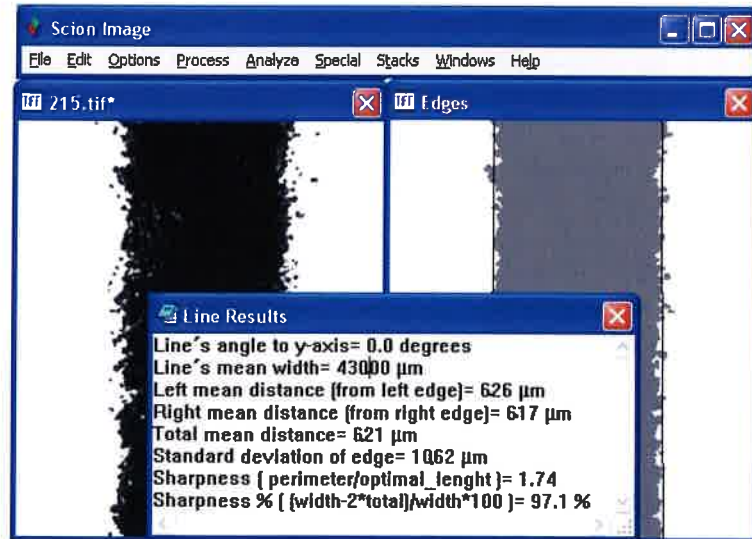


Figure 2: Microscopic line processing

The edge noise of a line such as the one shown in Figure 2 is expressed by the standard deviation of edges calculated as horizontal distance from the centre of the line to the right and left edges. Sharpness percentage quantifies in percentage units how much the line pattern resembles the ideal line pattern. Raggedness of lines is calculated from the following simple formula:

$$\text{Raggedness} = \text{perimeter/optimal length} \quad (5)$$

Figure 3 shows the 25% halftone dots before and after processing, and the edge noise of each dot (presented by raggedness) is calculated by the software according to the following equation:

$$\text{Edge noise} = \frac{P^2}{A * 4 * \pi}, \quad (6)$$

where p is perimeter, which is obtained by fitting the dots to some geometrical shape, in this particular case circles, and A is the area of the dot.

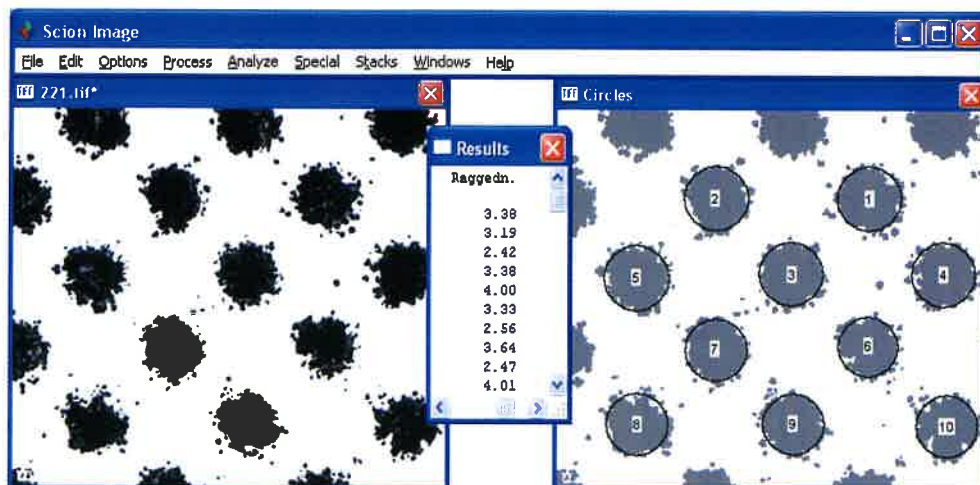


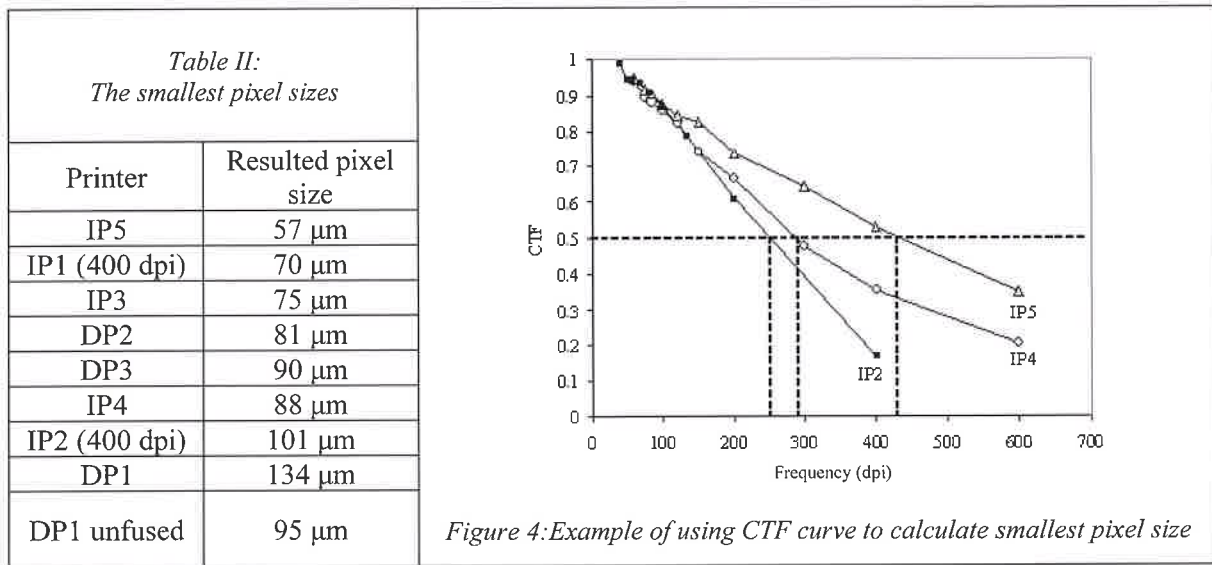
Figure 3: Microscopic dots processing

3.4 Subjective evaluations

Sharpness was evaluated visually using eight observers. The subjective method was based on pair comparison using the 2-1-0 point system. When one sample is observed sharper than the other it is awarded 2 points whereas the other gets 0 points. If the observer sees no difference, both samples get 1 point. Each sample is compared with any other sample in the group. The sum of points awarded to each sample was calculated statistically. The mean of all observers' assessments were compared with microscopic and image analysis tests.

4. Results and discussion

Smallest reproducible pixel size is calculated from $CTF_{0.5}$ from the lines printed using the different printers in the direction to the fibre orientation of the paper. This direction can be the same as the feeding direction (printing direction) in some printers which are designed for A4 format, and perpendicular to the feeding direction in some others designed for A3 format. Figure 4 illustrates the calculation technique for three printers. For instance, the $CTF_{0.5}$ of IP2 is at the frequency of 250 (dpi). The pixel size obtained using equation 4 is 101 μm . The pixel size from $CTF_{0.5}$ curves of all the printers are shown in Table II.



The results in Table II show that practical pixel sizes reproduced by IP1 and IP2 are close to the nominal design value, which is 64 μm for the 400 dpi printers. The detail rendering of IP5 is the best among the others. This printer is designed for black and white prints, so it has fewer process parameters which need to be optimized compared to the four-colour printers. The uncoated paper used in the experiments was especially suitable to this printer which is meant to use uncoated grades of 80 gm^{-2} . The smallest toner particles and the lowest fusing temperature of IP3 explain the smaller pixel size compared to the other four printers. The influence of fusing on detail rendering is clearly expressed as the 95 μm pixel size of unfused image compared to the 134 μm pixel size of the corresponding fused image. Both fused and unfused images were printed by the same printer (DP1). The result does not mean that the rest of the printers have poor detail reproduction, but rather that the measurement or the concept of CTF may have limitations. Also may be the papers do not very well meet the requirements of some of the printers.

Frequency (dpi) expressed as the 95 μm pixel size of unfused image compared to the 134 μm pixel size of the corresponding fused image. Both fused and unfused images were printed by the same

printer (DP1). The result does not mean that the rest of the printers have poor detail reproduction, but rather that the measurement or the concept of CTF may have limitations. Also may be the papers do not very well meet the requirements of some of the printers.

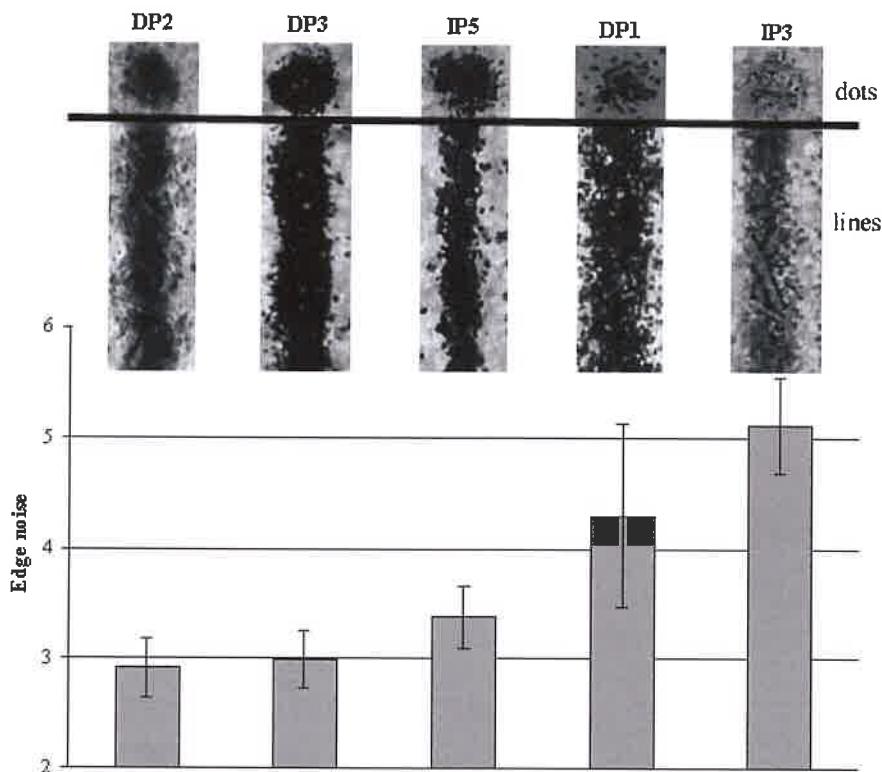


Figure 5: The microscopic images for dots produced by different printers with their respective edge noise values

In Figure 5, microscopic images of dots printed by different printers used in the study are depicted together with calculated values of edge noise of the dots. The frequencies of the printed lines are half of the nominal frequency and the dots are 25% halftones. The calculated values are a general indicator of the appearance of the printed microscopic images. Clearly the appearance varies a lot; each of the printers has a distinct fingerprint of its own. Subjectively determined impression of sharpness proved to be consistent with the appearance. Subjective assessments were related statistically with print darkness and edge quality; the way in which the edge quality was calculated influenced the correlation.

Figure 6 shows how quality deteriorates with increasing frequency. When measured as CTF at highest frequency the resolving power of the industrial printers is better than that of the desk top printers. The figure shows that the printer IP5 has produced better quality than the rest. This is because it is designed as a black and white printer, where the process parameters are fewer and more easily controlled than in colour printers. The results of IP5 in Figures 4, 5 and 6 give confidence that this is so. And then IP4 which is new technology with fairly low fusing temperature applied by soft and long fusing nip which is essential to produce better detail rendering. The transfer corona under the belt and the 6 μm toner particle size used in this machine are powerful factors in transferring the toner to paper efficiently (AL-Rubaiey & Oittinen, 2001). IP1 and IP2 printers have exactly the same engine, but IP2 is faster than IP1. To overcome the short dwell time in the fusing stage, the manufacturer has increased the fusing temperature of IP2 and the high fusing energy has caused more spreading of melt toner. Therefore the CTF curve produced by IP2 runs much lower than the CTF of IP1, especially at high frequencies.

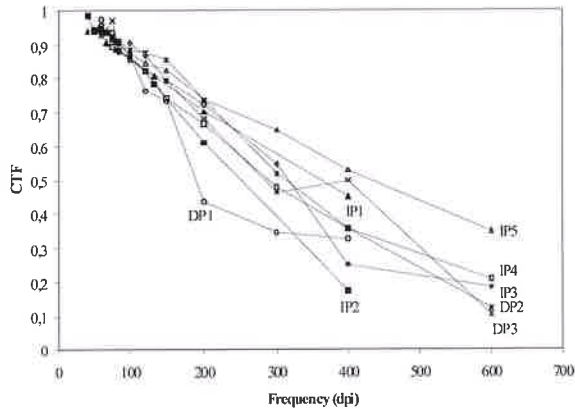


Figure 6

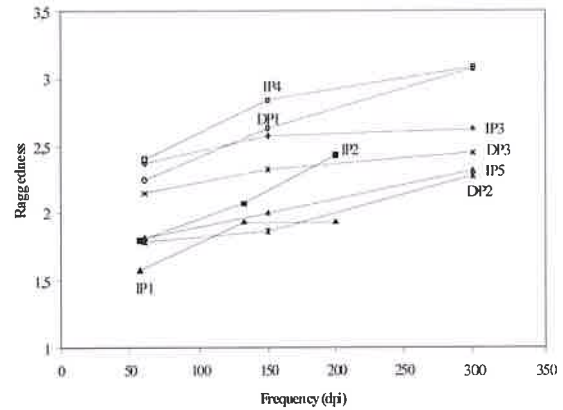


Figure 7

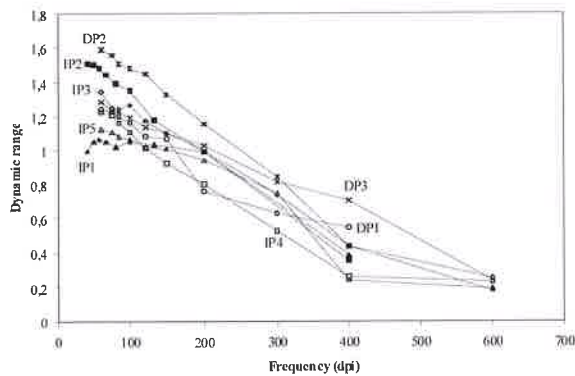


Figure 8

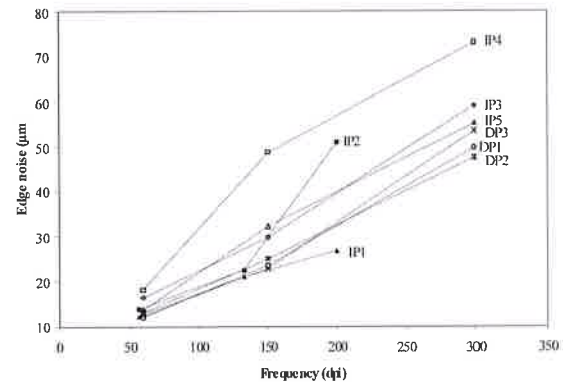


Figure 9

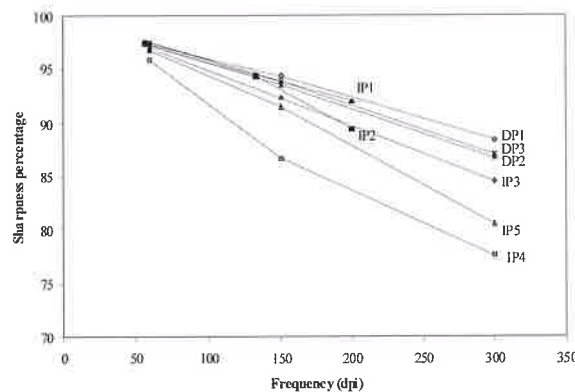


Figure 10

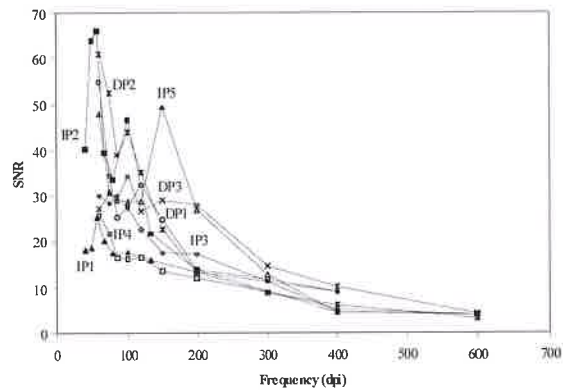


Figure 11

Figures 6-11: Spatial frequency domain performance of the printers measured by microdensitometric and image analysis methods

These same reasons apply for the performance of IP4 and IP3 in terms of raggedness shown in Figure 7. It is also valid for the desk top printer DP1 compared to the other two similar range printers. The fusing temperature is higher in this printer, but the thermal energy is applied indirectly through the fusing belt. High level of detail reproduction requires less fusing energy and efficient transfer of small toner size, so that less satellite particles arise. When they are melting with less energy, they will not spread much at the edge of the line. In the reverse case raggedness increases and sharpness deteriorates.

The dynamic ranges of the printers presented in Figure 8 can be used to evaluate the quality at low frequency. Most likely, the dynamic range is a good measure for functional quality, because it is a contrast indicator. Figure 9 shows that the edge noise is higher for industrial printers than office printers, and sharpness percentage illustrated in Figure 10 is lower, respectively. It may be observed that the edge noise values at the highest frequencies have the same order of magnitude as reproduced pixel size shown in Table II. Figure 10 shows that desk top printers have produced higher sharpness percentage than the industrial presses. The printing speed and the resolution are clearly influencing the sharpness percentage.

Signal to noise ratio (SNR) presented in Figure 11, was not found to be reliable in characterizing detail rendering. This may be related to the difficulty in determining “rms” noise from the data. In general low-speed electrophotography produces lower edge noise than high-speed processes at the same line width (Schein et al, 1993). Edge noise is strongly frequency dependent (Räsänen, 2004). Due to the absence of the deformation, non-contact fusing methods such as flash or infrared fusing lead to stronger edge noise than hard nip and soft nip fusing.

A printed line which lies in the axis direction of the photoconductor cylinder (cross to the printing direction) requires less time to be exposed, developed, transferred and fused, than the one printed in the same direction as the printing process. Less time means avoiding the variation of several parameters along the printing process. It was found that this appears to be true at least in the exposure and development stages, but definitely not in the transfer and fusing stages where other factors such as pre and post transfer, and the flow directions of melt toner under the hot deformation of the fusing nip influence the detail rendering in opposite direction more strongly than the speed. The difference in CTF of two perpendicular lines is shown in Figure 12.

Most criteria of image quality are subject to change at the final stage in electrophotographic printing process, where the image is fused to be fixed onto paper. Figure 13 shows the effect of fusing parameters on detail rendering.

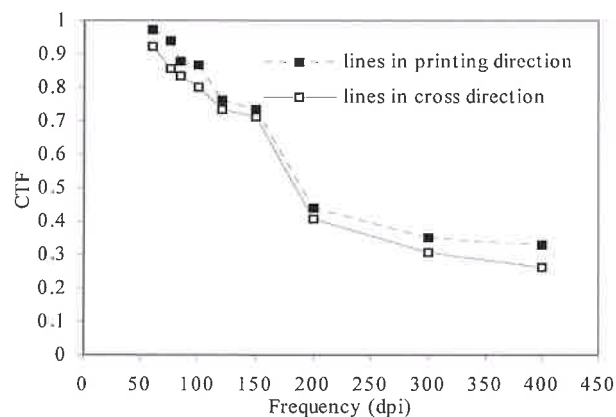


Figure 12: CTF of two lines perpendicular to each other

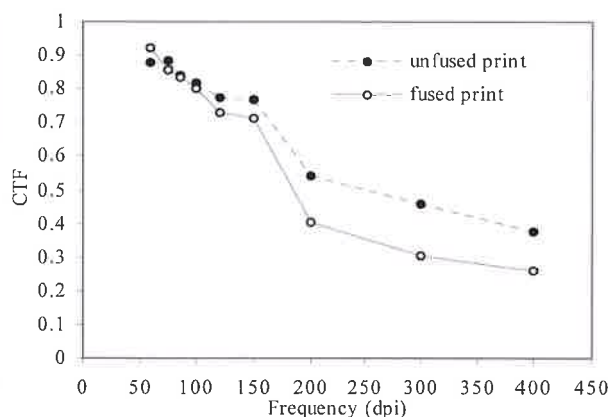


Figure 13: CTF, before and after fusing

In Table III, mutual correlation of the image quality criteria are shown as correlation coefficients. Statistically significant (95 %) correlations are bolded. The correlations between pair comparison (colour samples) and CTF and SNR are significant at 90 % confidence level (Laininen, 1995).

Values for raggedness, edge noise and sharpness percentage have been calculated from the lines that correspond to half the highest spatial frequency. In calculating the correlation coefficient between analytically determined image measures and dynamic range, CTF and SNR, values of the last mentioned also correspond to half of the highest frequency. Otherwise dynamic range, CTF and SNR values are calculated at the highest frequency. Pair comparison values used for correlations are the sum of points awarded for each sample by the group of judges. The values used to calculate correlations in Table III

are averages from lines in the two directions; printing and cross directions “the lines are perpendicular to each other”. From the table, it can be seen that dynamic range decreases as edge noise and raggedness increase and sharpness percentage decreases respectively. Raggedness decreases with decreasing detail/pixel size and increasing CTF. The higher dynamic range, CTF and signal-to-noise ratio yield also higher subjective quality (higher observed sharpness).

Table III: The relation between different measures at 95 % level of confidence

	Dyn. range (highest frequency)	CTF (highest frequency)	SNR (highest frequency)	Edge noise (half of the high. freq.)	Raggedness (half of the high. freq.)	Sharpness % (half of the high. freq.)	Smallest repr. pixel	Edge noise of halftones
CTF (half of the high. freq.)				-0,475	-0,713	0,240		
Dyn. Range (half of the high. freq.)				-0,772	-0,826	0,752		
SNR (half of the high. freq.)				-0,336	-0,498	0,363		
Dyn. Range (highest frequency)								0,004
CTF (highest frequency)	0,793							-0,037
SNR (highest frequency)	0,855	0,912						-0,199
Edge noise (half of the high. freq.)								0,869
Raggedness (half of the high. freq.)				0,801				0,697
Sharpness% (half of the high. freq.)				-0,906	-0,621			-0,206
Smallest reproducible pixel size	-0,823	-0,746	-0,650	0,201	0,641	0,115		0,224
Edge noise of halftones								
Pair comparison (colour), n = 6	0,847	0,711	0,712	-0,407	-0,509	0,386	-0,561	
Pair comparison (B/W), n = 8	0,528	0,266	0,418	-0,386	-0,010	0,512	0,118	0,821

5. Conclusion

The results of this study suggest that understanding of detail rendering on a fundamental level requires analysis and reference to process technology. Currently detail rendering is better controlled in B/W printers than colour printers, especially at the high speed range.

This study also indicated that not only CTF-based measures but also edge noise and raggedness are frequency dependent. Regardless of the exact measures used in characterization of detail rendering whether edge noise, CTF or SNR, it is important to understand the mechanisms and phenomena which influence the different types of characteristics. It is also important to understand the exact need for the different characteristics in different types of applications. For instance, the lower raggedness fused images fixed by heat roller is due to pressure that connects neighbouring toner particles at the edges.

This -of course- will not improve the detail rendering and is not good for photo printing, but it is important from the standpoint of slab (layer) melted toner which is essential in some functional applications such as those based on electrical conductivity.

The correlation coefficients calculated between the different image quality measures indicate that the data results given by different measuring methods were in accordance with each other. (For instance when CTF increases raggedness decreases etc.) Thus, image quality measures determined with microdensitometer correlated well with measures obtained image analytically. The same holds true for microdensitometric measurements and subjective tests -for colour samples- respectively.

References

- AL-Rubaiey & Oittinen, (2001), *Transfer Current and Efficiency in Toner Transfer to Paper*, IS&T, NIP 17, Pages 648-652
- AL-Rubaiey & Oittinen, (2004), *Controlling Fusing Parameters by Optical Image Quality in Electrophotographic Printing*, Graphic Arts in Finland, Volume 33, Number 1, Pages 1-5
- AL-Rubaiey et al, (2002), *The Influence of Flash Fusing Variables on Image Fixing Quality*, ICIS'02 Tokyo, Pages 496-498
- Anderson, (1997), *A Comparison of Experimental Data and Model Predictions for Tribocharging of Two-Component Electrophotographic Developers*, Recent Progress in Toner Technology, Pages 189-194
- Christy, (1997), *Surface Adhesion Properties of Field Charged Toners in a High Speed Toner Applicator*, Recent Progress in Toner Technology, Pages 203-206
- Hayashi & Shimizu, (1997), *Charge Stabilization of Toner using Polymer Resin*, Recent Progress in Toner Technology, Pages 93-99
- Kipphan, (2001), *Handbook of Print Media*, Springer-Verlag, Berlin 2001, page 1207
- Kipphan, (2004), *Personal discussion during the 31st iarigai International Conference*, Sep. 5-8, 2004 Copenhagen, Denmark
- Laininen, (1995), *Todennäköisyyslasku ja tilastomatematiikka (Finnish Language)*, Otatieto Oy, Espoo, Finland, Pages 254
- Majava, (1994), *Methods to Characterize Dry Electrophotographic Toners*, Graphic Arts in Finland, Vol. 23, No. 3, Pages 3-8
- Melnyk, (2002), *Higher Resolution for Color Laser Printers and Copiers: Why and How*, Journal of the Imaging Society of Japan, 41, 4, Pages 408-413
- Nash et al, (1997), *Toner Charge Instability*, Recent Progress in Toner Technology, Pages 169-180
- Oittinen & Saarelna, (1994), *Elektronisen painatuksen suorituskyky (Finnish Language)*, Helsinki University of Technology, Laboratory of Media Technology, Internal Report No. 22, pages 36
- Rushing et al, (2001), *Toner Satellite Formation in Electrostatically Transferred Images*, Journal of Imaging Science and Technology, 45, 2, pages 187-197
- Räsänen, (2004), *Detail rendering of dry toner based digital electrophotography*, Master's thesis, Helsinki University of Technology, pages 108
- Schein et al, (1993), *Offset Quality Electrophotography*, Journal of Imaging Science and Technology, 37, 5, pages 451-461
- Schleusener et al, (1994), *The Influence of Toner and Paper Properties on Electrophotographic Print Quality*, IS&T, NIP 10, Pages 545-548
- Tsunemi et al, (1997), *Influence of charge Control Agent and Development Roller Surface on Toner Charging*, Recent Progress in Toner Technology, Pages 292-297
- Vallenius, (2001), *Inkjet deposition of conductive polymers*, Master's thesis (Finnish Language), Helsinki University of Technology, Laboratory of Media Technology, Pages 65
- Weigert, (2003), *Solution to reduce the Impact of Paper Properties to Print Quality and Runnability in the NexPress 2100*, IS&T's International conference, DPP2003, Pages 216-217



CIEDE2000 – a tool for the determination of colour differences in inkjet?

Marianne Klamán, Per-Åke Johansson, Åsa Hägglund

STFI-Packforsk AB
P. O. Box 5604, SE-114 86 Stockholm, Sweden
E-mail: marianne.klamán@stfi.se
E-mail: perake.johansson@stfi.se

STFI-Packforsk AB
Järnvägsgatan 3, Örnköldsvik, Sweden
E-mail: asa.hagglund@stfi.se

Abstract

The objective of the research presented here was to seek an answer to the question:

- Is the CIEDE2000 a better metric to use in the media industry, here specifically for inkjet printing, than the earlier colour difference formulae?

Technical measures of colour differences have been compared with results from perception studies. Prints from two inkjet photo printers on ten different photo quality paper grades were measured and evaluated visually. The CIEDE2000, CIE94 and CIELAB formulae were compared. Four colour patches and two images were used in the study.

The outcome of the investigation with results in the form of correlation coefficients as well as response variations indicate that the CIEDE2000 formula seem to perform more uniformly than the other colour difference formulae, particularly CIELAB.

In order to be able to use images for assessment and compare with instrumental measures there is a need to develop methods where the real colour content of images can be extracted and measured.

1. Introduction

The CIELAB (CIE 1976) ($L^*a^*b^*$) formula for calculating colour differences has been found unsatisfactory, particularly in the textile industry where colour difference tolerances are extremely narrow, since the CIELAB colour space is not sufficiently uniform in different hue regions. The most recently presented colour difference formula CIEDE2000 (Luo, Cui and Rigg, 2001) is based on CIELAB. It includes not only weighting functions for lightness, chroma and hue, but also an interactive term for chroma and hue differences to improve the performance for blue colours and a scaling factor for the a^* -scale in order to improve the performance for gray colours (Luo et al., 2001 p. 340). The authors claimed that the CIEDE2000 formula “outperformed CMC and CIE94 by a large margin” (Luo et al., 2001, p 340). CIE has also adopted it as an improvement for industrial colour-difference evaluation (CIE, 2001). CIE describes the model as an extension of the CIELAB colour-difference model with corrections for variation in colour-difference perception dependent on lightness, chroma, hue and chroma-hue interaction. The formulae for CIEDE2000, CIE94 and CIELAB are found in the Appendix.

The results reported by (Johnson and Green, 2001) are partly contradictory to the results of Lou et al. Johnson and Green reported experimental work to evaluate the magnitude of colour differences that may be accepted according to different formulae for critical comparisons in the Graphic Arts field. The authors claimed that neither CIE94 nor CIEDE2000 offered any significant improvement over CIELAB

in their study. The CIEDE2000 was developed, as was the CMC formula earlier, to be used in the textile industry where the colour difference tolerances are narrow. In the media industry however the limits are wider. Nevertheless the need to find a uniform colour space is also important in the graphic arts applications. Comparisons have to be made between different images, prints and proofs and between prints from different devices to find the best combinations of ink and paper. One way to make this kind of comparison is by visual assessment. If the test sets are comprehensive visual assessment is time-consuming and expensive. If the colour differences compared with a reference could be used to rank different test images or patches, this could be a time-saving tool.

(Bassemir, 1995) found a reasonable correlation between perceived colour differences and CIELAB ΔE^*_{ab} . (Paul, 1998) on the other hand found a low correlation between perceived colour differences and ΔE^*_{ab} but an improved correlation when using CIE94.

Against this background, we wish to contribute some experiences gained from a study concerning the quality of inkjet photoprints, which was expanded to also include colour difference measures, even though our study is very restricted compared to other more deeply penetrating studies in this area.

The quality of inkjet printing has increased very rapidly during recent years and it is in many ways well adapted to meet the demands of different product segments. In a preliminary study (Klaman, Wedin, 2003), it was shown that photo prints produced with inkjet achieve at least the quality of professionally produced photographs or even, as is claimed in the literature, exceed what it is possible to achieve with conventional photography.

Since the study included a broad spectrum of different paper grades for high quality inkjet photoprints, the material seemed well adapted for an evaluation of the CIEDE2000 formula in comparison with the CIELAB and CIE94 colour difference formulae. The object of the study was to investigate to what degree, the new formula provides positive improvements and to what extent it may serve as a tool for critical comparisons in the media industry for the kind of graphic arts products that inkjet prints represent.

2. Method

The technical measures of colour differences have been compared with the results of perceptual studies.

2.1 Preparation of prints

Two printers, A and B, were used with six dye based process inks: cyan, magenta, yellow, black, light cyan and light magenta. Printer A was based on piezoelectric technology and printer B on thermal technology.

Glossy, semi-glossy (satin) and matte papers were printed. All these were commercially available. The characteristics of the papers used are given in Table I.

2.2 Colour measurement

Four colour patches were used for the comparative study: magenta, blue, skin and lime. In the Appendix, the colour patches are specified and their coordinates plotted in a^* , b^* -diagrams.

The printed test chart also included two images for visual evaluation, one with skin tones and one high-key image, see Figure 1, and also the TC9,18 test chart (from ProfileMaker). The patches on the chart were measured using GretagMacbeth SpectroScan (D50/2°). Paper number 3 was chosen as a reference, since the prints on this paper looked quite neutral within the group of prints.

Table I: Characteristics for the papers used

Paper number	Man.	Type of paper	Grammage g/m ²	Surface roughness PPS μ m	Gloss 75 %
1	a	Inkjet photo gloss	180	1,4	85
2	b	Inkjet gloss for imaging	180	1,5	79
3	b	Inkjet Satin for imaging, Reference paper	160	3,5	3
4	c	Photo paper matte	240	2,6	55
5	c	Photo paper gloss	240	0,8	94
6	d	Photo paper gloss	255	0,5	63
7	e	Paper for Imaging	225	0,16	92
8	f	Paper for imaging, budget	180	1,9	50
9	f	Paper for imaging, premium	200	1,0	85
10	f	Paper for imaging, Pro	270	0,6	70

From the CIELAB values obtained, the colour differences between each patch and the corresponding patch on the reference, as well as the mean colour difference for the entire chart were calculated. The CIEDE2000, the CIE94 and the CIELAB values were calculated in Matlab using the plug-in Colour Engineering Toolbox (Green, 2003).

*Figure 1: Images used for the perceptual study the High-key image and Baby Boy image*

2.3 Perceptual assessment

The perceptual study was performed under D50 illumination with a panel of 10 persons who were asked to judge the colour differences between the test prints and the reference. In this test, pairs of prints were compared with the reference and a slightly modified (referring to the use of a reference) 2-0 pair comparison method was used, where 2 points were given to the print that was most like the reference. If both prints were considered to be equally alike, or equally different from the reference, both prints were given 1 point. The points for each print were added together to give a total point sum. This sum was then divided by the number of persons in the panel and the number of prints in each set and multiplied by 200. This pair comparison index (Bristow, Johansson, 1984) is a measure of how close to the reference the prints assessed are and the higher index the more similar the print was to the reference. On this scale a sample that is preferred by all judges will gain 200 points and 100 points will indicate a sample that is considered to be on the average within the test set. Provided that samples are sufficiently similar for the judges not to be in agreement, it has been shown that a pair comparison index of this type has an approximately linear response to the visual stimuli (Bristow, Johansson, 1984).

2.4 Comparisons

The colour difference measures were compared with the result of the perceptual study to determine which of the three sets of colour difference data gave the best correlation with the visually assessed values.

From the three sets of colour difference data and the pair comparison indices the colour differences between all pairs within the print sets were calculated and plotted in diagrams. From these the corresponding values at a given level were estimated for analysis.

Taken together the perceptual studies and the measurements were performed on:

- Four colour patches, blue, magenta, skin and lime, from two printers.
- Two images and a colour chart printed on 10 paper grades, reference included, using two printers.
- Colour differences were calculated for all pairs of the colour patches for measured and calculated and for perceived values for all sets.

3. Results

3.1 Colour Patches

Table II - V present the measured and calculated and the assessed values for the four colour patches.

Table II: Colour difference and pair comparison index values for the **Blue** colour patches. Reference was paper 3

	Printer A				Printer B			
Paper number	CIEDE2000	CIE94	CIELAB	PC Index	CIEDE2000	CIE94	CIELAB	PC Index
1	5,92	5,67	8,17	40	3,26	4,17	4,24	135
2	2,78	3,80	4,07	160	2,18	2,90	3,76	161
4	8,11	11,10	18,94	46	3,74	4,03	5,54	111
5	9,61	12,80	20,84	25	4,17	4,09	6,30	121
6	4,81	6,95	13,75	141	5,37	5,99	8,80	20
7	2,86	4,00	6,56	80	3,71	4,58	5,07	63
8	4,23	4,52	7,00	142	3,83	4,91	5,51	108
9	2,86	4,00	6,56	148	3,38	4,43	5,64	83
10	5,58	7,95	15,72	116	2,08	3,00	7,24	99

Table III: Colour difference and pair comparison index values for the **Magenta** colour patches. Reference was paper 3

	Printer A				Printer B			
Paper number	CIEDE2000	CIE94	CIELAB	PC Index	CIEDE2000	CIE94	CIELAB	PC Index
1	5,91	6,34	12,29	14	10,51	12,28	24,39	69
2	4,70	4,75	5,27	55	11,58	13,51	24,55	50
4	1,82	1,85	3,81	138	11,54	13,50	24,79	69
5	4,58	4,88	9,64	59	11,36	13,22	22,81	79
6	2,77	2,77	4,75	115	9,78	11,50	21,62	159
7	2,45	2,49	3,75	95	12,17	14,35	27,31	69
8	2,62	2,62	3,24	156	10,34	11,94	24,02	98
9	2,45	2,49	3,75	129	9,51	11,22	21,99	161
10	1,82	1,82	4,94	140	11,44	13,62	26,48	148

Table IV. Colour difference and pair comparison index values for the *Skin* colour patches. Reference was paper 3

Paper number	Printer A				Printer B			
	CIEDE2000	CIE94	CIELAB	PC Index	CIEDE2000	CIE94	CIELAB	PC Index
1	2,07	2,70	2,89	143	1,32	1,61	1,76	121
2	3,06	3,31	3,92	65	1,68	1,62	1,95	116
4	3,62	4,37	5,23	71	4,98	4,80	6,12	63
5	4,59	5,71	6,82	53	5,22	4,83	6,13	38
6	4,08	3,42	4,04	100	5,27	3,90	4,36	19
7	4,06	5,23	5,76	11	1,21	1,25	1,36	94
8	2,44	2,60	3,45	114	2,45	2,47	3,17	124
9	0,70	0,74	0,93	183	1,10	1,65	1,70	180
10	1,26	1,26	1,49	161	1,87	1,60	1,76	146

Table V: Colour difference and pair comparison index values for the *Lime* colour patches. Reference was paper 3

Paper number	Printer A				Printer B			
	CIEDE2000	CIE94	CIELAB	PC Index	CIEDE2000	CIE94	CIELAB	PC Index
1	5,30	5,98	8,20	134	1,23	1,23	4,93	176
2	6,60	7,07	11,12	67	1,08	1,27	2,23	133
4	3,36	3,76	4,79	87	2,64	2,45	6,01	81
5	6,89	8,23	9,01	73	3,16	2,78	9,09	94
6	1,22	1,23	3,37	162	6,87	7,22	15,21	16
7	8,17	9,54	11,44	82	4,19	3,35	6,58	18
8	9,62	10,34	16,16	62	1,83	1,97	5,51	119
9	6,32	6,26	10,67	109	1,61	1,66	3,82	151
10	3,34	3,79	4,42	165	3,95	3,91	7,34	113

The CIEDE2000, CIE94 and CIELAB values are plotted against the corresponding perceptual values for Blue and Lime in Figure 2. These diagrams are also typical of the appearance of the other colour patch diagrams, showing CIEDE2000 and CIE94 more similar regarding the proportionality factor between the measures and pair comparison index values (with a steeper “slope”) than CIELAB. Table VI presents all the correlation values for the different sets of colour difference data in this study.

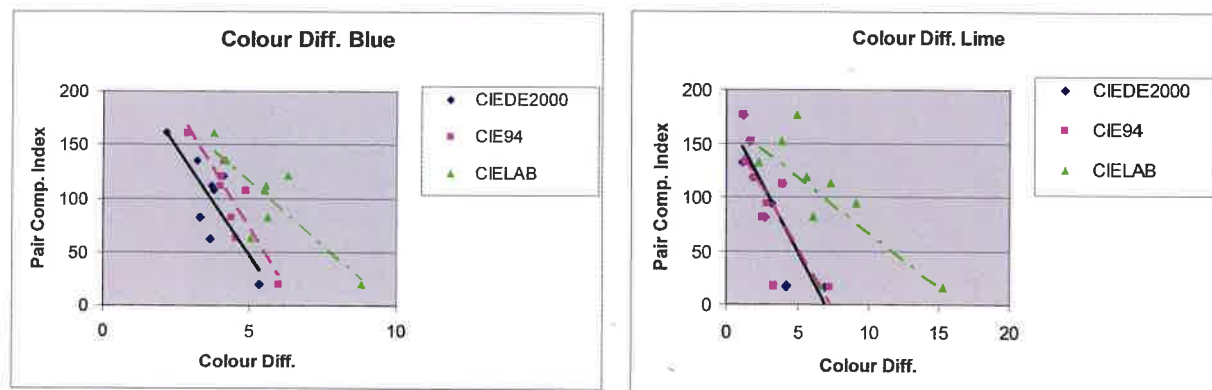


Figure 2: Calculated and perceived colour differences for Blue and Lime for one of the printers

Table IV. Correlation coefficients between the different colour difference sets for the four single- colour patches

Colour patch	Printer	Correlation Coefficients		
		CIEDE2000/CIE94	CIEDE2000/CIELAB	CIE94/CIELAB
Blue	A	0,96	0,90	0,97
Blue	B	0,90	0,94	0,84
Magenta	A	1,00	0,85	0,88
Magenta	B	0,99	0,81	0,83
Skin	A	0,95	0,95	0,99
Skin	B	0,97	0,95	0,99
Lime	A	0,99	0,96	0,92
Lime	B	0,98	0,92	0,94

The correlations between the data sets are naturally high, since the different sets are obtained by a mathematical transformation from the same data. This is particularly the case for CIE94 and CIEDE2000. A high correlation is obtained when these data are plotted for all the patches in the same diagram. This is not however the case when the data for CIE 94 or CIEDE2000 are plotted against the CIELAB data in a single diagram, since the transformation is, as indicated in the introduction, different in different hue regions.

The plot of CIEDE2000 values against the corresponding CIELAB values indicates that, for any given colour difference, the mathematical transformation is such that the CIEDE2000 value is about half the CIELAB value.

3.2 Images

In order to compare the perceptual image assessments with measured data, the mean colour difference for the whole set of patches in the TC9,18 colour chart was calculated. These mean colour difference values for the colour chart and the pair comparison perception index values for the two images are shown in Table VII for the two printers.

Table VII: Mean colour difference values for the colour chart and the pair comparison index values for the two images

Printer A Paper no	CIEDE2000	CIE94	CIELAB	Pair Comp. Index	
	Mean colour difference values for colour chart			High Key	Baby Boy
1	5,23	5,40	8,34	66	153
2	5,03	5,33	7,29	90	95
4	3,93	4,63	5,82	184	178
5	7,09	8,04	10,10	75	125
6	3,63	3,85	6,98	130	99
7	6,82	7,73	9,66	115	90
8	5,05	5,40	8,03	109	28
9	4,72	4,95	7,39	49	36
10	3,89	4,22	6,92	83	98

Printer B

Paper no

1	2,46	2,61	4,99	60	151
2	1,85	2,05	3,32	125	145
4	2,85	3,25	4,86	68	103
5	2,97	3,25	5,63	164	89
6	5,32	5,69	9,48	26	5
7	3,33	3,40	5,93	145	96
8	1,57	1,68	3,08	156	169
9	2,91	3,14	5,43	86	106
10	2,97	3,22	5,94	70	36

3.3 Correlation between measured and perceived colour differences

The correlation coefficients between measures and perception are tabulated for *colour patches* in Table VIII and for *images* in Table IX.

Table VIII: Correlation coefficients between measured and perceived colour differences for *colour patches*. An * indicates a non-significant value

Colour Diff. method	Blue	Magenta	Skin	Lime
Printer B				
CIEDE2000	0,68	0,68	0,87	0,85
CIE94	0,77	0,61*	0,79	0,78
CIELAB	0,76	0,43*	0,76	0,70
Printer A				
CIEDE2000	0,78	0,94	0,89	0,78
CIE94	0,68	0,94	0,93	0,78
CIELAB	0,59*	0,85	0,92	0,75

Table IX: Correlation coefficients between measured and perceived colour differences for *images*. An * indicates a non-significant value

Colour Diff. Method	Images	
	High-key	Baby Boy
CIEDE2000	0,57*	0,88
CIE94	0,60*	0,89
CIELAB	0,59*	0,89

The results from the two tables can be summarised:

- For the *colour patches* the correlation between the CIEDE2000 values and the perceptual values is *mostly* higher than the correlations between the other measures and the perceptual values. The differences between the correlations CIEDE2000 vs. perceived value and the CIE94 vs. perceived value are small. There is a larger difference between these correlations and the CIELAB vs. perceived value correlations, although the difference is not significant.
- For the *images*, there was no difference between the various correlation coefficients.

3.4 Pairwise Colour Differences

Assuming that the pair comparison index values make up a linear scale of achieved quality differences corresponding to the perceived differences, both measured and perceived colour differences for all pairs in each set were calculated and diagrams such as those shown in Figure 3 and 4 were obtained.

For a certain level, 100, corresponding ΔE values were estimated from the diagrams. These values are presented in Table X.

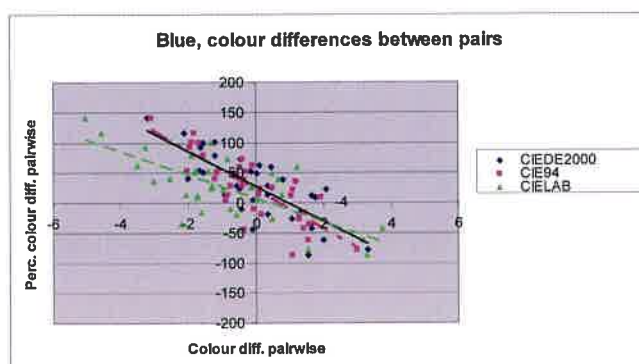


Figure 3: Pairwise colour differences for the Blue print

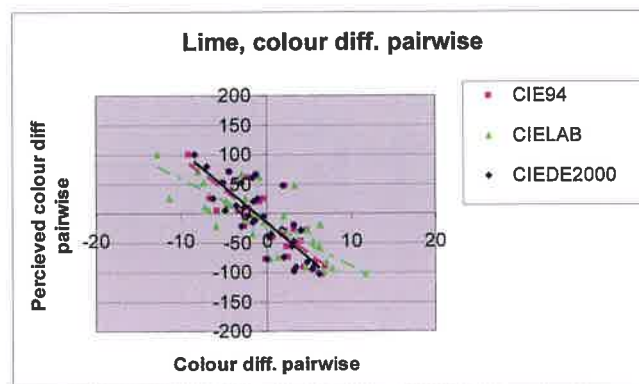


Figure 4: Pairwise colour differences for the Lime print

Table X: Estimated ΔE values from the diagrams with pairwise colour differences

Printer	Method	Blue	Magenta	Skin	Lime	Mean	Std. Dev.	Var. coeff.
A	CIEDE2000	5,5	2,5	2,5	8			
C	CIEDE2000	2,5	3,5	5,0	4	4,2	1,93	0,46
A	CIE94	11,0	3,0	3,0	9			
C	CIE94	2,5	5,5	4,5	4	5,3	3,09	0,58
A	CIELAB	25,0	10,5	4,0	15			
C	CIELAB	6	10,0	7,0	11	11,1	6,58	0,59

The estimated ΔE values are smaller for CIEDE2000 than for CIELAB, but – as indicated earlier – this is an intrinsic feature of the transformation from CIELAB to CIEDE2000 data. In this limited small-scale study, it is doubtful whether the differences in the coefficients of variation shown in this table are

significant. The fact that the coefficient of variation is smallest for the CIEDE2000 data may support the claim that, of all the formulae, this formula gives colour difference values which are the most uniform over the full colour space.

4. Discussion

The effect of a more or less uniform measure on the correlation between measured and visually assessed differences need to be commented on.

If a less uniform ΔE formula leads to difference values that are, say, too large by a constant factor in a certain region of the CIELAB space, this will not influence the correlation coefficient between the visual and the instrumental assessments in that region. It will however affect the proportionality factor (“the slope”) between the ΔE values and the visual differences. If, however, the less uniform ΔE measure contains differences in visual response in different $L^*a^*b^*$ directions in the CIELAB space, then the correlation between the visual and the instrumental values would be directly impaired by the ΔE dysfunction within the region of investigation.

The implications of our present investigation are not very strong. Nevertheless, the correlation coefficients and the response slopes suggest that the CIEDE2000 performs more uniformly than the other colour difference formulae, particularly CIELAB.

In the assessment of the images, mean colour difference measures were calculated from the colour chart. These values are the same although the images are different. In Figure 5, where the perceptual values are shown for all prints of the two images on the different paper grades, some of the prints are evaluated very differently although the paper is the same. Depending on the motif, one image can be assessed as being almost the most similar to the reference and the other one as being almost the most dissimilar to the reference although they are printed on the same paper. This must be kept in mind when a colour chart is used for calculating mean colour differences. Although it may be helpful for the characterisation of many images it may be less reliable for sensitive motifs. As soon as the colour control is not optimal and causes defects such as colour shifts, this may imply defects in colour for these sensitive motifs. Such a colour cast may not impact most images, or at least the cast may not be recognised as a disturbance, but for sensitive images the cast can have a large effect on how the image is assessed. For one of our sets and the Baby Boy image with a large content of skin tones, a slight colour cast, although not heavy, did not affect the high key image but it did affect the skin tones quite considerably. Different papers will expose this defect more as is shown in Figure 5 (compare papers 1 and 7). A better solution would be to extract the real colour content of each image and base the calculations on these data.

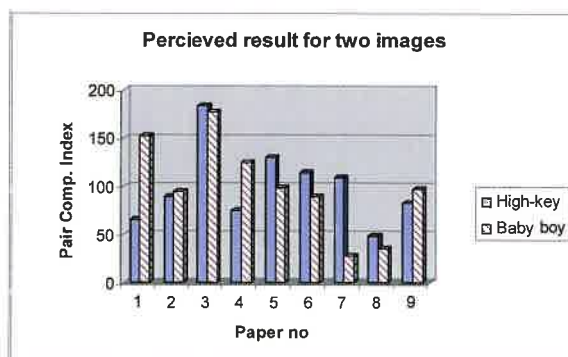


Figure 5: Perceptual results for the two images printed on the different photo print qualities

5. Conclusions

The implications of the present investigation are not very strong. Nevertheless, the correlation coefficients and the response slopes suggest that the CIEDE2000 performs more uniformly than the other colour difference formulae, particularly CIELAB.

The test material utilised in this study in the form of printed colour patches and images was not optimal for mapping colour differences over the whole available colour space but they were rather typical for a test of inkjet print performance in a few colours.

One outcome from the study is that there is a need to find methods where the real colour content of images can be extracted and measured and thus more relevant for perceived quality.

Acknowledgements

We express our gratitude to Kristina Wågberg and M-real for the permission to use the prints for this study and Malin Wedin for skilful assistance and organizing of the perceptual studies. We extend special thanks to Dr. J.A. Bristow for valuable comments and criticism of the study.

Literature

- Bristow, J.A. and Johansson, P.-Å, (1984), *Subjective evaluation by pair comparison: Pitfalls to avoid and suggestions for the presentation of results*, *Advances in Printing Science and Technology*, Vol 17 (Ed: W. H. Banks) Pentech press, 1984
- CIE Publication 142, (2001), *Improvement to Industrial Colour-Difference Evaluation*, CIE
- Green, P. J., (2003), *A Colour Engineering Toolbox*, <http://www.digitalcolour.org/toolbox.htm>
- Johnson, T., Green, P., (2001), *The CIE2000 colour difference formula and its performance with a graphic arts data set*, 28th Research Conference of IARIGAI, September 2001
- Klaman, M., Wedin, M., (2003), *Print quality and market potential for Ink-jet technology*, Paper presented at the 30th IARIGAI Conference on Advances in Printing Science and Technology, Cavtat 2003
- Luo, M. R., Cui, G., Rigg, B. (2001), *The Development of the CIE 2000 Colour-Difference Formula: CIEDE2000*, *Color Research and Application*, Volume 26, Number 5, October 2001

Appendix

Colour Difference formulae

CIEDE2000

$$L^* = 116 f(Y/Y_n) - 16$$

$$a^* = 500 [f(X/X_n) - f(Y/Y_n)]$$

$$b^* = 200 [f(Y/Y_n) - f(Z/Z_n)]$$

$$C_{ab}^* = \sqrt{a^{*2} + b^{*2}}$$

where

$$f(I) = \begin{cases} I^{1/3} & \text{for } I > 0.008856 \\ f(I) = 7.787I + 16/116 & \text{Otherwise} \end{cases}$$

$$L' = L^*$$

$$a' = (1 + G)a^*$$

$$b' = b^*$$

$$C_{ab}' = \sqrt{a'^2 + b'^2}$$

$$h'_{ab} = \tan^{-1}(b'/a')$$

where

$$G = 0.5 \left(1 - \sqrt{\frac{\overline{C_{ab}^{*7}}}{\overline{C_{ab}^{*7}} + 25^7}} \right)$$

where $\overline{C_{ab}^*}$ is the arithmetic mean of the C_{ab}^* values for a pair of samples.

$$\Delta L' = L'_b - L'_s$$

$$\Delta C'_{ab} = C'_{ab,b} - C'_{ab,s}$$

$$\Delta H'_{ab} = 2\sqrt{C'_{ab,b}C'_{ab,s}} \sin\left(\frac{\Delta h'_{ab}}{2}\right)$$

$$\text{where } \Delta h'_{ab} = h'_{ab,b} - h'_{ab,s}$$

$$\Delta E_{00} = \sqrt{\left(\frac{\Delta L'}{k_L S_L}\right)^2 + \left(\frac{\Delta C'_{ab}}{k_C S_C}\right)^2 + \left(\frac{\Delta H'_{ab}}{k_H S_H}\right)^2 + R_T \left(\frac{\Delta C'_{ab}}{k_C S_C}\right) \left(\frac{\Delta H'_{ab}}{k_H S_H}\right)}$$

where

$$S_L = 1 + \frac{0.015(\overline{L} - 50)^2}{\sqrt{20 + (\overline{L} - 50)^2}}$$

and

$$S_C = 1 + 0.045 \overline{C_{ab}'}^2$$

and

$$S_H = 1 + 0.015 \overline{C_{ab}'}^2 T$$

where

$$T = 1 - 0.17 \cos(\overline{h_{ab}'} - 30^\circ) + 0.24 \cos(2\overline{h_{ab}'}) + 0.32 \cos(3\overline{h_{ab}'} + 6^\circ) - 0.20 \cos(4\overline{h_{ab}'} - 63^\circ)$$

and

$$R_T = -\sin(2\Delta\theta)R_C$$

where

$$\Delta\theta = 30 \exp\left\{-\left[\left(\overline{h_{ab}'} - 275^\circ\right)/25\right]^2\right\}$$

$$\text{and } R_C = 2 \sqrt{\frac{\overline{C_{ab}'}^7}{\overline{C_{ab}'}^7 + 25^7}}$$

CIE94

$$\Delta E = \sqrt{\left(\frac{\Delta L^*}{k_L S_L}\right)^2 + \left(\frac{\Delta C^*}{k_C S_C}\right)^2 + \left(\frac{\Delta H^*}{k_H S_H}\right)^2} + \Delta R$$

where

$$\Delta R = R_T f(\Delta C^* \Delta H^*)$$

CIELAB

$$\Delta E = \sqrt{\Delta L^{*2} + \Delta a^{*2} + \Delta b^{*2}}$$

Colour specifications

Blue and magenta were taken from the test patches created for the project, with 100% M and 100 + 100% of M and C. Skin is the patch 2C8 and lime is the patch G6 on the TC9.18 chart. The diagrams for each colour are found in Figures 6a-d.

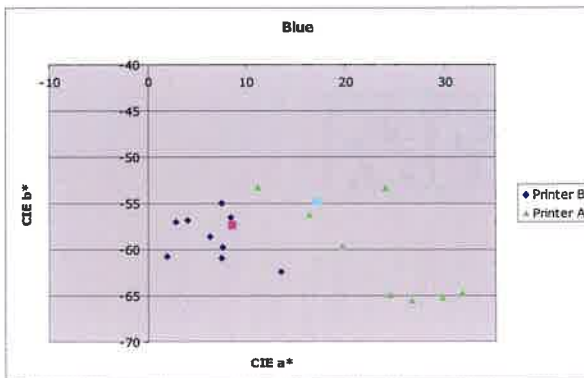


Figure 6a:

The Blue colour patches used. • and κ are the references for printer A and B respectively

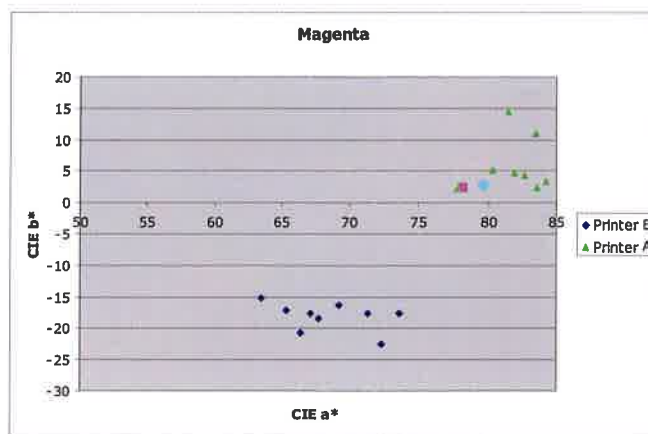


Figure VIb: The Magenta colour patches used. \bullet and κ are the references for printer A and B respectively

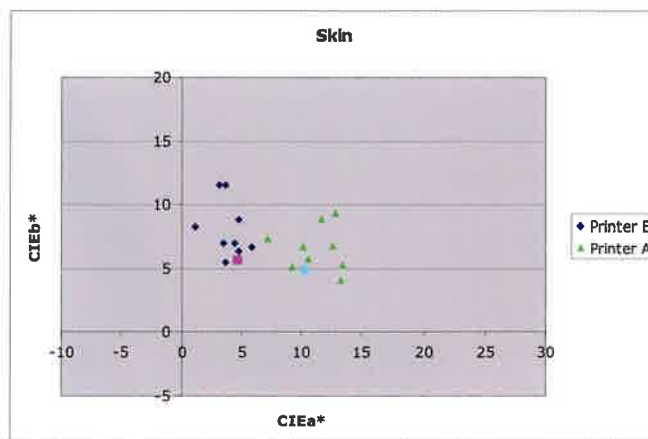


Figure VIc: The Skin colour patches used. \bullet and κ are the references for printer A and B respectively

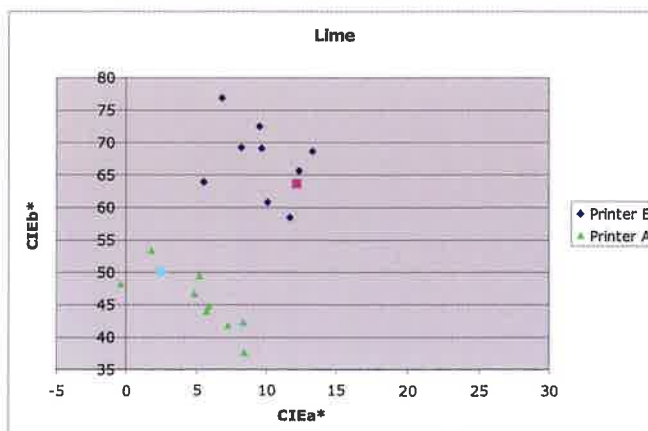


Figure VIid: The Lime colour patches used. \bullet and κ are the references for printer A and B respectively





2

Prepress and color



Testing colour accuracy of PDF files

Lidija Mandić¹, Darko Agić¹, Dean Žvorc²

¹ Faculty of Graphic Arts, University of Zagreb
Getaldićeva 2, HR-10000 Zagreb, Croatia
E-mail: mandic@grf.hr

² Punctum Studio
Gregorčičeva 8, HR-10000 Zagreb, Croatia
E-mail: dean@punctumstudio.hr

Abstract

Adobe Portable Document Format (PDF) is common used for digital exchange. The PDF overcomes several of the limitations of the PostScript language. A PDF file is designed to be viewed on screen as well as print, and this makes it possible to check the page content before imaging onto hard copy. The aim of this research is to check the reproduction of colors via output systems such as proofers. In experiment different inkjet and laser printers were used. Two target tests were printed on different digital output devices. The Altona Measure and Altona Visual Targets contain all necessary elements for checking compliance and colour accuracy and to identify product limitations. Tests are measured with the aim of spectrophotometric and visual judgement.

Key words

Color accuracy, Portable Document Format, Proof

1. Introduction

The Portable Document Format (PDF) was created for exchange of digital data across a wide variety of machine configurations, operating systems and communication networks. Despite the support of graphics industry vendors, PDF did not gain rapid acceptance as a format for the submission of digital files to printers and publishers. The PDF files did get exhibited many problems, like missing fonts and low-resolution images, making them worthless for high-quality print production (Marin, 2003).

The PDF is based on the same imaging model as PostScript, and it incorporates the majority of PostScript operators. The structure of a PDF file is like a database of the object, instead of a program that has to be executed in order to render a page description. A PDF file consists of a header, a body, a cross-reference table and a trailer. The body takes the place of the script in a PostScript file, and it contains a sequence of numbered objects that represents all the text, graphics and images in the document (Green, 1999). A PostScript file is converted to PDF with Acrobat Distiller. Job options are set in Distiller to control compression, font embedding, and high-end options such as Open Prepress Interface (OPI), overprint settings and color processing. Distiller offers a range of compression options according to the type of object and the quality requirements. These are highly efficient, and the process of conversion from PostScript to PDF usually reduces the file size dramatically. It can then be viewed with Acrobat Reader. PDF files are also intended for use as a means of distributing documents in electronic form, and they have a range of multimedia capabilities such as sound and video.

Acrobat Exchange, with its open architecture, allowed for the development of plug-ins to enhance PDF capabilities for the printing industry. These documents should be viewable on any display and should be

printable on any modern printer. With improvements, PDF files become widely used. PDF files are platform-independent, it can be viewed on any of the most common platforms in use including Mac and Windows. They eliminate the need for layout applications.

2. Experiment

The Altona Test Suite consists of a set of PDF files, specially designed for testing digital output devices - in particular, proofing solutions, conventional and digital printing systems. The purpose of the Altona Test Suite is to check PDF/X-3 compliance and color accuracy for all software and hardware modules used in a composite PDF workflow for print production. (www.eci.org). The Altona Test Suite comprises three PDF-files each designed for specific purposes. Two target tests were used, Altona Measure and Altona Visual. They were printed on free printers, laser printer-HP 8500 DN, and two ink-jet printers (HP designjet 10PS and Epson 9600 - both use Best RIP). They were printed on glossy paper. We printed tests also on mat and semi mat paper (Epson 9600).

“Altona_Measure.pdf” contains test elements for setting up and checking output systems such as proofers or conventional or digital printing systems. These charts were measured with spectrophotometer.

“Altona Visual” is a PDF/X-3 file focusing on visual testing of the PDF/X-3 applicability. As PDF/X-3 allows a color-managed workflow, this page comprises not only CMYK and spot color elements, but also several components containing device independent colors such as CIE L*a*b* and ICC based RGB. The Altona Test Suite addresses a set of six criteria well known for being critical in proofing and print production of PDF/X-3 files. For the evaluation of each criterion several elements are to be taken into consideration. For easy reference, numbers has marked all elements. The criteria for visual evaluation are process color, duotone and spot color, device independent color, overprinting, smooth shades and resolution. This test charts were printed from three different programmes, Acrobat, Photoshop and Quark. Thirty students were visually judged. An ordinal scale is used (M. Fairchild, 1997), numbered from one to six, for checking elements 19-25 and 39.

3. Results

Altona Measure test was measured with spectrophotometer Spectrolino (Gretag). The measured data are presented in Table I.

Table I: Measured colorimetric data of Altona measure.pdf test

		cyan	magenta	yellow	red	green	blue	black
HP 10PS (glossy)	L*	49,5	46,1	87,1	48	44,8	19,5	13,0
	a*	-37,9	70,5	-2,7	60,3	-65,6	14,9	-3,2
	b*	-46,8	2,1	98,5	48,2	30,0	-33,6	-3,0
HP 8500 (glossy)	L*	45,6	46,7	87,8	47,4	40,4	22,6	19,9
	a*	-23	74,4	-4,3	64,3	-54,8	24,9	0,5
	b*	-56	-16,1	97,5	24,6	24,3	-45,7	0,2
Epson 9600 (glossy)	L*	59,3	46,9	87,6	46,6	51,6	27,5	21,6
	a*	-37,4	72,9	-4,3	66,4	-68,9	21,4	1,8
	b*	-46,9	-6,0	95,8	48,8	34,6	-45,9	1,8
Epson 9600 (mat)	L*	59,5	47,7	86,1	51,3	56,4	36,5	30
	a*	-34,2	67,5	-2,8	57,8	-59,1	14,3	1,9
	b*	-46,5	-10,4	90	42,0	31,5	-48,4	-1,5
Epson 9600 (semi-mat)	L*	54,3	44,2	85,9	45,1	49,7	23,7	19,1
	a*	-36,4	70,4	-5,2	62,4	-62,3	17,6	0,4
	b*	-43,9	-5,1	89,2	43,9	29,2	-44,1	-1,4

After measurement, we were constructed device gamut which are shown in Figure 1.

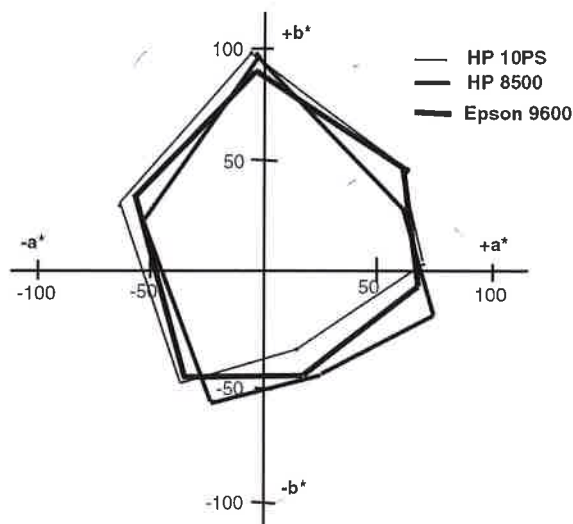
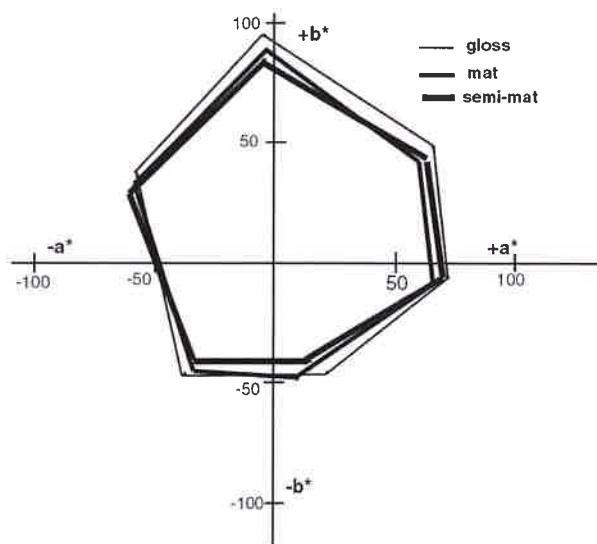


Figure 1: Printer's gamut

We checked whether gamut is changing a lot with using different type of paper and it is shown in Figure 2.



Figur 2: Changing gamut with paper

Duotone image (26, spot color-orange and process color black, was created in Adobe Photoshop. A small blue square in the upper right corner that indicates that the system is not able to correctly deal with spot colors appears on test printed on HP 10PS and HP 85000.

Marked elements 22 and 24 are used for testing PDF/X-3 functionality. A cross shaped section in the centre of the motif contains an RGB image. The image was assigned an embedded source ICC profile (ECI-RGB) and the perceptual rendering intent. The rest of the image is in CMYK mode. There are

noticeable color difference in the centered cross shaped section on test printed on Epson 9600 (all papers). This indicate that the respective system does not support color transforms as defined in PDF/X-3. In the case of cross shaped section in neutral image (22), all prints were acceptable. The purpose of the five patches (34-38) is to check weather or not rendereing intents and source profiles of a PDF/X-3 file are processed correctly. Each square consists of four triangular sections marked by small elements (rhomb, square, circle and triangle)Light gray strokes from underneath leading into the patches 36,37 and 38 indicate along which virtual line noticeable color differences shall be visible in correct output. The segments are coded in the color spaces CIELab and ECI-RGB in such a way as to match colorimetric identical colors. As all four segments have been assigned the relative colorimetric rendering intent (RI) no distinct color differences should be visible. A distinct color difference between ECI-RGB and CIELab after conversion to the CMYK destination color space indicates an error, as both color spaces should be treated identically. Color differences between elements - vector versus pixel - within the same color mode indicate an unwanted difference during color conversions of vector and pixel elements.

Purpose of ECI-RGB and CMYK (34) element is to check whether or not the color transformation of device independent colot into the CMYK color space of the output intent matches the result of the same conversion carried out in Adobe Photoshop.

Different device independent color spaces (35) is used for checking whether the color transformation of different device independant color spaces produce identical color results.

The patches 36 and 38 are used for checking whether the rendering intent (perceptual and relative) is correctly taken into account during color conversions into the destination color space.

The patch 36 is entended for the evaluation of the consistency of color transformations to the destination color space based on colors characterized by different ICC source profile.

Table II: Results for color management patches

	Patch 34	Patch 35	Patch36	Patch 37	Patch 38
HP 10PS-gloss	√	√	√	-	√
HP 8500-gloss	√	-	√	√	√
Epson-gloss	-	-	-	-	√
Epson-mat	-	-	-	-	√
Epson -semimat	-	-	-	-	√

Overprinting patch 28 consists of three circles colored with solids of the process colors: yellow, magenta and cyan. Printed test on Epson 9600 has correct overprint simulation. HP 10PS has partly wrong simulation of process colors and partly wrong simulation, and HP85000 has missing overprint simulation.

The quality of gradients and the support of PostScript3 smooth shadows are visually evaulated as good on all printed tests.

The gray background (19) consists of all four process colors (c25m19y19k20) were visually checked for color casts and wrongly adjusted overall gradation. All prints give satisfactory results. The contrast is good only on print that is printed on HP 10PS, other printers haven't get good contrast.

The portrait skin tones is reproduced correctly on HP 10PS, sufficient with Epson 9600. Laser printer HP 8500 is failed down in reproduction of skin tones. Neutral colors (22) are good reproduced with all printers.

Images from 23-25 contain high light tonal reproduction, saturated colors and the dark areas. The results are presented in figure 3.

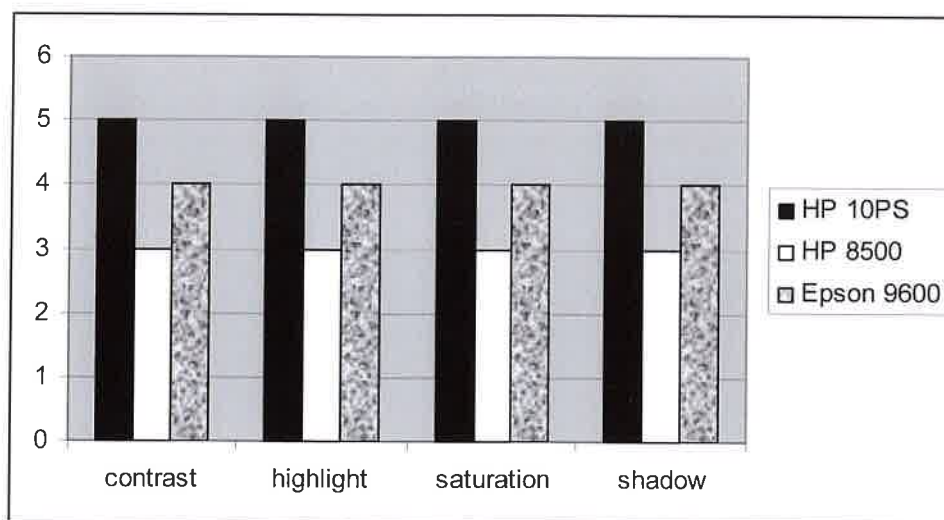


Figure 3: Subjective assesement derived by using ordinal scales

Visual tests were also printed through Photoshop and Quark, but they show unsufficient results in reproduction colors.

4. Discussion

The results showed that reproduction of neutral colors is satisfactory on every print. Also the visual difference between inkjet and laser printer is still big. RIP that printer used influences on the reproduction, with the use of better RIP more elements were correctly reproduced. Laser printer had wrong printing simulation, the system can not correctly deal with spot colors. Although laser printer had good contrast, the colors are not reproduced well, specially skin tone and highlight. For proofing better inkjet printers achieved better quality. There is not significant visual dependence of the type of paper used.

5. Conclusion

Testing two targets on different systems, indicates that processing PDF files is different on different printers, support with appropriate profile, and it is given different results. Although PDF files are independent on various platforms, they are rather dependent on output device. The need for improvement of the ripping for the target device is necessary, and it appears that inkjet output devices show better color matching according to the original.

5. References

- Green, P. (1999). *Understanding DigitalColor* Pira International, 1-85802-450-1, Pittsburg
- Marin, J. & Shaffer, J. (2003). *The PDF Print Production Guide* GATF Press, 0-88362-431-1, Sewickley
- www.eci.org



Online and automatic RGB to CMYK colour conversion

Jean-Pierre Gervasoni, Robert Catusse

EFPG

BP 65, 461 rue de la Papeterie

F-38402 Saint Martin d'Hères CEDEX, France

E-mail: Robert.Catusse@efpg.inpg.fr; jgervasoni@9online.fr

1. Introduction

Most colour prints are made up of CMYK (Cyan, Magenta, Yellow, and Black) ink layers. The printing process quality is often quantified with optical densitometers. RGB CCD cameras are also used on printing presses, mainly for visual inspection, seldom for quality measurement. Our motivation was to study whether a smart camera (gathering in the same box a CCD colour sensor, an image processing chip with some memory and an I/O block) could be programmed to control online printing quality on industrial presses: is it possible from an RGB picture to obtain data describing with enough information the CMYK ink layers? Moreover what are the requirements to allow a camera to measure colour with a good accuracy? Such a device could also advantageously replace spectrophotometer which can't be used for online measurements.

2. Methods

2.1 Experimental device

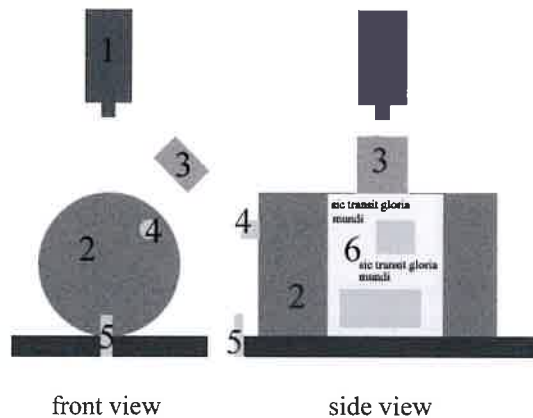


Figure 1

The main part of our device (fig. 1) is the smart camera model VC65c from Vision Components (VC, 2000). The camera layout is given in (fig. 3). The CCD detector ICX075AK (Sony, 2000) is made of an array of 782x582. To retrieve color information, this array is covered by a colour filter array (CFA), organized following a Bayer pattern (fig. 2). The CCD sensor (1) can send data to a VGA monitor or to DRAM (Dynamic Random Access Memory). What is stored into memory is not the RGB picture, but the 782x582 Bayer mosaic (Bayer, 1971). The camera is able to communicate with the surrounding industrial world through a block of logical I/O (4 inputs, 4 outputs), and through a serial port. As we can see in (fig. 1) a piece of metal (4) is glued on the rotating cylinder (2), a fixed inductive captor (5) triggering a camera input each time it passes near the piece of metal. This can be used to estimate the

speed. A logical output can trigger the flash (3) at any time. The camera is then able to take a picture of the print (6) and trigger the flash in synchronization with the movement.

green cell	red cell	green cell	red cell
blue cell	green cell	blue cell	green cell
green cell	red cell	green cell	red cell
blue cell	green cell	blue cell	green cell

Figure 2

Under the current measurement conditions (camera lens, size of the CCD sensor ...) a pixel corresponds to $27\mu\text{m}$. The area covered by the camera is $2.1 \times 1.5 \text{ cm}$. We used the language C to program our camera. The C code is then compiled with the ADSP 2181 tool chain from Analog Devices (AD, 2004). The resulting binary code is sent to the camera through the serial port and stored in EEPROM memory, ready to use.

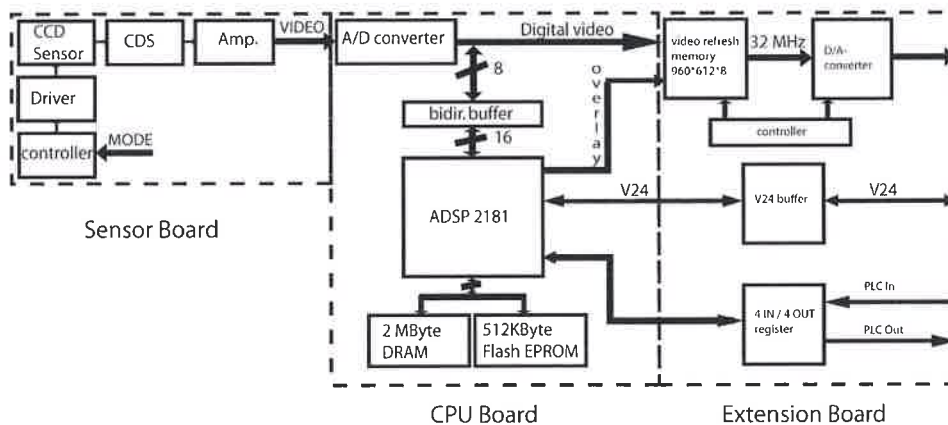


Figure 3

2.2 RGB image acquisition

The taking of pictures is software driven, and is synchronised with both flash triggering and cylinder rotation. The picture is then stored in the camera DRAM under its Bayer mosaic representation. In (fig. 4) we have represented the histogram of a picture corresponding to a matt white paper. This histogram is established from the original Bayer mosaic stored in memory.

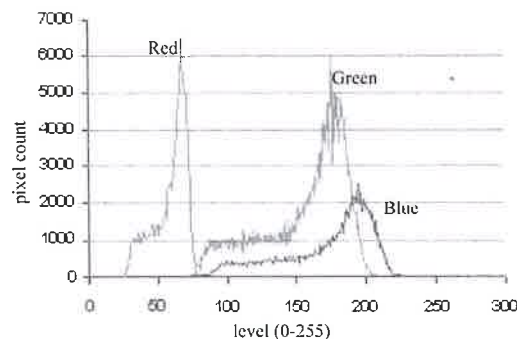


Figure 4

As the print to be analysed is continuously moving (due to cylinder rotation) we used a flash in order to freeze the movement. However this has one drawback: the picture tends to be bluish (fig. 4). Moreover the actual lighting geometry and the curvature of the cylinder imply that the lighting intensity is not uniform upon the print. We have implemented an algorithm (Gervasoni, 2003) in order to correct the picture. It works on data stored into camera memory (RGB measured values).

2.3 RGB image correction

Let's call the mosaic corresponding to an ink free area stored into memory **Mref**. Then for each new picture acquisition (different print on the same paper), we divide pixel per pixel the current mosaic **Mcur** and the reference mosaic **Mref**. This division corrects the lighting non uniformity, but does nothing about white balance, for which we require another step applying three different weights (one for each R, G and B channel), established from previous work. Let **Wr**, **Wg** and **Wb** be the weights respectively for the Red, Green and Blue colour channel. **Mcur**, and **Mref** can be considered like two rectangular arrays (**width** = 782, **height** = 582). Our algorithm can be described by the following pseudo-code:

```

1- For w=0 to w=width
2-   For h=0 to h=height
3-     If Mcur(w,h) is a Red pixel
4-       let P=Wr
5-     endif
6-     If Mcur(w,h) is a Green pixel
7-       let P=Wg
8-     endif
9-     If Mcur(w,h) is a Blue pixel
10-      let P=Wb
11-    endif
12-
13-      Mcur(w,h)
14-    Mcur ← P -----
15-      Mref(w,h)
16-   endfor h
17- endfor w

```

The pattern of the mosaic is known (fig. 2) which is why we can retrieve the corresponding channel for each pixel stored into memory. As we can see from the previous pseudo-code, this algorithm is easy to implement. It gives fast and very satisfying results. The resulting mosaic is then transferred to a PC through the camera serial port for further exploitation.

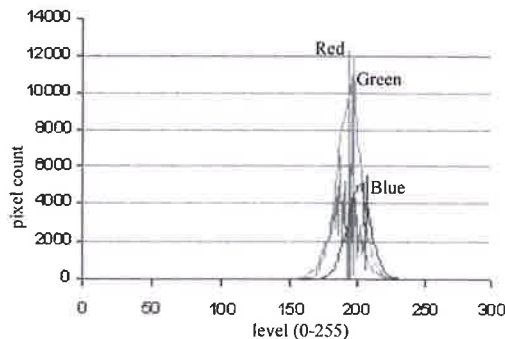


Figure 5

We took a picture of an ink free area, *not the same as the reference*, and applied the previously described algorithm. The histogram of the resulting picture (fig. 5) must be compared to the one of the reference (fig. 4). In (fig. 4) peaks are very large, and the optimum is not located at the same level for each colour channel (roughly Red: 60, Green: 175 and Blue: 200), whereas in (fig. 5) peaks are narrower and the optimum is the same for each channel and located at level 200. Re-establishing a correct white balance implies that peaks optimum are located at the same level. If we had chosen a value higher than 200, we would have obtained values through calculus greater than 255, which are truncated to 255 (we work on 8 bits, 0-255).

2.4 Demosaicking (Gervasoni, 2003) (Longère, 2000) (Cok ,1984,1986,1987)

As we have previously seen, the camera transfers to a computer a mosaic representation of the current picture. Demosaicking is the operations chain needed to interpolate all the missing values. We have explored many algorithms, trying to find a good compromise between result quality and time consumption. Adaptive algorithms analyze the mosaic and try to detect edges (vertical, horizontal, or any orientation), while non adaptive ones apply the same computations to each pixel and give faster results but more noisy pictures. We present some of the reviewed algorithms.

	w=0	w=1	w=2	w=3
h=0	R(0,0)	R(1,0)	R(2,0)	R(3,0)
h=1	R(0,1)	R(1,1)	R(2,1)	R(3,1)
h=2	R(0,2)	R(1,2)	R(2,2)	R(3,2)
h=3	R(0,3)	R(1,3)	R(2,3)	R(3,3)
....

Figure 6

(fig. 6) represents a rectangular array corresponding to the red channel of a picture. Some values are known from mosaic: R(1, 0), R(3, 0), R(1, 2), But some values are “missing” and need to be computed: R(0, 0), R(2, 0),

2.4.1 Non adaptive algorithms

- nearest neighbour interpolation

This is the simplest way of retrieving missing values, which are taken equal to the nearest neighbour value. Example:

$$R(0,0)=R(1,0)$$

$$R(0,1)=R(1,0)$$

$$R(1,1)=R(1,0)$$

Even if the computation time is near 0, this method leads to so many colour artefacts that it's never used.

- bilinear interpolation

In this case, we compute mean values. Example:

$$R(1,1)=(1/2)*[R(1,0)+R(1,2)]$$

$$R(2,1)=(1/4)*[R(1,0)+R(3,0)+R(3,2)+R(1,2)]$$

When looking at such interpolated images, we notice less colour artefacts (compared to the previous method), but they are still visible on edges.

- median filtering (Freeman, 1987)

In a first step Red, Green and Blue channels are computed using a bilinear interpolation. Then we compute the following colour plans:

Cr=red channel - green channel
Cb=blue channel - green channel

A median filter is then applied to **Cr** and **Cb**, in order to smooth colour artefacts. The red and blue channels are easily deduced:

Final red channel =filtered **Cr** + green channel

Final blue channel =filtered **Cb** + green channel

The green channel is not filtered. There remain artefacts, but they are less visible.

2.4.2 Adaptive algorithms

- horizontal and vertical edges detection using two gradients (Hibbard, 1995)

Colour artefacts are especially noticeable on next to edges inside a picture. That's why it could be relevant to detect horizontal and vertical edges. Let's define horizontal and vertical gradients **dH** and **dV**:

$$\mathbf{dH}(2,1)=\text{abs}[V(1,1)-V(3,1)]$$

$$\mathbf{dV}(2,1)=\text{abs}[V(2,0)-V(2,2)]$$

Using a threshold **T**:

$$\text{If } (\mathbf{dH} < \mathbf{T}) \text{ and } (\mathbf{dV} > \mathbf{T}) \quad V(2,1) = (1/2) * [V(2,0) + V(2,2)]$$

$$\text{If } (\mathbf{dH} > \mathbf{T}) \text{ and } (\mathbf{dV} < \mathbf{T}) \quad V(2,1) = (1/2) * [V(1,1) + V(3,1)]$$

$$\text{If } (\mathbf{dH} < \mathbf{T}) \text{ and } (\mathbf{dV} < \mathbf{T}) \quad V(2,1) = (1/4) * [V(1,1) + V(3,1) + V(2,0) + V(2,2)]$$

The choice of **T** depends on the images, but could be taken equal to $(1/2) * (\mathbf{dH} + \mathbf{dV})$.

- any orientation edges detection using a variable number of gradients (Chang, 1999)

NW	N	NE
W	X	E
SW	S	SE

Figure 7

Height gradients (fig. 7) are defined on a 5x5 neighbourhood. A rather complex procedure is then used to retrieve missing pixels.

2.4.3 Results



Figure 8

In order to benchmark (fig. 9) the previously reviewed algorithms (alongside others), we used RGB pictures (cf. fig. 8 for a grey level representation). The two pictures in the middle are subsets of the left one. The last picture on the right is a simple black disk on a white background. All these images were converted to Bayer mosaic, and then reconstructed using different algorithms. We defined two criteria, the first being the *mean time per pixel*, given in microseconds, defined as the total computation time divided by the number of pixel in the mosaic (all the computations were done on the same platform). The other criterion is the *mean square error* between the *Lab* representation of original and the reconstructed image.

		Time (us)	MSE			
			Disk	Bucket	Lys	Flowers
non adaptative	nearest neighbour	4	8,8	18,3	11,2	12,6
	bilinear	6	10,6	11,5	18,6	7,6
	median filtering	15	4,0	9,1	16,9	6,6
adaptive	horizontal and vertical edges	50	5,9	7,2	16,9	7,0
	any orientation edges	1757	8,4	8,1	18,9	13,4

Figure 9

The best compromise between computation delay and result quality is the median filtering algorithm, and that will be our default demosaicking method.

2.5 CMYK colour conversion (Gervasoni, 2003)

Converting a RGB picture to CMYK is a rather complex task. In our approach, we use a colour lookup table (*CLUT*) for two important reasons, the first being that *CLUT* based methods don't require lots of computation power compared by example to the Neugebauer approach (Neugebauer, 1937), the other reason being that under the current measurement conditions the pixel size (27 μ m) is much smaller than the printing resolution range commonly used in offset printing, a pixel corresponds to a small set of colours, defined by all the possible ink overlapping (15 combinations when using CMYK inks). In practice, overlapping of 3 and 4 inks can't be efficiently measured due to a lack of sensibility of our camera.

	L	a	b
C	52.5	-15.0	-33.3
M	62.7	60.6	7.6
Y	76.0	- 0.8	56.3
K	10.3	- 9.5	- 4.3
C+M	21.8	19.9	-35.3
C+Y	36.6	-37.5	10.4
C+N	4.8	- 3.7	- 9.0
M+Y	59.3	61.2	48.3
M+N	1.0	1.4	0.5
Y+N	15.0	-15.9	22.0
No ink	91.2	0.5	- 1.8

Figure 10

To establish a *CLUT*, we have measured with our camera mean RGB values corresponding to all combinations of two or less inks, and then converted them into Lab coordinates (fig. 10). For a picture of any print realized with the same inks and paper, we convert RGB data to Lab, and then we compute the distance between a pixel lab coordinate to each reference values (given by fig. 10). When the distance is

minimized we have found the ink combination corresponding to the currently processed pixel. In (fig. 11), one can find an example of RGB to CMYK conversion. The original picture represents four crosses (the upper left is printed in cyan, the upper right in magenta, the lower left in black and the lower right in yellow). The crosses are correctly detected, even if there remain some artefacts on their edges. The method gives good results when the zooming factor is high enough to distinguish printed dots on the picture. However, this factor should not be too high otherwise we'll lose information about the print. In order to smooth the four CMYK pictures, we've chosen to apply a 5x5 gaussian filter.

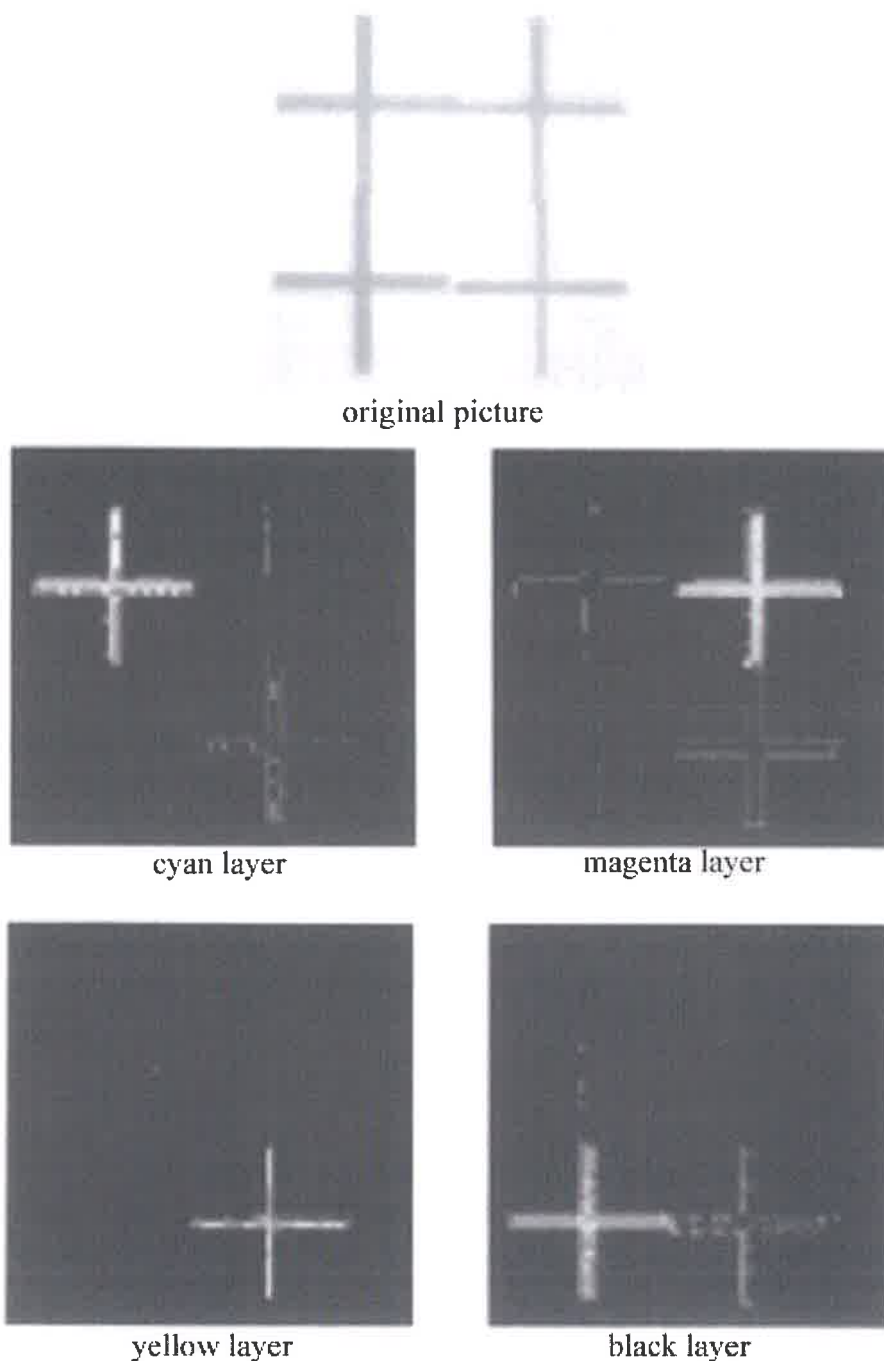


Figure 11

3. Results: dot area percentage measurement on single colour halftones

After the RGB to CMYK colour conversion, but before applying the gaussian filter, each value stored into the Cyan, Magenta, Yellow or Black arrays is either 0 or 1. It's very straightforward to compute the ratio (*number of ink pixels*) / (*total number of pixels*) for each array. We have compared these values to those given by the Murray-Davies formula (using an optical densitometer). The curves on figures (fig. 12) and (fig. 13) are obtained by putting on the x-axis the Murray-Davies values and on the y-axis the values computed with our method, for a set of cyan halftone prints (fig. 12) and black (fig. 13).

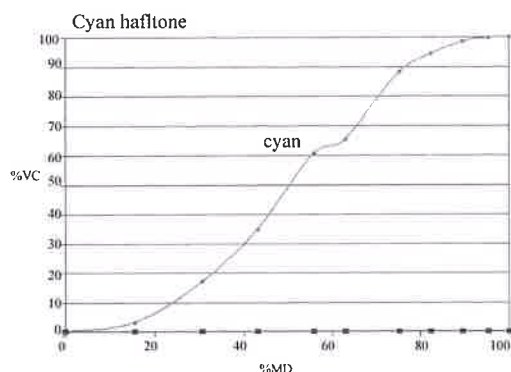


Figure 12

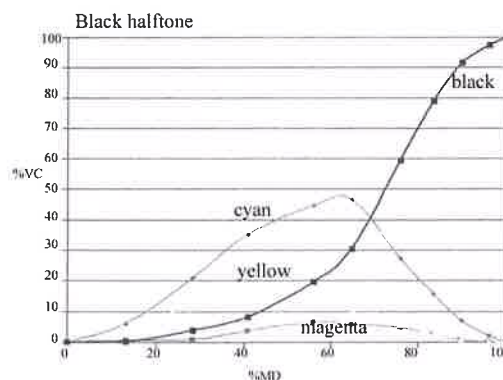


Figure 13

In the case of cyan prints (fig. 12) only cyan ink is detected, and the shape of the curve is very classical. For black prints (fig. 13) cyan, magenta and yellow inks are detected whereas there are only black inks on the prints. We do believe that this is mostly due to the demosaicking step which introduces colour artefacts, concentrated on edges inside the picture.

4. Conclusions

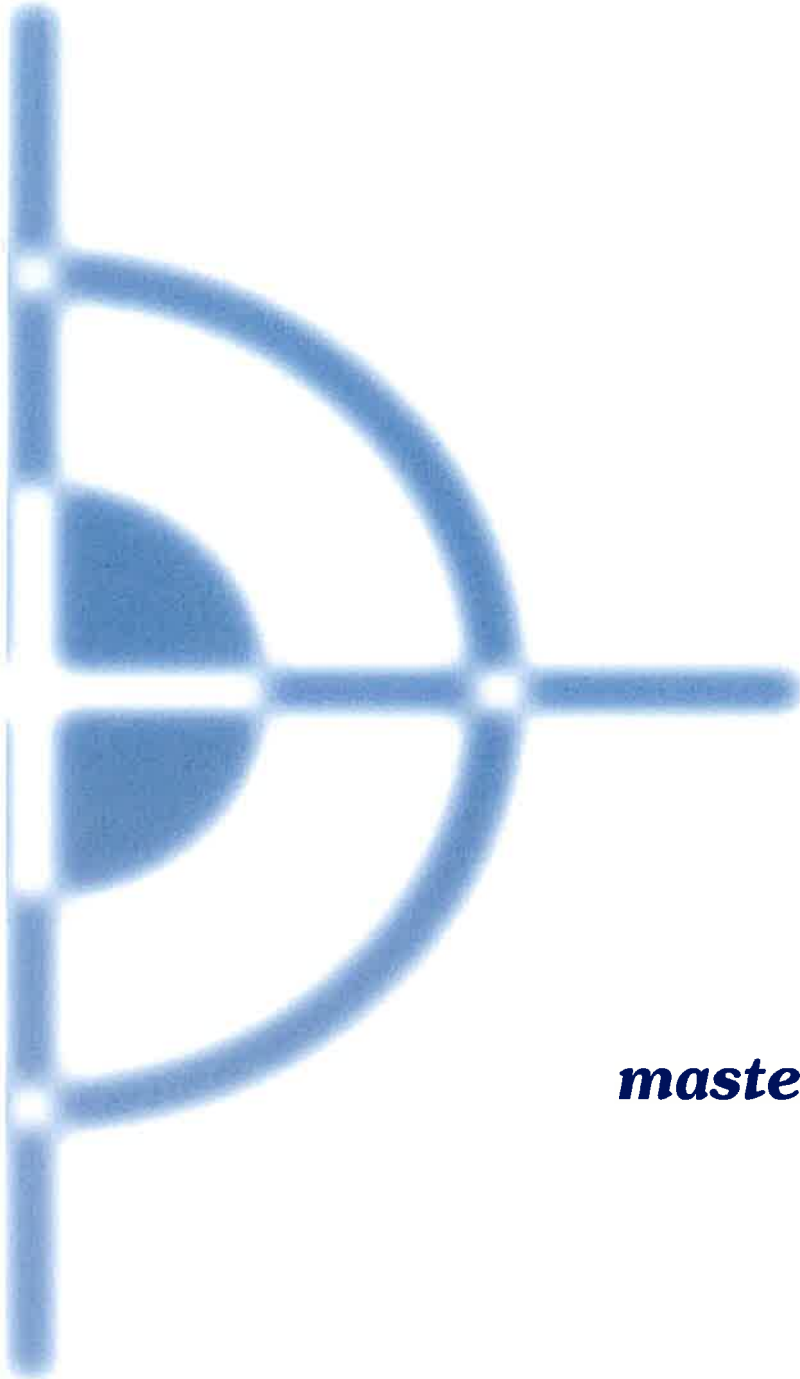
In this work we used a smart camera as a replacement of classical the image processing tool chain: camera + frame grabber + computer. We have developed a fast algorithm giving good corrected RGB pictures. The demosaicking step was done using the *Freeman* (Freeman, 1987), which was found to be a good compromise between computation time and image quality. The RGB to CMYK conversion was achieved through using a *CLUT* (colour lookup table). When applying our method to the dot area percentage measurement, we found it gave good results for cyan halftones, and unreliable ones for black halftones, this lack of reliability being due to the demosaicking step which introduce colour artefacts. We now have a clear idea of the requirements that must be fulfilled for a smart camera to be used as a print quality monitor in an industrial environment.

Literature references

- (AD, 2004), Link to Analog Devices web site <http://www.analog.com/index.html>
- (Bayer, 1971), Bayer 1971, *Colour imaging array*, U.S. Patent 3,971,065
- (Chang, 1999), Chang and Cheung, 1999, *Color filter array recovery using a threshold based variable number of gradients*, International symposium on electronic imaging: science and technology, 3650
- (Cok, 1984), Cok 1984, *Single chip electronic color camera with color dependent birefringent optical spatial frequency filter and red and blue signal interpolating circuit*, US Patent 4,605,956
- (Cok, 1986), Cok 1986, *Signal processing method and apparatus for sampled image signals*, US Patent 4,630,307

- (Cok, 1987), Cok 1987, *Signal processing method and apparatus for producing interpolated chrominance values in a sampled color image signal*, US Patent 4,642,678
- (Freeman, 1987), Freeman, 1987, *Method and apparatus for reconstructing missing color samples*, US Patent 4,663,665
- (Gervasoni, 2003), Gervasoni Jean-Pierre 2003, *Système de repérage sans cible pour rotatives d'imprimerie*, Phd. Thesis, EFGP
- (Hibbard, 1995), Hibbard, 1995, *Apparatus and method for adaptively interpolating a full color image utilizing luminance gradients*, US Patent 5,382,976
- (Longère, 2000), Longère, Zhang, Delahunt and Brainard, 2000, *Perceptual assessment of demosaicing algorithm performance*, IEEE
- (Neugebauer, 1937), H.E.J. Neugebauer 1937, *Die theoretischen grundlagen des mehrfarbendruckes* (The theoretical foundation for multicolor printing), Z. Wiss Photogr., pages 73-89
- (Sony, 2000), Link to ICX075AK technical references, <http://www.sony.co.jp/~semicon/english/img/sonyde01/a6802541.pdf>
- (VC, 2000), Vision Components web site: <http://www.vision-components.de/>





3

***Conventional,
master based printing***

Emulsifying of dampening solution in offset ink in short inking units

W. Beier¹, A. Hübler¹, G. Marx², C. Klinger¹, N. Meyer² et al.

¹ Institute for Print and Media Technology, Technical University of Chemnitz
Reichenhauser straÙe 70, D-09126 Chemnitz, Germany

² Institute for Chemistry, Technical University of Chemnitz, Germany

Abstract

There is a tendency in short inking units of offset printing machines that resplitted dampening accumulates so highly in the printing ink that the offset process destabilises. As has been proven especially with multi-colour ink, this so-called over-emulsification of ink leads to a sudden increase in density on the printed matter. The process tips over. Prior to the tip-over, a gradual density decrease occurs with progressive emulsification.

This phenomenon has been reproduced in an experimental printing unit at the University of Technology Chemnitz, Germany. Thereby the incident, well known to the practitioner, has been confirmed that the process tips over as soon as the surface water appears on the anilox roller.

The tests showed a correlation between the sudden appearance of water drops on top of the cell walls of the anilox roller with the rapid increase of the optical density of single solid areas.

Using ultra-fast photography, microphotos have been taken of the surface of the anilox roller during the ongoing printing process, clearly displaying the surface of the roller. Water drops can be precisely identified and localised on the surface. Furthermore, the emulsified and free amounts of water contained in the ink have been verified discretely using DSC (Differential Scanning Calorimetry).

The cause for the formation of surface water on top of the cell walls of the anilox roller is the transgression of the dew point leading to the formation of condensed water from the wet air in the inking unit.

The density increase on the printing matter can be explained that the surface water on the anilox roller causes the displacement of the emulsion gradient in the roller gap between anilox and application roller and thus relocates the ink splitting level towards the anilox roller. Consequently more ink is picked up and delivered to the printing forme.

As soon as the surface water has been removed from the anilox roller, the density increase subsided to its initial value -even without changes of the dampening concentration of the ink in the fountain.

The abrupt density increase could effectively be counteracted by influencing the microclimate in the inking units in a way that kept the relative humidity well below the dew point. The evaporated amount of water is exemplarily calculated.

1. Introduction

The inking unit's function in an offset printing press is to provide a constant supply of ink on the printing plate during the production run, so that the image areas on the plate constantly receive an ink film of the same thickness. It is vitally important that there is only a close tolerance of the ink film thickness. With the aim of solving this problem, the short inking unit technology has been introduced in addition to the already well-established vibrator-type and continuous-feed inking systems.

To create a constant ink film of exactly the same thickness along the whole machine width, short inking units employ an anilox roller. The anilox roller has a smooth surface into which pits, e.g. cells,

are engraved. The circumferential speed of the anilox roller is equivalent to the printing speed. When the anilox roller dips into the inking fountain of the chambered doctor blade system, the cells are completely filled with ink. An ink blade, which is adjusted to the inking fountain, rests with its leading edge on top of the cell walls of the anilox roller, so that it removes the ink from the cell walls. The ink, thus, remains only in the cells. This exactly dosed and uniform ink film of the width of the machine is then split by the flexible ink form roller, which has the same size as the plate cylinder, and transferred to the printing plate (fig. 1).

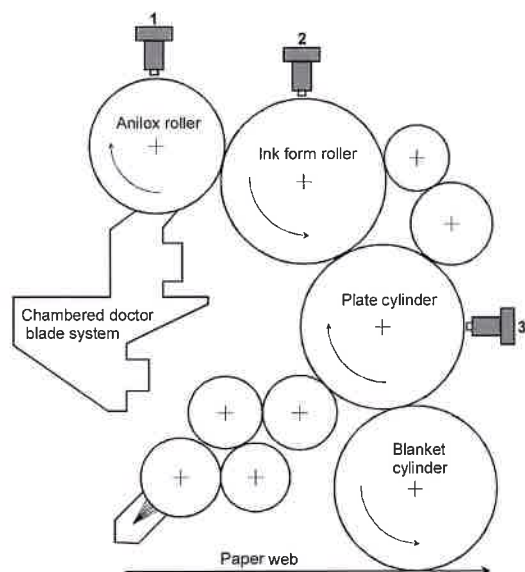


*Figure 1:
Plan of a short inking unit (1, 2, 3:
camera position with microscope header
for takings of the surface while printing
press is operating)*

The great advantage of these inking units is their simple design. Due to the cell metering system, the correct ink film thickness is already achieved at print start. Therefore, the inking unit has an extremely short start-up phase. Moreover, these inking units are characterised by a very stable inking process virtually from the print start. Stable production printing conditions are achieved only after a few revolutions.

Recently, short inking units are increasingly employed in waterless offset. This general tendency continued at DRUPA 2004. Besides the advantage that the printing presses require less space (due to the missing dampening units), the reason for this trend is the elimination of the short inking units' tendency that the wet offset process can become instable during the production printing (e.g. after several ten thousand prints). This sporadic phenomenon is differently strong pronounced depending on the kind of ink. The printer refers to this as "over-emulsifying" of the printing ink. This happens when the printing ink absorbs too much dampening solution. A "breakdown" of the offset printing process is the result. The optical density on the printing product increases abruptly by leaps and bounds (after a slight decrease immediately before). The consequences are piling and the build-up of printing ink in the printing unit. The ink flow breaks down, as the printing ink loses its splitting ability. A stable offset process cannot be restored, until the "over-emulsified" printing ink has been replaced with fresh ink.

Scientific publications deal with the interdependency of printing ink and dampening solution, as well as the measurement of the dampening solution content in the printing ink and the resulting influences for the printing process. Moreover, they address topics such as the influence of the percent area coverage of the printing forme on the dampening solution content in the printing ink, as well as characteristic effects of short inking units on the printing quality (cf. Lin 1991, Lin 1990, Stu 1995, Loi 1991, Ros 1986, Pyl 1981, Ros 1989, Ros 1990).

There are, however, hardly any information about topics like "overemulsifying" of the printing ink and the abrupt increase of the optical density.

The mechanism leading up to this “breakdown”-phenomenon is closely analysed in the following paper.

2. Printing Experiments with a Laboratory Printing Press

In order to define the causes leading to the abrupt increase of the optical density, standard printing press conditions have been reproduced on the laboratory printing press “LaborMAN”, which is set up in the research centre of the Institute for Print and Media Technology at Chemnitz University of Technology. One of the four printing units of this laboratory printing press is equipped with a short inking unit (fig. 2).

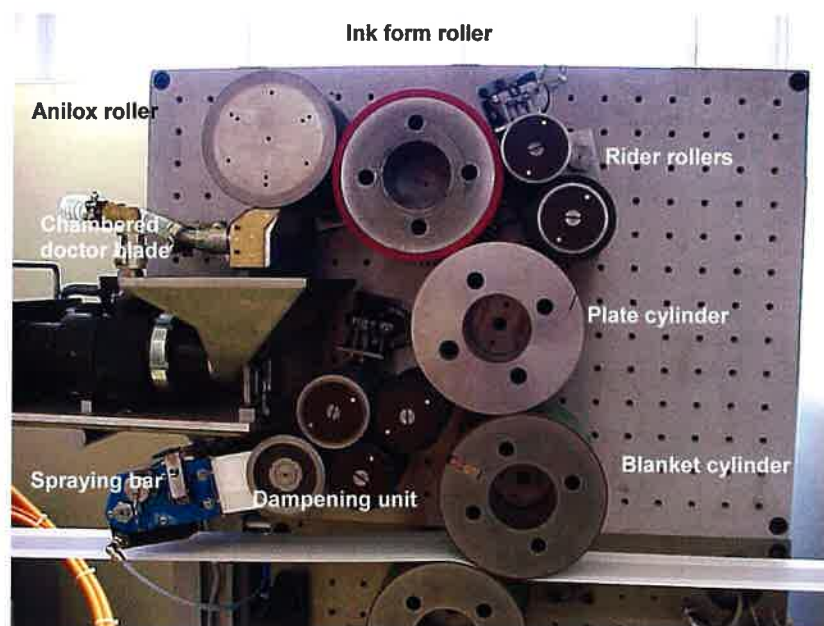


Figure 2: Short inking unit of the laboratory printing press LaborMAN

Standard magenta cold-set ink with the corresponding dampening solution has been used according to manufacturer’s instructions in the experiments.

The test printing forme consisted of a solid area, corresponding in length to the print format, common test elements and zones with solid single elements. Figure 3 shows the test printing forme, which has been used for the following experiments.

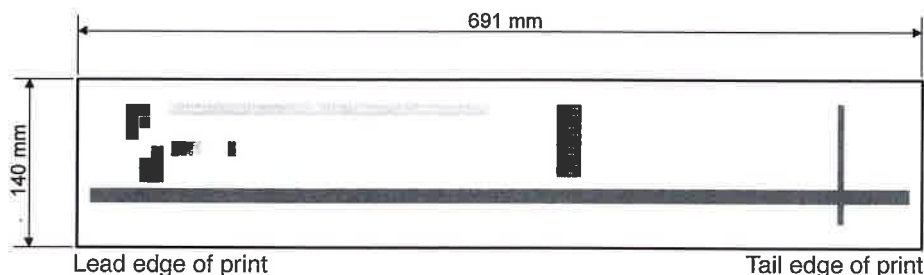


Figure 3: Test printing forme

The open-type design of the printing and inking unit of the laboratory printing press, which is equipped with cantilever cylinders and rollers, allows a constant and intensive air exchange with the ambient air in the inking, dampening and printing unit. The microclimate in these areas differed only insignificantly from the pressroom climate. In an extensive series of testing, we could not verify a breakdown of the

offset process. That means that there was no abrupt increase of the optical density on the print product. Even with the use of already emulsified ink, which contained more than 25% dampening solution, it was not possible to provoke an optical density jump. During production printing, the printing ink constantly contained a dampening solution level of 18% to 22%.

The climatic conditions inside a rotary offset press, e.g. a newspaper rotary press, are notably different from those in the laboratory printing press. The printing unit with inking and dampening unit is arranged between the two machine frame walls, which make an air exchange on either side virtually impossible. Moreover, the inking and dampening unit rollers, which have a width of more than 1000 mm, as well as the printing unit cylinders and the paper web seriously constrain the air exchange in machine direction, upwards and downwards. Therefore, air exchange with the pressroom air is severely limited. According to experience, the relative humidity rises up to $\varphi_{\text{rel}} = 90\%$ and more during production printing in this almost hermetically sealed inking unit area. In order to create comparable conditions in the laboratory printing unit, the whole unit has been enclosed with Plexiglas windows (fig. 4).

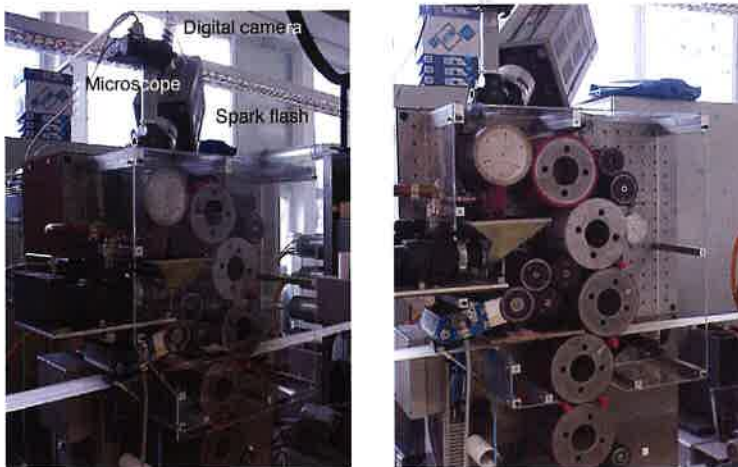


Figure 4:
Printing unit, enclosed with
Plexiglas windows (on the left
photo with front panel, on the
right photo without front panel)

The relative humidity within this enclosure rose locally up to values of $\varphi_{\text{rel}} = 90\%$ to $\varphi_{\text{rel}} = 95\%$. Under these conditions, a breakdown of the offset process could be observed after more than 45,000 copies, which had been stably printed with good quality. This resulted in an abrupt increase of the optical density. This phenomenon was especially visible in areas with few picture elements. This optical density jump is diagrammed in fig. 5. The printing ink contained approximately 25% dampening solution.

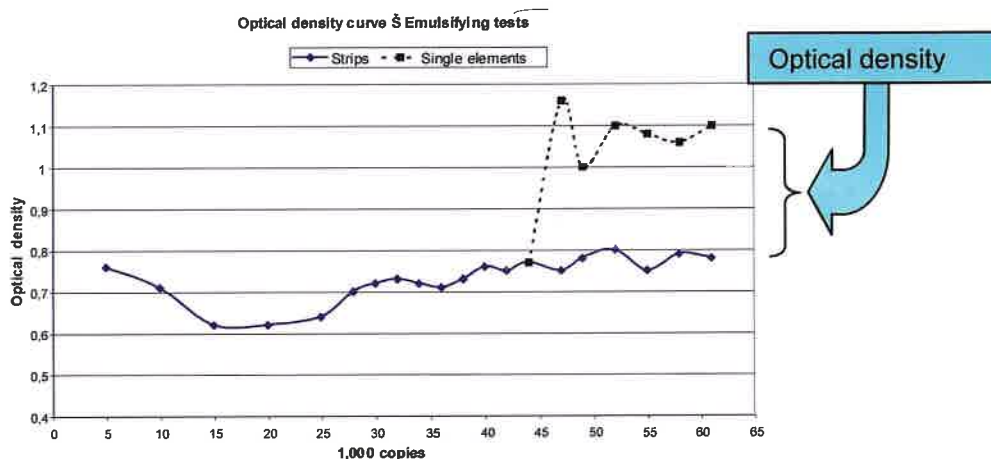


Figure 5: Measured values of the optical density during production printing. After 47,000 copies had been produced, the optical density of the solid single elements increased abruptly. Printing ink: Magenta, cold-set

3. Measuring Equipment

The optical density of the solid areas on the printing product has been measured with the help of a type "Gretag D 19 C" **densitometer**.

Ink samples have been taken from the inking fountain as well as the surface of the ink form roller at different stages of the printing process. These samples have then been tested for water concentration. Additionally, we analysed the dispersion type of the water in the printing ink. For this purpose, **DSC analyses** (Differential Scanning Colorimetry) (cf. Doe 2002, Ros 1986) have been conducted. Characteristic examples for curves of the DSC analyses results are presented in figure 6.

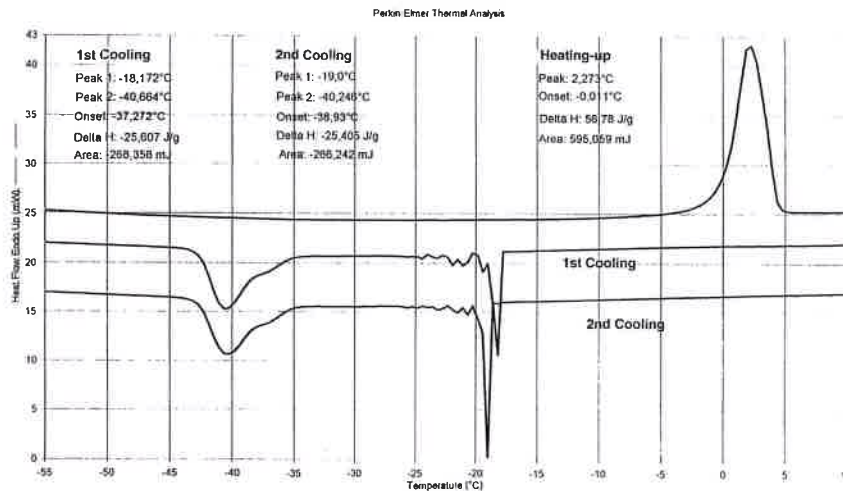


Figure 6:
DSC analysis of an ink sample, which has been taken from the operating printing press

The water lying on the surface of the printing ink cannot be measured with the DSC analysis. However, the curve progression, which represents the heat flow, absorbed or emitted by the sample, versus temperature, provides information about the quality and quantity of the water. This water is contained in the printing ink in form of emulsified droplets according to the water-in-oil emulsion model. The cooling curve shows a first major peak around $t = -18^\circ\text{C}$. There is a second peak at $t = -40^\circ\text{C}$. This characteristic curve progression results from the fact that the water is contained in the printing ink in two distinctive forms:

- as free water, i.e. in the form of coarsely dispersed droplets (equals the peak at $t = -18^\circ\text{C}$)
- as bound water, i.e. in form of a fine dispersed emulsion (equals the peak at $t = -40^\circ\text{C}$)

In case of shear load or splitting of such an ink film, the coarsely dispersed part of the water tends to discharge from the ink first. It accumulates in the form of droplets on the surface of the ink film (cf. Ros 1986). This means that ink with a high coarsely dispersed water content accumulates a larger amount of water on the surface under these conditions than ink with a low level of coarsely dispersed water. Water on the surface evaporates provided that the water vapour partial pressure of the surrounding air is lower than the saturation pressure. The bigger the difference, the higher the evaporating mass flow.

In order to prove the existence of water on the surface of rollers, which rotate at print speed, **short-time microphotography** has been employed (cf. Ros 1986). For this purpose, a digital colour camera has been equipped with a 55x magnifying microscope header and pointed at the roller surface. In a darkened room the roller surface has been exposed for a microsecond with a fast short-time flash while the camera shutter was open. With the help of this extremely short exposure time, enough sharp and detailed photos could be taken of the moving roller surface. The fuzziness of the photos due to motion was in the region of few μm at a rotation speed of 1 to 5 m/s. The photos are suitable for a local qualitative and semi-quantitative analysis of the surface conditions. Water droplets, cell walls, colour surface details and edge transitions were clearly visible and could be evaluated. The experiment set-up is presented in fig. 7.

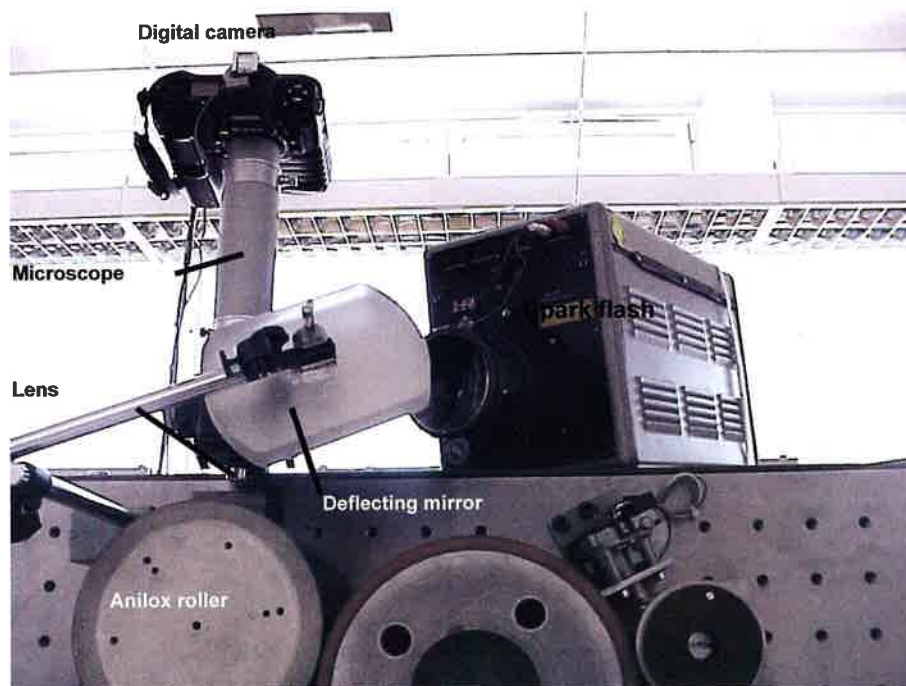


Figure 7: Experiment set-up for taking microphotos of the surface of anilox rollers when laboratory printing press is operating

Fig. 8 shows a photo that was taken with this experiment set-up. Dampening solution, which lies on the surface of the ink in the form of droplets, is visible as white spots on the photo.



Figure 8: Microphoto of the anilox roller surface (55x magnified). The cell walls appear dark, while the cells appear brighter. Water on the surface is visible as white areas. (This photo shows a section of the anilox roller on the border between solid area and non-printing area of the printing forme. The solid area is located in the left part of the photo.)

The relative humidity in the printing and inking unit, as well as in the laboratory has been measured with the help of a **hair hygrometer**. The accuracy of measurement, reached with this method, was sufficient for the ventilation calculations. The required space for the relatively big hygrometer was considered in the constructive design of the printing and inking unit enclosure.

A **pyrometer** was used for the contactless measurement of the surface temperature of the rollers. The air temperature as well as the temperature of the printing ink, which was constantly repumped between ink tank and inking fountain, were measured with laboratory **mercury thermometers**.

4. Test Evaluation

The printing tests have been conducted at the printing press LaborMAN (cf. fig. 2). For one part of the tests the printing press's open-type design has been retained unchanged. For the other tests the printing unit was enclosed with Plexiglas windows. The evaluation mainly focussed on the difference between the operating conditions in the stable printing process and the operating conditions at the stage of the density jump and after the density jump. The printing process parameters did not show any noticeable problems. Serious alterations could, however, be observed on the anilox roller.

a) operating conditions of the stable offset process: The photos of the anilox roller show little or no surface water. There is no dampening solution on top of the cell walls of the anilox roller.

b) operating conditions at the stage of increased optical density values according to fig. 5: The photo of the anilox roller shows water drops on top of the cell walls (cf. fig. 11).

In both cases, the camera was exactly pointed on the trace with the solid single element, whose optical density changed according to fig. 5. The test was repeated several times. The conditions proved true again and again. The occurrence of water drops on top of the cell walls correlates with the abrupt optical density increase of the solid area on the printing product.

This behaviour raises two questions:

1. Is there a functional connection between water on top of the cell walls and the optical density increase? If yes, what is this connection?
2. What causes the water on top of the cell walls? In fact, the ink has been properly wiped off from the surface of the cell walls by the doctor blade. Remaining binding agents and solvents provide for a hydrophobic behaviour of the cell walls. It seems very unlikely that surface water floats out of the cells, which are filled with printing ink.

4.1 Water on Top of the Cell Walls and Optical Density Increase

A plausible reason for the sudden alteration of the ink flow quantity in the case of water on top of the cell walls are the conditions in the roller nip between anilox roller and inking roller. Water on top of the cell walls, from which the ink has already been wiped off, functions like a separating layer when getting into contact with the returning ink layer of the inking roller. In the present case less ink of the returning ink layer is splitted in comparison to cell walls with no water on top. The part of the returning ink layer that is not splitted remains on the inking roller. More ink is transported resulting in a higher optical density on the printing product.

A low heating of the anilox roller surface, which results from the condensation heating of the water vapour, may intensify the effect. I will come back to this point later.

4.2 Origin of the Water Drops on Top of the Cell Walls

The water on top of the cell walls may be caused by the humid air, which prevails in the inking unit. The air humidity in the upper part of the inking unit increased considerably as the number of printed copies grew. The highest values have been measured close to the anilox roller. The photo of the printing unit in fig. 9 shows that water has condensed on the windows of the enclosure. The dew point has been transgressed on the windows.



*Figure 9:
Humidity condensation on the
insides of the Plexiglas windows.
It indicates the transgression of the
dew point in the steamy areas*

It can be supposed that condensation water accumulates on the anilox roller, too. When the air temperature, the relative humidity and the air pressure are known, it is possible to read off the dew point temperature from the Mollier h,x diagram (cf. fig. 10 and Hae 1969). The point of intersection of the air temperature straight line with the φ -curve describes the condition of the humid air. At the point where the vertical line through this intersection intersects the saturation curve $\varphi = 1 = 100\%$ is the dew point. The dew point temperature has to be read off the ordinate. In the case that an object, which comes into contact with this air, has a lower surface temperature than the dew point temperature, water condenses on its surface.

Moreover, it can be read off the diagram (fig. 10) at which relative humidity $\varphi_{rel, T}$ the dew point is reached. However, the air temperature and the surface temperature t_L , t_O have to be known. Table I shows examples for the values $t_L = 35\text{ }^{\circ}\text{C}$ and $t_O = 30\text{ }^{\circ}\text{C} \dots 33\text{ }^{\circ}\text{C}$.

Table. I: Examples for $\varphi_{rel, T}$ against t_L and t_O

t_L in $^{\circ}\text{C}$	t_O in $^{\circ}\text{C}$	$\varphi_{rel, T}$ in %
35	30	75
35	31	80
35	32	85
35	33	90

The following values have been measured in the area of the anilox roller of the laboratory printing unit at a stage when the optical density of the solid area has been increased.

Air temperature	t_L	$= 35\text{ }^{\circ}\text{C}$
Relative humidity	φ_{rel}	$= 95\text{ }%$
Anilox roller temperature	t_O	$= 32\text{ }^{\circ}\text{C}$
Air pressure	p	$= 10^5\text{ Pa}$

These measured values illustrate that the dew point on the anilox roller surface has been markedly transgressed (cf. table 1). Water condenses on the anilox roller from the humid air. The thermodynamic conditions, which are described by the Mollier h,x diagram, have no time reference. The conditions are, thus, valid for the quickly rotating anilox roller surface, too. Water condenses on the roller surface despite the high circumferential speed.

The cell wall areas are coated with a binding agent and solvent film. Therefore, they have hydrophobic properties. The condensed water immediately forms droplets. These droplets are visible as white-spots under the microscope. Fig. 11 shows microphotos of the anilox roller surface, which have been taken during production printing with the test printing forme. The water on top of the cell walls is clearly visible after 47.000 copies (cf. also fig. 5).

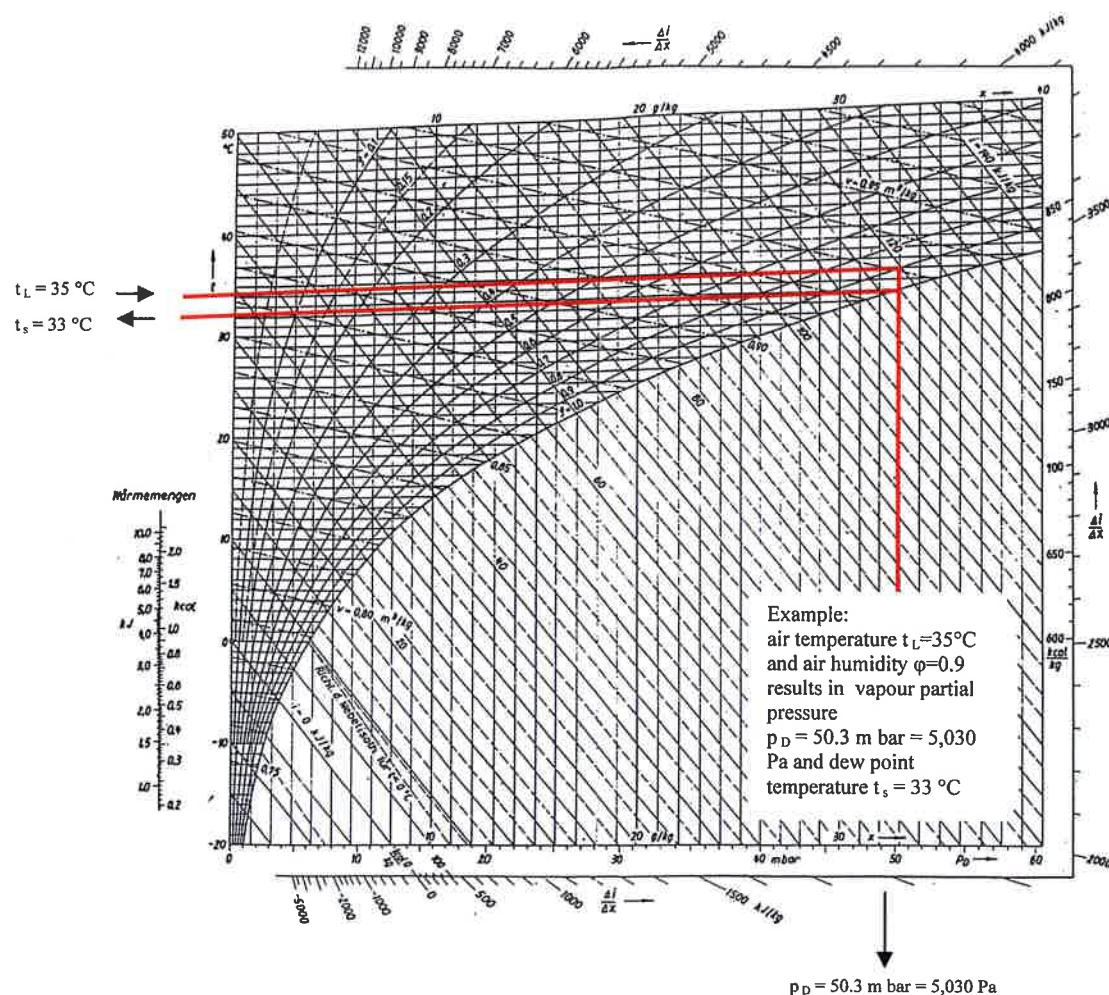


Figure 10: Mollier h,x diagram for humid air with $p = 1 \text{ bar} = 10^5 \text{ Pa}$ total pressure (cf. Hae 1969) with example



After 10.000 copies



After 30.000 copies



After 35.000 copies



After 44.000 copies



After 50,000 copies



After 55,000 copies

*Figure 11: Microphotos of the anilox roller surface.
Water droplets are visible as white spots on top of the dark cell walls*

When considering the dew point, it becomes clear that water condenses in the area of the anilox roller under the analysed operating conditions. Evaporation cannot occur in this area. Nevertheless, the relative humidity remains stable at $\varphi = 95\%$. Fig. 12 shows the temperature distribution in the printing unit. The printing ink in the inking fountain has a temperature of $t_L = 42^\circ\text{C}$. Printing ink constantly flows out of the inking fountain into the ink catch pan. Surface water accumulates on top of the ink. The temperature of this ink is high enough, so that the water can evaporate. The heated and humid air ascends to the anilox roller. The cooling down of the air to $t_L = 35^\circ\text{C}$ results in an increase of the relative humidity to the measured 95%. The extreme condensation on the Plexiglas windows in the area of the anilox roller, which is completely missing in the area of the ink catch pan, confirms these circumstances.

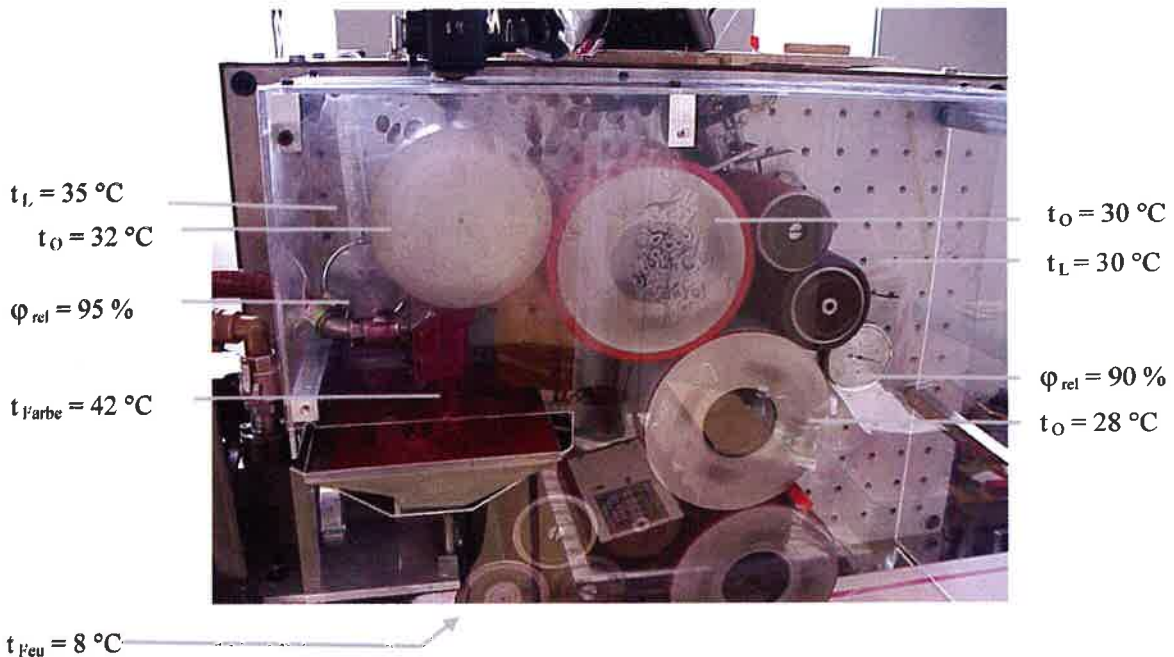


Figure 12: Temperature and air humidity values in the printing unit

4.3 Major Parameters Influencing the Evaporation in the Printing and Inking Unit

With the aim of finding the main parameters influencing the air humidity in the printing unit, the evaporation quantities, which have been emitted from the inking and printing unit, have been calculated. The calculation has been conducted for the open-type laboratory printing unit, as stable values can only be assessed for this case. Another major reason is that the temperature remains relatively constant in the open-type printing unit.

The evaporation is calculated on the basis of the model of an even, wet plate, which is overflowed with air. The following values have been applied:

Average overflowed free length of the wet plate $l = 0.22 \text{ m}$

Air velocity, in this case circumferential speed of the rollers $w = 5 \text{ m/s}$

Temperatures, air humidity, air pressure, saturation vapour pressure

$$t_L = 22^\circ\text{C}; \varphi_L = 0.5 \rightarrow x_L = 0.0084 \text{ kg/kg}$$

$$t_O = 30^\circ\text{C} = t_S$$

$$p = 10^5 \text{ Pa}; p_{D,s} = 4,241 \text{ Pa}$$

Properties of the air at average boundary layer condition (reference condition):

$$t_{bez} = 0.5(t_L + t_S) = 0.5(22 + 30) = 26^\circ\text{C}$$

$$x_{bez} = 0.5(x_L + x_S)$$

$$x_S = 0.622 \frac{p_{D,s}}{p - p_{D,s}} = 0.622 \frac{4,241}{10^5 - 4,241}; x_S = 0.02755$$

$$x_{bez} = 0.5(0.0084 + 0.02755) = 0.017975$$

The following equation applies for the laminar flow of air:

$$\left(1 - \frac{p_{D,s}}{p}\right) \overline{Sh}_l = 0.664 \sqrt{\text{Re}_l} \cdot \sqrt[3]{Sc} \quad \text{if} \quad \text{Re}_l < 3.5 \cdot 10^5 \rightarrow \text{laminar flow}$$

Explanation of symbols:

Sh_l	Sherwood number, based on length l
Re_l	Reynolds number, based on length l
Sc	Schmidt number
Pr	Prandtl number
ρ_l	density of the humid air
η_l	dynamic viscosity of the humid air
λ_l	thermal conductivity coefficient of the humid air
R_l	gas constant of the air
D_p	diffusion coefficient vapour-air, based on Δp
	(cf. Pli 2001)

$$\text{Re}_l = \frac{w \cdot l \cdot \rho_l}{\eta_l}$$

$$\rho_l = \frac{p}{R_l \cdot T_{bez}} \cdot 0.622 \frac{1 + x_{bez}}{0.622 + x_{bez}} = \frac{10^5}{287(273.15 + 22)} \cdot 0.622 \frac{1 + 0.017975}{0.622 + 0.017975} = 1.16799 \text{ kg/m}^3$$

$$\eta_L = 1.82 \cdot 10^{-5} \text{ kg/ms}$$

$$Sc = 0.619$$

$$D_p = \frac{1.7441816 \cdot 10^{-6}}{T_{bez} + 190} \cdot \frac{T_{bez}^{1.5}}{p} = \frac{1.7441816 \cdot 10^{-6} \cdot 299.15^{1.5}}{(299.15 + 190) \cdot 10^5} = 1.844944 \cdot 10^{-10} \text{ s}$$

$$Re_l = \frac{5 \cdot 0.22 \cdot 1.16799}{1.82 \cdot 10^{-5}} = 7,0592.8 < 3.5 \cdot 10^5 \rightarrow \text{consequently: laminar flow}$$

$$\bar{\beta} = Sh_l \cdot \frac{D_p}{l}$$

$$\overline{Sh_l} = \frac{0.644 \sqrt{Re_l} \cdot \sqrt[3]{Sc}}{(1 - \frac{p_{D,s}}{p})} = \frac{0.644 \sqrt{7,0592.8} \cdot \sqrt[3]{0.619}}{(1 - \frac{4,241}{10^5})} = 157.012$$

$$\bar{\beta} = 157.012 \cdot \frac{1.844944 \cdot 10^{-10}}{0.22} = 1.31672 \cdot 10^{-7} s/m$$

The rate of flow of evaporation is consequently:

$$\dot{M}_D = \bar{\beta} \cdot (p_{D,s} - p_{d,\infty}) \cdot A$$

A is the wet total surface area of the inking and printing unit and

$$p_{d,\infty} = p \cdot \frac{x_L}{0.622 + x_L} = 10^5 \cdot \frac{0.0084}{0.622 + 0.0084} = 1,332.483 Pa$$

The rate of flow of evaporation at a total evaporation area of 1 m² is consequently

$$\dot{M}_D = 1,31672 \cdot 10^{-7} (4241 - 1332,4873) \cdot 1 = 1,31672 \cdot 10^{-7} \frac{s}{m} \cdot 2908,513 Pa \cdot 1 m^2 = 3,8297 \cdot 10^{-4} \frac{kg}{s}$$

or the specific rate of flow

$$\dot{m}_D = 3.8297 \cdot 10^{-4} \frac{kg}{m^2 s} = 1.379 \frac{kg}{m^2 h}$$

If you consider not only the mass exchange, but also the connected heat and mass transfer, you receive a more exact value for the rate of flow:

$$\dot{M}_D = \beta_m \cdot (p_{D,s} - p_{d,\infty}) \cdot A$$

$$\bar{\beta}_m = \bar{\beta} \pi^{-n} \quad \text{with} \quad \pi = \frac{p - p_{D,\infty}}{p - p_{D,s}} = \frac{10^5 - 1,332.4873}{10^5 - 4,241} = 1.03037$$

and $n = 0.7 \rightarrow$ for laminar flow (cf. Pli 2001, p. 4)

$$\bar{\beta}_m = \bar{\beta} \cdot 1.03037^{-0.7} = 1.31672 \cdot 10^{-7} \cdot 1.03037^{-0.7} = 1.28943 \cdot 10^{-7} \frac{s}{m}$$

$$\dot{M}_D = 1.28943 \cdot 10^{-7} \cdot 2,908.513 = 3.7503 \cdot 10^{-4} \frac{kg}{s} \quad \text{for a total evaporation area of 1 m}^2 \text{ or}$$

$$\dot{m}_D = 3.7503 \cdot 10^{-4} \frac{\text{kg}}{\text{m}^2 \text{s}} = 1.350 \frac{\text{kg}}{\text{m}^2 \text{h}}$$

Major parameters influencing the evaporation quantity:

- temperature of the roller surfaces
- air temperature
- relative humidity
- printing speed
- total wet surface area of the rollers in the printing and inking unit (It must be pointed out, however, that the surface water, which is spread in drops, just partly covers the total surface area of the rollers. The total wet surface area is, thus, considerably smaller than the total surface area of the rollers. It decreased and increases depending on the amount of the surface water)

5. Summary and conclusions

On the one hand, the surface photos of the inking and printing unit rollers have been analysed for the open-type printing unit, and on the other hand for the enclosed alternative. Significant differences could be found at the anilox roller. In fact, surface water of different amounts could be found at all process stages with stable offset conditions. Even water accumulations in the cells could be detected. In all cases, however, there was no dampening solution on top of the cell walls of the anilox roller.

The same findings were made for the enclosed printing unit.

The optical density abruptly increases on the printing product simultaneously involved surface water accumulations on top of the cell walls of the anilox roller. It is plausible that ink transfer and splitting conditions in the roller nip between anilox roller and ink form roller are affected by these characteristic changes. If water on top of the cell walls locally prevents their inking in the roller nip to the ink form roller with reflowing ink, the splitting in these areas is limited.

As a consequence of the local ink splitting processes, there is a larger quantity of ink on the ink form roller. The quantity of ink transferred to the printing forme and ultimately to the printing substrate increases. The result is an increased optical density on the printing product.

The quantity of the surface water mainly depends on the water concentration and the water distribution in the printing ink. At stable conditions, an increasing surface water quantity involves an increased evaporation. Condensation on the anilox roller is caused by a transgression of the dew point, resulting from rising air humidity and restricted air exchange in the inking and printing unit.

The balance of dampening solution content, consumption and evaporation should guarantee that the dampening solution contained in the ink is well below 25%. An effective measure to avoid the abrupt increase of the optical density could be to dissipation of the humid air from the inking unit area. At the same time, dry air should be supplied. Goal is to limit the air humidity, so that the dew point on the anilox roller surface cannot be reached in any case.

The findings just apply for the enclosed laboratory printing unit as well as for the used ink and dampening additive. Further research has to be conducted in order to prove that the conclusions are also valid for production printing presses.

Literature References

- Doe 2002, Dörfler, H.-D., (2002), *Grenzflächen und kolloid-disperse Systeme*, Springer-Verlag, Berlin Heidelberg New York, ISBN 3-540-42547-0
- Hae 1969, Häußler, W., (1969), *Lufttechnische Berechnungen im Mollier-i,x-Diagramm*, ES 18 B 4/20 D 2, Verlag Steinkopff, Dresden
- Lin 1991, Lindqvist, U., (1991), *Das Vermeiden von Emulgierproblemen in farbzonenfreien Offsetdruckwerken*, ifra Special Report 3.15
- Lin 1990, Lindqvist, U., (1990), *Welche Entwicklungsdefizite bestehen noch bei Anilox-Offset?*, Ifra Special Report 3.12
- Loi 1991, Loibl, D., (1991), *Kurzfarbwerke für den Zeitungsdruck*, FOGRA-Forschungsbericht 3.008
- Pli 2001, Plichta, J. / R. Arnold, (2001), *Stationäre Wärme- und Stoffübertragung, Berechnungsunterlagen*, Technische Universität Chemnitz
- Pli 1984, Plichta, J., (1984), *Prallströmung in der Gasfeuchtigkeitsmesstechnik*, Dissertation, TH Karl-Marx-Stadt
- Pyl 1981, Pylotis, D., (1978 and 1981), *Wechselwirkungen zwischen Druckfarbe und Feuchtmittel beim Offsetverfahren*, FOGRA-Forschungsbericht 5.205 and 5.205/2
- Ros 1990, Rosenberg, A., (1990), *Einfluss von Füllstoffen auf die Feuchtmittelaufnahme von Offsetdruckfarben*, FOGRA-Forschungsbericht 5.212
- Ros 1989, Rosenberg, A., (1989), *Zusammenhänge zwischen der Konsistenz von Offsetdruckfarbe und ihrem drucktechnischen Verhalten*, FOGRA-Forschungsbericht 5.211
- Ros 1986, Rosenberg, A. / K.-H. Schirmer, (1986), *Feuchtmittelaufnahme von Skalendruckfarben Cyan, Magenta und Gelb für den Offsetdruck*, FOGRA-Forschungsbericht 5.208
- Stu 1995, Stutz, H., (2/1995), *Offsetdruck mit Emulsionsfarben*, Zeitungstechnik, pp. 64-66

The effect of speed on image transfer in rotogravure printing

Glyn R. Davies, Timothy C. Claypole

Welsh Centre for Printing and Coating
School of Engineering, University of Wales Swansea
Singleton Park, Swansea, SA2 8PP, UK
E-mail: meprint@swansea.ac.uk

Abstract

An experimental investigation of the effect of speed on image transfer in rotogravure has been undertaken comparing under controlled conditions a low speed proofing press (1.2 m/s) with a range of production speeds (2.5 to 7.5 m/s) on a web fed six colour gravure press. Measurements of tone gain, trap and colour gamut were made on a bespoke fingerprint image.

The tone gain and colour gamut were found to be highly dependent on the print speed. This can be attributed to the effect of the interaction of the cohesive viscous and body forces of the ink, the cell size and geometry and the capillary/suction of the printing process. The nett effect is that with increasing speed there was an increased ink release in high coverage areas, whilst the ink release from the low coverage areas fell. The cell dimensions in the direction of print were also found to have an effect at high coverage.

Keywords

Colour gamut, Gravure, Ink transfer, Press speed, Tone gain

1. Introduction

Speed is significant process variable in rotogravure printing, as it dictates amongst other things the time available for the ink to flow from the engraving to the substrate. The speed will also effect the flow of ink from the chamber into the engraving and within the cell after doctoring. Thus, changing press speed will have a significant influence on the ink transfer and hence the colours of the image, as well as phenomena such as dot skip.

Proofing presses are used to check the engraved cylinders before they are used on the press and as a guide to press settings. Such proofing presses have a similar mode of operation to the press, use similar inks and print on the production substrate. However, they operate at far lower speeds, so while they ensure the integrity of the image, the colour rendition can be difficult to relate directly to the print obtained at production speeds.

An investigation was undertaken into the effect of production press speed on print quality and its relationship to the proof press. This is part of a long-term investigation to quantify the effect of process parameters and establishing the underpinning science, with the goal of developing a predictive model of the rotogravure printing process. The experimental procedure is first described before the results of the effect of speed on tone gain, trapping and colour gamut are presented and their implications discussed.

2. Experimental programme

A test image was printed on a proof press (at approximately 1.2 m/s) and a web fed six colour Gravure press at four speeds (2.5, 4.2, 5.8 and 7.5 m/s). The prints were made on a 52 gsm Supercalendered

(S/C) and 51 gsm Lightweight coated (LWC) paper. The four colour process liquid inks were nitro-cellulose resin based, near Newtonian, with viscosity of 0.012 Pas. The viscosity of the ink was checked at the start and end of each test to confirm that they were unchanged.

A single cylinder proof press was used that printed each colour separately to build up the four colour image. The print cylinder was brought in to contact with the drum and the doctor blade positioned on the cylinder (Figure 1). Ink was poured into the reservoir formed between the doctor blade and the cylinder. As the drum revolved the print cylinder rotated and ink was dispensed into the engraved cells on the cylinder and metered by the doctor blade.

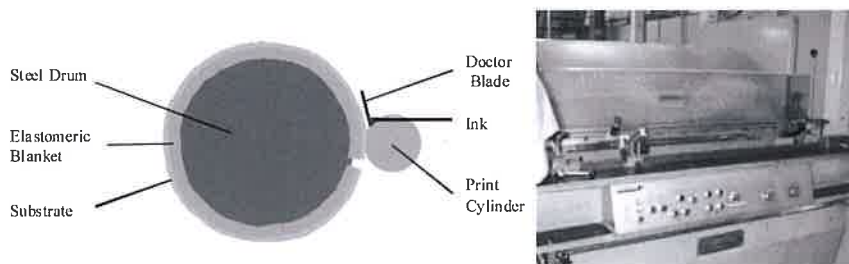


Figure 1: Photograph and diagram of a single cylinder drum proof press

A set of four process colour test cylinders was manufactured for the print trial. The test image provided areas for assessment of different quality characteristics (Figure 2). The tone gain could be accessed both parallel and orthogonal to the direction of print, as well as gamut and trap. The printed sheets were measured with a Gretag SPM 55 spectro-densitometer. The results for the production press are based on an average of five consecutive sheets to improve accuracy and eliminate errors due to copy to copy variation (Bohan et al, 1998).

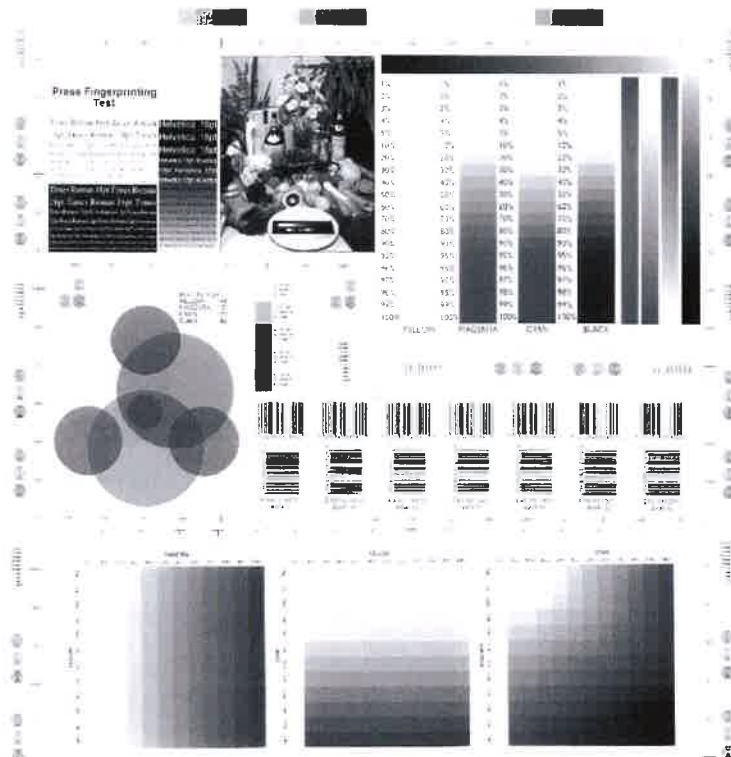
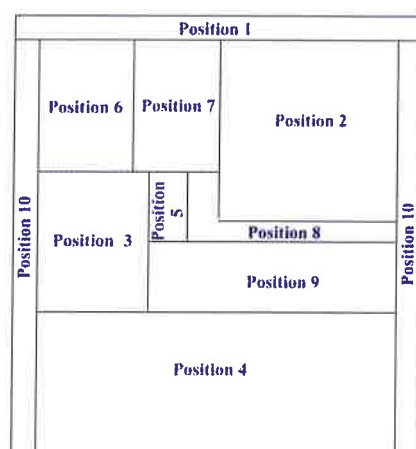


Figure 2a: Test image



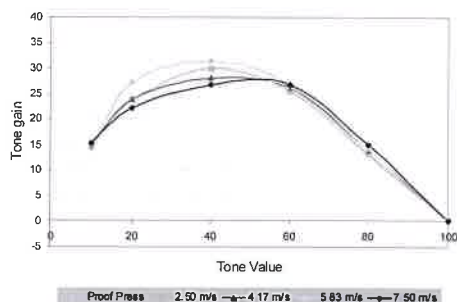
- Position 1 – Horizontal gradation bars
- Position 2 – Vertical gradation bars
- Position 3 – 50% Tone circles
- Position 4 – Calibration Squares
- Position 5 – Neutral Grey Gradation bar
- Position 6 – Positive and negative print for text
- Position 7 – Four colour Process image for visual
- Position 8 & 10 – Area for testing print slur
- Position 9 – Bar codes for line print sharpness

sharpness
assessment

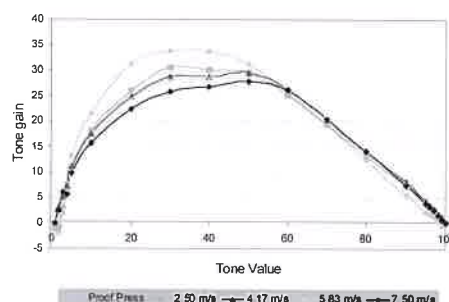
Figure 2b:
Sub division key of test sheet to illustrate significance of test areas

3. Results

As all the colours show similar trends, the effect of speed on tone gain is illustrated using the magenta curves (Figure 3). There is a high value of tone gain because of the use of uncorrected cylinders. When the machine speed is increased the tone gain decreases for all tonal values, but particularly in the mid tone regions between 20% and 60%. The largest effect of speed was seen on the black print (10 %), with the yellow, magenta and cyan having reductions of between 5 and 8%. The tone gain curves obtained exhibit the same trend for both the vertical and horizontal gradation scales.



Magenta tone gain
curve for horizontal gradation scale



Magenta tone gain
curve for vertical gradation scale

Figure 3: Tone gain curves for supercalendered paper

When comparisons are made between the machine and the proof press, the variations for the vertical tone wedges, are more marked. The measured tone gain is greater for the proof press than for the production press. The higher tone gain of the proof press may be due to the dynamics of the proof system where the ink is held and metered out from above the doctor blade and not carried up from below the blade as with the print press.

There was a negligible effect of the paper type on tone gain, the results with the LWC being within 2% of the S/C at all speeds. However, the inks display different tonal reproduction characteristics (Fig 4). This suggests that the ink and cell geometry are dominant in determining absolute value.

The two-colour trap value of cyan on yellow (green), magenta on yellow (red) and cyan on magenta (violet) were measured to evaluate the effect of speed on overprinting (Figure 5). As the press speed increases, there is no significant change in the measured trap for either the S/C or the lightweight-

coated paper. The small variation of trap on the print press suggests that the dry film thickness is changing little with increase of speed.

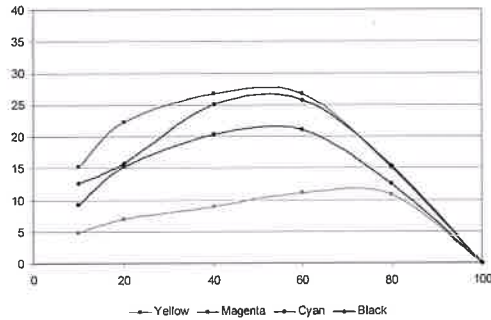
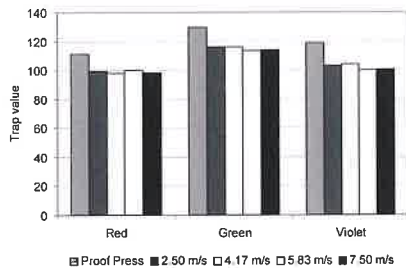
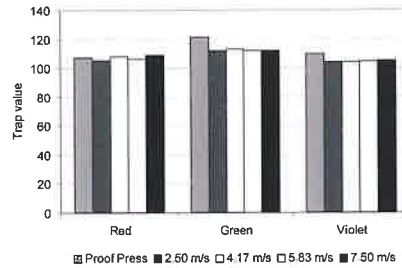


Figure 4:
Horizontal Tone gain curves for
supercalendered paper at 7.5 m/s

However, the trap was higher on the proof press for both substrates with the S/C showing a greater magnitude of change. This may be due to its method of operation as much as the reduced printing speed. Unlike the production press where the printed ink is force dried between the print units, the ink printed by the proof press is allowed to dry without assistance. This allows the ink time to be absorbed into the surface of the substrate before the application of the overprinted ink. This would effect the profile of the pigment in the surface and present a more absorbent surface than if it had been forced dried. This would be further exacerbated by the differences in the absorption characteristics of the substrates.



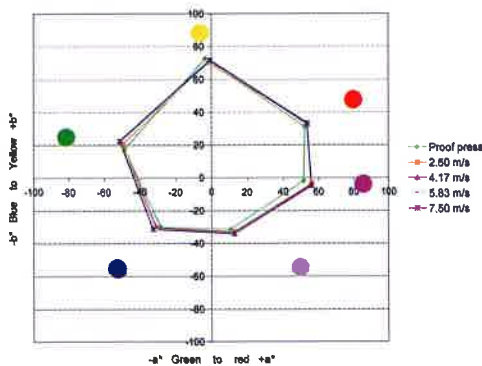
Supercalendered



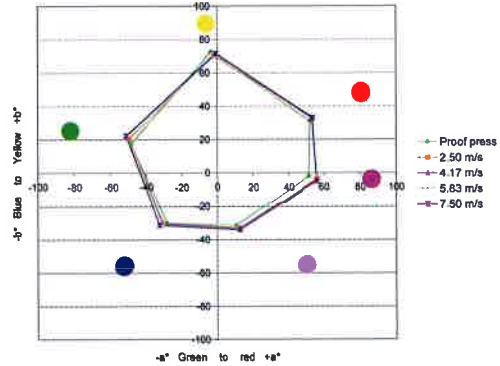
Lightweight Coated

Figure 5: Comparison of trap values at varying print speeds

The change in maximum colour gamut for the process inks at 100% solid and 100% overprint on S/C and LWC paper is shown in Figure 6. For each substrate the maximum colour gamut achievable at press speeds show little variation. However for both substrates the colour gamut of the proof press is different to that of the gamut



Supercalendered Paper



Lightweight Coated Paper

Figure 6: Colour gamut at varying print speeds

achieved with the production press. While the single colours and overprints on the production press move predominantly in terms of saturation with speed, there is a shift in hue between the overprints on the proof press and those on the production press. This is particularly noticeable in the green. This reflects the measurements of trap, reflecting the change with ink transfer mechanism due to the different drying conditions.

A comparison of the maximum colour gamut for S/C and LWC paper for the proof press and the print press at 7.50 m/s, illustrates the different responses obtained with the two substrates (Figure 7). Although both substrates exhibit similar trends i.e. the proof press having a smaller colour gamut than the production press, the initial gamut achieved with the LWC on the proof press is larger than that observed with the S/C printed with the production press. This is significantly increased when the LWC is printed using the production press.

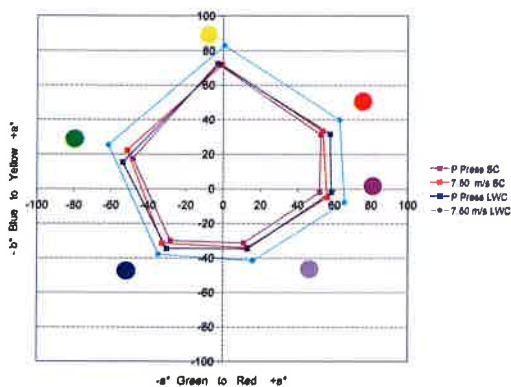
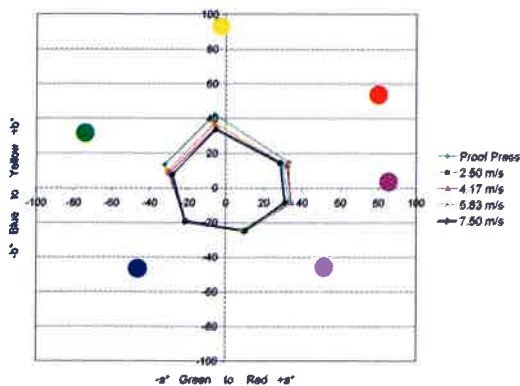
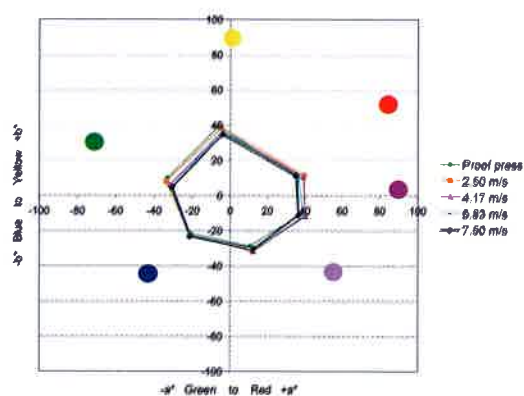


Figure 7:
Comparison of maximum colour gamut

The Gamut plot for the same process colours at a 50% tone, show the expected reduced colour space (Figure 8). Unlike the colour gamut obtained with the 100% print, where the proof press gamut is slightly smaller than the production machine, the gamut obtained for the 50% tone on both substrates is equal to or slightly larger than the printing press. The yellow and colours containing yellow showing larger shifts than the cyan or colours containing cyan. There is a more pronounced colour shift with press speed, which are predominately in terms of saturation, even for the overprints. Unlike the maximum colour gamut, the second colour is being printed on a 50% coverage, thus the substrate surface would be altered far less by the already printed layer and hence it has less effect on the ink transfer for the second colour.



Supercalendered Paper



Lightweight Coated Paper

Figure 8: Colour gamut of 50% tone at varying print speeds

4. Discussion

Although tone gain gives a guide to the visual impact, it is a relative measure of image change that assumes the solid density remains sensibly constant. It is thus only a symptom of the effect of ink transfer from the engraved cylinder to the substrate. As the viscosity and the concentration of the pigment were held constant during these trials, then the print density can be used as a measure of the ink transfer. The effect of cell size can be studied by plotting density against speed for different coverage (Figure 9). For the 100% solid coverage, the density increases with speed, regardless of print direction. This suggests that at these larger cell sizes the effect of centrifugal force as the cylinder rotates faster is a dominant effect. The paper type also has an influence as it effects the capillary forces and produces a different print density at the 100% coverage, the LWC enhancing the ink transfer.

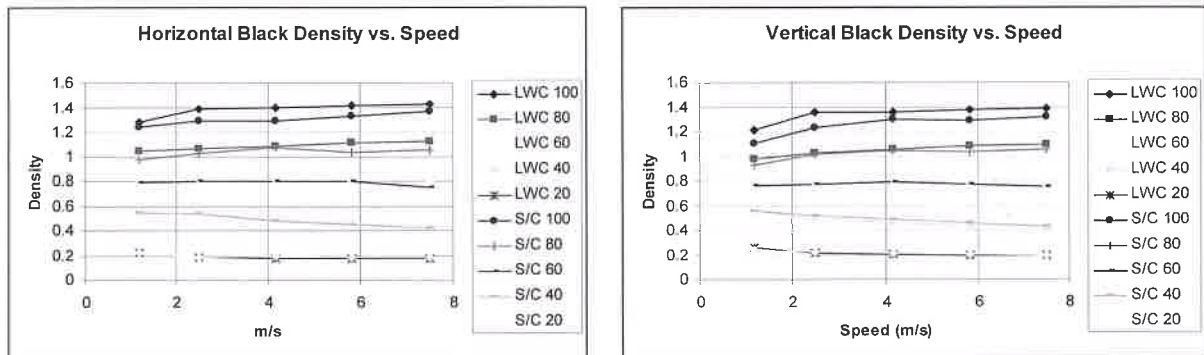


Figure 9: Black Density vs. print speed for various coverage on two papers

At 80% coverage there is an increase of density with speed, although reduced compared to the 100% coverage. This is almost entirely due to the interaction of the centrifugal and suction forces with the cell, as the density is independent of paper type. At 60% coverage, the forces balance at all speeds and the density remains constant.

For the lowest coverage, the ink released falls with press speed. As the press goes faster there is less time for the ink to fully evacuate the cells. At the same time, the cohesive viscous also become more dominant in the smaller volume and so the capillary/suction forces require more time to remove the ink from the cells. So as speed increases, so the amount of ink transferred decreases. This is in line with the theories of Kunz 1975 and Jeske 1990, who suggested that a finite time was required for ink transfer. However, this work suggests it is most relevant at low coverage.

These trends have been observed for the black, yellow and cyan inks. The black has the finest engraved cells of regular geometry, while the yellow has larger rectangular cells and the cyan has cells of the same dimensions in the print direction as the yellow, but that have been elongated orthogonally to the direction of print. The magenta cells are similar geometry, but elongated in the direction of the print. While the density follows the similar trends for the coverage from 20 to 80%, the ink released from the 100% solid magenta coverage falls with increasing speed (Figure 10). Kunz 1975 had suggested the doctor blade drags the ink meniscus back in a wave on the trailing edge of the cell after which it relaxes back to fill the cell. As the speed of the process increased then there is less time for the ink in the cell to relax. Whilst this does not validate the process physics Kunz's hypothesis, these results imply that there is an interaction of the ink in the cell with the wiping action of the doctor blade. This may cause flow perturbations in the ink contained in the engraved cells.

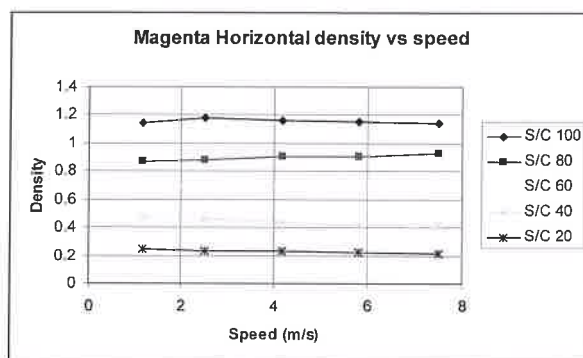


Figure 10:
Magenta density vs. print speed on
S/C paper for various coverage

The mode of operation and construction of the proof press will also account for some of the differences observed. The proof press had a large circumference drum with a thin elastomeric layer 2% of the diameter, when the print cylinder is in contact there is little deformation of the elastomeric layer, therefore a relatively low pressure drop occurs on the exit of the nip. The forces pulling the ink from the cell and transferring the ink to the paper i.e. film splitting, will be lower and therefore less ink will be transferred. The production machine had a pressure roller of approximately quarter the diameter of the proof press with a 10% elastomeric layer. Even at the same speed, the pressure drop on the nip exit will be much higher than the proof press because a larger deformation and the geometry of separation. This will effect the ink film splitting so more ink is pulled from the cell and transferred to the substrate.

The lower difference observed between the proof press and the production machine for the S/C paper may be a result of its more absorbent nature when compared to lightweight-coated. On the proof press, due to the size of the nip and the reduced speed of the press, the substrate has a longer contact time with the ink in the cylinder cells. The effect of capillary action pulls more ink from the when the proof press prints are compared to production machine.

5. Conclusions

A study on the effect of print speed on the rotogravure printing process has been undertaken. Traditionally tone gain and colour gamut have been assumed to be constant for a given gravure press substrate combination. This research has shown speed has a significant effect on ink transfer. It may even be necessary to have a knowledge of the intended printing speed at the prepress stage of image production.

The main conclusions can be summarised as follows:

- The tone gain curve and colour gamut changes with increasing speed as a consequence of the increased ink released at high coverage and reduced ink release at low coverage.
- Centrifugal force, capillary action and suction dominate the ink release at high coverage. The paper type has an influence on the release of solids.
- At low coverage, the cohesive-viscous forces reduces the rate at which the ink leaves the cells. As increasing speed reduces the time available for ink transfer and as a consequence the cells are not fully evacuated.
- There is reduced ink release with increasing speed from the solid with cells elongated in the print direction.
- The absorption of the ink between prints on the proofing press, effect the structure of the paper and has a significant effect on overprints (i.e. trap and gamut).

- The speed difference between the proof press and the production press is the main source of colour discrepancies. This is exacerbated by the increased rate of film splitting due to the relative geometries and construction of the production press compared to the proof press. There is a need to compensate for these effects when comparing the proof with the production print.

Acknowledgements

The authors wish to acknowledge the financial support of the Rotogravure Printing Technology Group for this work.

References

- Bohan, M.F.J, Claypole, T.C. and Gethin, D.T, 1998. "An investigation into ink transfer in rotogravure printing" Proc. TAGA, pp484 – 494
- Kunz, W, 1975 "Ink Transfer in Gravure Process", TAGA Proceedings
- Jenske, D.R., 1990, "Impulse Press Simulation Of A Gravure Printing Nip", International printing and graphic Arts Conference, pp 97-104

Tone gain due to deformation of the flexographic plate

David C. Bould, Timothy C. Claypole, Mark F. J. Bohan, D. T. Gethin

Welsh Centre for Printing and Coating
School of Engineering, University of Wales Swansea
Singleton Park, Swansea, SA2 8PP, UK
Email: t.c.claypole@swansea.ac.uk

Abstract

The engagement in the printing nip leads to the application of mechanical loads to the flexographic plate. These cause the structures carrying the image to distort. The amount of distortion is a function of the local coverage, i.e. the dot structure. This is combined with the spread of the ink carried by the plate to produce tone gain. The microscopic nature of the dot substrate interface makes direct experimentation difficult. Therefore, the distortion of the plate for different coverages has been analysed using finite element modelling techniques. Three different models were developed for the highlight, mid tone and shadow areas of the plate. The tone gain due to distortion of the dots was evaluated for different engagements, line rulings and plate thickness.

Two different mechanisms were identified for dot gain, expansion of the surface of the dot and barrelling of the dot edges. Dot barrelling was found to make the most contribution to the tone gain for most of the coverage range. However, dot expansion and dot barrelling were found to be equally important at low coverages, due to the inherent instability of the dot shape. The low coverage was particularly sensitive to the effect of engagement. A complex relationship was found between the coverage and tone gain in the low coverage (3-15%). This implies that particular attention has to be paid to the engagement to successful print images that rely on low coverage areas for reproduction.

This study has created a methodology that will enable the effects of the plate distortion to be separated from the tone gain due to ink transfer and spreading in experimental trials.

Keywords

Distortion, Finite element modelling, Flexography, Plate, Tone gain

1. Introduction

The tone gain in the flexographic printing process is governed by the deformation of the plate as it passes through the printing nip and the spread of the ink as it is transferred from the plate to the substrate. Although the overall tone gain can be measured from the plate coverage and print, it is difficult to allocate the proportion of gain due to the compression of the plate in the printing nip and to ink spreading. The deformation of the plate on a micro scale is difficult to investigate experimentally without disturbing the physics of the process. Finite element modelling techniques (FEM) were initially developed by the aircraft industry primarily to allow the detailed analysis of structures without physical testing. However, these can also be applied to study situations, such as occur in the printing nip, to which physical access is difficult or where intrusive measurements would disturb the physical behaviour.

This paper describes the use of finite element modelling techniques to derive an understanding of the role of plate distortion in the tone gain. FEM simulations have been developed of a single dot on a plate for various coverages. These have been used to study the effects of percentage coverage, line

ruling, engagement and plate thickness on the tone gain due to the mechanical distortion of the plate. The practical implications of these findings are also discussed.

2. Development of an FEM simulation

In Finite Element modelling (Chandrupatla & Belegundu 1997, Smith & Griffiths, 1998), the structure is divided into a series of small elements bounded by nodes around their perimeter. The solution is then obtained by solving fundamental equations for force and displacement for each individual element, throughout the structure, with the boundary conditions for each element being dependent on neighbouring elements. Boundary conditions are defined along lines of symmetry to reduce the complexity of the model. The FEM was developed using a proprietary finite element software package, *Elfen* (Rockfield Software 1998).

The models were based on three dimensional profiles of series of dots obtained using white light interferometry (Bould 2001). For low coverages, up to 30%, the dots were circular free standing structures (Figure 1). The dot areas for coverages up to 30% were obtained by measuring the diameter of the top surface of the dot profile and calculating the area. For the 40% coverage the dot shape changed to a square, each dot receiving structural support via the corners. For this coverage the width of the square dot was measured and the area obtained. For all other coverages, the dots linked such that the non-printed region of the dot was circular. The radii of the circles of the non-printing regions of each dot were measured and the area obtained. This was then subtracted from the total area of the square bounding the dots. The width of the square was dependent on the line ruling, and was obtained by inverting the line ruling in lines per cm to give cm per line.



Figure 1: 20% 40% and 60% dots on printing plate

Each model consisted of a single flexographic dot only, which was bounded by the theoretical square (Figure 2), with the deepest parts of the dot at its four corners. As the profile at 45° to the line ruling was different to the profile along the line ruling, it was necessary to build 3 dimensional models to incorporate this. Analysis was restricted to a single dot due to the computational time required to run models consisting of more than one dot.

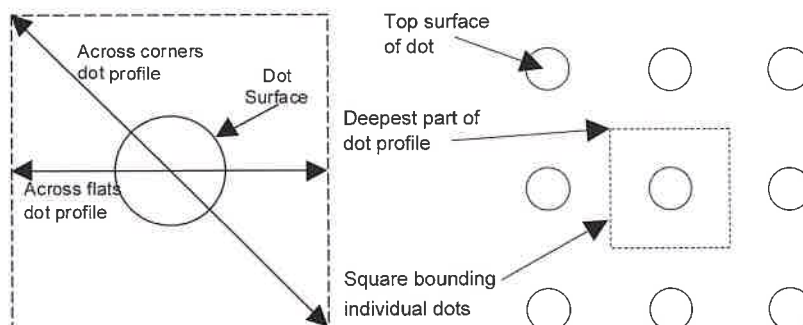


Figure 2: Plan view of dot profile on plates

The dot shapes used for the three model types are shown in Table I, and are illustrated in Figure 3. The entire plate thickness and the mounting tape were included. The models were constructed using an unstructured mesh to simplify the geometry. An unstructured mesh permitted a high mesh density around the top of the dots, which was the main region of interest. The mesh density of other parts of the models, where a high resolution was not required was reduced to improve the computational efficiency. The mesh for a 20% nominal coverage is shown in Figure 4. The mesh for the full model is shown, as well as an enlarged view of the dot itself, illustrating the increased mesh resolution around the top of the dot. Tokens were assigned instead of numerical values to define the geometry and load conditions. This enabled the model to be defined parametrically, permitting the geometry or value of the load to be adjusted by modifying the value of the token. Tensile and compressive tests were performed on samples of the plate and the mounting tape to establish their physical properties. The materials were assumed to be isotropic. The Young's Modulus for the tape was found to be consistent. The Young's Modulus for the plate material was found to increase with compression. However, this was not deemed to be significant over the range of distortion considered and therefore a constant mid range value for young's modulus was used.

Table I: Dot geometry for different dot types

	Model type 1	Model type 2	Model type 3
Coverage Range	1% - 30%	40%	50% - 90%
Dot Shape	Round	Square with leaders connecting adjoining dots	Quarter circles of non-dot at four corners

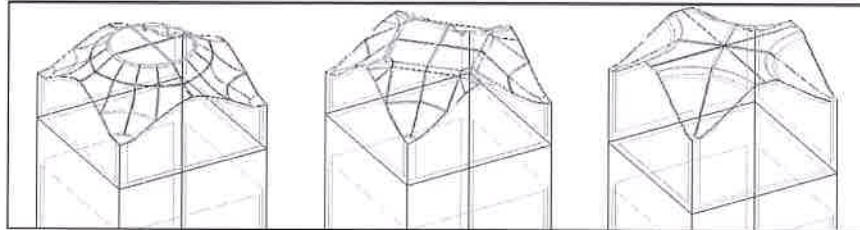


Figure 3: Illustration of dot types

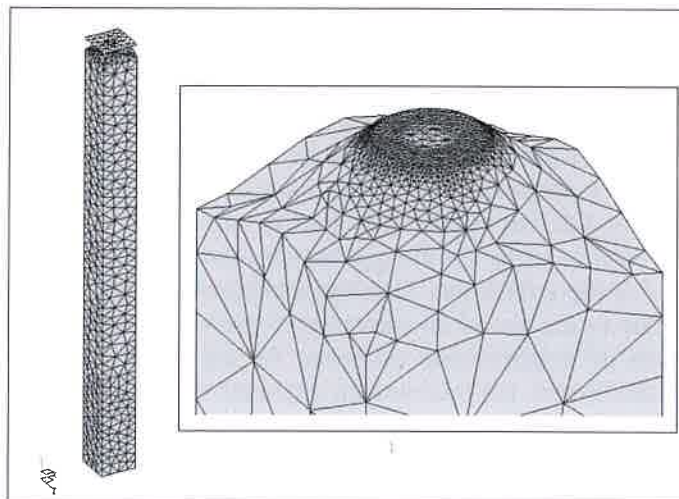


Figure 4: Mesh of full model and enlarged view of dot

An applied displacement of a steel shell normal to the dot surface was used to simulate the engagement in the printing nip. The deformation of the dots on a printing plate could then be considered to be a series of steady state problems. This simplified the model further as the number of elements used to deform the flexographic dots was reduced. The shell was assumed to be flat, as the radius of the impression cylinder was large in comparison to the size of the dot. The models were dry contact models with no ink, reducing the problem to a single phase analysis, although the friction could be varied to simulate the lubricating effect of the ink. A dry contact analysis also enabled the deformation of the printing plate to be quantified.

The possibility of reducing the computational requirements by modelling only a quarter of the dot was investigated. A model of a quarter dot was developed for a 1% dot with a line ruling of 39.4 lpcm for a 1.70mm plate thickness. The model was constrained so that elements along the planes of symmetry were able to displace tangentially to the planes, but were restrained normal to the planes of symmetry. The outer sides of the model were also constrained in the same way, as these faces were also planes of symmetry against neighbouring dots. A full dot for the same coverage, line ruling and plate thickness as the quarter dot was also developed. The boundary conditions for the full dot were set along the sides of the square bounding the dot, so that displacement tangential to the faces was possible, but movement normal to the faces was not permitted. The boundary conditions for the two models are shown in Figure 5.

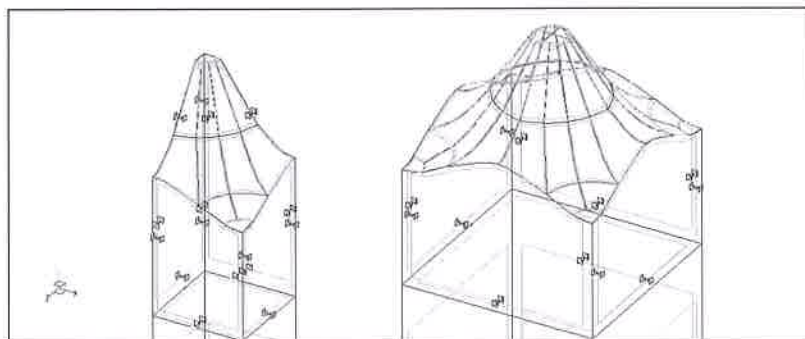


Figure 5: Models of quarter and full dots

Both models were tested using an engagement of $50.8\mu\text{m}$. When the results for the two models were compared, the results for the maximum stress were higher for the quarter dot than for the full dot. This was because the constraints for the quarter dot were positioned along the planes of symmetry of the dot, which extended to the dot surface itself. For the full dot however, the constraints stopped below the shoulder of the dot, and the whole dot was free to displace in all directions as shown in Figure 6. Table II compares the displacement and the maximum stress for the same node for the quarter dot and the full dot models. The selected node is situated along the perimeter of the dot, along a plane of symmetry, which for the quarter dot model, was constrained in the z direction, but was able to move in the x and y directions. The node for the full dot model was free to move in the x, y and z directions. The displacement in the x direction is larger for the quarter dot model than for the full dot model. A small displacement also occurred in the z direction. This was attributed to the discretisation of the model into irregular finite elements, due to the use of an unstructured mesh, where the force and displacement on each element is a function of neighbouring elements. As the displacement in the z direction was restrained for the quarter dot model, the surrounding elements were affected, which resulted in higher maximum stress, and a larger displacement in the x direction to compensate for the restricted movement in the z direction. It was concluded that the use of an unstructured mesh, whilst allowing specific regions to be examined in greater detail, increased the error when used in conjunction with a plane of symmetry cutting a region of interest. Therefore, the modelling was performed using the full dot model as the quarter model introduced computational errors.

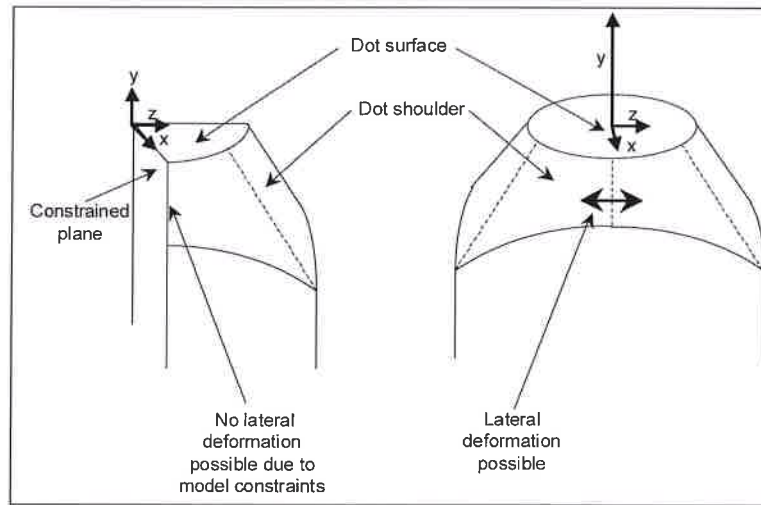


Figure 6: Deformation mechanisms for quarter dots and full dots

Table II: Comparison of displacement for quarter and full dots

	x displacement (μm)	y displacement (μm)	z displacement (μm)	Max. stress (Nmm^{-2})
Quarter Dot	4.004	-50.8	0.000	3.118
Full Dot	2.853	-50.8	0.021	2.682

To analyse the deformed dot profile, nodes on the shoulder of the dots were identified, starting from the top of the dot, working downwards. The height of each node was calculated to determine how much of the shoulder had bulged to form part of the dot surface. A tolerance of $1\mu\text{m}$ was applied from the top of the dot, due to the discretisation of the structure into finite elements and to simulate the natural surface roughness of the dots on the plate. All nodes within the tolerance were considered to be part of the top surface. It was necessary to interpolate between the two nodes directly above and directly below the tolerance threshold, so that the radius of the dot surface after deformation could be determined.

The effect of the shoulder profile at 45° to the line ruling and along the line ruling was analysed to investigate its effect on the dot radius. Two nodes on the perimeter of a 10% coverage dot were determined, and their co-ordinates obtained. One node was on the edge of the dot at 45° to the line ruling and the other was on the edge of the dot along the line ruling. Using the final co-ordinates of the nodes, dot areas and hence coverages were determined based on the two radii. The effect of the shoulder profile is minimal affecting the results for the coverage by 0.04% only (Table III). Coverages were subsequently calculated using the profile at 45° to the line ruling, as the profile along the line ruling existed up to the 30% coverage only.

Table III: Effect of shoulder profile on coverage

Profile	Dot radius (mm)	Coverage	Difference
45° to line ruling	23.03	5.81%	0.04%
Along line ruling	23.12	5.85%	

3. Analysis of the flexographic plate

Two mechanisms were identified from the FEM analysis for the deformation of a flexographic dot (Figure 7). The first is lateral expansion of the dot surface as it is compressed. The amount of expansion is dependent on the Poisson's Ratio (ν) of the material. As Poisson's Ratio increases, the lateral strain increases, for a given longitudinal compressive strain. For the flexographic plate, which has a high Poisson's Ratio, lateral expansion is a significant mechanism of tone gain. The second mechanism of deformation concerns the shoulders of the dot barrelling, and becoming part of the dot surface. Barrelling is governed by the Young's Modulus (E) of the material. For a stiff material with a high value of Young's Modulus, little or no barrelling will occur. The flexographic plate, with a low value of Young's Modulus, is much less rigid, allowing barrelling to occur.

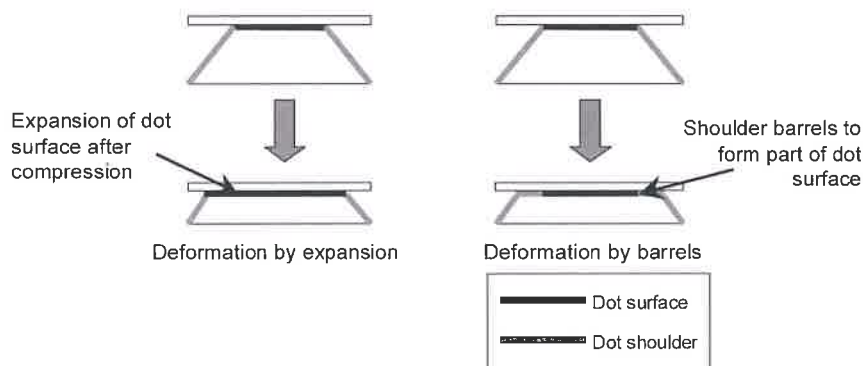


Figure 7: Two mechanisms of dot deformation

Through the highlight region, the contribution to plate gain caused by dot expansion increased as coverage increased (Figure 8). Through the midtones, the plate gain due to dot expansion decreased slightly as coverage increased. Between 40% and 50% nominal coverages, a sharp decrease in gain due to dot expansion was observed, as the dot structure changed from square to linked dots. As coverage increased further towards solid, the effect of dot expansion was negligible. The curve of plate gain due to dot barrelling shows that for low coverages, there is an initial sharp decrease, as the dot area increases and the dot gains stability. As the coverage increases further, the dot perimeter increases, permitting increased gain due to dot barrelling. As the coverage approaches solid, the perimeter decreases, resulting in decreasing plate gain due to barrelling.

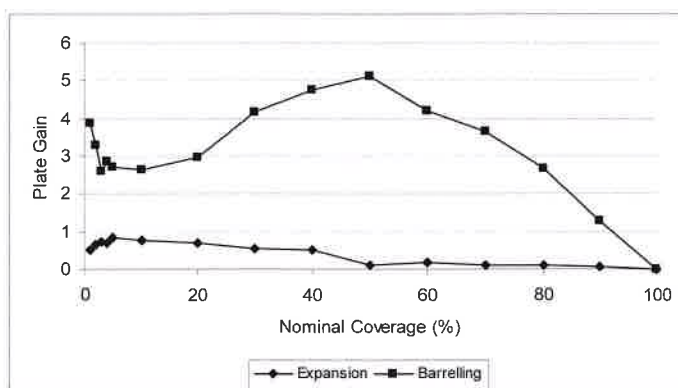


Figure 8: Effect of plate gain mechanisms for increasing coverage

The effects of dot expansion and dot barrelling on the three dot structures are shown in Figure 9 for the 59.1 lpcm line ruling at an engagement of 50.8 μ m. At low coverage, the gain due to deformation of the dot is large for both dot expansion and dot barrelling. As the coverage increases and the dot structure

changes to square, there is little change in the gain due to the expansion of the dot surface, with most gain due to the barrelling of the dot shoulders. For the high coverage linked dot structure, no gain due to dot expansion was observed, with only a slight amount of gain due to dot barrelling evident.

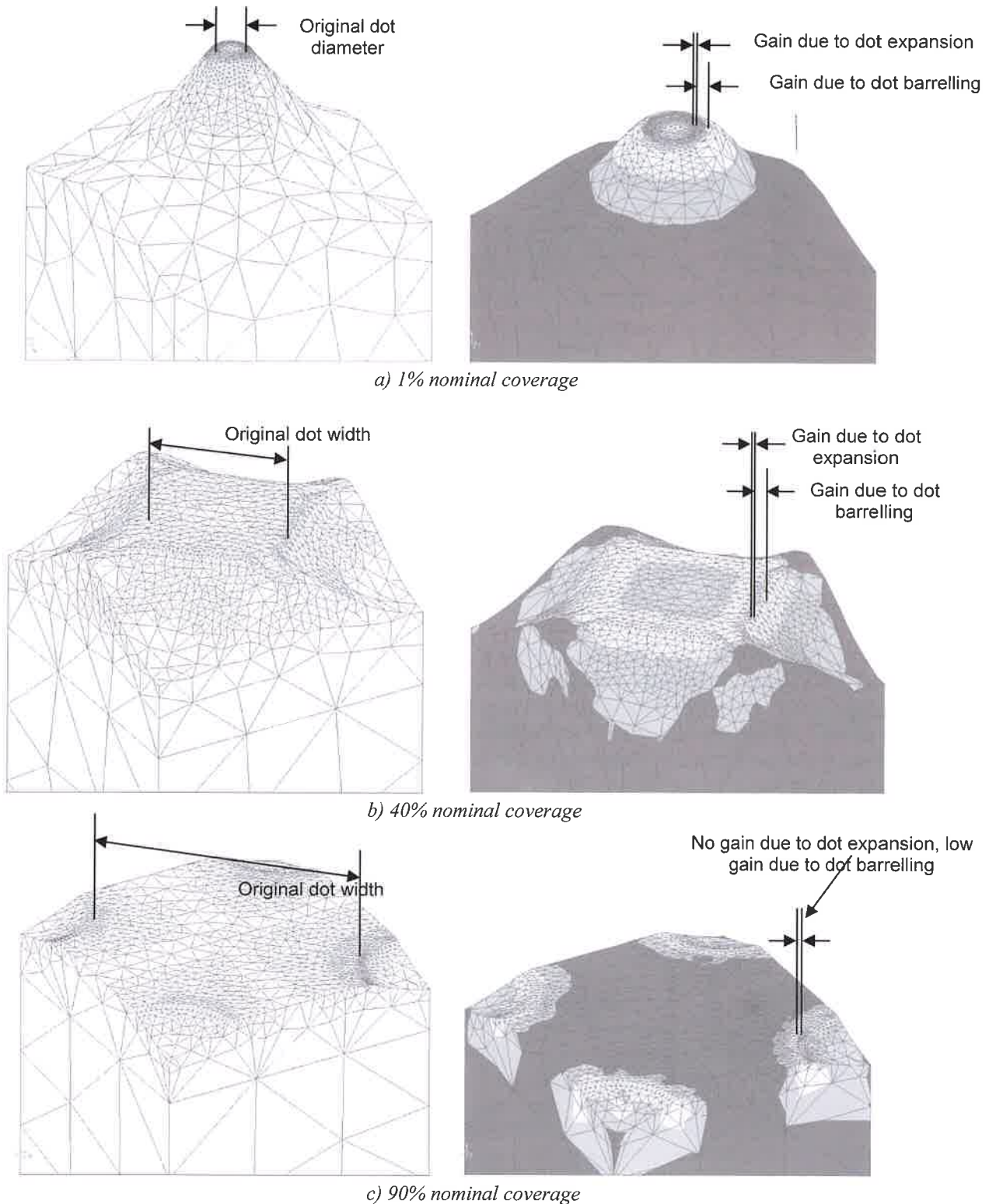


Figure 9: Effects of dot expansion and barrelling for different dot structures

The effect of variations in line ruling on tone gain is shown in Figure 10 for a 50.8 μ m engagement on the 1.70mm plate. The tone gain is calculated relative to the dot coverages measured in (Bould 2001) and not the nominal coverages quoted on the plate itself. As line ruling increases, tone gain increases. As line ruling increases, there is little change in the tone gain resulting from the expansion of the dot surface. All of the increased plate gain is therefore due to the barrelling of the dot shoulder, which is caused by a greater dot perimeter to dot area ratio, due to the smaller dot area of higher line rulings.

In terms of overall print quality, the use of higher line rulings, while enabling more complex images to be printed results in greater tone gain. This analysis does not show how the effect of a rolling contact between the impression cylinder and the printing plate would affect the two mechanisms of tone gain. However, the radius of the impression cylinder is large compared to the size of a single dot on a plate and therefore the effect is likely to be small.

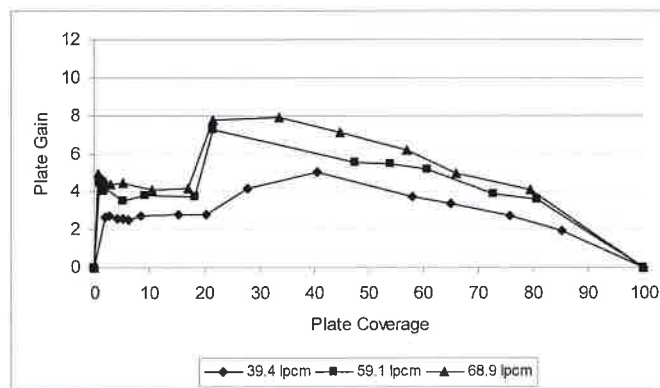


Figure 10: Effect of line ruling on plate gain for actual plate coverages

The effect of engagement on tone gain is shown in Figure 11. As engagement increased, tone gain increased, with larger differences between consecutive engagements for low coverages. For higher coverages however, there was very little difference between consecutive increases in engagement. The difference was attributed to the effects of the two mechanisms of plate gain at the two coverages. It was shown in Figure 8 that both mechanisms contribute to plate gain at low coverages, but only dot barrelling affects the gain for higher coverages. Therefore, as engagement increases, the increase in plate gain is due to increases in both mechanisms at low coverages, but due to only one mechanism in the shadow region of the tonal curve.

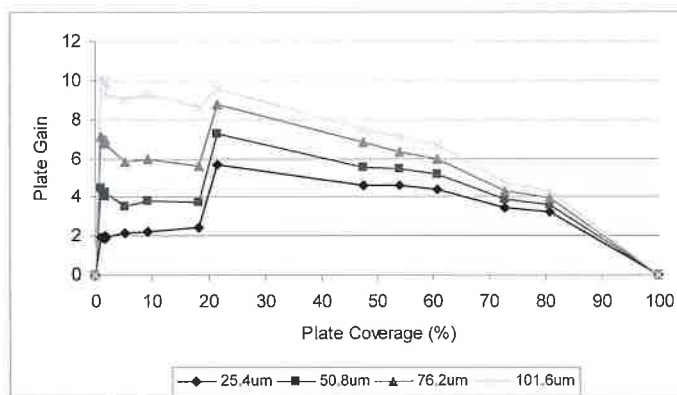


Figure 11: Effect of engagement on tone gain

The effect of engagement on the two mechanisms of tone gain is highlighted by determining the dot expansion and dot barrelling for each engagement of the 5.2% (10% nominal) coverage (Figure 12). As engagement is increased, both dot expansion and dot barrelling increase, with dot barrelling producing the largest effect on tone gain.

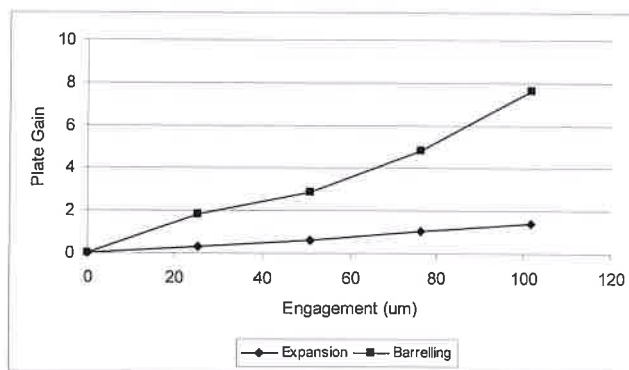


Figure 12: Change in tone gain mechanisms with increasing engagement

The results for the effect of dot expansion and dot barrelling show that engagement is an important parameter, particularly for low coverages, as both mechanisms cause increased plate gain for increasing engagement. Therefore, it is necessary to have accurate control of the amount of impression between the impression cylinder and the printing plate, especially when setting up the press to re-print a job. Unless the press is run with exactly the same impression settings as when it was originally printed, the different tone gain will result in a different image being produced. Although flexographic printing uses a light impression (Hall, 1999), studying the effect of higher engagements aids the understanding of plate deformation, as it enables the two mechanisms of deformation to be examined for a wider range of printing conditions.

The effect of plate thickness on tone gain is shown in Figure 13. The models were tested using a line ruling of 59.1 lpcm and an engagement of 50.8 μm. Both tonal curves display similar trends, with the gain for the 1.14mm plate higher than for the 1.70mm plate. After the 40% nominal coverage, the gain decreases as coverage increases. Analysis of the two mechanisms of plate deformation show that the plate gain due to both dot expansion and dot barrelling is higher for the thinner plate. As engagement increases, the amount of dot barrelling and the dot expansion also increase (Figure 12). For a thinner plate, an engagement of 50.8 μm is a higher percentage of the total plate thickness than the same engagement for a thicker plate. Therefore, the higher gain of the thinner 1.14mm plate may be attributed to a higher relative engagement compared to the thicker 1.70mm plate.

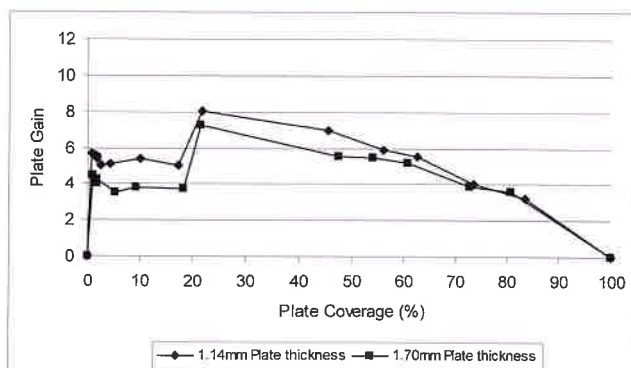


Figure 13: Effect of plate thickness on tone gain

4. Discussion

Analysis of the dot profiles from the measurement of the printing plates revealed three different types of dot structure, dependent on the coverage and accordingly, three types of model were developed. The models were representative of actual plate profiles to obtain results which could be related to the experimental investigation and were defined parametrically using tokens, so that each model represented the conditions that occurred during the experimental investigation. Although the models quantify the levels of tone gain due to the deformation of the plate, they have several limitations. The plate deformation is a dry contact analysis and therefore does not consider any effects of the ink on the process. Due to the comparatively large radius of the impression cylinder, the shell that represented the impression cylinder was assumed to be flat. Displacement was also applied normal to the dot surface instead of rolling across the dot as occurs in the printing nip. The load was also static and therefore did not consider any cyclic effects due to repeat impressions. Although these will affect the results for tone gain due to plate deformation, the models that have been developed provide a good initial assessment of the role of the plate in flexographic printing.

As the flexographic printing plate passes through the nip to transfer ink to the substrate, deformation occurs, which results in tone gain due to plate effects. The deformation is due to two mechanisms, which occur in different proportions under different printing conditions. These two mechanisms of plate deformation are expansion of the dot surface and barrelling of the dot shoulders.

After increasing in the highlight region, dot expansion decreases as coverage increases. Dot barrelling was shown to decrease sharply in the highlight region, due to increasing dot stability. However, it then increased as coverage increased through the midtone region, as the dot perimeter increased. In the shadow region, plate gain due to dot barrelling decreased as the dot perimeter decreased.

Dot expansion and dot barrelling increase linearly as engagement increases for a constant coverage, line ruling and plate thickness, with the majority of gain due to dot barrelling. The decreasing gap between the tone gain curves for higher coverages can be attributed to the decreased significance of dot expansion at higher coverages.

Plate deformation is most significant for low coverages, where the majority of the total gain is due to plate deformation. Large dot depths and small dot areas combine to form unstable dot structures, which deform easily. This has implications for high quality printing of tonal work and the printing of vignettes, as the large dot growth of low coverages prevents the reproduction of coverages approaching zero.

Line ruling has been shown to be a critical parameter for tone gain in flexography. As line ruling increases, the dot area decreases resulting in a greater dot perimeter per unit area of the dot surface. This results in increased plate gain due to barrelling of the dot shoulders. Dot expansion had no effect on line ruling, with all the changes in the plate gain due to dot barrelling.

Engagement has the largest effect on tone gain in flexographic printing with the majority of tone gain due to dot barrelling. As engagement increases, dot expansion and dot barrelling both increase, due to the high Poisson's Ratio and low Young's Modulus of the printing plate material. For high engagements, resistance in the material retards deformation and the tone gain plateaus. In practise the Young's Modulus increases as engagement increases, resulting in a stiffer material. This also retards deformation, causing plateauing of tone gain. Although little further dot growth on the plate will occur, the large amount of plate deformation that has already occurred results in high gain due to the printing plate.

Plate thickness was shown to have a small effect on plate deformation in comparison with parameters such as line ruling and engagement. However, greater deformation occurs for thinner plates than thicker plates, due to a higher relative engagement between the plate and the impression cylinder. Both dot expansion and dot barrelling were greater for the thinner plate. Thinner plates are generally used when

printing halftones and thicker plates are used to print solid regions [5]. However, using thicker plates, where the engagement is a smaller proportion of the total plate thickness, could reduce tone gain.

5. Conclusions

Finite Element Modelling analysis techniques have been used to study the distortion of flexographic printing plates in the printing nip, as these deformations occur at a microscopic level and cannot be assessed experimentally. Models have been developed of three different dot shapes that cover the full tone range. This will enable the allocating the proportion of tone gain due to plate distortion, thus allowing the gain due to ink spreading to be isolated in experimental trials.

The models have generic implications for the distortion of any dot shape. The numerical models assessed the distortion under dry contact conditions with planar contact. This is a precursor to developing a full understanding of the tone gain effects due to the printing plate.

These models have been used for a systematic evaluation of the influence of process parameters on the contribution of the plate to tone gain. The following conclusions can be drawn from this work:

- Deformation of the printing plate is due to two mechanisms, expansion of the dot surface and barrelling of the dot shoulder.
- The contribution of plate deformation to tone gain has been quantified for different printing conditions
- Dot barrelling is the dominant effect in plate distortion.
- Engagement and line ruling have the greatest effect on plate deformation.
- Increasing engagement results in increases in both dot expansion and dot barrelling.
- Increasing line ruling has little effect on dot expansion, but results in greater dot barrelling.
- Dot expansion and dot barrelling are both important mechanisms for low coverage dots.
- Low coverage dots have the highest gain relative to their size, due to low dot stability resulting from a low dot area.
- The high gain and sensitivity at low coverages has implications for the production of images with fine detail.
- Thicker plates may give improved fine detail by making the low coverage dots less sensitive to engagement.

Acknowledgment

The authors wish to acknowledge financial support of the EPSRC, EFTA and the Flexographic Printing Technology Group for this work.

References

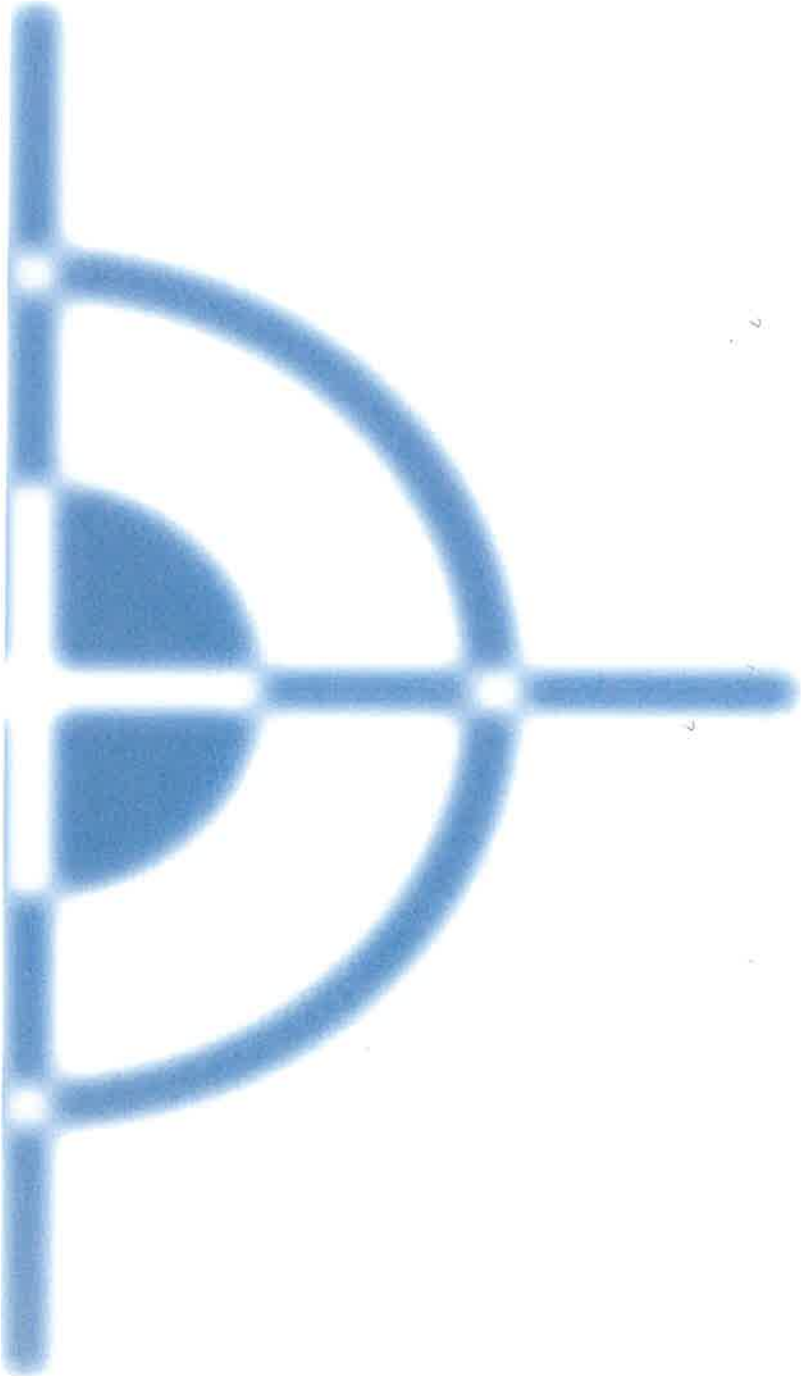
- Bould, D.C. 2001. "An Investigation into Quality Improvements in Flexographic Printing" PhD Thesis, University of Wales Swansea
- Chandrupatla T.R. & Belegundu A.D 1997. "Introduction to Finite Elements in Engineering" 2nd Edition Prentice-Hall
- Rockfield Software Ltd, 1998. ELFEN User Manual, Version 2.7
- Hall R., 1999 Private Communication
- Smith I.M. and Griffiths D.V. 1998 "Programming the Finite Element Method" 3rd Edition, Wiley





4

Printing inks



Drying of water based ink by use of microwave

Ashraf A. El Rhman Saad, Jorge M. Rodriguez Giles

Wuppertal University
Printing and media Technology
Gaußstraße 20, D-42119 Wuppertal, Germany
E-mail: rodi@kommtech.uni-wuppertal.de
E-mail: elsaid@kommtech.uni-wuppertal.de

1. Introduction and aims of the development

Water based inks are seen more and more as an interesting alternative in the aim to reduce the environmental impact of the printing industry, especially to avoid a later release of retained solvent in the ink in the areas of printing packaging material for the food industry. It can not be avoided that some amount of solvents remain retained in the ink, and these solvents, as they later evaporates may cause a potential health hazard and a potential danger to the product through negative effects in the perception of aroma and taste of the packed good. Therefore, the use of water based inks play a vital role in food packaging.

Whereas the printing inks, whose solvent is water has evident advantages such as reducing the environment impact, health and safety hazards as already stated, the drying of water based inks is technically much more difficult than the drying of solvent based inks, namely:

- Owing to the larger vapour heat of water, the length of the dryer is much longer as in for organic solvents. With the usual dryer systems the whole sheet (printing and non-printing areas) is heated, which may be a source for the problems arise with hygroscopic and thermoplastic materials.
- The water content of the ink leads to an unequal distribution of moisture in hygroscopic substrates with unequal change of dimensions as consequence.

Actually, for drying the water based inks, we require a technique which produces only heat on to the printed areas of the sheets, as long as the ink still contains water, without causing thermal effects on to the non- printed areas on the sheets. This means to generate the needed evaporation heat directly to the water molecules in the ink, but not to those in paper.

Dielectric heating and drying in intensive microwave fields fulfil these requirements:

A material with dielectric losses exposed to strong microwave electric field inside a waveguide applicator absorbs energy from the electric field and convert this energy into heat. Materials containing water (such as water based inks and lacquer) belong to those with large dielectric losses, as the strong dielectric dipolar moment of the water molecules rotate following the oscillating electric field, they collide with another molecules and converts electromagnetic energy into heat (ref. 1).

As shown in this paper, an efficient microwave drying system needs also an adequate air circulation to transport away the evaporated water from the ink and keep the temperature to an optimum. Therefore the waveguide applicators where microwave fields are build up have slots for the web passing through it and also outlets for air input and air exhaust.

It is important to note that only such water molecules which can freely rotate, as those in a liquid, show large dielectric losses. This is the case for the water molecules in the ink film. The water molecules in the paper, attached to cellulose fibres are comparable to crystal water and can not rotate freely. This means that with high frequency electromagnetic fields we can dry the ink without drying up the substrate such as paper.

We work at a frequency of 2.45 GHz; this means the same frequency as used in well known microwave ovens in households.

2. Theory of water based ink drying with microwave

In conventional drying, the surface is the warmest part, and temperature decreases towards the interior, when a temperature gradient is built up in a hygroscopic material. More water is vaporized in warm areas than in cool areas and a partial vapour pressure gradient is built up. The gradient is equalized through water movement towards cooler areas.

In microwave heating, the top surface may be cooler than in the inner layers of the substrates, and the moisture may move toward the top surface, and it can escape towards the circulating air.

When a printed paper web is exposed to a strong high frequency electric field, the generation of heat towards the water based inks on the web is achieved by dielectric heating.

The absorption of electromagnetic energy is mainly a consequence of interaction between the alternating electric field and the water molecules as such molecules, which have a very large dielectric moment, rotate trying to follow the direction of electric field.

The generation of heat to evaporate the water from water-based inks depends upon the Frequency f , the dielectric properties, and the square electric field strength (ref. 2):

$$(dP/dV) = 2\pi f \varepsilon_0 \varepsilon' \tan \delta E^2 \quad [1]$$

Where:

- dP/dV : Power per volume unit,
- E^2 : the square of electric field strength,
- f : the wave frequency in MHz,
- $\varepsilon' \tan \delta$ loss factor,
- ε_0 Relative permittivity of vacuum.

This equation is actually the same as the well known for everyone from the classical electro technique for a condenser, with V/d for E and $A \varepsilon_0 \varepsilon' / d$ for the capacity C of a plane capacitor with plate area A at a distance d from another; V is the voltage.

As said in the introduction, the drying of water based ink using microwaves makes possible to overcome the contradiction between following opposite aims:

- to get away the water from the printed ink film in the printing areas,
- to let nearly unchanged moisture of the paper in the non-printing areas.

To achieve this optimal aims the temperature of the printed substrate must be kept nearly at room temperature by using the air circulation in the microwave applicator.

With this low temperature we achieve:

- $\varepsilon' \tan \delta$ is high for water molecules in the ink film (printing ink),
- $\varepsilon' \tan \delta$ is low for paper (non-printing areas).

Now we will try to find an expression for the water evaporation from the ink film in the microwave electric field under the assumption that the temperature of the print remains unchanged (and low, near to room temperature) through convection.

The power P demanded for evaporation of the process in the wave guide for a surface unit is:

$$P = r \frac{dm_w}{dt} \quad [2]$$

Where:

- r : evaporation heat,
- m_w : water remaining in the ink per surface unit.

From [1] we can see that

$$P = c m_w E^2 \quad [3]$$

Where the constant c depends on ϵ_0, f , and the density of water and $\epsilon' \tan \delta$.

From [2] and [3]

$$\frac{dm_w}{dt} = \frac{-cE^2 m_w}{r}$$

This differential equation is easy to solve obtaining:

$$\ln m_w = -\frac{c}{r} E^2 t + C$$

Where C is the integration constant. To get the remaining water in the ink as function of the time we build the exponent of e :

$$m_w = e^C e^{-\frac{c}{r} E^2 t}$$

The value of the integration constant C can be determined from the initial conditions; in the beginning of the drying process, at $t = 0$ is $m_w = m_{w0}$ obtaining:

$$m_w = m_{w0} e^{-\frac{t}{\tau}} \quad [4]$$

Where the characteristic drying time τ is:

$$\tau = \left(\frac{K f E^2 \epsilon_0 \epsilon' \tan \delta}{r} \right)^{-1} \quad [5]$$

K is a coefficient which includes the coupling of the external field in the dielectric; here the water based ink film.

Equation [4] and [5] say us that: In a microwave dryer the amount of water in the ink goes down exponentially, therefore we can not speak of a drying speed in g/m^2s , as in the case of convection or infrared drying, but rather about the characteristic drying time τ or a half time, equivalent to $(\ln 0.5 \times \tau)$. This means that microwave drying is meant specially for the initial drying and should be followed by a convection dryer in order to complete the drying process.

Relevant: the value of $\epsilon' \tan \delta$ remains high as long as the viscosity η of the ink is low, this means as long as a larger amount of water remains in the ink; this is the situation in the first stage of the drying process, as it can be inferred from the Debeye equation: $\epsilon_0 \epsilon' \tan \delta$ is high as long as the so called relaxation time (orientation time) for the water molecules is shorter than the period of the microwave oscillation; this relaxation time Z given by the Debeye equation (ref. 3):

$$Z = \frac{4 \pi \eta a^3}{k T}$$

Where:

- η : the viscosity of the ink film,
- a : radius of the molecules,
- k : Boltzmann constant (1.38×10^{-16} erg/grad),
- T : absolute temperature.

3. Experimental setup

The aim of the experimental part of this work is to confirm that the combination of microwave irradiation with convection leads to a drying of the water in the ink which follows the equations [4] and [5], with low moisture losses for the paper. This means to keep trough convection of the temperature of the web at room temperature, because, as said before:

- this is necessary to evaporate the water in the ink with low moisture losses for the paper,
- The equation [4] assumes that the whole heat developed in the ink film is used to evaporate water from the ink.

We build up the microwave electromagnetic fields in a hollow metallic tube called wave guide applicator. This wave guide, with rectangular cross section may be slotted at the centre of its broad walls (Figure 2) without reducing its ability to keep the fields inside the applicator (ref. 4). The slots are necessary to allow to the printed paper web going through the applicator (Figure 3).

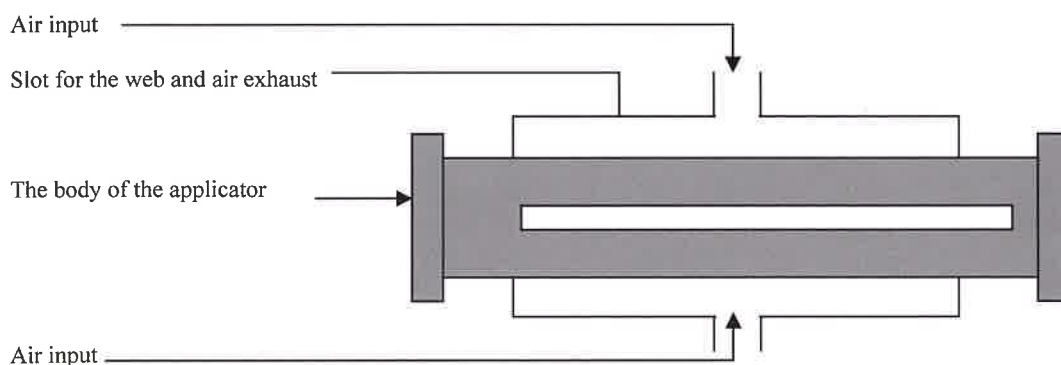


Figure 1: the microwave applicator, including a slot for the web and an air input for convection

On the narrow walls of the waveguide are punched holes which feed an adequate air circulation to remove evaporated water from the ink and keep the temperature of the web trough convection at room temperature.

This dryer system was fixed on a gravure laboratory web press for conducting experiments; to set the relevant process magnitude drying time without changing the applicator, it produces a microwave field over a width of about 4, 3 cm. The work was conducted in four different printing speeds namely 10, 20, 30 and 40 m/min.

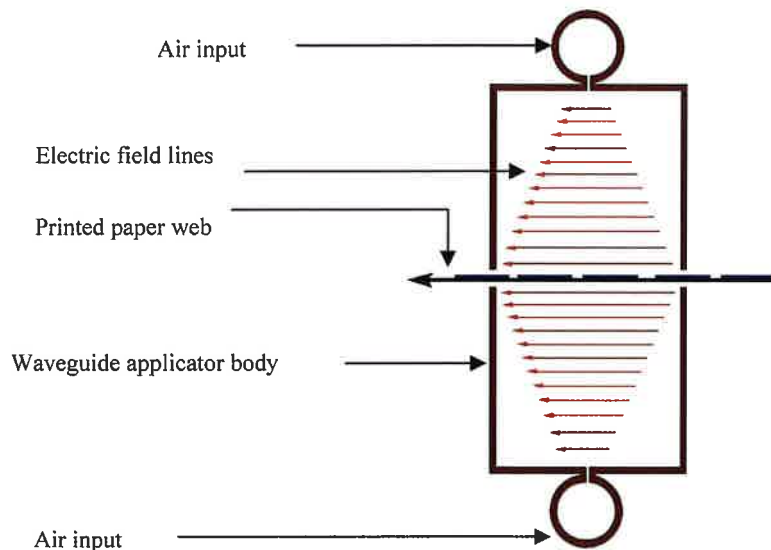


Figure 2: Section of the microwave applicator, including a slot for the web and an air input for convection

Another process parameter was the amount of ink, and thereby the water content in the paper, this parameter was measured in the engraving of the cylinder. We have used cylinders which printed solid tones with different ink film thicknesses. The ink film thickness on the paper corresponded to the following amounts of water on the paper:

Table1:

The ink film thickness on the paper corresponded to the following amounts of water on the paper

Gravure thickness (for 100% transferred ink film) [μ]	Water in the actually transferred ink film [g/m ²]
6	1.8
8	3.7
12	4.4
18	6.1

Further the process magnitudes electric field, air circulation and the status of temperature and relative moisture in the microwave dryer were controlled. The measurement of the water amount in the printing areas and paper without printing were determined from the weight loss after an oven drying of 30 minutes at 105°C.

Now some information about the paper and the inks used in the experiments: we have used 70 g/ m² uncoated paper, with 3- 4% moisture content in the paper and water based inks with a casein based binder having non conductive (*specially no carbon black*) pigmentation. The water amount in the ink was *about* 60 %, with a viscosity of 21-23 s measured with a "Zahn" cup Nr. 4 (ref. 5, 6).

4. Results

As the difference between weight losses of paper with ink on it and naked paper is the amount of water in the ink, to test if the drying results actually follow the equation [4] and [5] we have drawn the diagrams for:

$$u = \ln \left(\frac{m_{w0}}{m_w} \right) \text{ Versus time}$$

Calculated as follows:

$$u = \ln \left(\frac{m_{WF0} - m_{WP}}{m_{WF} - m_{WP}} \right) \quad \text{for} \quad u = \ln \left(\frac{m_{w0}}{m_w} \right)$$

Where:

$$m_{w0} = m_{WF0} - m_{WP} \quad \text{with:}$$

m_{WF0} : Weight loss in the oven of printing areas without MW-drying

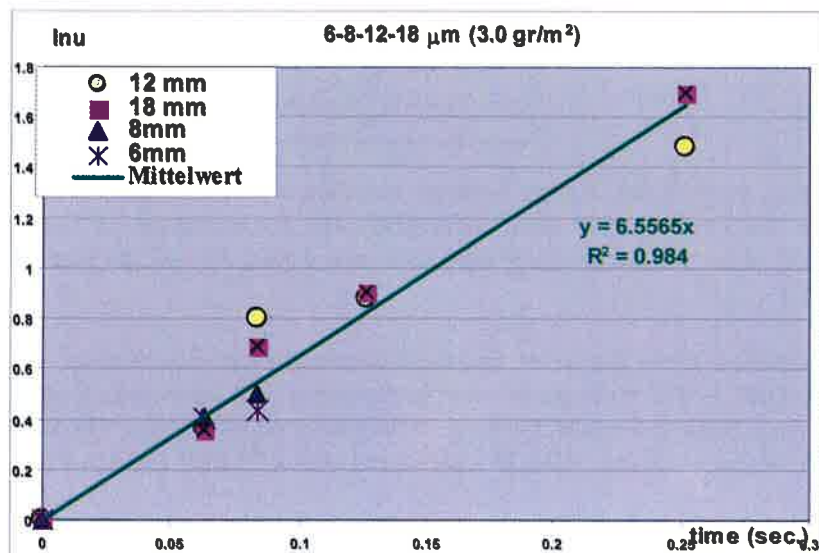
m_{WP} : Weight loss in the oven of naked paper

and: $m_w = m_{WF} - m_{WP}$ with:

m_{WF} : Weight loss in the oven of printing areas with MW-drying

Such diagram should show a linear relationship, with the same slope for different values of m_{w0} . (Picture 1) show the results for a constant electric field value, well under the arc discharge threshold, using a non conductive pigment. This means that an industrial microwave dryer could be operated at this field strength continuously. As it may be seen in picture 3, the time to reduce the amount of water in the ink is of about 0,115 s; it is important that in this time, in which up to 4 g/m² water from the ink was evaporated, the paper reduces its moisture on only 0,4 g/m² or less than 0.3%. With heavier papers the moisture losses of the paper (absolute and relative) increases with the weight of the paper also very quickly.

With carbon black pigmented inks the water evaporation from the ink is still larger as with non conductive pigments.



Picture 1

5. Conclusion and resume of the results

The drying of water based inks with the aid of microwave fields is an interesting alternative because it makes possible to evaporate very efficiently the water of the ink without a strong drying or heating of the substrate. We have found that:

1. The microwave drying, and therefore the applicators must combine the irradiation with microwave energy with an effective air convection to transport the water vapour and to keep the substrate at a low temperature.
2. The drying effects increase exponentially with the amount of water: it evaporates very well the water from thick ink films; the losses of moisture of paper substrates are absolutely and comparatively lower on light papers.
3. As a consequence of the point no. 2, the microwave drying is advantageous especially for the initial drying the microwave stage should be followed by warmed air convection dryer to complete the drying process.
4. As a consequence of the point nos. 2 and 3, the microwave drying is advantageous specially for the drying if thick ink films on light weight papers.
5. As another consequence of the point no. 2, the microwave drying leads to equalization of the amounts of water on the substrate.

As the results of the study shows, we can easily reduce the drying time to an extent of 50%, namely 0.115 s, in other words the water can be dried from 8 g/m² to 4 g/m². During this drying period the naked paper (70 g/e m²) losses only 0.4 g/ m².

This means negligible changes of the dimensions of the paper. The best results were achieved in view of the drying time by use of carbon black pigmented inks, namely about 0, 08 s.

Reference:

- R.V Decareau and R.A .Peterson, Microwave processing and Engineering, Ellis Harwood Ltd. Chichester,England, 1986
- Roger Meredith, „Engineering Handbook of industrial microwave heating“, Short Run Press Ltd., Exeter, England, 1998
- Josef Gefahrt, „Hochfrequenz- Erhitzung in Holz“, Helmut Bücking Verlag Prien/ Chimsee 1962
- Tse V.Chow Tingchan and Howard G. reader, Understanding Microwave Heating Cavities, Artech House, INC, 2000
- Terry Scarlett & Nelson R. Eldred, what the printer should know about ink, GATF, 1984
- FFTA, Flexography printing and practices, Fourth Edition, FTA, Inc & FFTA Inc, USA, 1992



Extensional viscosity of lithographic inks

Anne Blayo

EFPG, 461, rue de la Papeterie, BP 65
F-38402 St Martin d'Hères, France
E-mail: Anne.Blayo@efpg.inpg.fr

1. Introduction – Context of the study

In the context of offset lithography, as well as in many coating processes, the flow of the liquid in a nip is particularly complex, since it results from the combination of shear flow and extensional flow. Several studies [Lyne, 1989; Fu et al. 1994] have pointed out that squeeze flow and fluid extension are the predominant modes of deformation of the ink as it passes through the nip. Consequently, extensional flow is of significant relevance in many practical situations, and its study is still evolving. However, extensional viscosity measurements are far more difficult to carry out than those related to shear experiments, such as flow, creep or oscillation. To our knowledge, no standard technique for ink analysis currently exists for this mode.

In this paper, some theoretical aspects are recalled. Then an experimental study on the evaluation of the extensional properties of offset inks is described. From the results obtained, correlations were found between tack and these properties.

2. Theoretical aspects

Extensional viscosity (η_E) is a measure of the resistance of a fluid to extensional deformation ($\dot{\epsilon}$). The extensional viscosity of a Newtonian liquid is exactly three times that of its shear viscosity: $\eta_E = 3\eta$. In general, η_E is a function of the extensional strain rate $\dot{\epsilon}$, just as shear viscosity is a function of the shear rate $\dot{\gamma}$, for non-Newtonian liquids. Besides, these two functions are often qualitatively different. Indeed, for example, shear-thinning elastic polymer solutions exhibit frequently extensional viscosities that increase dramatically with strain rate [Barnes et al, 1989]. Given their shear-thinning and elastic nature, offset inks may be expected to display similar '*tension-thickening*' behaviours.

In the printing context, tack may be interpreted as a manifestation of the extensional viscosity of offset inks. In most studies concerning the tack of printing inks, there is no clear-cut correlation between tack and other rheological properties. Zang et al. [1991] defined the tack as the magnitude of the peak negative pressure at the exit of a nip which depends on both roller surface speed and fluid properties. The magnitude of this was between 0,2 and 0,4 10^3 Pa, at roller surface speeds of 236 and 690 feet/min, respectively, with ink film thicknesses in the nip of up to 15 μm . It is generally assumed that the tack is strongly related to polymer structure and content in the ink. Thus the inks must be conceived so as to fulfill the requirements of high press speeds, and the tack is one of the critical properties to control.

Tack rises with an increase in the press speed, and this increase might become detrimental to the printing quality, since an ink with excessive tack can even pick the paper surface. This increase in tack with roller speed can be explained by the extensional viscosity variations. A judicious choice of the vehicle formulation (gelling agent and/or "structured" resins) may limit this phenomena. However, as mentioned above, no correlation exists between the tack and the ink properties. As Lyne [1989] pointed out, an attractive idea is to explore the similarity between the rise in storage modulus G' with

increasing oscillatory shear rate (ω), and the rise of extensional viscosity with increasing extensional rate. He recognized however that the major distinction between the storage of elastic energy in oscillatory shear and in extensional flow is the magnitude of the absolute strain. In an oscillatory experiment (linear viscoelasticity), the samples are submitted to very small deformations with respect to their equilibrium position, while very large strain are usually encountered in extensional flow.

In a previous work [Blayo et al, 2000], we studied the variations of tack values of offset inks with the tackmeter roller speed. The experiments were conducted on a Tack-o-Scope. A general pattern of the curves tack vs. speed was obtained (see Figure 1).

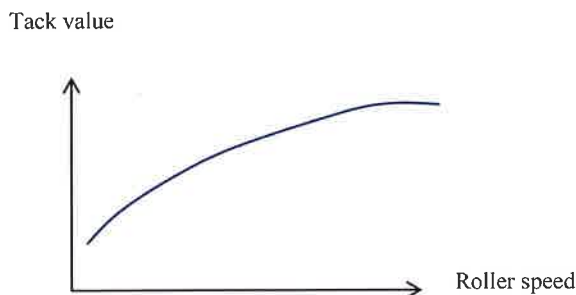


Figure 1: General pattern of the curves tack vs. roller speed

This suggested that the dependence of the tack on roller speed could be represented by a general model, characterised by the following features:

- One can expect the existence of an asymptotic value of tack as the roller speed becomes very high. This value is probably related to the cohesive energy of the ink, i.e. the force necessary to split a viscoelastic liquid at a very high strain rate is likely to be related to its internal cohesion.
- The curve can reach its asymptotic value for small or large values of the roller speed, depending on the rheological properties of the ink, which in turn depend essentially on the polymer properties.
- When the roller speed tends to zero, the tack value is likely to reflect the viscous flow at very low strain rate and could be considered as the counterpart of the limiting value of the extensional viscosity η_E when $\dot{\epsilon}$ tends to zero. It should therefore show the same variations as η_0 and/or η_E .

Given these assumptions, a relationship between the tack and the roller speed was proposed:

$$\tau = \tau_{\infty} - (\tau_{\infty} - \tau_0) \cdot \exp(-\alpha v) \quad (1)$$

where τ is the tack value measured at the speed v (m.s^{-1}),
 τ_{∞} is the 'asymptotic' value of the tack, maximum value,
 τ_0 is the tack value when v tends to zero, minimum value
and α is the inverse of a characteristic velocity.

These three parameters were estimated using the data obtained in this work. In this first approach, τ_{∞} was estimated directly from the curve, whereas α and τ_0 were calculated by a least squares method.

In the present study, we first analysed the flow behaviour and measured the viscoelastic characteristics of a series of offset inks. In parallel, measurements of tack as a function of roller speed were conducted. The curves obtained were analysed according to a model described by equation (1). Then, the extensional viscosity values are deduced from the variations of the filament diameter after step strain, and compared with the tack results.

3. Experimental

3.1 Measurement methods

Flow properties

The steady shear flow analyses of the ink samples were conducted on a rotating rheometer (TA Instr. CSL²₅₀₀), with the cone-plate geometry (diameter = 2 cm, top angle = 4°). Controlled-stress flows were performed from 0 to 500 Pa, during 2 min, at 28 °C.

Viscoelastic behavior

The oscillatory flow experiments were conducted on the same cone-plate rheometer, within the appropriate stress and frequency ranges. Preliminary experiments were performed in order to establish the linear viscoelasticity domain. Oscillation frequencies were scanned in a linear mode, from 0,1 to 10 Hz, at 28°C.

Tack measurements

The tack of the ink samples was measured with a Tack-o-Scope device. Experiments were carried out, using samples of 0,6 cm³, with rotating speeds varying from 50 to 350 m/min, at 28°C.

Filament rheometry

Two geometries have mainly proved optimal in this context: the Filament Stretching Extensional Rheometer (or FiSER) and the Capillary Breakup Extensional rheometer (or CaBER, for simplicity). In the present study, the latter was used. The Capillary Breakup Extensional Rheometer (CaBERTM) is an original concept by Entov and co-workers [1997]. This technique gives a measure of rheological parameters, and, in addition, a measure of characteristic values, such as break-up time, stringiness, etc, which are relevant for the industry. It is already used in the field of paper coating, polymers, foodstuffs, adhesives, etc.

In this device, a small sample of ink is placed between two circular parallel plates (6 mm in diameter). A rapid uni-axial extensional step strain of order unity is imposed to the plates to generate an unstable 'necked' liquid bridge, connecting two cylindrical disks. Then, the plates are held at a fixed axial separation. The filament subsequently evolves under the influence of viscous, elastic, gravitational and capillary forces, without further input at the boundaries. Large extensional strains can still be attained as the mid-region of the filament progressively necks down and eventually breaks. Measuring the time rate of change in the diameter allows material properties of the test fluid to be quantified. For a purely Newtonian material, the diameter vs. time results should be independent of the length of the stretch. A laser micrometer monitors the diameter of the sample at the axial midpoint, as the diameter decreases under the influences of surface tension and gravity.

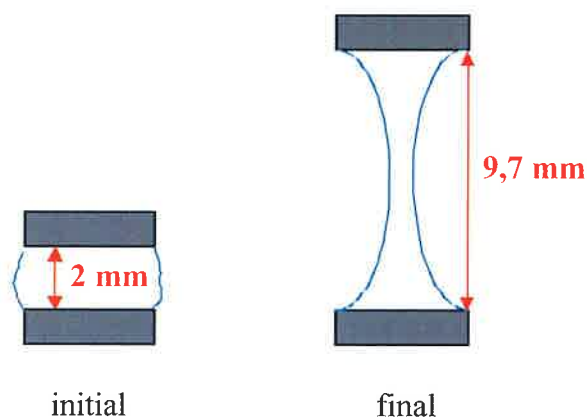


Figure 2a:
Operating principle of the
CaBER rheometer

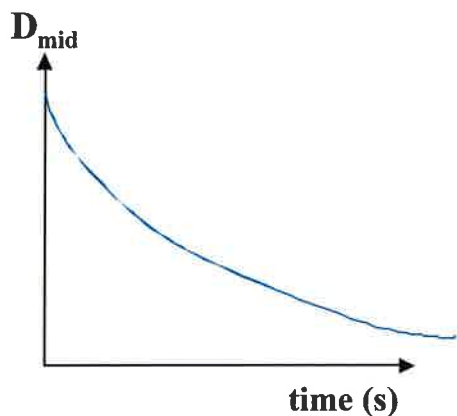


Figure 2b:
Variations of D_{mid} vs. time,
corresponding to Fig.2a

Typically, the raw data is registered as midfilament diameter D_{mid} vs. time, during the necking. The operating principle of the CaBER is described on Fig.2a and the pattern of the corresponding curves D_{mid} vs. time is shown on Fig.2b.

In our experiments, we used the CaBER rheometer of the Technical Center of Paper (Grenoble). The initial gap was 2mm, and the final gap was 9,7mm, the extension being completed within 20 ms. Temperature was 28°C. For each sample, the measure was made at least twice, in the same operating conditions.

According to Anna and McKinley [2001], the initial axial separation of the plates may be viewed as the elongational equivalent of a “step-strain” experiment, provided that the separation rate E is much faster than the viscoelastic relaxation time in the fluid ($E \gg 1/\lambda$) and the time scale for capillary drainage ($E \gg 2\sigma/\eta_0 D_0$, where D_0 is the initial diameter of the mid-region of the filament).

The Hencky strain $\varepsilon(t)$ experienced by the fluid element at the axial mid-plane at time t can be defined, using the mid-filament diameter by [Schümmer and Tebel, 1983; Anna and McKinley, 2001]:

$$\varepsilon(t) = 2\ln(D_0/D_{mid}) \quad (2)$$

Thus, the extensional instantaneous deformation rate at the axial midplane ($\varepsilon'(t)$) can be deduced from $R_{mid}(t)$ measurements by:

$$\varepsilon'(t) = -2/R_{mid}(t) \cdot dR_{mid}(t)/dt \quad (3)$$

Then, an instantaneous extensional viscosity η_{Eapp} can be defined:

$$\eta_{Eapp} = -\sigma / (2dR_{mid}(t)/dt) = -\sigma / (dD_{mid}(t)/dt) \quad (4)$$

where σ is the surface tension of the liquid.

3.2 Ink samples

In this paper, the results presented concern a series of 8 offset inks, designated by Ink1, Ink2...Ink8, respectively, with different gradually increasing tack values. Their basic formulations are similar, unless their resin contents. These inks have similar surface tension, from 30 to 35 mNm⁻¹.

4. Results and discussion

4.1 Shear viscosity

All the samples presented at 28°C a classical shear-thinning behaviour, which can be modelled by the Cross model [Barnes et al, 1989].

Table I gives the values of the viscosity at low shear rate ($\sim 0,02 \text{ s}^{-1}$) and the value of the viscosity at the end of the shear experiment (500Pa). The values of second group tend to the values of η_{∞} , of the Cross model, whereas the first group of viscosity values tends to the zero-shear viscosity η_0 of the model.

Table I: Viscosity (Pa.s) of ink samples, at 28°C

	Viscosity at $0,02 \text{ s}^{-1}$	Viscosity at 500Pa
<i>Ink1</i>	377	12,5
<i>Ink2</i>	402	17,2
<i>Ink3</i>	424	25,3
<i>Ink4</i>	1412	48,5
<i>Ink5</i>	1586	75,5
<i>Ink6</i>	1314	76,6
<i>Ink7</i>	1066	109
<i>Ink8</i>	700	165

As expected, given the composition of these inks, the viscosity measured at 500 Pa, which is similar to the plastic viscosity (according to Bingham), is increasing with the number of ink. On the contrary, anomalous results were obtained for the low shear-rate viscosity (at $0,02 \text{ s}^{-1}$), especially for Ink5, Ink7 and Ink8. This was confirmed by the viscoelastic characterisation below.

4.2 Viscoelastic properties

Oscillatory shear experiments gave the viscoelastic characteristics of the samples, at 28°C.

The values of elastic modulus G' (Pa), dynamic viscosity η' (Pa.s) and loss tangent $\tan\delta$ measured at 1Hz, are presented in Table II.

Table II: Viscoelastic properties of ink samples, at 28°C

	G' (Pa)	η' (Pa.s)	$\tan\delta$
<i>Ink1</i>	6,4	16,3	19,2
<i>Ink2</i>	10,2	26,1	19
<i>Ink3</i>	17,9	41	17,3
<i>Ink4</i>	123,3	108	6,6
<i>Ink5</i>	148,6	125	6,4
<i>Ink6</i>	194	150	5,8
<i>Ink7</i>	152	126	6,2
<i>Ink8</i>	265	200	5,7

As previously mentioned for the shear results, Ink7 and Ink8 have unexpected behaviour. On the other side, the properties of the inks of this series is coherent from Ink1 to Ink6: the elastic character is less pronounced for Ink1 to Ink3 (large values of $\tan\delta$).

4.3 Tack measurements

Figure 3 presents the variations in the tack of the samples as a function of the roller speed. Similar curves were obtained by Oittinen [1976], with different laboratory inks. Then, the model proposed in equation

(2) was applied to these results. Table III regroups the values of the constants of the model calculated for the ink samples. The model was not successfully applied to the samples Ink5, Ink7 and Ink8, given the errors of measure on these samples. This corroborates the particularities already observed in other rheological experiments for these samples, and may be attributed to a lack of homogeneity of these inks. However, for the other samples, the results confirm some of the observations made in a similar context [Blayo et al., 2000]. The constant α follows the elastic character of the sample, at last for the four first inks. The constant τ_0 varies in the same manner as the viscosity at low shear rate, which was also previously noted.

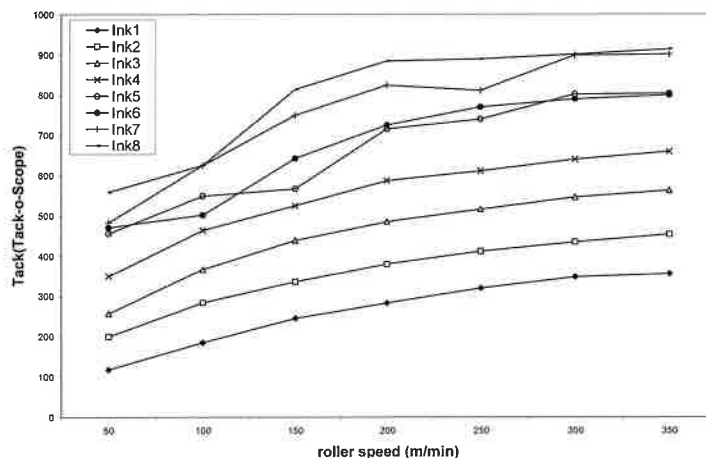


Figure 3: Tack vs. roller speed

Table III: Constants of equation (2), for the ink samples

	τ_0	τ_∞	α
Ink1	23	420	0,0053
Ink2	96	499	0,006
Ink3	107	595	0,0074
Ink4	200	693	0,0073
Ink6	308	915	0,0052

4.4 CaBER results

Figure 4 gives an example (here for Ink3) of the variations with time of the diameter of the filament at the mid-point. Similar curve patterns were obtained with all the ink samples. One can notice that the filament diameter came to an equilibrium value, but it did not break. From these curves, the values of $dD_{mid}(t)/dt$ at the beginning of the extension was calculated. It was then possible to calculate the apparent extensional viscosity η_{Eapp} according to equation (4). For this calculation, the surface tension σ of the inks was estimated at 35 mNm^{-1} . This value may be taken identical for all the samples, given their oleo-resinous nature.

Table IV compares the apparent extensional viscosity, estimated from the curves and the τ_0 values obtained from the model (equation (2)).

Table IV: Constants of equation (2), for the ink samples

	$\eta_{Eapp}(\text{Pa.s})$	τ_0
Ink1	72	23
Ink2	94	96
Ink3	135	107
Ink4	226	200
Ink6	388	300

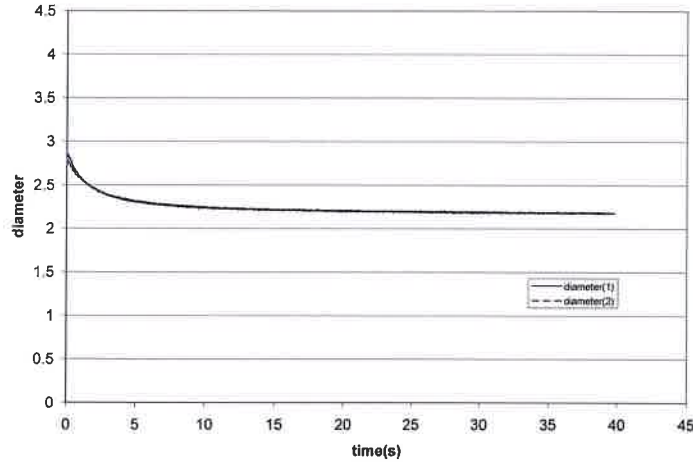


Figure 4: Example of variations of diameter vs. time

It is interesting to note that these two values follow the same tendency, although they were obtained from distinct devices. The two measurements consist in the extension of the same liquid, but η_{Eapp} has the dimension of a viscosity and is obtained from the CaBER experiments, while τ_0 may be considered as a stress and is obtained from the Tack-o-Scope. These observations confirm the hypothesis mentioned in our previous work, namely, the value of τ_0 reflects the extension characteristics of the ink filaments.

5. Conclusion

In this paper, a complement of interpretation is proposed to the tack phenomenon. It was possible to compare classical tack measurements on a tackmeter on the one hand, and extensional viscosity, measured on the CaBER extensional rheometer, on the other hand. In addition to flow and viscoelastic properties of the inks, this type of measurement contributes to a better understanding of tack, and brings another knowledge of the ink properties. This can also help to predict typical behaviours on the press, such as picking of the paper or ink misting. Picking is directly related to the tack, thus to the extensional viscosity of the ink. Misting occurs when an ink filament is likely to break at several points; one can expect that experiments on CaBER rheometer can help in a better analysis of this phenomenon, as the filament break may be observed by this technique.

Further investigation is still needed in this context.

Acknowledgements

We wish to thank David Guérin, from the Technical Centre of Paper, Grenoble, who allowed us to use the CaBER rheometer, and Fatou Diop for her work on this project.

Literature references

- Anna S.L. and McKinley G.H. (2001), *Elasto-capillary thinning and breakup of model elastic liquids*, *J. of Rheology*, **45**, pp. 115-138
- Barnes, H. A., Hutton J. F. and Walters, K. (1989), *An introduction to rheology*, Elsevier

- Blayo A., Gandini A. and Medlege F., (2000), *Rheological characterization of printing inks: correlation between laboratory and press performance*, *TAGA Proceedings*, pp. 662-679–
- Entov V.M. and Hinch E. J., (1997), “*Effect of a spectrum relaxation times on the capillary thinning of a filament of elastic liquid*”, *J. Non-Newtonian Fluid Dyn.* **72**, 31-45
- Fu, T. Z., James, D. F. and Lyne, M. B., (1994), *Measuring the extensional rheology of printing inks*, *International Printing and Graphic Arts Conference*, pp. 3-12
- Lyne M. B., (1989), *The importance of extensional viscosity in the impression of ink into paper during printing*, *Advances in Printing Science and Technology*, vol. ??, pp.236-248
- Oittinen, P. (1976), “*Fundamental rheological properties and tack of printing inks and their influence on ink behaviour in a printing nip*”, *Ph.D. Thesis, Helsinki University of Technology*
- Schümmer P. and Tebel K.H., (1983), *A new elongational rheometer for polymer solutions*, *J. of Non-Newtonian Fluid Mechanics*, **12**, pp. 331-347
- Zang, Y. H., Aspler, J. S., Boluk, M. Y. and De Grâce, J. H., (1991), “*Direct measurement of tensile stress (tack) in thin ink films*”, *Journal of Rheology*, Vol. 35, n°3, pp.345

Examining the mechanism of ink transfer

Ikuo Naito, Yoshiaki Nitta, Satoshi Fujiki, Kazuyuki Shibata, Keiko Koga*

Dept. Photography, Kyushu Sangyo Univ.
Matsugadai 2-3-1, Higashi-ku, Fukuoka 613-8503, Japan
E-mail: naitou@ip.kyusan-u.ac.jp

Abstract

We studied ink transfer by observing the printed surface immediately after printing using cast-coated papers and black offset proofing ink. There are many ink peaks on the surface. As there was the same number of ink peaks on the ink roll after trapping, we concluded that the ink transfer progressed via cavitation theory. The number of the peaks decreased as the amount of trapped ink (y) increased for various nip widths. We observed many ink peaks in ink trapping using plastic sheets. At $y = \text{ca. } 1.0 \text{ g m}^{-2}$, air from the paper seems to affect ink trapping because there were one fourth fewer ink peaks on the plastic sheet than on the cast-coated paper. Therefore, we studied ink trapping using coated papers (air permeances = 1500 and 5000 s; cast-coated paper, 28000 s). The number of the ink peaks increased as the air permeance decreased. At small y value, small air bubbles from the paper caused cavities during ink transfer as the number of the ink peaks roughly matched the number of pinholes on the paper surface.

Keywords

Air permeance, Cavitation theory, Height of the peak, Number of ink peaks

1. Introduction

Banks and Mill¹⁾ proposed cavitation theory of ink transfer. The photographs of Sjodahl²⁾ and Hull³⁾ of ink lengths between rolls showed that ink trapping progressed according to cavitation theory. There are three hypotheses for the generation of cavities. Lepoutre et al.⁴⁾ proposed that the cavities arise from air from inside paper, while Taylor and Zettlomoyer⁵⁾, and Myers⁶⁾ proposed that they result from the heating of ink owing to dynamic viscosity.

Figure 1 shows a model of ink trapping according to cavitation theory. The ink trapping has the following mechanism. Ink on a roll (ink roll) is pressed on the paper. The pressure between the ink roll and the paper increases initially and then decreased with rotation of ink roll. Under reduced pressure, air bubbles from inside the ink layer. The bubbles grew as the roll pulls away from the paper and ink walls between the bubbles became thin. Sufficiently thin ink walls rupture. The small figure in the right shows a model from bubble formation to cutting of ink walls. Myers et al.⁶⁾ and De Grace et al.⁷⁾ photographed ink filaments and ink peaks immediately after trapping from a horizontal direction. Since these studies produced uni-axial measurements, the cavity measurements are not the unit area. Although Carlsson and Lindberg⁸⁾ photographed ink peaks, but they did not count them.

We studied how to obtain high quality printed matter on a dry printed surface using a gloss meter,⁹⁾ a roughness meter,¹⁰⁾ a scanning electron microscope (SEM),¹¹⁾ and an atomic force microscope.¹²⁾ When a small amount of ink was trapped (y), many ink particles adhered on the surface ($\phi = 5 - 10 \text{ }\mu\text{m}$). Around these particles were very small particles, which looked like ink mists ($\phi = \text{ca. } 0.2 \text{ }\mu\text{m}$). Increasing the amount of ink, the ink particles adhered to the paper in a net-like structure. For $y > 1 \text{ g m}^{-2}$, the surface was completely covered with ink, although unevenly, as the SEM images clearly show. Although these images

are important, direct observation of the wet surface is the most important way to study the ink trapping. We used digital microscopy to analyze the wet surface immediately after trapping.

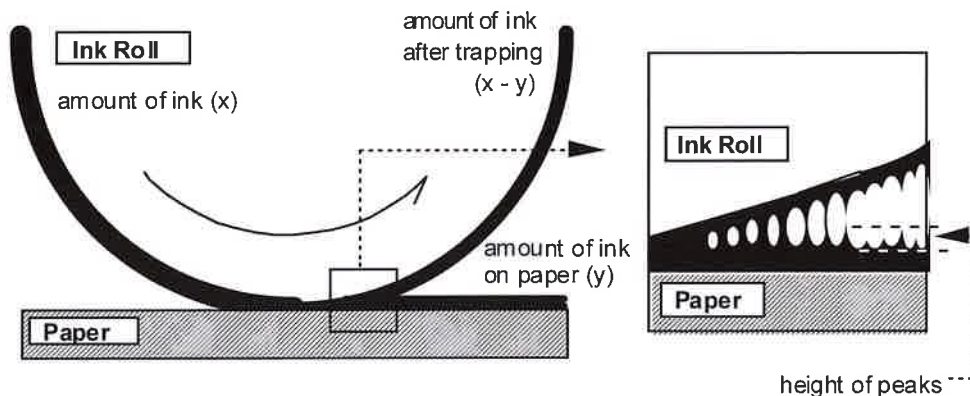


Figure 1: A model of a ink transfer by cavitation theory

2. Experimental

2.1 Sample

Cast-coated paper (Oji paper Co. Ltd.) and two coated paper (Nippon Paper Co. Ltd.) were used as the print substrates with plastic film (PET film, 0.20 mm thickness) and polypropylene film (20 mm film thickness) overcasted paper. The data on the print substrates are listed in Table I. The weight and air permeance are the values reported by the maker. The average roughness (JIS B-0601-1982) of the paper was measured using a Tokyo Seimitsu Co. Ltd. Surfcom type 1400D-12 with a non-contact type laser detector E-DT-SL12A type (cut-off value: 0.8 mm). Three black inks (offset proofing, synthetic paper and web-offset) were used (tack = 15.7, 20.4 and 9.8 at 293 K, respectively). The cast-coated paper (150 g m^{-2}) was used after twice carender treatments ($1.5 \times 10^5 \text{ N m}^{-1}$).

Table I: Physical data of paper

paper	weight / g m^{-2}	air permeance / s	Ra / mm
coated-paper A	128	1700	1 - 2
coated-paper B	128	5000	1 - 2
cast-coated paper	112	28000	0.2
cast-coated paper	157	15500	
cast-coated paper ⁺)	157	18200	
PET film	—	—	0.1
PP overcoated paper	ca. 150	—	0.1

+: after carender treatments

2.2 Ink Trapping

Ink trapping was performed using an AKIRA Seisakusyo Co. Ltd. RI tester RI-4 type at around 293 K. The nip width between the inking and paper rolls was adjusted to 2, 3 and 4 mm. After 10 minutes to

distribute the ink, the ink trappings were carried out. The ink transfer ratio was determined using a Kumagai Testing Machines Co. Ltd. printability tester KRK type at 293 K (printing pressure = 4.9×10^3 and $9.8 \times 10^3 \text{ N m}^{-1}$). The amounts of ink on the ink roll before trapping (x) and on a paper after trapping (y) were determined gravimetrically.

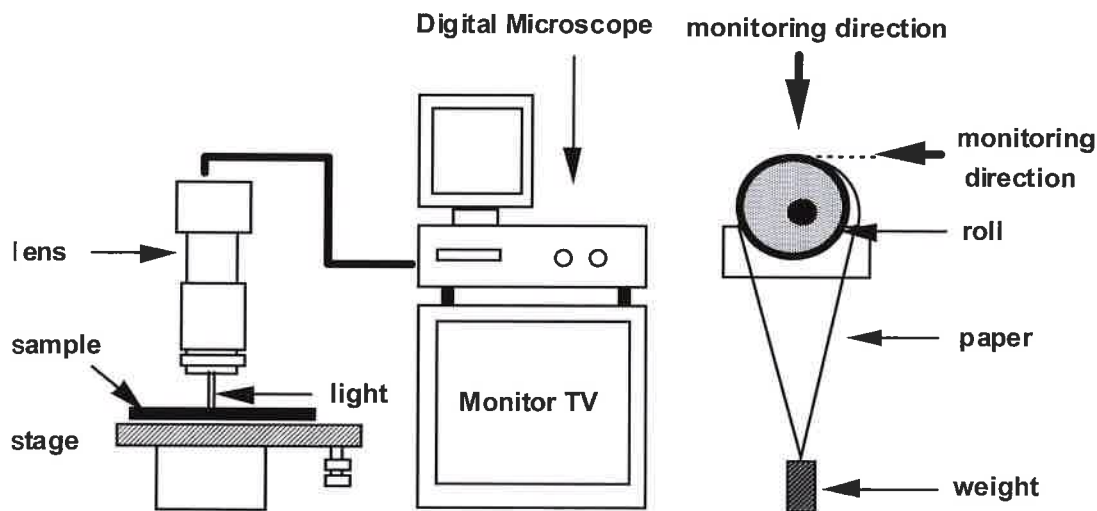


Figure 2: Apparatus of measurement

The surfaces were also observed using a Hitachi S-510 scanning electron microscope (SEM; Hitachi Co. Ltd., Tokyo Japan). Each sample was coated with gold four times for 30 seconds each time to avoid heating the sample at ca. $1 \times 10^2 \text{ Pas}$ using an ion coater (IB-2, Eiko-Engineering Co. Ltd., Ibaragi, Japan). Observations were made from directly above (0°) and at an angle of 70° to the surface (acceleration voltage: 15 - 30 kV; vacuum, ca. $1.3 \times 10^{-3} \text{ Pas}$).

3. Results and Discussion

3.1 Effect of amount of ink on the wet-surface

We studied the ink trapping by direct observation of wet surface immediately after trapping ($30 \pm 3 \text{ s}$).

Figure 3 shows photographs of printed surface [amount of ink (y) = 0.14 (1), 0.89 (2), 1.58 (3) and 3.80 g m^{-2} (4)]. There are many ink peaks on the wet printed surface that seems to be mottles reported by Carlsson and Lindberg.¹³⁾ We measured ink particles on dry printed surface using a SEM and an atomic force microscope. The ink peaks appeared to correspond to the ink particles.

We counted the ink peaks over five times and averaged the result to give the number of ink peaks on the paper ($5.8 \times 10^9 \text{ m}^{-2}$ at $y = 1.1 \text{ g m}^{-2}$). The average deviations are about 10 %. The number of the peaks decreased drastically as the amount of ink trapped (y) increased. Figure 4 shows the relation between the number of the ink peaks and the y value. We studied the effect of nip width as a function of printing pressure on the number of the ink peaks. Although we carried out the ink trappings at several nip widths (1, 2, 3 and 4 mm), a single relation was obtained. Therefore, under the experimental conditions, the effect of printing pressure was small.

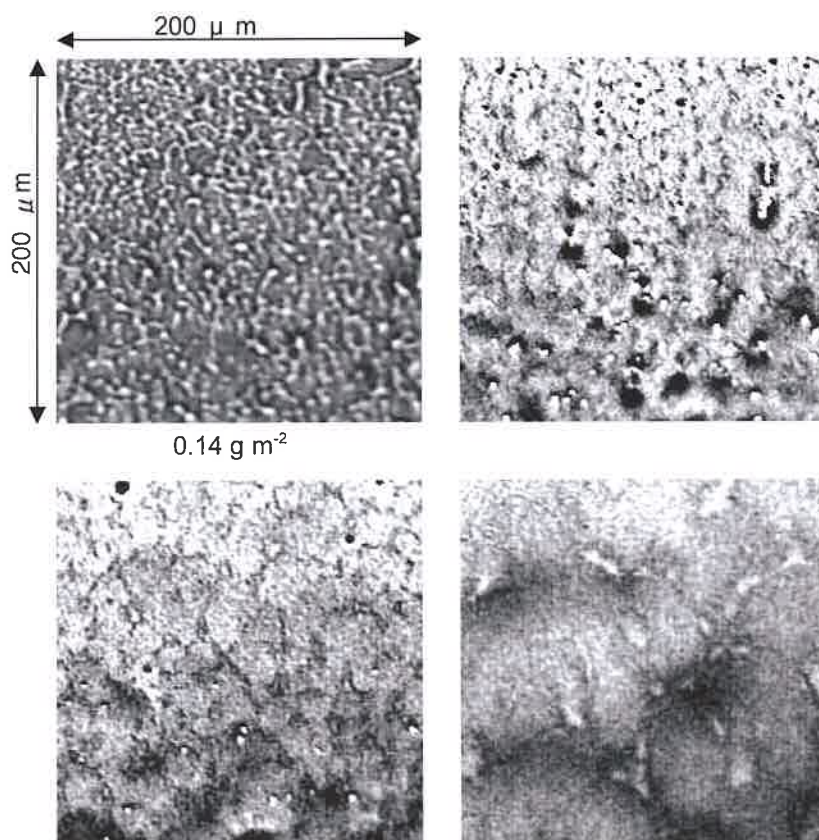


Figure 3

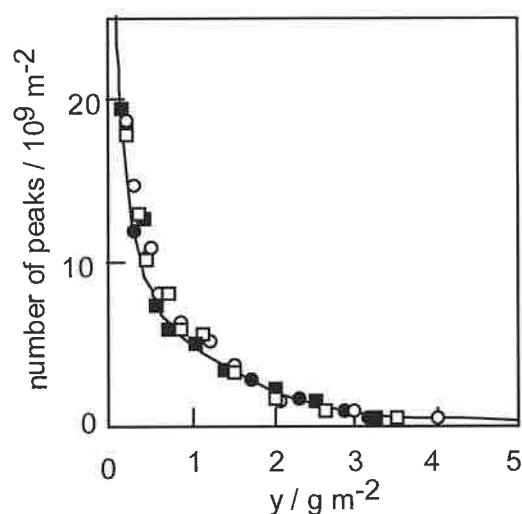


Figure 4: Relation between amount of ink on paper (y) and number of ink peaks. Ink, black ink for offset proofing; paper, cast-coated paper; nip width, 1 (○), 2 (□), 3 (●) and 4 mm (■)

In cavitation theory, the ink trapping progresses via the rupture of thin ink walls between bubbles. The ink peaks are the mark of ruptured bubbles and form on both the paper and the ink roll symmetrically. We expected to detect the ink peaks on the ink roll. The ink peaks on the paper and the roll were counted after sudden stopping the tester during trapping. There were many ink peaks on the ink roll

and the number decreased as the amount of ink increased. When we plotted the number of the ink peaks on the paper (**P**) against the number on the ink roll (**IR**), a good linear relation was obtained with its slope = ca. 1.0 (0.961) [correlation coefficient (**R**) = 0.998], as shown in Fig. 5. The relation can be written as equation 1.

$$P = 0.96 IR + 2 \times 10^7 \quad (1)$$

Therefore, ink trapping must progress according to cavitation theory and the ink peaks result from trapping.

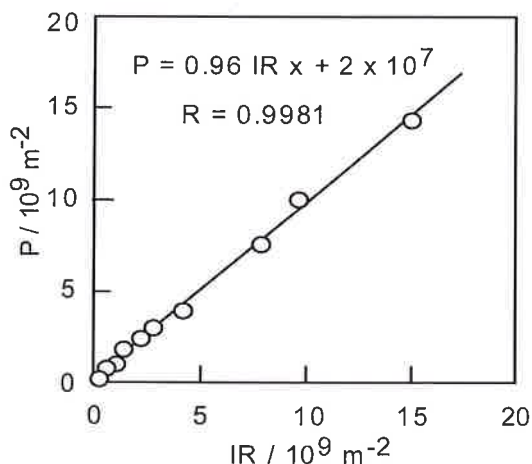


Figure 5: Plots of number of ink peaks on the roll vs. number of ink peaks on the paper in the ink trapping using the cast-coated paper and the black ink for offset proofing

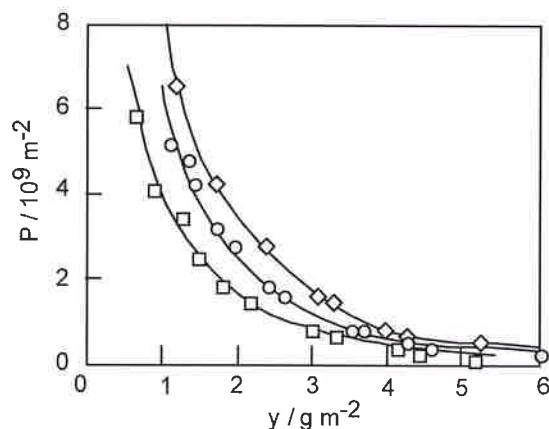


Figure 6: Relation between the amount of ink on paper and number of ink ink peaks. Ink, black inks for web-offset (\diamond), offset proofing (\circ) and syntetic paper (\square). Paper, cast-coated paper; nip widht, 2 mm

3.2 Effect of ink variation

We studied the effect of ink variation using the cast-coated paper and black inks for synthetic paper and web-offset, and detected many ink peaks. With each ink, the number of the ink peaks decreased with increasing the y value as with the black offset proofing ink (Fig. 6). Since it is impossible to adjust the y value, we compared the number at $y = 1.5 \text{ g m}^{-2}$, estimated using regression curves. The order of the number was inversely proportional to tack value of the ink [synthetic paper ink ($P = 2.5 \times 10^9 \text{ m}^{-2}$ at 1.5 g m^{-2} , $1.6 \times 10^9 \text{ m}^{-2}$ at 2.0 g m^{-2}) < offset proofing ink ($3.8 \times 10^9 \text{ m}^{-2}$, $2.5 \times 10^9 \text{ m}^{-2}$) < web-offset ink ($4.9 \times 10^9 \text{ m}^{-2}$, $3.5 \times 10^9 \text{ m}^{-2}$)]. Although we controlled the ink distribution (milling) time on the tester (5 to 30 minutes) using the offset proofing ink before trapping, the number was independent of the time.

Unlike the number of the ink peaks, the peak height 30 s after the trapping increased slightly with increasing the y value for each ink, as shown in Fig. 5.¹⁴⁾ At same y value, the height of the peak increased with the tack value [web-offset ink (6 - 13 μm), offset proofing ink (10 - 15 μm) and synthetic paper ink (17 - 23 μm)].

3.3 Effect of print substrate

To clarifying the effect of printing substrate on the number of ink peak, we studied the ink trapping using three coated papers with different air permeances [= 1500 s (coated paper A), 5000 s (coated paper B) and 28000 s (cast-coated paper)]. Figure 7 shows SEM image of the paper surface. Black dot on the image seems to be pinhole on the paper. The black dots in the images are small pinholes in the paper.

There are small pinholes ($\phi = \text{ca. } 2 \mu\text{m}$) and some relatively large ones in the coated papers. By contrast, the cast-coated paper has many very small pinholes ($\phi = \text{ca. } 0.2 \mu\text{m}$), which formed during vapor evaporation in paper making. Because the air permeance reflects the average pinhole size and its number, the cast-coated has the largest value.

Using these papers, the ink trapping was examined. The number of the ink peaks decreased with increasing the y value, as shown in Fig. 8. Using the regression curves, the estimated number at $y = 1.5 \text{ g m}^{-2}$ (1.0 g m^{-2}) estimated were $4.1 \times 10^9 \text{ m}^{-2}$ ($7.5 \times 10^9 \text{ m}^{-2}$, coated paper A), $3.1 \times 10^9 \text{ m}^{-2}$ ($6.5 \times 10^9 \text{ m}^{-2}$, coated paper B) and $2.5 \times 10^9 \text{ m}^{-2}$ ($5.0 \times 10^9 \text{ m}^{-2}$, cast-coated paper). For $y = 4 \text{ g m}^{-2}$, the number is small as $4 \times 10^8 \text{ m}^{-2}$ and agrees with that in the plastic film, described below.

The number of the ink peaks seems to depend on the air permeance. Ink trapping was carried out using cast-coated paper after twice carender treatments ($1.5 \times 10^5 \text{ N m}^{-1}$) to increase the air permeance. For the small difference in the air permeances (15500 s and 18200 s), two relations agreed each other.

Since the air permeance of plastic films approaches infinity, they are a good printing substrate to study the ink trapping. We used 0.2 mm poly (propylene terephthalate) (PET film) and 20 μm poly(propylene) (PP) over-coated on cast-coated paper. The relations between the number and the y value are shown in Fig. 8. The relations for the two plastic film agreed each other. Although the number at $y = 1.0 \text{ g m}^{-2}$ ($1.4 \times 10^9 \text{ m}^{-2}$) is one fourth smaller than that of the cast-coated paper at 1.0 g m^{-2} ($5.0 \times 10^9 \text{ m}^{-2}$), the number at $y = 4.0 \text{ g m}^{-2}$ ($4 \times 10^8 \text{ m}^{-2}$) agreed with that of cast-coated paper at 4.0 g m^{-2} .

To increase the air supply from the plastic surface, we used plastic films covered with many scratchers made using emery powder (sand-breathing processing, using three processing steps), as shown in Fig. 7d. The ink adhered to the surface unevenly; attaching in some areas and not in other. The percentage area where no ink adhered, increased with the processing time. This means that the air from the shallow surface scratches partial prevented the adhesion of ink.

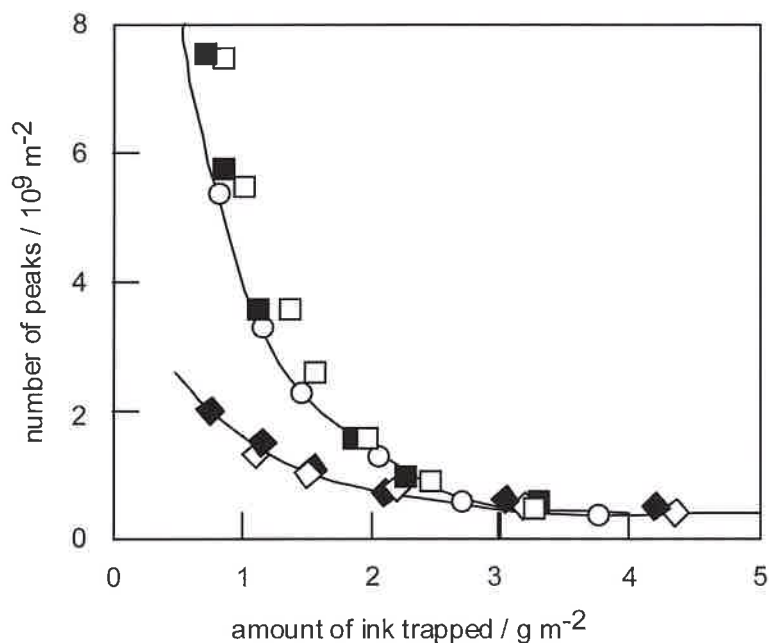


Figure 8:

Plots of the number of the ink peaks (P) vs. the amount of ink trapped (y).

Ink, black ink for offset proofing; printing substrate: cast-coated paper (○), coated paper A (□), coated paper B (■), PET film (◇) and PP overcoated paper (◇); nip width: 2mm.

3.4 Ink transfer equation

Walker-Fetsko's equation¹⁵⁾ for the ink trapping is shown in eq. 2,

$$y = f(x - b) + b, \quad (2)$$

where, x and b are amount of ink before trapping and amount of ink fixed on the printing substrate. The symbol f is a ratio of fractionation for transfer to the paper after fixation ($x - b$). In this equation, the f value suggests that fractionation position; at $f = \text{ca. } 0.5$, the ink layer divides inside of layer; when f is small, the ink layer divided near the surface of the printing substrate.

Using black ink for offset proofing and cast-coated paper, when the y value plotted against the x value (Fig. 9), a good linear relation was obtained with $f = \text{ca. } 0.4$ [$f = 0.41$ ($R = 0.999$) under $4.9 \times 10^3 \text{ N m}^{-1}$; $f = 0.39$ ($R = 0.968$) under $9.8 \times 10^3 \text{ N m}^{-1}$]. This means that the bubbles are generated near the paper surface. Ink trapping was carried out using same ink and the PET film. A good linear x - y relation was obtained. Since $f = \text{ca. } 0.5$, the ink layer was divided inside within itself [$f = 0.52$ ($R = 0.997$) under $4.9 \times 10^3 \text{ N m}^{-1}$, $f = 0.48$ ($R = 0.999$) under $9.8 \times 10^3 \text{ N m}^{-1}$].

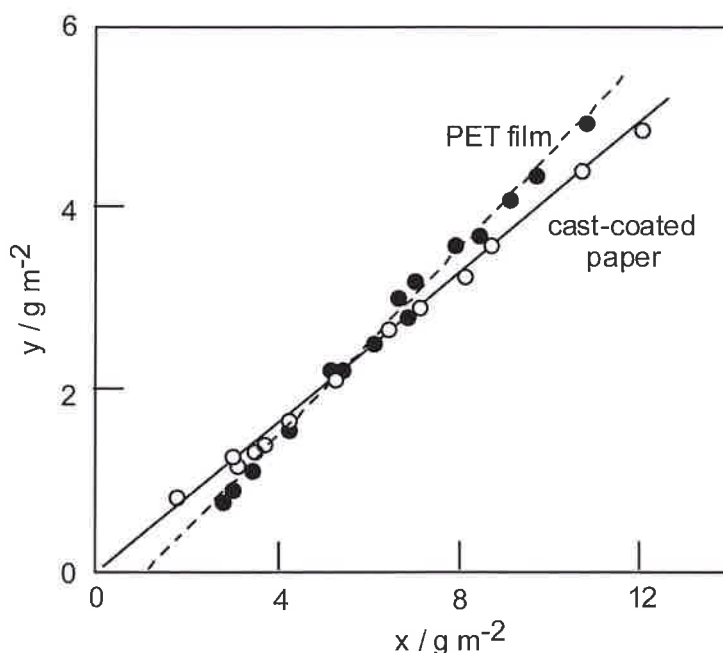


Figure 9: Relation between the amount of ink on ink roll (x) and amount of ink trapped (y).
Ink: Black ink for offset proofing; printing substrate cast-coated paper (O) and PET film (●)

3.5 Generation of cavity

In cavitation theory, why are the bubbles generate? Mechanisms produce printed matter at high speed. Under such conditions, bubbles seem to form under reduced pressure in the ink layer, if the ink contains compounds that are volatile at low temperature. Although the offset proofing ink is a non-solvent type, scentless material, it contains a small amount of low molecular weight compounds. There are many pinholes on the paper surface, as shown in Figure 7. Before the ink transfer, we must distribute ink sufficiently. Since the ink is pressed and separated between the rolls, many small air bubbles seemed to be suspended in the ink layer. Therefore, the nucleus of a cavity seems to arise via the following mechanisms:

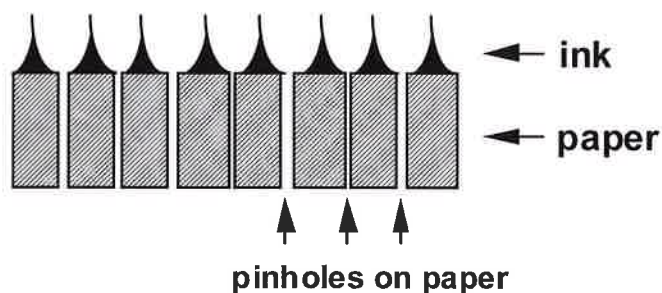
- Mechanism 1: effect of volatile compounds,
 2: air supply from paper surface,

- 3: fixed air between paper surface and ink surface,
- 4: suspended air bubbles.

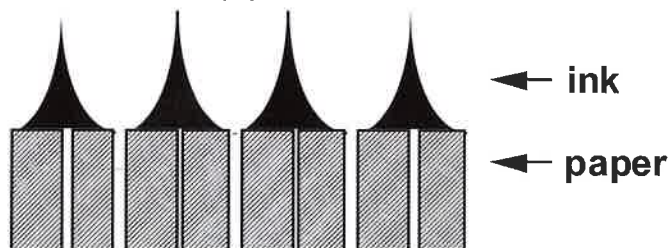
The number of the ink peaks is larger on the paper than on the plastic film. Since the effects of mechanisms 1, 3 and 4 are independent of the printing substrate, this difference must depend chiefly on the printing substrate. When a small amount of ink trapped, the number increased with decreasing the air permeance. Nozima calculated the number of the pinhole to be $7 \times 10^9 \text{ m}^{-2}$ on the cast-coated paper.¹⁶⁾ This number agreed well with that of the ink peaks at $y = \text{ca. } 0.8 \text{ g m}^{-2}$. The air permeance is the time required for a constant amount of air to pass through the constant area independent of pinhole size. In fact, the ink attached unevenly to the surface of the plastic sheets with many small shallow scratches. Therefore, the ink peaks must depend on the pinholes at small y value. Increasing the y value, the number of the ink peaks decreased to that on the plastic sheet.

We propose a model that gives the number of the ink peaks, as shown in Fig. 10. At small y value, the ink peaks formed pinholes on the surface (Fig. 10a). Increasing the y value, narrow pinholes are covered by the ink (Fig. 10b). Around $y = \text{ca. } 4 \text{ g m}^{-2}$, almost all pinholes are covered by the ink and the ink peaks result from other effects (Fig. 10c).

small amount of ink (a)



medium amount of ink (b)



large amount of ink (c)

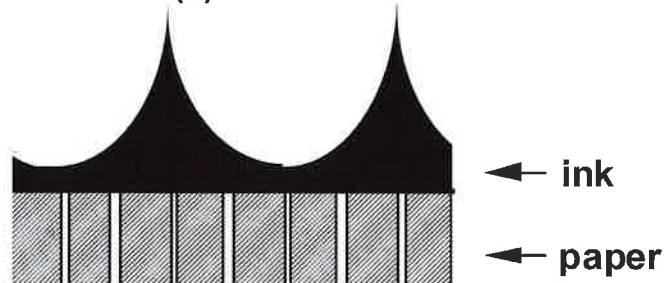


Figure 10: A model for adhesion of ink on paper

If the trapping proceeds by mechanism (1) or (4), the f value must be 0.5, since the cavities form inside of the ink layer. Lower *et al.*¹⁷⁾ and Ichikawa¹⁸⁾ reported the localized generation of heat inside the ink layer during dynamic ink transfer. Aoki¹⁹⁾ reported the relation between the speed ratio of two ink rolls and velocity of laminar flow in the ink layer. Under reduced pressure, the ink appeared to divide at the heated layer owing to shearing stress (mechanism 1). The shearing stress seemed to increase according to the decrease of the y value. Under these experimental conditions, the ratio of speeds was be 1. For the plastic film, the f value for was determined to be 0.5. The number of the ink peaks decreased as the y value increased. Since there is no reason to rule out Mechanism 4, further study of ink trapping on plastic film is needed.

4. Conclusion

We studied the mechanism of ink trapping using cast-coated paper and black offset-proofing ink. Immediately after the trapping, many ink peaks were detected on the surface. As the number of the ink peaks on the paper surface matched that on the ink roll, ink trapping must progress via cavitation theory.

Detailed observations of the number and height of the ink peaks were made. The number decreased and the height increased as the y value increased. Same results were obtained in the ink trappings using the synthetic paper and web-offset inks. Comparing the ink, the number decreased and the height increased as the tack value of the ink increased at the same y value. For the papers, the number increased as the air permeance decreased for the same amount of ink trapped. On the plastic films, the same results were obtained, although the number was one fourth smaller than that on the cast-coated paper. Since the difference in the numbers agrees with the number of pinholes on the cast-coated paper, most cavities likely arise from air supplied from the paper.

5. Acknowledgment

We are grateful to Mr. H. Yamazaki of Metso-SHI Co. Ltd. and K. Nozima of Oji Paper Co. Ltd. for useful many discussions, K. Oshima of Dinippon Ink and Chemicals Co. Ltd and T.Mikuni of Oji paper Co. Ltd. for donating materials. I.N. also thanks H. Watanabe of Tokyo Seimitsu for the measurements of surface roughness of paper.

References

- 1) W.H. Banks and C.C. Mill, *J. Colloid. Sci.*, **8**, 137-147 (1953)
- 2) L.H. Sjodahl, TALI Proceedings (1949) in referece of H.H. Hull [TAGA, (1951) 83-90.]; L.H. Sjodahl, *Am. Inkmaker*, **39** (3), 31-33, 57 (1951)
- 3) H.H. Hull, TAGA, (1951) 83-90
- 4) P. Lepoutre, J.H. De Gracê and J.P. Mangin, *Coating Conference Proceedings*, (1979) 21-25
- 5) J.H. Tayer, Jr. and A.C. Zettlemoyer, *TAPPI*, **41**, 749-757 (1957)
- 6) R.R. Myers. J.C. Miller and A.C. Zettlemoyer, *J. Colloig. Sci.*, **14**, 287-299 (1959)
- 7) J.H. De Gracê and P.J. Mangin, W.H. Banks edit., "Advances in Printing Science and Technology, vol. 19", Pentech Press, London, UK, (1988) 146-167; J.H. De Gracê, J.E. Dalphond and P.J. Mangin, W.H. Banks edit., "Advances in Printing Science and Technology, vol. 21", Pentech Press, London, UK, (1991) 312-327
- 8) G.E. Carlsson and B. Lindberg, "A Study of Ink Mottle", W.H. Banks edit., "Recent Development in Graphic Arts Research", Pergamon Press, Oxford, UK, (1971) pp. 283-310

- 9) I. Naito, Y. Ezaki, S. Tsuzumi and A. Kinoshita, Preprint of the meeting of Japan Society of Printing Science and Technology, No. 87, pp.37-40; I. Naito, A. Kinoshita and Y. Yonekawa, Kyushu Sangyo Univ. Res. Rep. Fac. Art., **23**, 97-102
- 10) I. Naito, T. Suzuki and A. Kinoshita, J. Printing Sci. Technol., **31** (3), 147-153
- 11) I. Naito, T. Hayano, K. Maki and A. Kinoshita, J. Printing Sci. Technol., **35** (3), 139-144
- 12) I. Naito, M. Deguchi, S. Tsumura and K. Koga, Proceeding of 30th IARIGAI Meeting in Dubrovnik (2003) 111-117
- 14) There are relatively large errors in the measurement
- 15) W.C. Walter and J.M. Fetsco, Am. Ink Maker, **33** (11), 38 (1955)
- 16) Private letter from Dr. Nozima of Ooji Paper Making Co. Ltd.
- 17) G. Lower, W. Walker and A. Zettemoyer, J. Colloid. Sci., **8**, 116 (1953)
- 18) I. Ichikawa, Insatsukyoku Jihou, **6**, 1 (1964)
- 19) S. Aoki, M. Eda, T. Matsushima, and K. Nishiyama, Tech. Report of Mitsubishi Heavy Industry, **39**, 198-201(2002); S. Aoki, Preprint of the meeting of Japan Society of Printing Science and Technology, No. 109, (2002) pp.55-57

Objective print quality assessment of complex images

Christine Antoine¹, Ola Diserud², Olav Solheim¹, Elisabeth Berli³

¹ PFI-AS, Høgskoleringen 6b, NO-7491 Trondheim, Norway

E-mail: christine.antoine@pfi.no

E-mail: olav.solheim@pfi.no

² PFI-AS but now at NINA, NO-7485 Trondheim, Norway

E-mail: ola.diserud@nina.no

³ Norske Skog Research and Development, NO-3701 Skien, Norway

E-mail: elisabeth.berli@norskeskog.com

Part 1: Print Quality Assessment by Means of the Fast Fourier Transform

Abstract

The printing of an image is a complex process involving numerous parameters. A good quality print, evaluated either subjectively or objectively, is usually the final goal of the printing process. As subjective evaluation of images is a difficult and time-consuming task, often done by considering complex (real) images, we propose a model that objectively evaluates print quality in images. First, the printed images are acquired by a high-resolution digital camera. Print quality is then evaluated from the power spectrum of the images, obtained in the Fourier domain. In the model, we can choose to include a reference image ('original') and / or a contrast sensitivity function (CSF) that models the sensitivity of the human eye. For multicolour images, we have included traditional colour difference indices as additional quality parameters.

1. Introduction

A good quality print is one of the final goals of any print process. For the printer, this is a tedious task since it requires a fine-tuning of several parameters, and the process itself is not stable during a printing run. Many printing defects may result from suboptimal settings, or imperfect consumables, such as low print density, mottling, print-through, linting, trapping, misting, scumming, etc.

Consumer demands regarding print quality are continuously increasing, partly because more and more paper products tend to be printed, but also due to the introduction of new printing methods, such as digital printing. Combined with a tougher competition, this leads to a great need for methods that evaluate print quality. The standard approach, subjective evaluation by panels, is both expensive and time consuming, and it requires very experienced judges. The need for objective, or instrumental, methods to measure print quality, imitating the human visual system, is therefore obvious. These indices should be inexpensive to acquire, suitable for online implementation while maintaining the sufficient precision. It will be difficult, if not impossible, to fulfil all these criteria, taking into account the intrinsic variability and uncertainty of the subjective evaluations. Nevertheless, even a suboptimal method to measure print quality would still be a large improvement.

The search for an objective method to measure image quality has been going on for quite some time, not only in the paper industry but also in other industries where good reproduction of images are essential (e.g. TVs and PC-monitors). The question is then which properties of print on paper are important for the paper producers, the printers and the advertisers regarding the apparent quality of the product? At present, much of the research is based on an approach that can be characterised as a 'signal evaluation approach'. The image is regarded as a complex signal that deviates more or less from the signal

representing the ‘original’. Images are defined in the physical, in the Fourier, or in the perceptual domain (in the latter case using models of visual perception), and quality measures are defined as distances in an appropriate function space, e.g. the Euclidean distance between the printed and original images.

Various image analysis software programs have been developed in order to evaluate print quality characteristics (e.g. Antoine, 1998; Berli et al., 1994; Collins and Rosson, 1988; Johansson, 1993; Johansson and Norman, 1996; Ness and Göttching, 1995; Nguyen et al., 1996; Shiratori et al., 1994; Spencer and Schwartzwald, 1996; Ångskog and Johansson, 1995). They usually focus on only one, or a few, of the numerous parameters that affect print quality, such as mottling, print density, dot gain, or dot shape. Screen evaluation is usually done on constant dot coverage areas, where the quality of the printed dots is evaluated (Berli et al., 1994; Antoine, 1998; Nguyen et al., 1996). This differs from what is done during a subjective evaluation. In solid areas, we can calculate characteristics such as print-density, mottling and print-through. Some of these are measured in the spatial domain (e.g. print density) while others are described in the frequency domain (e.g. mottling). Some attempts have been made to evaluate the quality of video images or prints by analysing complex images, as done during a subjective evaluation (Foyn et al., 1996; Jin et al., 1998). Foyn et al. (Foyn et al., 1996) evaluated print quality in black and white images by means of the Fast Fourier Transform (FFT). Our work continues their work on the evaluation of black and white images, and proceeds to the evaluation of coloured images. Here, we describe the different steps of the proposed methods, starting with the acquisition of the printed images. The statistical analysis of the results will be presented in Part 2 of this work (Diserud, 2004).

2. Equipment and sampling

A high-resolution digital colour camera ‘EyeLike’ with maximum resolution 6144×6144 pixels was used to acquire the images from the printed samples. After a preliminary study, we found that a 60mm AF Micro Nikon lens was the most suitable lens for our printed samples. Lenses with other ranges did not allow us to reach the required resolution for the complete region of interest. For this particular set of samples, resolutions around 25 $\mu\text{m}/\text{pixel}$ did not allow a differentiation of image quality between samples. The same samples could be differentiated applying resolutions in the range from 5.6 to 10 $\mu\text{m}/\text{pixel}$ (see study reported in (Nybakk, 2000) Four linear fluorescent lights (Orsam Dulux® L 36W/12), placed two by two on both sides of the sample, and illuminated the samples during image acquisition. The distance from light source to sample was 65 cm. The angle between light and sample was approximately 120 degrees, yielding a light luminance on the sample set around 255 Lux. The light illuminance was recorded for each image, together with the lens aperture and the exposure time, in order to detect possible changes of illuminance due to e.g. electrical power variations.

Adjustable parameters when acquiring images are: Scan size, image size (cropping), lens, lens aperture, exposure time, lighting power, distance between lens and sample, black/white balance and colour balance. The settings we applied for acquiring the different images are reported in Appendix 1.

The test samples we used during the development of the image analysis routines, were a set of 28 different newsprint qualities printed in a Norske Skog Research benchmarking study. The samples were printed in a full scale printing trial in Germany, on a CSWO Colour Man M printing press. Press parameters were kept as constant as possible during printing. Both the black and white and the colour images were printed on both the inside-reel (IR) and outside-reel (OR) side of the paper.

The black and white image of the ship ‘Galtesund’ was acquired at two different magnifications. First, the whole image was acquired from both the IR and OR-side at a resolution of 40 $\mu\text{m}/\text{pixel}$ (Figure 1a). Second, a small part from the centre of the image was acquired on the OR-side only, at a resolution of 8.33 $\mu\text{m}/\text{pixel}$ (Figure 1b). This cropped image section was chosen since it had small details in both light and dark areas, as well as areas with more homogeneous grey levels. The same applies for the full ‘Galtesund’

image. A black and white image, picturing an old car with large uniform areas, was also acquired in order to compare different measures of mottling (Figure 1c). The 'Old car' image was acquired at a resolution of $42.5 \mu\text{m}/\text{pixel}$, and from the OR-side only. Similarly, two colour images were acquired. The full image of the 'Fuji-lady' was acquired from both the IR and OR-sides at resolution $56 \mu\text{m}/\text{pixel}$ (Figure 1d). From the 'Three musicians' picture, the face of the leftmost lady was acquired from the OR-side at a resolution of $25 \mu\text{m}/\text{pixel}$ (Figure 1e). Digital originals of all the printed images were obtained from Norske Skog Research. The images were then rescaled according to the size of the acquired images.

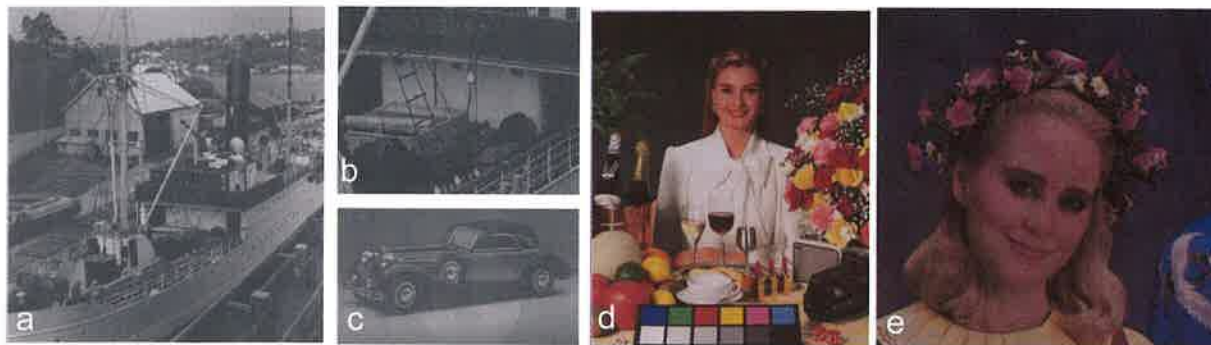


Figure 2: a) The full 'Galtesund' B/W picture, b) Part of 'Galtesund'
c) The 'Old car' picture, d) The 'Fuji-lady', e) Part of the 'Three-musicians'

3. Analysis of black and white images

The development of print quality assessment methods by means of FFT is part of a work focusing on objective measures of perceptual print quality. The results obtained from this FFT-analysis of complex images will, together with data from optical measurements of the formation of paper, be the most important explanatory variables in an objective model on experienced judges' evaluation of print quality. The routines described below are implemented in Image-Pro (www.mediacy.com) and Matlab (www.mathworks.com).

3.1 Image alignment

When performing operations on images element-by-element, it is critical that the images we compare are aligned, both with respect to translation and rotation. Therefore, we have developed an algorithm that calculates the cross-correlation between the two images that is to be aligned. After translating one of the images both horizontally and vertically, the algorithm finds the optimal translation from the maximum correlation between the two images. The image is then rotated within a defined angle interval, and the angle that gives the maximum correlation is chosen as the relative rotation angle between the two images. Edge detection was applied in order to obtain the most distinct peak of the between-images correlation. To speed up the calculations, the cross-correlation was calculated in the Fourier domain (Nybak, 2000). It is not necessary to calculate the cross-correlation for the whole images, so the algorithm cropped them to a size of power of two and the correlation was then calculated from these images sections. The size of the cropped image is specified as an input parameter in the alignment program. When the optimal rotation angle and translation is found, the image, or a part of it specified by the user, is translated, rotated and then stored in a file.

3.2 The contrast sensitivity function (CSF)

The human vision is often modelled by a so-called contrast sensitivity function (Maffei, 1978; Watson et al., 1983). Contrast sensitivity measurements yield information about an individual's ability to see low-

contrast targets over an extended range of target size and orientation. Many neurophysiological and psychophysical studies have been dedicated to the sensitivity of the human vision and more complex models than the CSF have been developed. The low-order processing of the visual system, i.e. from the optics to the cortex, can be modelled by three main sensitivity variations as a function of light level, spatial frequency and signal content (DeValois et al., 1982; Blakemore and Campbell, 1969; Stromeyer and Julesz, 1972). In a comprehensive study, Daly proposed a Human Visual System model called Visual Differences Predictor implemented in three steps (Daly, 1993). This model is developed for B/W images, but can be adapted to colour images also by working simultaneously on the three colour channels (Jin et al., 1998). However, this model is rather complex to implement and the gain in a benchmarking study questionable, so in our initial approach we prefer to keep the model of the human vision simple. CSFs are known to depend on various parameters, such as age of the observer, illumination, eccentricity, viewing distance or viewing angle (DeValois and DeValois, 1988; Sullivan et al., 1993). The first CSFs applied were band-pass filter shaped, but later studies have demonstrated that a low pass filter CSF leads to better correlation between objective and subjective image quality (Mitsa et al., 1993; Limb, 1979). In this project, we have implemented a low-pass CSF that takes into account the viewing distance and angle, as described in (Sullivan et al., 1993), (Figure 2). Note that our CSF also takes into account the eye's increased sensitivity for the horizontal and vertical orientations. The intended viewing distance for the analysis of the full Galtesund image was set to 260 mm. For the cropped Galtesund image the viewing distance was set to 190 mm, assuming that we look closer at images when we want to evaluate minor details.

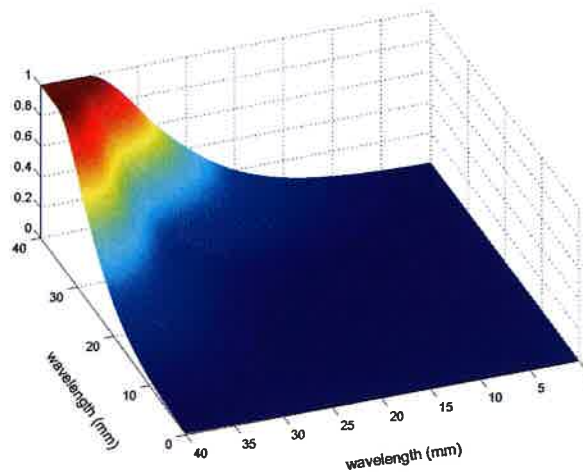


Figure 2: The low pass filter CSF with a viewing distance of 260 mm and an image size of 40×40 mm

3.3 Fast Fourier Transform 2D and 1D

Frequency analysis is an important tool when filtering images. The Discrete Fourier Transform (DFT) has traditionally been the most common method for determining the frequency spectra of digital images or signals. Further, the Fast Fourier Transform (FFT) is an algorithm that efficiently calculates the DFT. In standard signal processing, the FFT is a one-dimensional calculation, whereas in image processing, the FFT is two-dimensional. A 2D-FFT power spectrum is not intuitively interpretable. If we believe that the actual spatial direction of essential image characteristics is of minor importance, e.g. the orientation of the wiremarks, we may summarise the 2D information in a 1D power spectrum. In a 'shifted' 2D spectrum, where the DC-term is placed in the centre of the plot, points with equal distance to the centre of the 2D spectrum represent the same frequency in the image (Figure 3a). The frequencies in the 2D spectrum were therefore sorted by applying a binary mask with the shape of a ring, with diameter running from zero to the length of the diagonal from centre to the corner of the spectrum.

Two different approaches to obtain this 1D power spectrum were tried out. First, we calculated the mean over each frequency ring (Figure 3b). This approach takes the average over all directions for a given frequency, and is suitable for describing features with assumed equal strength in all directions. Secondly, the maximum value for each frequency ring was found (Figure 3c). This second approach is more efficient if we want to quantify high-energy features, such as wiremark-peaks and halftone dot peaks, which have a dominant direction in the 2D spectrum that would have been ‘smeared’ out by applying the first approach. This last 1D representation of the 2D spectrum is by nature more sensitive to frequency peaks, but also to noise. The main peaks detected in these 1D spectra corresponds to the halftone dot frequency and its harmonics. The amplitude of the main and harmonics peaks can theoretically be linked to the amplitude of the halftoning, i.e. halftone dot contrast. The number of harmonic peaks, and their relative amplitude compared to the main peak, is influenced by the grey scale intensity gradient of the dot edge, i.e. dot sharpness. When wiremarks are detectable in printed samples, the corresponding 2D spectrum and 1D-max plot exhibit an additional peak, corresponding to the wiremark frequency, located to the left of the halftone dot frequency peak (see Figure 4).

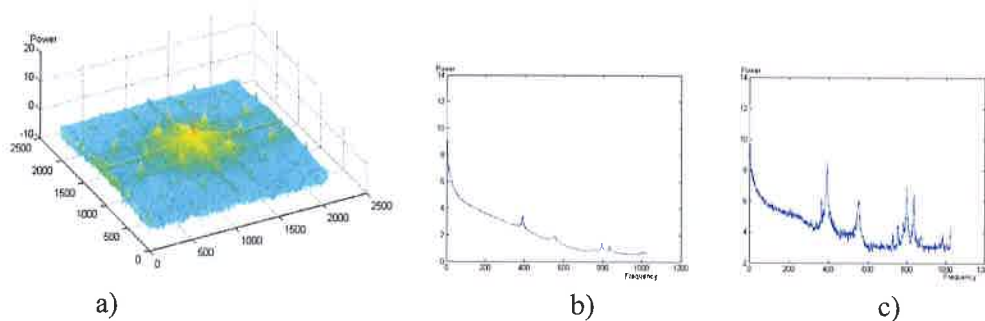


Figure 3: a) 2D-power spectrum, b) 1D-power spectrum obtained from the mean values for each frequency, and c) 1D-power spectrum based on maximum values for each frequency

3.4 Power spectrum partition

Little is known about the factors that influence the perceived quality of complex halftone images. Some of the common image quality measures applied today includes edge correlation, mean square error (MSE), frequency-weighted MSE, and maximum local error. Another quality index is the Figure of merit. First, both the Fourier transform of the halftoned image and that of the original image are weighed by a model of the human visual system (usually a CSF). Then, the average difference between the two FTs is presented as the Figure of merit.

Image quality can also be quantified by partitioning the power spectrum into different frequency ranges. This is a common approach when formation or mottling are quantified (Johannsson, 1993, Johannsson, 1999). Following this approach, we divided the 1D-power spectrum into 5 different frequency intervals that correspond to specific image wavelengths and characteristics (Figure 4).

These five intervals are:

1. Wavelengths longer than 8 mm. This range corresponds to the larger image features.
2. Wavelengths between 1 and 8 mm. This range includes information on mottling, but will also describe actual details of these wavelengths in the image.
3. Wavelengths between that of the halftone dot peak (approximately 0.2 mm for our samples) and 1 mm. These wavelengths correspond to very small details, but also the smaller wavelengths required to represent sharp edges in an image. Wiremarks, if observable and graininess are also represented by these wavelengths.

4. The interval under the halftone dot peak. The width of this interval may vary between images, and is calculated automatically from the first derivative of the spectrum.
5. The shortest wavelengths. Halftone dot characteristics, such as raggedness, may be detected in this interval. Harmonic peaks from the halftone dot frequency are also visible in this range. In addition, high frequency noise from the acquisition procedure can give a large contribution to the energy in this interval.

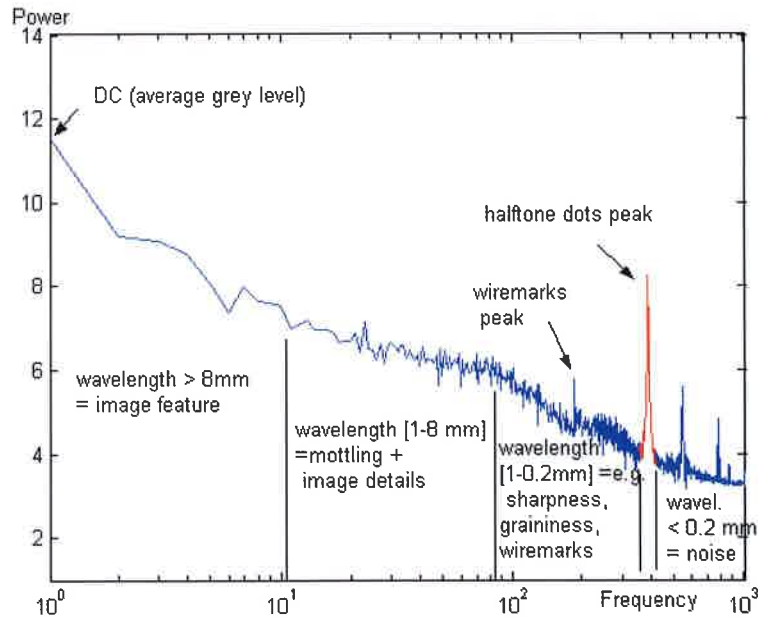


Figure 4: 1D-FFT spectrum partitioned into 5 frequency, or wavelength, intervals. Peaks of particular interest are also marked

The integral of each of the intervals and of the complete power spectrum are calculated for both the 1D-mean and 1D-max spectra by the discrete approximation in Equation 1.

$$P_{ij} = \sum_{f=i}^{f=j} P_f$$

Equation 1

where P_{ij} is the total power in the interval $[i, j]$ and P_f the power at frequency f . The height of the halftone dot peak is measured in both plots, as well as the height of the wiremark peak, when detected, in the 1D-max plot. The width of the halftone dot peak and the observed halftone dot frequency are also measured.

3.5 Models

When quantifying image quality, the printed image can either be compared to a reference image, or evaluated on its own. If the original image is available, we can evaluate the quality of the printed version by measuring the difference between the two images. However, a relevant reference image is not always available, so we have tested both approaches. Moreover, in order to test the efficiency of applying a model for the human visual system, here the CSF, we have performed analysis both with and without the CSF. Figure 5 shows a flowchart of the model where both the original image and the CSF are taken into account. The three simpler models can be deduced from this figure by removing the original image-branch and/or the CSF input.

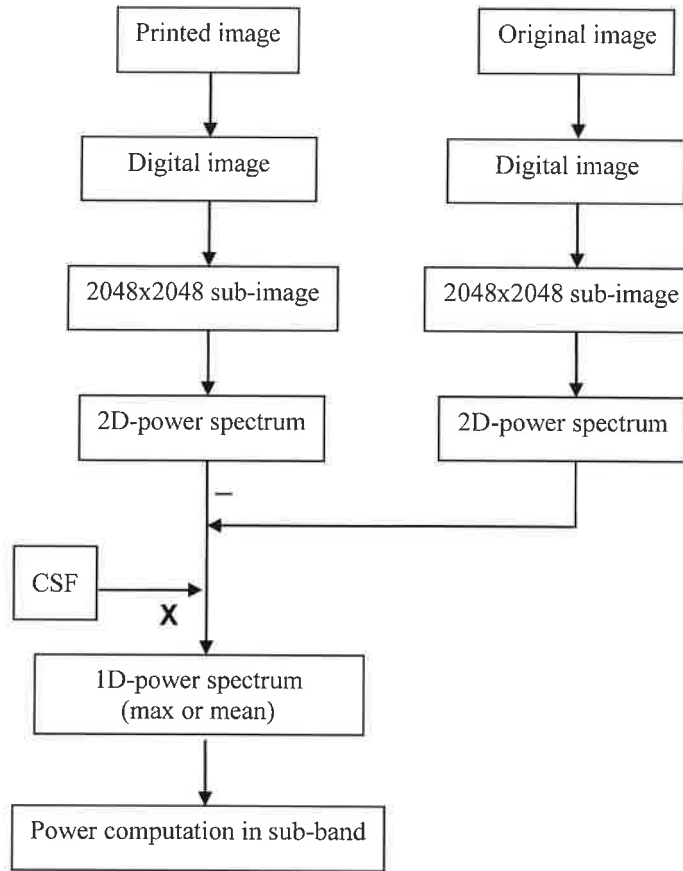


Figure 5: Flowchart of the model where the difference between the original and the halftoned images, as well as a CSF low pass filter, are taken into account.

3.6 Print mottle

Variations in print density in solid areas, i.e. print mottle, is known to have a large influence on the overall print quality. As explained above, the frequency range corresponding to mottling is also representing the smaller details in the image. This gives a confounded effect; a negative feature (mottling) and a positive feature (good rendering of the details) have the same influence on the power spectrum. It is therefore difficult to measure print mottle in a complex image by the means of FFT. If the evaluated image contains an area with more or less homogeneous intensity (no details in the mottling frequency range) we can be more certain that we actually measure print mottle.

In this work, we have developed and implemented a routine that calculates print mottle from the 2D-FFT. The 2D-information is summarised to 1D by the same approach as described above, i.e. by averaging the power of a given frequency in all directions. From there, already developed 1D mottling index can be used: a mottling index, developed at STFI, takes the paper basis-weight into account (Equation 2; (Johannsson and Norman, 1996)); an alternative mottling index, not including the basis-weight, has been developed at PFI (Equation 3). The octave bands of interest have traditionally been 1-2 mm, 2-4 mm and 4-8 mm. These bands have been found to give the highest correlation between subjective mottling evaluations and the respective mottling indices (Johannsson, 1993).

$$MI_{STFI}(\lambda_a - \lambda_b) = \sqrt{\frac{1}{BW * l} * \sum_{i=\lambda_a}^{i=\lambda_b} i^2 * P_f(i)^2} \quad \text{Equation 2}$$

$$MI_{PFI}(\lambda_a - \lambda_b) = \sqrt{\sum_{i=\lambda_a}^{i=\lambda_b} i^2 * P_f(i)^2} \quad \text{Equation 3}$$

Where *MI*: Mottling Index

$\lambda_a - \lambda_b$: octave band considered (mm)

i: frequency (mm⁻¹)

$P_f(i)$: mean power of the 2D power spectrum at the frequency *i* (W)

l: image scanned length (mm)

BW: paper basis weight (g/m²)

4. Analysis of colour images

Due to the large increase in four-colour printing in newspapers, and colour advertising in other media, calls for less colour deviation and reduced colour variation in newspaper offset printing are becoming louder. The images printed in four-colour are acquired with the same acquisition system as described for the black and white (BW) images, and are stored as RGB images, i.e. divided into the three colour channels Red, Green and Blue respectively. The images are aligned following the same procedure developed to align the BW images. One colour-channel only is used to define the angle of rotation and translation. The three channels in an image are then rotated and translated simultaneously by the same angle and translation.

The trichromatic theory of colour vision says that a mixture of no more than three differently coloured lights can reproduce all colours (Pratt, 1991). Any colour can thereby be described by a set of three colour coordinates. Many colour systems have been defined, the best known being the different variants of the RGB-systems for video monitors, and the device independent standard systems CIE-La*b* and CIE-LUV. In the paper industry, the CIE-La*b* system is commonly used to describe paper colour. This system is known as a good descriptor of human perception of colour difference (Williams, 1996). We have therefore preferred the CIE-La*b* colour system in this work. The ‘Eyelike’ camera has a device specific RGB coordinate system. When linear, the conversion from RGB to CIE-XYZ space can be done by the determination of a first order matrix equation with 9 coefficients. In our case, the camera producer (Jenoptik L.O.S. GmbH) has provided us with a conversion program from RGB to CIE-XYZ. From CIE-XYZ, the conversion to CIE-La*b* colour coordinates is well-defined (Equation 4).

$$\begin{aligned} L &= 25 \cdot \left[100 \cdot \frac{Y}{Y_0} \right]^{1/3} - 16 \\ a^* &= 500 \cdot \left[\left[\frac{X}{X_0} \right]^{1/3} - \left[\frac{Y}{Y_0} \right]^{1/3} \right] \\ b^* &= 200 \cdot \left[\left[\frac{X}{X_0} \right]^{1/3} - \left[\frac{Z}{Z_0} \right]^{1/3} \right] \end{aligned} \quad \text{Equation 4}$$

The FFT is performed separately for each colour channel. We then obtain three power spectra that are analysed individually. The 2D information is subsequently compressed to 1D and the 1D spectrum partitioned as previously described for the BW images. The results obtain from the study of BW images

may allow us to narrow down the number of bands of interest. This must be done with caution, since other frequency bands or elements may be crucial for print quality of colour images. The same applies for the four different models described in the section on analysis of BW images.

A computational model predicting perceived quality of colour reproductions will be a very useful tool in digital image processing. Thus, it is beneficial to develop a colour quality index that evaluates the perceived quality of reproduced colours in accordance with observers' judgements. Since the eye's sensitivity varies with the wavelength of the light, i.e. the colour, we apply three different CSFs, one for each colour channel. The low-pass filter CSF used for the evaluation of BW images is also applied for the luminance L. Two almost identical low-pass filter CSFs are used for the a^* and b^* channels (Jin et al., 1998; Mullen, 1985). Both have constant sensitivity (normalised to unity) in the low spatial frequency range, and start to decline when passing a transition point (0.8 cpd - cycles per degree). The a^* -channel CSF has a cut-off frequency of 11.5 cpd, while the b^* -channel CSF has a cut-off frequency of 11 cpd (Figure 6). When converting from cpd units to metric units (mm), we use the same formula as used for the luminance CSF (Sullivan et al., 1993).

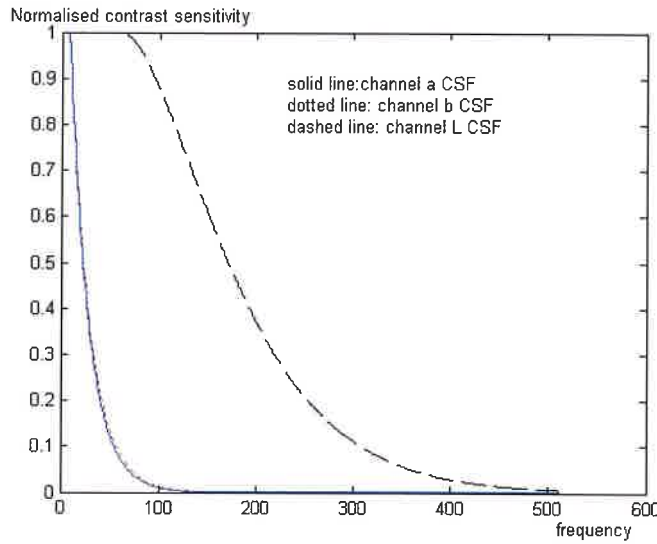


Figure 6: Profiles of the CSFs for colour channels L, a^* and b^* respectively

The total colour difference ΔE_{ab}^* between two colour stimuli, each given in terms of L, a^* , and b^* coefficients, can be calculated from Equation 5 (Hunter and Harold, 1987; Wyszecki and Stiles, 1982).

$$\Delta E_{ab}^* = \left[(\Delta L)^2 + (\Delta a^*)^2 + (\Delta b^*)^2 \right]^{1/2} \quad \text{Equation 5}$$

Colour difference can also be expressed in terms of perceived lightness, chroma, or hue. We then apply cylindrical coordinates; see Figure 7 (Hunter, 1987). ΔE_{ab}^* can then be expressed by these coordinates as follows,

$$\Delta E_{ab}^* = \left[(\Delta L)^2 + (\Delta C^*)^2 + (\Delta H^*)^2 \right]^{1/2} \quad \text{Equation 6}$$

where $\Delta L = L_1 - L_0$ (difference in lightness), and $\Delta C^* = [(a_1^*)^2 + (b_1^*)^2]^{1/2} - [(a_0^*)^2 + (b_0^*)^2]^{1/2}$ (difference in chroma). We are then able to deduce the difference in hue ΔH^* as

$$\Delta H_{ab}^* = \left[(\Delta E_{ab}^*)^2 - (\Delta L^*)^2 - (\Delta C^*)^2 \right]^{1/2} \quad \text{Equation 7}$$

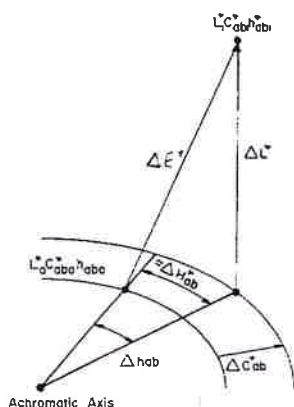


Figure 7: Distance between two points in a cylindrical coordinate system (Hunter and Harold, 1987).

These four differences (ΔE , ΔL , ΔC , ΔH) can be calculated in two ways: First, they can be calculated separately for each pixel, before the final result is given as the average over all pixels. Secondly, we can start by finding the average L , a^* and b^* -values of the whole image, and then calculate the colour differences from these 'global' coordinates.

5. Conclusion

We have here presented different models aimed at finding an objective measure for print quality in complex images. Both B/W and multi-colour images have been considered. The models all operate in the frequency domain, obtained by the Fourier transform. Some of the models require a reference image, or an 'original'. The human visual system has been modelled by contrast sensitivity functions. An elaborate analysis of printed images from a full-scale printing trial is presented further (Diserud et al., 04).

Part 2: A Model for Perceptual Print Quality in Complex Black and White Images

Abstract

We have in the preceding paper presented a new optical method that objectively evaluates print quality in complex images (Antoine et al., 2004). Our approach is based on analysis of high-resolution digital images acquired from commercially printed newsprints. These objective measurements are tested for their ability to differentiate between samples with almost equal print quality (papers from the same market segment). Their precision are found to be satisfactory, so also their ability to capture the most important elements of subjective print quality.

Based on these optical measurements, we have developed a multivariate model for the evaluation of perceptual print quality. The model is constructed from three variables, all describing image features from the high frequency part of the spectrum, i.e. features with wavelengths less than 1 mm. These variables can be linked to detail reproduction and edge sharpness, half tone dot characteristics and the regularity of the dot localization. With this model, we can predict how a panel of expert judges will rank samples from a benchmarking study focusing on print quality in black and white images on newsprint.

1. Introduction

The evaluation of paper and print quality can be separated into two main approaches, instrumental measurements of specific paper and print characteristics (objective measurements) and visual evaluation (subjective perception). Visual evaluation can include both single profile characteristics such as gloss, print sharpness, contrast and evenness in solid print, or overall evaluation of image quality. The problem today is the lack of acceptable objective methods that can quantify perceptual print quality; printed images are often ranked solely by panels of judges. This subjective approach is both expensive and time consuming since it requires a regular training of participants with experience from both paper production and printing. The difference between paper qualities is decreasing while the quality level improves, so the task will not be any easier in the near future.

We presented in the preceding article optical methods for measuring features in complex images relevant for subjective evaluation of print quality (Antoine et al., 2004). Our approach is based on Fourier analysis of high-resolution digital images acquired from commercially printed newsprint. The results obtained from the FFT (Fast Fourier Transform) analysis of complex images will, together with data from optical measurements of the formation of paper, be the most important explanatory variables in our model for experienced judges' evaluation of print quality.

2. Experiments and methods

The image acquisition and FFT-analysis are described in detail in Antoine et al. (2004). It is highly recommended to read this article first in order to get a good understanding of the following statistical analysis. Nevertheless, we will briefly summarize the essential steps of the experiments and methods.

The samples are from a full scale printing trial on newsprint, CSWO, performed by Norske Skog Research & Development, Runability & Printability Department. From the outside of the reel (OR) side we have 23 different samples (different newsprint qualities) and from the inside of the reel (IR) side 20 samples. We acquired 5 parallels from each of the samples, in order to average out 'noise' from the image acquisition or the press. The images were acquired with a high-resolution digital camera; 'EyeLike' from JenOptik.

The black and white (BW) image of the ship 'Galtesund' was acquired at two different magnifications. First, the whole image was acquired from both the IR and OR-side with resolution 40 $\mu\text{m}/\text{pixel}$. This image will from now on be named 'Full'. Second, a part of the image with small details in both dark and light areas (denoted 'Part') was acquired on the OR-side only, with a higher resolution of 8.33 $\mu\text{m}/\text{pixel}$ (see Figures 1a and 1b in Antoine et al., 2004).

The images were then aligned and analyzed. In order to extract indices relevant for perceptual print quality from the two-dimensional FFT spectra, we must first reduce them to one-dimensional FFT spectra. Two additional options are available in the analysis; we can choose to include a model of the human vision, the so-called contrast sensitivity function (CSF), or we can compare the spectra from the halftoned prints with the spectrum from the original digital image. Following common procedures from the quantification of mottling and formation, we divide the 1D-spectra into different frequency intervals, and treat the peaks separately (Figure 1). For this particular spectrum, we let the direction with the maximum contribution represent the frequency in the 1D spectrum and we have not applied the CSF. The spectrum from the original digital image is included in Figure 1 (upper line) in order to illustrate how the original is reproduced. The original is useful when we compare frequencies below the half tone dot frequency, but when evaluating the quality of the half tone dots, we must rely on assumptions on how an optimal half tone dot will be represented in the spectrum. Our selected OPQ (Optical Print Quality) variables from the 1D power spectrum are presented in Table I.

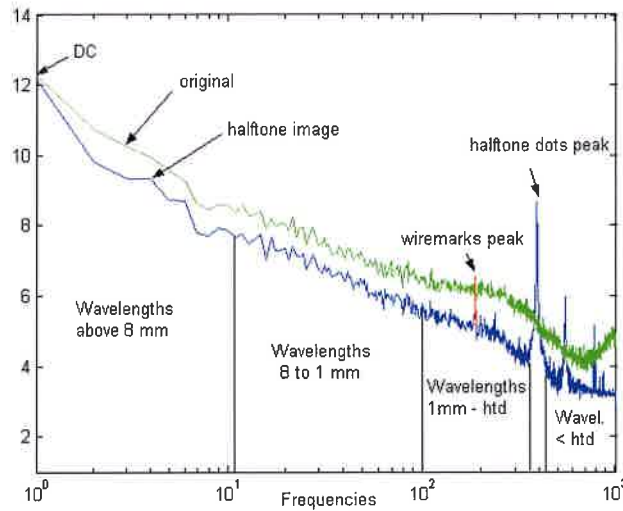


Figure 1: The partition of the 1D FFT power spectrum into OPQ-variables.
The higher the frequency in the FFT spectrum, the smaller is the wavelength that generates this frequency

Table I: The selected OPQ-variables from the 1D FFT spectrum

Variable	Definition
DC	The average grey level of the image.
WL[>8mm].	The area under the spectrum for the lower frequencies, i.e. wavelengths over 8 mm. Corresponds to large size image content.
WL[1-8mm]	Wavelengths between 1 and 8 mm. This range is representing mottling (in solid print), and details in the image that corresponds to these wavelengths.
WL[HTDP-1mm]	Wavelengths between 1 mm and the wavelength of the halftone dot peak (approximately 0.2 mm). This range includes wavelengths representing small details or sharp edges.
WL[HTDP]	The area under the half tone dot peak.
WL[<HTDP]	This range includes the shortest wavelengths. It represents half tone dot characteristics (e.g. raggedness), but also high frequency noise from the acquisition procedure.
WIDTH[HTDP]	The width of the base of the half tone dot peak.
HTDPWL	The wavelength of the half tone dot peak.
HEIGHT[HTDP]	The height of the half tone dot peak.
WMP	The wavelength of the wire mark peak.
WMH	The height of the wire mark peak.

Trained judges from the NSR&D Runability & Printability department have evaluated these prints. The OR and IR sides are evaluated separately. The results from these subjective evaluations are then analyzed statistically by a so-called multidimensional scaling (MDS). MDS refers to a group of techniques that help the researcher to identify the key dimensions underlying respondents' evaluation of objects. We are thereby able to create a multidimensional spatial picture, or map, of observer judgments in a psychological space. Once the data is acquired, MDS can help determine 1) which dimensions the judges use when evaluating samples, 2) how many dimensions they may use in a particular situation, 3) the relative importance of each dimension, and 4) how the objects are related perceptually.

The final subjective ranking of the samples, based on the judges' preference evaluations, will in this paper be denoted *STPREF* (standard preference). The ranking is scaled so that the best sample is given the value 100, and the least preferred sample 0. *STPREF* will be the response, the 'target' variable, in the multivariate analysis of perceptual print quality.

The prints were also evaluated by traditional halftone dot quality indices acquired with a microscope camera (Berli et al., 1994), in order to check whether our interpretations of the high frequency variables are reasonable. The most interesting variables regarding our application are *Print sharpness*, i.e. the gradient of the density change when going from an unprinted to a printed area, *Dot Raggedness* and *Contrast*. When performing a factor analysis, we find that especially these three half tone dot variables correspond well with the high frequency variables from 'Part'. For example, *Print sharpness*, where a low value indicates good dot sharpness, has correlation $r = -0.88$ with $WL[HTDP]$. Our interpretation that a large area under the peak (high value of $WL[HTDP]$) indicates a dot of good quality seems to be supported. A scatter plot of *Print sharpness* vs. $WL[HTDP]$ is presented in Figure 2. We conclude that the OPQ-variables obtained from 'Part' can, when predicting perceptual print quality, replace measurements from the traditional half tone dot analysis performed by a microscope camera.

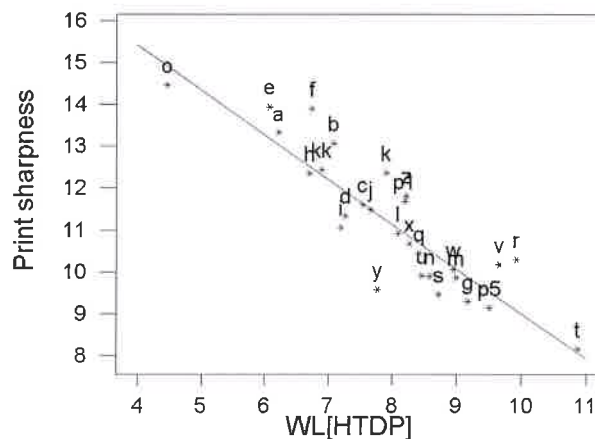


Figure 2: Scatter plot of *Print sharpness* vs. $WL[HTDP]$ with regression line inserted

3. Results

From each paper quality, we acquired 5 parallel samples. We then performed an analysis of variance (ANOVA) in order to check if the uncertainty in the measurements were minor compared to the variance between averages for the different paper qualities. If not, the measure would be useless in differentiating between paper samples. The basic idea in an ANOVA is to check whether the variance between groups (paper qualities) is significantly larger than the variances within the groups ('measurement error').

For all but two of the variables from 'Full', the variance between the quality averages was significantly larger than the variances within the quality. Note in particular that the wiremark variables (WMH and WMP) had a very small within-group variance for several of the qualities. When the wire mark of a certain paper quality is detectable, we do not expect any difference in measured wavelength between parallels of this quality. The two rejected variables were $WL[HTDP]$ and $HEIGHT[HTDP]$, with p -values equal to 0.26 and 0.48 respectively. These are both variables that describe some elements of the half tone dot peak.

Previously, we argued that in order to obtain the necessary resolution in the higher frequencies we had to 'zoom in' on a section of the image. The improved resolution in 'Part' gives less 'within-group' variance, i.e. less 'noise' in the high frequency variables. All measurements from 'Part' are accepted with p -values less than 0.001. To sum up; in order to obtain values with sufficiently small measurement error in the high frequency ranges, we have to acquire a section of the image with sufficiently high resolution. For the remaining part of the analysis, we will apply the mean value calculated for each set of 5 parallels for all the variables.

The samples from the OR and IR sides will be analyzed separately. This is not necessarily due to a twosidedness of the papers, but rather that the press parameters for the two sides may have been different during printing. Some of the samples may even have been re-rolled so that the actual sides are switched. In general, all the paper machines are ‘different’ in some sense, so we would not expect any consistent differences between the sides due to paper or machine parameters. If we were to pool the two sides together, we may end up modelling the differences due to varying press conditions rather than varying paper properties between the qualities. This is illustrated in Figure 3 where the first 31 samples are from the OR side and the last 29 from the IR side. The sample order is randomized and does not reflect any physical or experimental characteristics (for example the order the samples were printed), so there should not be any systematic trends in this plot. If we look at the two sides separately, we see that there is a small, non-significant, negative trend. If the two sides are pooled together, we get a significant positive trend (unbroken line from 1-60), indicating that there is a positive correlation between *DC* and the sample order. Level shifts like this may give ‘false’ models if the two sides (subpopulations) are analyzed together. This effect often occurs when data from different sources are pooled together, e.g. Newsprint and LWC in the same study, or when important variables are left out (‘side’) with the result that the explained relations can be spurious.

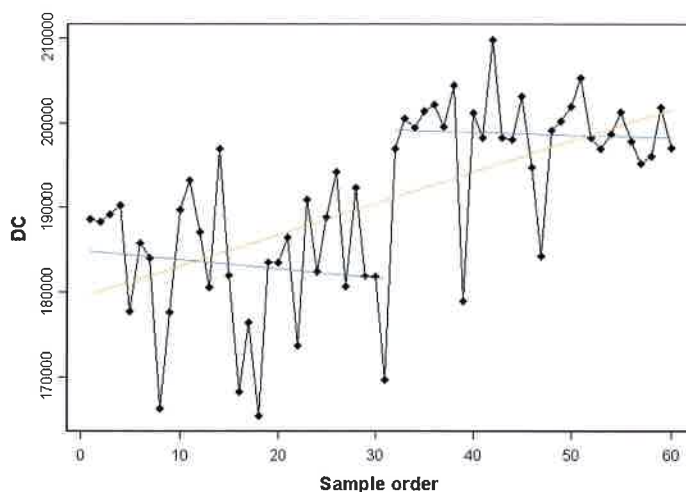


Figure 3: The DC-level for the OR (no. 1-31) and IR samples (no. 32-60) plotted together

For each of the sides of ‘Full’ and for ‘Part’, we have calculated the list of variables by several approaches (Antoine et al., 2004). We have applied both the ‘max’ and the ‘mean’ transformation from 2D to 1D spectrum, we have used both the sample spectrum as it is and the difference between the original and sample spectra, and we have calculated the variables both with and without applying the CSF. In total, we obtain eight different lists of variables from the same images. Different approaches may be the optimal choice for different variables.

Our final goal is to construct a model for the human perception of quality in images, represented by the standard preference *STPREF*. Since we are dealing with strongly correlated input variables, or predictors, we cannot apply a multiple linear regression model where one of the basic assumptions is independent predictor variables. PLS, projection on latent structures or partial least squares (see e.g. Martens and Martens, 2001), models both the predictors and response simultaneously to find the latent structures in the predictor space that are best in explaining the response. These latent structures are similar to principal components, and will be referred to as PCs. In our analysis we use the multivariate data analysis software Unscrambler (<http://www.camo.com/rt>).

The statistical analysis will be based on the OR-side, since we only have the ‘Part’ images from this side. The variables obtained from the ‘Full’ image will have the prefix *F*, e.g. *F-WL[HTDP]*, and the variables

from the 'Part' image the prefix P . In order to see if a more complicated model is 'worth the trouble', we fit the simplest model possible to our data; a univariate linear regression model. The best predictor for the OR side is $P\text{-}WL[<HTDP]$ with an R^2 of 64 %. This variable, obtained from the highest frequencies, have much less noise when obtained from 'Part' than from 'Full' and is therefore better in predicting the standard preference of the judge panel. The quality of the half tone dots seems to be an important element in the judges' preferences.

The optimal PLS model for 'Full', OR-side, based on $F\text{-}WL[HTDP]$ and $F\text{-}WL[HTDP\text{-}Imm]$, has for comparison an adjusted R^2 of 52%, indicating that the information found in the higher frequencies is more important than lower frequency information. The adjusted R^2 tries to compensate for the sample size and for the number of variables included in the model. Although the addition of new variables will always cause R^2 to rise, the adjusted R^2 may fall if the added variables have little explanatory power and / or if the degrees of freedom become too small. Finding the optimal model will usually be a trade off between maximizing R^2 , minimizing the model validation variance and including theoretical knowledge in the model. For the IR-side, we find the same optimal model for 'Full', i.e. predictors $F\text{-}WL[HTDP]$ and $F\text{-}WL[HTDP\text{-}Imm]$, but R^2 is now only 47%. The coefficients for the models for the two sides differ, so if we would try to model the two sides together the explained variance would be even worse.

The optimal PLS model based on variables from 'Part' only has an R^2 of 68%. Predictors are $P\text{-}WL[<HTDP]$ and $P\text{-}WL[HTDP\text{-}Imm]$, i.e. high frequency information. The improvement from the univariate regression model is just 4%, so one can argue that the gain is too small to "defend going multivariate".

The question is then if we gain any additional explanatory power by combining the variables from 'Full' and 'Part' in the same model, or do they contain more or less the same information? A principal component analysis indicates that the two sets of variables do not correlate very well. The first principal component consists mainly of 'Part' variables, whereas the second is constructed from the lower frequency 'Full' variables. The complete model of $STPREF$, complete in the sense that all variables from both 'Full' and 'Part' were included, gave an R^2 for the two first PCs on 79%. Combining the two sets of variables greatly improved the model. Further, we found that most of the variables were redundant, so without losing too much of the model's predictive power, we can remove all but three predictors.

The main results of a PLS analysis include score plots, loading plots, predicted response values and residual validation variance. PLS scores are basically the sample coordinates along the PCs (Figure 4). This plot gives information about patterns (groupings, asymmetric distributions, outliers etc.). The closer the samples are in the score plot, the more similar they are with respect to the two PCs concerned, so this plot can be used to interpret differences and similarities among samples.

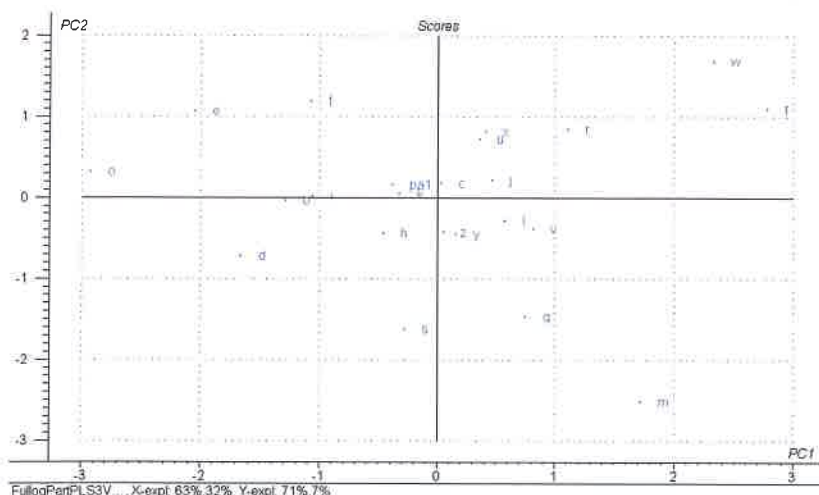


Figure 4:

Score plot for the final PLS model for the OR-side based on both 'Full' and 'Part' variables

The PLS loadings express how each of the predictor and response variables is related to each other and to the PCs summarized by the scores (Figure 5). Variables close to the response have a large (positive) influence; variables opposite of the origin have a negative influence, whereas variables close to the origin contribute little to the model. The score plot and the loading plot should be interpreted together. This can help in determining which variables are responsible for differences between samples. For example, samples to the right of the score plot will usually have a large value for variables to the right of the loading plot.

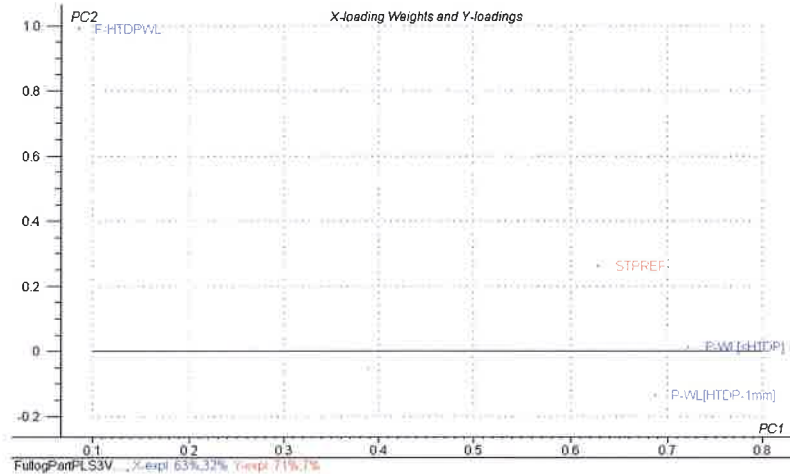


Figure 5: Loading plot for OR-side model based on both 'Full' and 'Part' variables

From 'Part', the variables $P\text{-WL}[\text{HTDP-1mm}]$ and $P\text{-WL}[\text{<HTDP}]$ are still the most influential, together with $F\text{-HTDPWL}$ from 'Full' (see Figure 5). This model explains 78% (adjusted) of $STPREF$; split into 71% from the first PC and 7% from the second PC. The two variables from 'Part' basically make up the first PC, so this direction can be interpreted as the representation of small details and sharpness ($P\text{-WL}[\text{HTDP-1mm}]$) together with the characteristics of the half tone dots ($P\text{-WL}[\text{<HTDP}]$). In order to represent sharp edges, both with respect to image content and dot sharpness, we generally need more energy in the higher frequencies. More sharply defined and regular dots will induce harmonics and more energy in the frequency interval covered by $WL[\text{<HTDP}]$. The second PC is surprisingly based on $F\text{-HTDPWL}$, i.e. the wavelength of the half tone dot peak observed in the 'Full' image. This variable was not found significant in the model based only on variables from 'Full', but the additional information it gives is apparently useful in the combined model. The wavelength of the half tone dot peak should be fixed from the press parameters for all qualities, so this variable must indirectly express 'something else', e.g. fan-out and the dimensional stability of the paper. By inspecting the corresponding score plot (Figure 4) we see that samples m , s and q have low values along the second PC, whereas samples w , e and f score high. These sample levels are also found in $F\text{-HTDPWL}$.

We validate our models to get an idea of how well a model would perform if it were used to predict new, unknown samples. A test set consisting of samples with known response values is usually used. Only the predictor values are fed into the model, from which response values are predicted and compared to the known, true response values. We will here use the cross-validation approach where the same samples are used both for model estimation and testing. A few samples are left out from the calibration set and the model is calibrated on the remaining samples. Then the values for the left-out samples are predicted and the prediction residuals are computed. The process is repeated with another subset of the calibration set, and so on until every sample has been left out once. Then all prediction residuals are combined to compute the validation residual variance (Figure 6). Large residual validation variances indicate that the model does not describe the data well. We see that a model with two or three PCs has an acceptable validation variance.

The predicted vs. measured response plot is another way to check the quality of the model (Figure 7). If the model gives a good fit, the plot will show points close to a straight line through the origin and with slope close to 1, indicating a high linear correlation between predicted and measured values. For each sample we have plotted two points; the point closest to the straight line shows the calibration sample and the other point shows the validation sample. The calibration samples are the samples on which the calibration of the model is based, whereas validation samples are samples that are not used during the calibration stage but only to validate an already calibrated model. If the calibration and validation points for a given sample are far apart, this sample has a strong influence on the model. Outliers and non-linear relationships can also be detected from the predicted vs. measured plot.

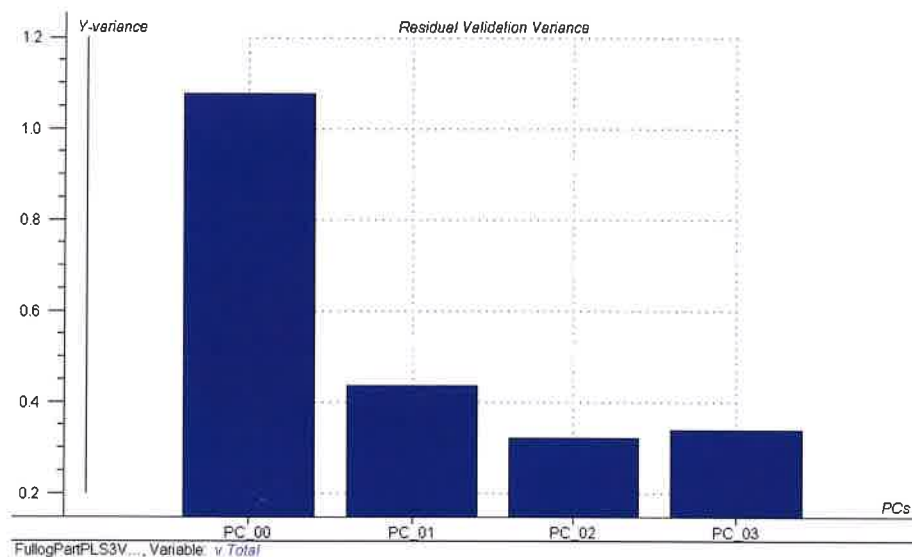


Figure 6: Residual validation variance plot for final OR-model

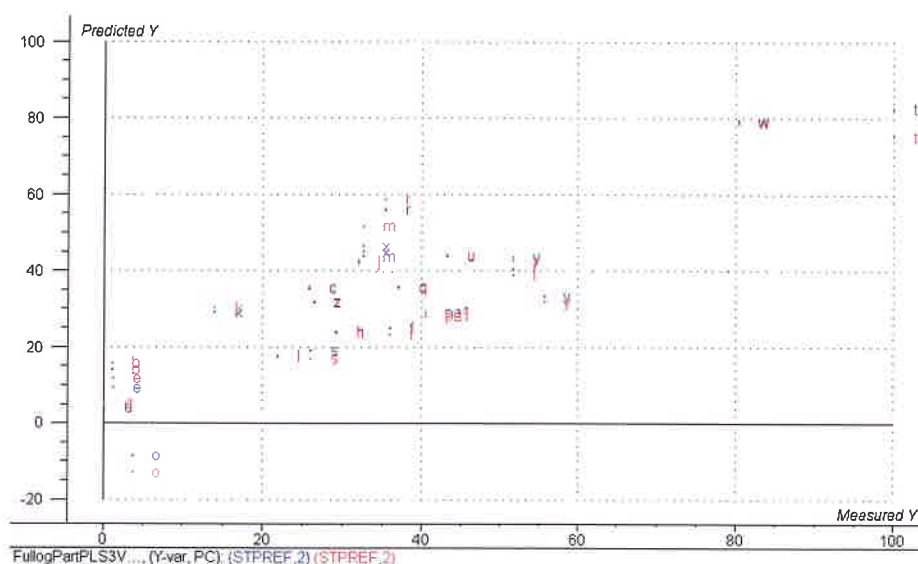


Figure 7: Measured and predicted response values plotted against each other; final OR-model

This predicted vs. measured plot is satisfactory; the points are fairly close to the straight line indicating a high correlation between predicted and measured responses, and the calibration and validation points are close, indicating that the model is good at predicting unknown samples in this quality range.

4. Discussion

Several authors (e.g. Antoine, 1998; Berli et al., 1994; Collins and Rosson, 1988; Foyn et al. 1996; Johansson, 1993; Johansson and Norman, 1996; Nguyen et al. 1996; Shiratori et al. 1994; Spencer and Schwartzwald, 1996; Ångskog and Johansson, 1995) have attempted to find these indexes that characterize image quality with respect to sharpness, mottling, contrast etc. Remember then that all paper and print quality measures are one-dimensional indices from a multidimensional space, so we should not expect them to be more than measures of this particular dimension. If we want a more robust analysis, we should apply several different indices, or rely on a more complete description of the image.

Instrumental measures must be able to distinguish between images not too different; it is the more subtle changes that we need analytic tools to discover. A measure's effectiveness will therefore depend on its ability to discriminate between images and the precision with which it can be estimated from samples. The OPQ-variables from 'Full' are acceptable when inferring from lower frequencies, but when we are interested in small details and higher frequency measures (e.g. dot characteristics) the image resolution must be improved. These higher frequency features are therefore obtained from 'Part'. Results from this analysis validate our theoretical interpretation of the OPQ-variables.

An ideal model is one that describes the system in as much detail as we have evidence for besides having a parsimonious structure. Predictions are always conditional and probabilistic statements depending on how the samples are selected, the images used in the printing form, the background of the judges etc. A note of warning; models validated in a limited domain are too often generalized on insufficient evidence. The search for generality may increase our understanding, but this generalization should be based on solid ground and not on excessive extrapolations. Since models and theories necessarily are simplifications, they cannot be expected to account for all the variance in a noisy world. The final model will therefore be a trade off between optimizing the fit to the present data set and considerations based on theory and 'facts' related to the involved variables. Our predictions will probably be both more accurate and certainly more convincing if we manage to link the observed pattern with some physical explanation.

It is hard to be precise when subjectively quantifying the difference or preference in a large pairwise comparison evaluation. Any inconsistencies or deviations from the ideal linear scale for the standard preference will show as a reduced R^2 for the model or, as in our case, problems in obtaining predicted values from the whole scale (0 to 100). For example, in Figure 7 we see that the predicted value for the best sample (t) is around 80. The OPQ measurements do not indicate that sample t is that much better than the other samples as the subjective evaluation states. Possibly, the scale is 'stretched' in the higher values in order to use the whole predefined scale. A more robust validation of the model can be to check if it detects the extreme observations. The general tendencies of the sample set should also be maintained, but there will always be some elements in the concept of subjective quality that are impossible to model by physical parameters.

The significant parameters of the model are already discussed in the text, but some additional comments are appropriate at this stage. The three OPQ variables left in the final model are all calculated from wavelengths of size 1 mm or smaller. Some would maybe expect that the longer wavelengths were more important in the print quality evaluation (e.g. wiremarks), but the paper grades in this sample set differed little with respect to these 'larger' features. The judges had to base their evaluations on the finer details of the print; details that models of the human visual system assume beyond the eye's maximum resolution. Even if the judges cannot pinpoint which element of print quality they apply in their evaluation, they 'sense' effects like deviations from an ideal dot (halftone mottle or dot raggedness). The positive correlation observed between $WL[<HTDP]$ and perceptual quality indicate that differences in dot characteristics are observed by the panel. A tentative explanation for the observed link between the second PC of the model and $F-HTDPWL$ is differences in the dimensional stability between samples. Papers with a poor dimensional stability will yield prints with irregular dot distances.

During a statistical analysis, one must always be cautious when inferring causalities from observed correlations or model relations. Our suggested interpretations are just that, i.e. suggestions. Any further interpretation must be based on the reader's experiences and/or additional data. Remember also that failure to detect a connection between parameters does not prove that a parameter has not influenced the print, but merely that its assumed effect cannot be deducted from the sample set. A basic assumption in most statistical methods is random sampling. Theoretically, we mean random in the sense that all 'individuals' have the same chance of being observed. This is usually hard to achieve in practice; randomness may instead refer to time of sampling, location, 'random' sections from 'non-random' batches (rolls) etc. Deviations from random sampling may produce a biased model; we may get only 'good' specimens, or at best; selective 'good's and 'bad's, rendering it difficult to estimate the true variance in paper quality.

We suspect that we will experience an increasing stochasticity with the length of the study period. On short time scales paper characteristics may vary slightly about some level, but when the time scale is prolonged, this level itself will vary and possibly even more than the short time variations. This stochastic time dependence makes long time predictions very uncertain. The reason for this should be pretty clear; there are continuous changes in paper quality itself, in our perception of an acceptable level of quality, and in which elements of paper quality we emphasize. A model of perceptual quality will therefore have a time-limited durability. At each major change in the production process, in the printing process or in the raw material composition, a new model will have to be fitted. We can 'never' become totally independent of human evaluation, unless a general agreement (consensus) is reached on which objective measures to use and how to measure these. Nevertheless, models like the ones presented in this report are needed in order to increase our knowledge of the 'evolutionary' causes for print quality. The models can also be used to ease the workload of the panel by applying them in between these 'quality alterations', and as an aid in product development and process optimization by simulation studies where important variables are varied, within acceptable limits, and the effect on the response evaluated.

5. Conclusions

We have here presented a statistical model for perceptual print quality in complex images on newsprint. The parameters included in the model are found by Fourier transforming high-resolution digital images of commercially printed newsprint. These instrumental measurements were found to be satisfactory in differentiating between samples of almost equal quality and in capturing the most important visual quality characteristics from complex images.

The multivariate model is based on two principal components that explain 78% of the variance in the response. The first component (explaining 71%) is calculated from two variables; one describing small details and the sharpness of the image, the other is linked to the characteristics of the half tone dots. The samples were thereby found to differ mostly in the high frequency features, i.e. the smallest wavelengths, such as the shape and sharpness of the dots. We found no significant influence on the response from image features with longer wavelengths (e.g. wiremarks). The second component explained 7%, and is based on the average distance between half tone dots. This is a surprising result, since this distance should be fixed in the press and thereby constant for all qualities, but is probably an effect of unevenness in fan-out, or shrinkage.

With this model, we can predict how a panel of judges will rank samples from this market segment in a benchmarking study focusing on print quality in black and white images on newsprint.

Acknowledgments (part 1)

The authors wish to thank Ola Nybakk, NTNU, Norway for his valuable work during his diploma work in the frame of this project (Nybakk, 2000) and Jacques Antoine, Supelec, France for useful discussion on Fourier Transform and signal filtering. The authors are also grateful to Norske Skog and the Research Council of Norway for financial support.

Acknowledgements (part 2)

The authors are grateful to Norske Skog and the Research Council of Norway for financial support.

References (part 1)

- Antoine, C., 1998, 'Development of Image Analysis Procedures for Print Quality Evaluation', *Pan-Pacific and IPAGAC Conference, Québec, 6-8 October 1998*
- Berli, E.L., Moller, K., Hansen, Å., Foy, B., 1994, 'The Dagbladet full-scale printing trials - Part 2: Print quality evaluation by subjective comparison and image analysis', *Tappi Journal* 77(4): 151-159
- Blakemore, C., Campbell, F.W., 1969, 'On the existence of neurones in the human visual system selectivity sensitive to the orientation and size of retinal images', *Journal of Physiology* 203: 237-260
- Collins N.J., Rosson, A.J., 1988, 'Image Analysis in Printability Testing', *Appita* 41(6): 475-479
- Daly S., 1993, 'The Visible Differences Predictor: An algorithm for the Assessment of Image Fidelity', chapter 14 of 'Digital images and Human Vision' ed. by Andrew B. Watson, Cambridge, MIT Press, ISBN: 0-262-23171-9
- Devalois, R.L., Albrecht, D.G., Thorell, L.G., 1982, 'Spatial frequency selectivity of cells in the macaque visual cortex', *Vision Research* 22: 545-559
- Devalois, R.L. and Devalois, K.K., 1988, 'Spatial Vision', Oxford: Oxford University Press
- Diserud, O., Antoine, C. and E. Berli, 2004, 'Objective Print Quality Assessment in Complex Images – Part 2: A Model for Perceptual Print Quality in Complex Black and White Images', *IARIGAI 31st International Research Conference, 5-8 September 04, Copenhagen*
- Foy, B., Solheim, O., Løvhaugen, O., 1996, 'Differential Spectra – A new method for print quality analysis from pictures', *TAPPI Proceedings, 1996 international Printing and Graphic Arts Conference*
- Hunter, R. S., Harold, R.W., 1987, 'The Measurement of Appearance', 2nd edition, A Wiley – Interscience publication, John Wiley & Sons, New York, ISBN: 0-471-83006-2
- Jin E.W., Feng, X.-F., Newell, J., 1998, 'The development of a color visual difference model' *IS&T's 1998 PICS Conference, 154-158*
- Johansson, P.-Å., 1993, 'Print mottle evaluation by band-pass image analysis', *IARIGAI 22nd International Research Conference, Munich, Advances in Printing Science and Technology 22, Pentech Press, p. 403*
- Johansson, P.-Å., Norman, B., 1996, 'Methods for evaluating formation, print unevenness and gloss variations developed at STFI', *Proc. TAPPI 1996 Process and Product Quality Control Conference, Cincinnati, TAPPI Press, Atlanta, pp. 139*
- Johansson, P.-Å., 1999, 'Optical homogeneity of Prints', *Doctoral thesis, KTH, Stockholm*
- Limb, J.O., 1979, 'Distortion Criteria of the Human Viewer', *IEEE trans. On systems, man and cybernetics, SMC-9(12):778-793*
- Maffei, L., 1978, 'Spatial frequency channels: Neural mechanisms', In R.Held, H.W. Leibowitz & H. Teuber (Eds.) *Perception. Berlin: Springer-Verlag. pp. 39-66*
- Mitsa, T., Varkur, K.L., Alford, J.R., 1993, 'Frequency-Channel-Based Visual Models as Quantitative Quality Measures in Halftoning' *SPIE vol. 1913 pp. 390-401*
- Mullen, K.T., 1985, 'The Contrast Sensitivity of Human Colour Vision to Red-Green and Blue-Yellow Chromatic Gratings', *Journal of Physiology* 359: 381-400
- Ness, C., Götsching, L., 1995, 'Formation of Paper and Mottling of Solid Prints', *IARIGAI 23rd International Research Conference, Paris, 17-20 Sept. 1995, Advances in Printing Science and Technology, Ed. Wiley. pp. 429-450*

- Nguyen, N.G., Jordan, B.D., Le-Ngoc, T., 1996, 'Print Sharpness Measurement by Image Analysis', *JPPS* 22(9): J356-J364
- Nybakk, O., 2000, 'Measurement of Print Quality in black/white offset print', Diploma thesis, ITK, NTNU, Trondheim
- Pratt, W. K., 1991, 'Digital Image Processing', 2nd edition, A Wiley - Interscience publication, N.Y., ISBN: 0-471-85766-1
- Shiratori, N., Yoshidomi, N., Ishimura, H., 1994, 'Quantitative evaluation of print mottle and correlation to subjective rating', 1994 Coating Conference, TAPPI Proceedings: 269-278
- Spencer, P., Schwartzwald, D., 1996, 'Automatic Print quality measurement using a scanner', International Conference on digital printing technologies, San Antonio, TX, USA, pp. 156-158
- Stromeyer, C.F., Julesz, B., 1972, 'Spatial-frequency masking in vision: Critical bands and spread of masking', *Journal of the Optical Society of America* 62: 1586-1592
- Sullivan, J., Miller, R., Pios, G., 1993, 'Image halftoning using a visual model in error diffusion', *Journal of Optical Society of America* 10(8): 1714-1724
- Watson, A.B., Barlow, H.B., Robson, J.G., 1983, 'What does the eye see best?', *Nature*, 302, 419-422
- Williams, A., 1996, 'Colour management systems', *IFRA Special report* 2.18
- Wysecki, G., Stiles, W.S., 1982, 'Color Science: Concepts and Methods, Quantitative Data and Formulae', 2nd Edition, a Wiley - Interscience publication, John Wiley & Sons, New York
- Ångskog, S., Johansson P.-Å., 1995, 'Measurement of detail rendering in print', IARIGAI 23rd International Research Conference, Paris, 17-20 Sept. 1995, *Advances in Printing Science and Technology*, Ed. Wiley. pp. 471-491

References (part 2)

- Antoine, C., Diserud, O.H. and Solheim, O., (2004), *Objective Print Quality Assessment of Complex Images. Part 1: Print Quality Assessment by Means of the Fast Fourier Transform*, IARIGAI 2004
- Antoine, C., (1998), *Development of Image Analysis Procedures for Print Quality Evaluation*, Pan-Pacific and IPAGAC Conference, Québec
- Berli, E.L., Moller, K., Hansen, Å., Foyn, B., (1994), *The Dagbladet full-scale printing trials - Part 2: Print quality evaluation by subjective comparison and image analysis*, *Tappi Journal*, 77(4), pp. 151-159
- Collins N.J., Rosson, A.J., (1988), *Image Analysis in Printability Testing*, *Appita*, 41(6), pp. 475-479
- Foyn, B., Solheim, O., Løvhaugen, O., (1996), *Differential Spectra – A new method for print quality analysis from pictures*, TAPPI Proceedings, 1996 international printing and Graphic Arts Conference
- Johansson, P.-Å., (1993), *Print mottle evaluation by band-pass image analysis*, IARIGAI 22nd International Research Conference, Munich, *Advances in Printing Science and Technology* 22, Pentech Press, pp. 403
- Johansson, P.-Å., Norman, B., (1996), *Methods for evaluating formation, print unevenness and gloss variations developed at STFI*, *Proc. TAPPI 1996 Process and Product Quality Control Conference*, Cincinnati, TAPPI Press, Atlanta, pp. 139
- Martens, H. and Martens, M., (2001), *Multivariate analysis of quality*, John Wiley & Sons, Chichester, England.
- Nguyen, N.G., Jordan, B.D., Le-Ngoc, T., (1996), *Print Sharpness Measurement by Image Analysis*, *JPPS*, 22(9), pp. J356-J364
- Shiratori, N., Yoshidomi, N., Ishimura, H., (1994), *Quantitative evaluation of print mottle and correlation to subjective rating*, 1994 Coating Conference, TAPPI Proceedings, pp. 269-278
- Spencer, P., Schwartzwald, D., (1996), *Automatic Print quality measurement using a scanner*, International Conference on digital printing technologies, San Antonio, TX, USA, pp. 156-158
- Ångskog, S., Johansson P.-Å., (1995), *Measurement of detail rendering in print*, *Advances in printing science and technology: Proceedings of the 23rd research conference of IARIGAI*, Ed. Wiley, pp. 471-491

Appendix 1 to part 1

Experimental: Acquisition parameters

Picture	Side	Size (pixels)	B/W balance	Lens Aperture	Exposure time ¹ (s)	Illuminance ² (lux)	Camera height on tripod ³ (cm)
Galtesund	OR	3336 x 3560	21/227	5.6	1/4	253	118.3
Galtesund	IR	3328 x 3560	19/232	5.6	1/4	254	118.3
Galtesund	OR	4644 x 3564	15/201	5.6	(1/4)+	257	96
Old car	OR	5316 x 2976	18/232	5.6	(1/4)-	264	120
Three musicians	OR	2200 x 2200	17/214	5.6	1/4	260	105
Fuji lady	OR	2488 x 3016	17/243	5.6	(1/4)+	260	132
Fuji Lady	IR	2488 x 3016	18/247	5.6	(1/4)+	260	132

1: the 1/4, 1/4+ and 17- are three exposure times offered by the software handling the acquisition of images. The exact meaning of the + and – is not known.

2: the illuminance given here is the one measured at the start of the series acquisition, the illuminance meter being place on the sample at the center of the region of interest to be acquired. During each acquisition, the illuminance were also recorded but with the illuminance meter lying close to the sample out of the region of interest so its place were fixed during all the series acquisition time. This allowed us to detect any important fluctuation in the illumination that happened due to electrical power fluctuation during the day. No samples were acquired during these unstable periods.

3: The tripod of the camera has an accurate rule suitable (millimetric graduation) to record the height of the camera with the ground. It would have been more appropriate to measure the distance between the sample and the camera, but as the table where the sample is lying is fixed, if needed this height can be known. We found so far much accurate and easy to record the camera height with the ground according to the tripod rule.

An innovative tool to ensure printing ink performances consistency

Christine Canet

ICGQ

999, Émile- Journault Avenue East

Montreal (Quebec), Canada H2M 2E2

E-mail: canet@icgq.qc.ca

Abstract

In order to ensure printing ink performances consistency, ICGQ carried out an applied development project. This study aimed to find a fast and reliable laboratory test that allowed printers to control ink performances consistency before going on press.

This innovative tool, which is a patent pending technology, is based on the usage of an FT-IR spectrophotometer. The novelty of this technology relies on the fact that spectrum are now directly linked with press performances, and no longer with ink components only.

This invention contemplates a method for comparing data from a whole printing ink sample to reference data, analyzing differences and predicting impact on its quality or performance in a printing process, in order to make a decision generally of the pass or fail type.

Context

The ICGQ is a world-class center that integrates innovation and expertise to proactively support the graphic communications industry, its partners and their employees in their technical and commercial development.

Key words

Consistency, Ink, Performances, Printing

1. Introduction

Although ink supplies represent the second highest expense after substrates, for the production of printed products, little care and efforts have been devoted so far to control properties of ink supplies and their impact on production costs and quality. For instance, slight changes in an ink formula may result in a reduction of coverage (mileage...), leading to substantial but hardly identified consumption and cost increases. For a large printing company, such variations in ink quality may result in millions of dollars of extra cost annually. Furthermore, introduction of improper ink in a printing process may require stop and cleaning a press, which is highly troublesome and costly.

In order to reduce occurrence of the aforementioned drawbacks, some quality control is carried out on printed samples or on whole (unprinted wet state as supplied by manufacturers) ink samples. However, while evaluation of printed samples (generally by simple photometric measurements) produces a late indication of a problem and mainly addresses visual quality problems, testing whole ink prior to printing is typically carried out in laboratory through an extensive series of physical and mechanical tests, such as pigment density, opacity, viscosity etc., requiring fair amounts of ink samples and time. Further, differences between the physical or mechanical properties of a sample with respect to reference values do not provide clear indication of the resulting impact on in-process performance of the tested ink.

It is worth mentioning that most of the existing technologies of the prior art concern jet-printing inks and writing instrument inks and that technologies used in connection with offset printing inks or the like are generally of the spectrophotometric type. Therefore, none of the existing techniques provide an appropriate means for evaluating properties and quality of a whole printing ink, and especially with regard to in-process performance. However, the prior art teaches that infrared (IR) and near-infrared (NIR) spectrometry enable extended characterization of an ink, providing some sort of distinctive signature (also referred to as fingerprint). Indeed, such techniques proved to be very effective for chemometric analysis of organic components such as resins, pigments or solvents found in media such as paints, dyes or inks, as well as for quality control in the pharmaceutical industry.

A few scientific publications confirm that FT-IR and FT-NIR spectra of a liquid ink solution provide a unique signature, usable for authentication purposes provides good results in matching spectra from ink solutions extracted from a questioned document with spectra from pure whole ink samples from a data base for identification purposes. The major causes of errors are related to the presence of substrate traces in the extracted ink solution.

2. Objective of this work

Although the above examples show that different existing methods contemplate detection or evaluation of ink properties, no method of the prior art is readily applicable to evaluation of a whole printing ink to enable reliable identification of any aspect that may negatively affect performance of the ink in a printing process such as offset, gravure, flexography etc.

There was thus a need for a novel method overcoming the limitations and drawbacks of the methods of the prior art, which can be carried out using a very small whole printing ink sample from an ink supply, to provide indication of the degree of compliance with reference ink data to enable a pass or fail decision and/or ensure consistency of in-process performance characteristics prior to introduction into the actual process.

3. Materials and method

3.1 Materials

The machine is a Mid and NIR FT-IR spectrophotometer from ABB with appropriate accessories. Ink samples were collected in 148 pressrooms worldwide. Among them, 132 were offset printing plants and the remaining ones were gravure printing pressrooms. A total of more than 1000 ink samples of each color were gathered, tested and analyzed.

3.2 Methodology

Two subprojects were conducted in parallel to ensure the completion of the development of this new tool:

- ✓ The first one consisted in developing adequate lab procedures to characterize accurately ink (either paste or liquid) with the IR technique. The principal objective was to reach an acceptable repeatability and reproducibility of the measurements. This phase included the selection of the Mid vs. the near infrared, the choice of accessories and of detectors and the development of the measurement procedure.
- ✓ The second phase of the project that was run in parallel with the above mentioned one consisted in building databases.

- The first step consisted in characterizing and defining theoretical parameters having a major influence (considered individually or in combination) on mileage. Determination of these factors was feasible thanks to extensive laboratory testing and thanks to the active participation of Quebecor World, which provides us a feedback on real ink performances behavior on press. In fact, multivariable analyzes were carried out, containing both laboratory data and feedback from the field. Each time a feedback from the field was introduced in the database, our customer sent a printing specialist to confirm that specific ink behavior was really due to specific ink properties and were not related to particular press set ups and press environment.
- The second phase consisted in establishing or revisiting existing laboratory procedures to obtain accurate measurements of pre-identified parameters (considered separately or in combination). This part of the project permitted to establish consistency of the procedures, their repeatability and their reproducibility. At the end of this stage, all procedures were revisited, validated and approved by the two major ink manufacturers in the world. This stage was fundamental as the data issued of the regular testing were then introduced in the databases, on which IR calibrations are built.
- ✓ Last phase of the project consisted in linking the FT-IR Mid & NIR spectrum with the data, on which calibrations are built. In fact, this last stage comprised several steps:
 - Feasibility of the calibrations related to ink performances on press should have been demonstrated;
 - Accuracy of the verdict (pass or fail) should have been obtained;
 - And finally calibrations should have been validated on unknown samples.

4. Results and discussion

The second and the three stages of the project were very long and fastidious as a very large number of data was collected and as printers are generally not used to work with such databases.

Establishment of the first calibrations was complex, as we had to demonstrate that some parts of a FT-IR spectrum could be correlated with specific ink printing behavior. After having established the feasibility of calibrations of that type, extensive work was carried out to fine tune calibrations. First acceptable calibrations were obtained in July 2003. Since that date, they have been revisited and fine tuned several times.

Between July 2003 and June 2004, both conventional lab and infrared tests were conducted in parallel. This period intended to ensure the methodology robustness, but was also used by ICGQ to prove the validity of the technology to the ink manufacturers.

Since June 2004, conventional testing measurements are gradually switched to FT-IR evaluation. Complete implantation in the field is planned for November the 1st 2004, as the two major ink manufacturers have decided to invest and to use this technology for a large group of printers.

At that stage, verdict (i.e.: an ink passes or fails printer specifications) is similar in more than 98 % of the case, when comparing regular and IR testing. As far as values are concerned, actual values measured by the IR correlate data issued of regular testing with a coefficient of correlation between 0,95 and 0,99 depending on the ink type, the color and the considered ink properties.

5. Conclusions

The present tool provides a printing ink evaluation method enabling acceptance or rejection of a printing ink supplies according to the degree of compliance with a reference master ink. This tool permits a fast

(less than one minute is needed to do the measurement) and reliable systematic ink quality control to ensure its consistency from batch to batch.

Infrared technology represents in fact a shortcut, which summarizes standard tests in one minute. It condenses several tests in a single measurement.

It is not a new technology; it is an already proven technology. It is only a new way to interpret the data. Results are related to performances and no more to ink composition only.

Acknowledgements

The author would like to thank Quebecor World for their active support, ABB Bomen for their cooperation and EFPG for their valuable help.

Literature references

- Bowers (1994), *US patent No 5,373,366*
Martin & al., (1990), *US patent No 4,935,628*
Nottke & al., (2001), *US patent 6,275,285*
Pfeiffer & al., (1999), *US patent No 5,967,033*
Rena A. Merrill & Edward G. Bartick, (1992), *Journal of Forensic Sciences, JFSCA, Vol 37, No 2, pp 528 – 541*
Sato & al., (1985), *Publication No 60-202172A*
Yanagida & al., (2001), *US patent No 6, 287,374*



5

Color and image quality



Effects of screen ruling on color of printed matter

Ikuo Naito, Syon u Lee, Akihiro Kinoshita*

Dept. Photography, Fac. Art, Kyushu Sangyo Univ.
Matsugadai 2-3-1, Hushashi-ku, Fukuoka 813-6503, Japan
E-mail: naitou@ip.kyusan-u.ac.jp

Abstract

The effects of screen ruling on color gamut were studied using 175, 330, 700 lines per inch (LPI) half-tone printed matter. The reflectance in the muddiness range, i.e., green (**G**) range of cyan (**C**) ink and blue (**B**) range of magenta (**M**) ink, improved with increasing screen ruling. Micro reflection spectra of dot and non-dot (paper) areas were measured. With **C** printed matter, the **G** reflectance of dots increased and that of non-dot area in red (**R**) range decreases with increasing the screen ruling. With **M** printed matter, the reflectance of dot area in **B** range increased and that of non-dot area in **R** range decreased with increasing the screen ruling. With accurate ink yellow (**Y**) printed matter, reflectance of the none-dot area in **B** region decreased with increasing the screen ruling. These phenomena can be explained by optical dot gain.

Keywords

Micro reflection spectrum, Optical dot gain, Screen ruling

1. Introduction

Recently, many new printing technologies have been developed, including high resolution printing, random dot printing (FM screen printing), seven color printing and printing by high density inks, etc.¹⁻⁵. High resolution printing is a representative high screen ruling [< 300 lines per inch (LPI)] method that is characterized by high color reproducibility (wide color gamut), high resolution, and an undetectable Moiré pattern. While the latter two characteristics of high screen ruling are understandable, it is difficult to understand why high screen ruling results in high color reproducibility. This can be explained by optical dot gain,⁴ yet there are no reports or they are not well known on the relation between the optical dot gain and the high color reproducibility.

We studied the optical dot gain using an image processor and samples printed in black square dot patterns (dot percentage: 10 - 90 %; screen ruling: 25 - 200 LPI). Because the optical dot gain is a phenomenon to observe dot larger than real size. A difference in them is one parameter of the optical dot gain. Since the reflectance changes continuously around dot edge, we measured width of the reflection change (reflectance range = 17 - 64 %) as about $30 \mu\text{m}$.⁶ A wavelength effect on the width was also detected. To clarify the optical dot gain, we measured reflection density changes around the edge of solid patch. Reflection density traces were divided to three parts: as low-, middle-, and high-density areas. In the middle density area, the reflection density changed linearly with length. Previously, we reported that the width (Δl) in the middle-density area ($d = 0.5 - 1.2$) to about $20 \mu\text{m}$ [14.1 (**R** filter), 18.2 (**G** filter) and 23.5 (**B** filter) and $20.5 \mu\text{m}$ (no filter)].⁷

The reflection spectra of the printed matter are far from the ideal spectra for the muddiness of the ink, i.e., lack of **B** and **G** reflectance of **M** and **C** printed matter, respectively. As more amount of ink is transferred (**y**), the colors of **M** and **C** printed matter changed to **R** and **B**, respectively, according to the **y** value. Improving the ink color should increase the color gamut a great deal. We studied the effect of the screen ruling on the color specification values (CIE- $L^*a^*b^*$) of printed matter using a geometric series of the screen ruling: 175, 330, 700 LPI (6.9, 13.0, 27.6 lines per mm, respectively).

2. Experimental

2.1 Samples

The half-tone printed matters were donated by Okamura Printing Industry Co. Ltd. (screen ruling: 175, 330 and 700 LPI; ink: for sheet feed offset printing; paper: art post paper 250 g m⁻²). The dot percentages were the values of original data. Reflection densities of solid patch are listed in Table I.

Table I: Solid densities of sample

ink	screen ruling / LIP	reflection density		
		d _B	d _G	d _R
cyan	700	0.29	0.59	1.67
	330	0.28	0.63	1.64
	175	0.31	0.64	1.68
magenta	700	0.72	1.65	0.20
	330	0.76	1.75	0.21
	175	0.69	1.64	0.20
yellow	700	1.92	0.21	0.16
	330	1.88	0.20	0.15
	175	1.76	0.22	0.16
paper		0.11	0.10	0.10

2.2 Apparatus

Every measurement was made in a dark room. Reflection traces were measured using an Olympus Co. Ltd. microscope BH2-UMA type with a long-working-distance objective lens (magnification: 5, 10 and 20 times; twice the magnification of relay lens). Photomicrographs were taken using a Tokyo Electronic Industry BV6404A9 CCD camera (analog camera) connected to the microscope and a Nippon Avionics Excel II image processor (6.55 × 10⁴ pixel, 8 bite). The printed matter was illuminated from two directions, 70 deg. apart, using two Moritex 150 SL cable illuminators and interference filters. A power supply was used for stabilization of illuminators. We lit the illuminators one hour before the measurements. Figure 1 shows a rough sketch of the apparatus. The distances in the photomicrograph were calibrated using a standard gauge (10 µm notch) and a test pattern for IC (0.5 – 5.0 µm line and space pattern). The reflectance was calibrated using a standard reflection plate (Machbeth, 10 steps).

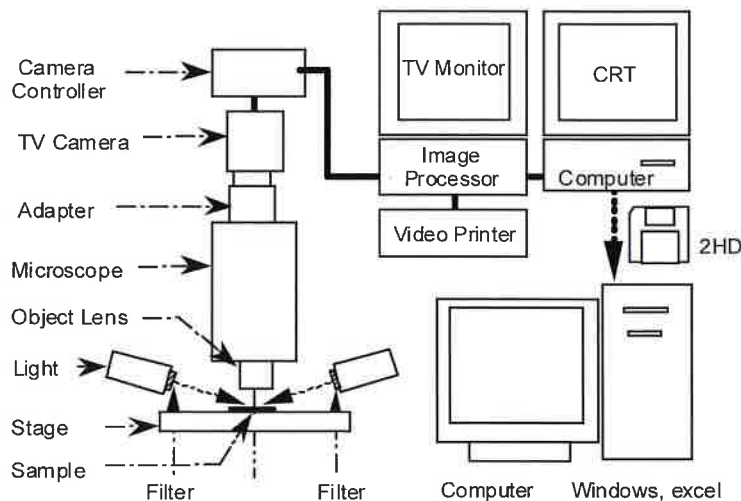


Figure 1: Apparatus of image processor

Reflection spectra were recorded using a Minolta CM2022 color meter (measuring area $\phi = 5$ mm; polychromatic integrating sphere mode). Color specification values (CIE1976 $L^*a^*b^*$) were measured as CIE1931 standard calorimetric values (light source: D65).

Micro reflection spectra were measured using an Otsuka electronics IMAC-7000 instantaneous multi-photometer (monitoring spot; $\phi < \text{ca. } 1, 2, \text{ and } 4 \mu\text{m}$ for the 20, 10 and 5 times object lenses, respectively). The spot size was sufficiently smaller than the dot size. A quartz fiber of the apparatus was connected to the head of the microscope instead of the CCD camera of the image processor. Measuring of spots was confirmed visually using marker spots (Fig. 2). The spectra were measured after adjusting the sample and cutting the spot lamp. We used the art post paper instead of white standard reflection plate. The average spectrum was recorded from ten measurements.

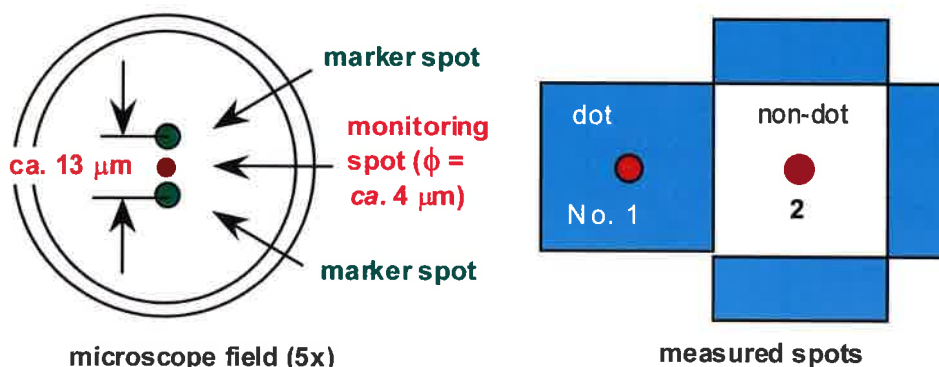


Figure 2: Microscope scope field and monitoring spot

3. Results and Discussion

3.1 Muddiness of printed matter

The reflection spectra of the printed matter are shown in Fig. 3 [amount of ink trapped (y): $\text{ca. } 1 \text{ g m}^{-2}$]. Ideal spectra are shown by colored area in the figure. The spectra of printed matter are far from the ideal spectra for the muddiness of the ink, i.e., lack of **B** ($\lambda = 400 - 500 \text{ nm}$) and **G** reflectance ($\lambda = 500 - 600 \text{ nm}$) of **M** and **C** printed matter, respectively. Lacks of the reflectance of the printed matter are shown in this figure by green arrows. On the other hand, the spectrum of **Y** printed matter is closely to the ideal one.

Clarifying the effect of the y value on the color, Figure 4 shows the changes in the a^*--b^* plots for the y value. For $y < 0.8 \text{ g m}^{-2}$, there is a good linear relation from the origin ($a^* = 0, b^* = 0$) for each printed matter in the a^*--b^* plots. Therefore, the printed colors appear relatively good. For $y > 0.8 \text{ g m}^{-2}$, the a^*--b^* plot of the **C** printer matter curved drastically toward the **B** area owing to the lack of the **G** reflectance, while that of the **M** printed matter curved toward the **R** area owing to the lack of the **B** reflectance. For $y > 2 \text{ g m}^{-2}$, the **C** and **M** printed matters looked like **B** and **R** materials, respectively. It must be caused by the muddiness of the ink and narrow color gamut is reflected to the muddiness. For **Y** ink, the curve in the a^*--b^* plot was smaller than for the other printed matter. Therefore, the effects of optical gain on the color specification values were studied using the high screen ruling printed matters.

3.2 Reflection spectrum

The reflection spectra of the half-tone printed matter were measured (screen ruling = 175 and 700 LPI). Figure 5a shows the spectra of the **M** samples with dot percentage (a) = $\text{ca. } 30 \%$ and $\text{ca. } 50 \%$.

At the same dot percentage, the reflectance of the 700 LPI sample in **B** range is higher than that of the 175 LPI sample. Conversely, in the **G** range, that of the former sample is lower. This means that the color appears better in the 700 LPI sample than in the 175 LPI sample. In the spectrum, the reflectance difference (ΔR) between the maximum and minimum values is a good parameter for evaluating color appearance. At $a = 30\%$, the ΔR value was larger for 700 LPI (25 %) than for 175 LPI (18 %). At $a = 50\%$, the difference in the ΔR values increased [$\Delta R = 30\%$ (700 LPI) and 18 % (175 LPI)]. The color of the 700 LPI sample approximates the ideal color. In this figure, the red arrows indicate the reflectance changes in the increase of the screen ruling.

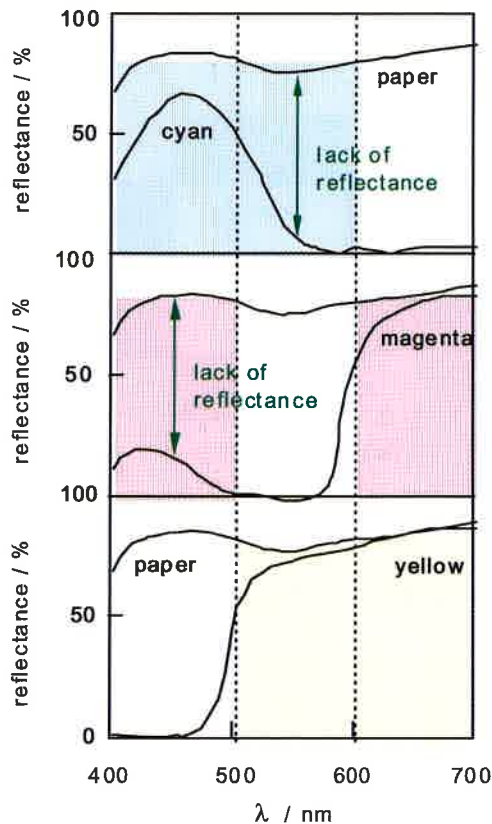


Figure 3:
Reflection spectra cyan, magenta and yellow
printed matter (amount of ink: ca 1 g m^{-2}). The
spectrum of paper is also shown

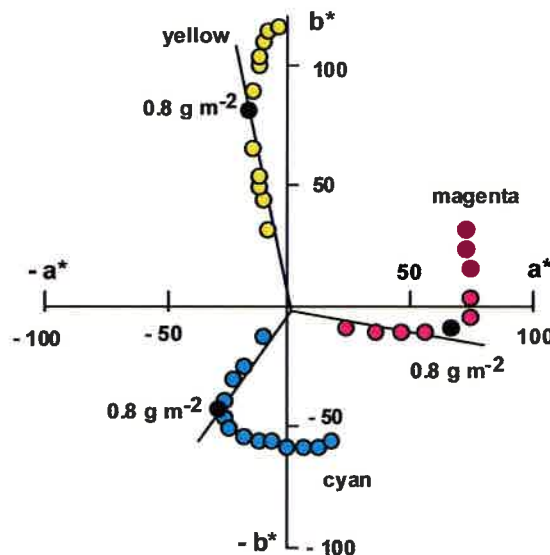


Figure 4:
Changes of the a^* - b^* plots in the
amount of ink transferred

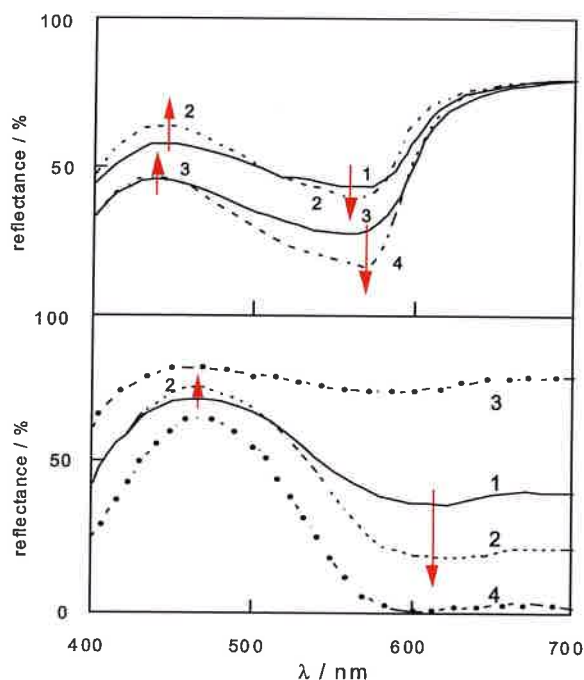


Figure 5:
Reflection spectra of magenta (a) and cyan (b) halftone printed matters.
Upper: screen ruling = 175 (1 and 2), 700 LPI (3 and 4), a = ca. 30% (1 and 3), ca. 50% (2 and 4). Lower: spectrum 1 (175 LPI, a = ca. 30%), spectrum 2 (700 LPI, ca. 50%), spectrum 3 (paper) and spectrum 4 (solid patch)

Similar results were obtained for the **C** half-tone printed matter (Fig. 5b). The reflectance of the 700 LPI sample in the **B** range was higher than that of the 175 LPI sample at the same dot percentage (a = ca. 50 %, ΔR = 3 %), while that in the **R** range (λ = 600 - 700 nm) was lower than that of the 175 LPI sample (a = ca. 50 %, ΔR = 21 %).

There were many crosses in the reflection spectra of the **M** and **C** printed matters. The samples were printed using the same ink, same paper, and same printing press, although the a value was not fixed. It is difficult to understand why there were crosses in the spectra, when we apply the Murray-Davis's equation to reflectance of each wavelength. The crosses clearly show that the color improves when we use high screen ruling.

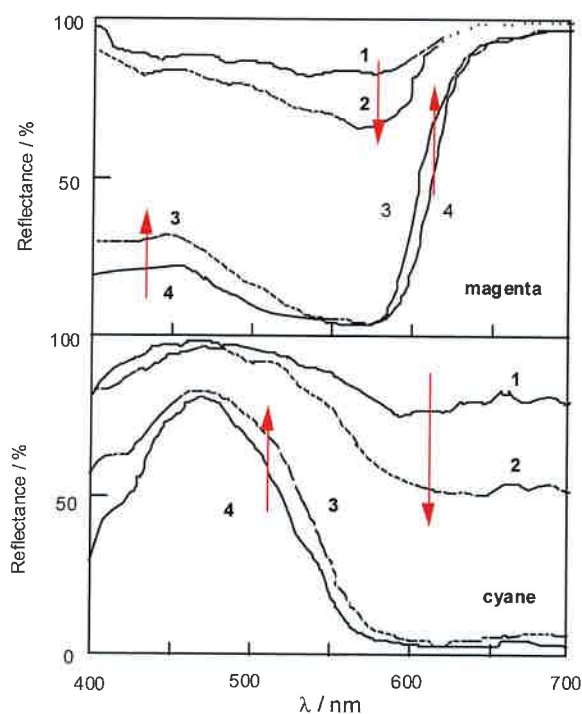


Figure 6:
Microreflection spectra of magenta (upper) and cyan halftone printed matter (a = ca. 50%). Spectra number: 1 and 2 (center of paper), 3 and 4 (center of dot); screen ruling: 175 (1 and 4) and 700 LPI (2 and 3)

Engeldrum⁸ reported that the color appearance of the non-dot area between dots was a pale version of the color of the dots. This is also explained by the optical dot gain. Clarifying the optical dot gain, we measured micro reflection spectra of the center of the dot and non-dot area of half-tone printed matter using 175- and 700-LPI half-tone printed matters ($a = \text{ca. } 50 \%$) with an object lens with a magnification corresponding to the screen ruling [measuring spot: $\phi = \text{ca. } 1$ and $\text{ca. } 4 \mu\text{m}$ for 700 and 175 LPI, respectively]. The average spectrum of ten measurements was recorded, as shown in Fig. 6. Although the reflectance of the 700 LPI **M** dot center at $\lambda = \text{ca. } 565 \text{ nm}$ equaled that of the 175 LPI sample, that of the 700 LPI sample at 450 nm was about 10 % higher than that of the 175 LPI sample. In **R** region, the reflectance of the former sample around 600 nm is also about 15 % higher than that of the latter sample. Therefore, the color at the center of the dot area improves as the screen ruling increases. Conversely, although the reflectance of the 700 LPI **M** non-dot area at $\lambda = \text{ca. } 450 \text{ nm}$ is only 4 % lower than that of the 175 LPI sample, that at 575 nm is about 18 % lower than that of the 175 LPI sample. Therefore, the color of the non-dot area appears to be the color of a very thin ink film. Changes in the micro reflection spectrum are listed in Table II.

Table II: Changes of color in increasing the screen ruling ($a = \text{ca. } 50\%$)

patch	area	reflectance			appearance
		B range	G range	R range	
C	dot	increased			better C
	non-dot	decreased			pale C
M	dot	increase	increased		better M
	non-dot	decreased			pale M
Y	dot				unchanged
	non-dot	decreased			pale Y

Although the reflectance of the 700-LPI **C** dot center ($a = \text{ca. } 50 \%$) at $\lambda = \text{ca. } 620 \text{ nm}$ equaled that of the 175-LPI sample, the reflectance at 400 and 500 nm were more than 10 % higher than those of the 175-LPI sample. Conversely, although the reflectance of the 700-LPI non-dot area at $\lambda = \text{ca. } 470 \text{ nm}$ equaled that of the 175-LPI sample, that at $\lambda > 600 \text{ nm}$ was about 30 % lower than that of the 175 sample.

The reflection spectra of the **Y** printed matter were also measured ($a = \text{ca. } 50 \%$). Although the screen ruling had no typical effect on the dot area, the reflectance of the 700-LPI non-dot area around 500 nm was about 15 % lower than that of the 175-LPI sample. The effect of screen ruling seems to be greater in the non-dot area than in the dot area. Since the reflection spectrum of the **Y** printed matter was very close to the ideal spectrum, no effect was seen in dot area.

3.3 Reflection trace

Reflection traces were measured to clarify the effect of screen ruling with the aid of the image processor connected to the microscope (magnification of object lens: 5) using 175-, 330- and 700-LPI half-tone printed matter ($a = \text{ca. } 50 \%$, black ink). The scanning angle was adjusted to 45° for the dot pattern, as shown in Fig. 2. Figure 7 shows the reflection traces of 175-, 330- and 700-LPI half tone printed matter. There were some small peaks in the dot area, which seemed to result from unevenness of the printed surface. For the 175-LPI half-tone printed matter, the reflectance of the trace increased to the paper value (R_p) at the non-dot area and decreased to the solid value (R_s) at the dot area. Near

the dot edge, the reflection changed. In the 330-LPI samples, the reflectance did not rise to the R_p value or fall to the R_s value. The traces of the non-dot area (between dots) appeared a half circle. In the 700-LPI sample, the reflectance traces between the dots appeared like pointed mountain, and the reflectance increased with the distance from dot edge. The difference between the maximum and minimum reflectance decreases increasing screen ruling. Therefore, the whole areas in the 700-LPI sample are regarded as the optical dot gain area.

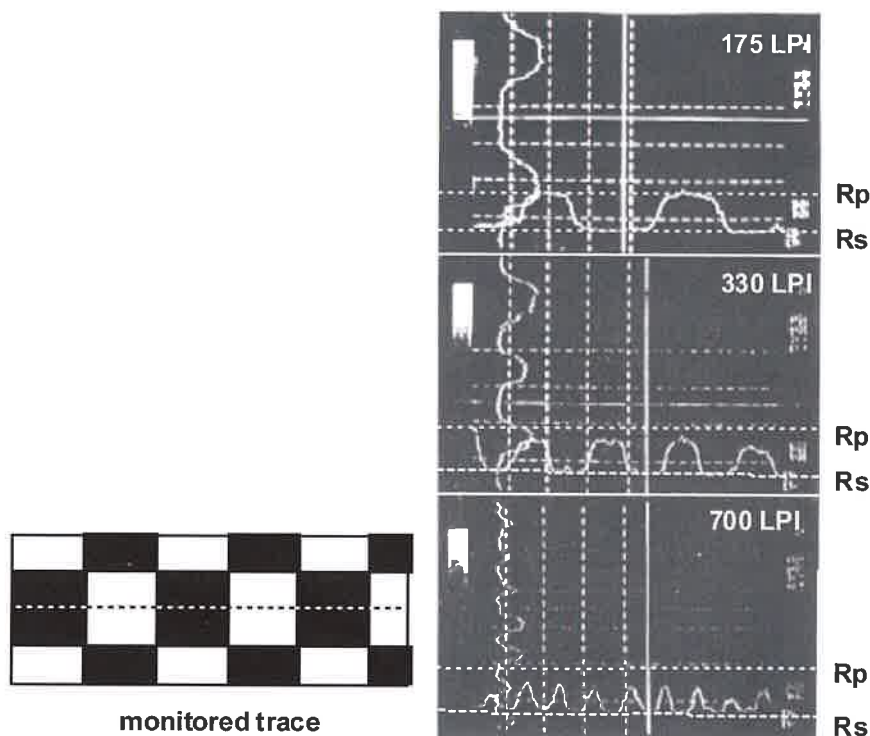


Figure 5: Reflection traces of *M* printed matter ($a = \text{ca. } 50\%$) monitored using *G* filter (screen ruling: 175, 330 and 700 LPI from the top)

The measured width of reflection change (17 - 64 %) was measured to be 27 (**R** filter), 32 (**G** filter) and 44 μm (**B** filter); sample, 25 - 200 LPI black half tone pattern printed on cast-coated paper].⁶ These values indicate that the width of the optical dot gain is assumed roughly to be about 30 μm . By using this value, the reflection traces were modeled roughly.

Figure 8 shows models of the reflection traces of the 175- and 700-LPI printed matter ($a = 50\%$). When the dot gain can be negligible, the reflection traces can be approximated to on-off pattern between the R_p and R_s values (Fig. 8b) resulting from the inking pattern on the paper surface (Fig. 8a). Considering the optical dot gain, the reflection trace of the 175-LPI sample was divided three parts, R_p part, R_s part and the middle reflectance part which is optical dot gain part demonstrated by a skew line. In the 700-LPI samples, because the sizes of the dot and non-dot area (26 μm) are smaller than the dot gain width 30 μm , reflection trace of the non-dot area dose not increase to the R_p value and that of the dot area dose not decrease to the R_s value. The reflection peaks must be observed at center of the non-dot area, as shown in Fig. 8c. We cannot divide to the dot and non-dot area by using the reflection trace. If the narrow color gamut is only caused to the muddiness reflectance of the solid patch, color appearance of the printed matter becomes better according to the increase of the screen ruling.

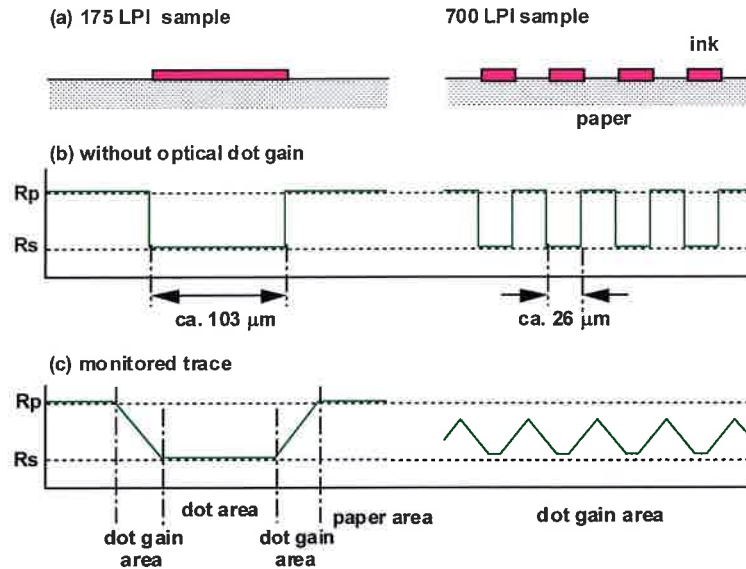


Figure 8: Models of reflection trace ($a = 50\%$)

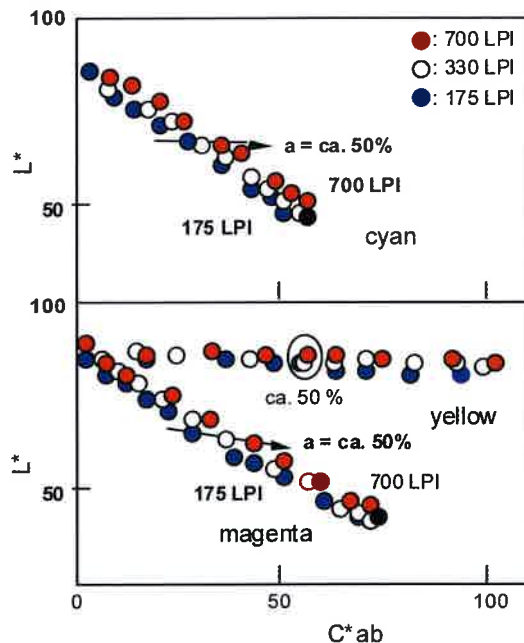


Figure 9: Plots of C^*_{ab} vs. L^* of half-tone printed matter

3.4 Characteristics of high screen ruling printed matter

Clarifying the effect of the screen ruling on color of the printed matter, the metric lightness L^* is plotted against the metric chroma $[C^*_{ab} = \{(a^*)^2 + (b^*)^2\}^{1/2}]$ for the mono-color printed matter, as shown in Fig. 9. For the Y half-tone printed matter, although L^* is nearly constant, the chroma value C^*_{ab} increases with increasing the a value independent of the screen ruling. For the C and M half-tone printed matters, there are good linear relationships between a and C^*_{ab} . The slope of the relation decreases with increasing the screen ruling. At $a = 50\%$, C^*_{ab} increases with increasing the screen ruling, as shown red arrows in this figure.

The color specification values of multi-color printed matter were also studied. We measured the color specification value of **C** ($a = 0 - 100\%$) - **M** (50 %) multi-color half-tone printed matters, because the effect of the optical dot gain was most detectable around $a = 50\%$. The metric lightness L^* decreased and C^*ab increased with increasing the a value of the **C** printed matter, as shown in Fig. 10. Conversely, the C^*ab value decreased initially with increasing the a^* value in the **C-M** half tone printed matter, but then increased with increasing the a value.

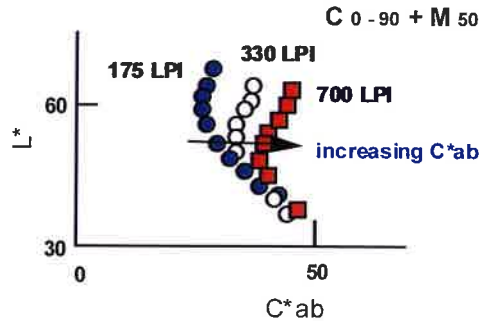


Figure 10: Plots of C^*ab vs. L^* of **C-M** half-tone printed matter

The effects of the optical dot gain should be clear around $a = 50\%$. We studied the color gamut of 175-, 330- and 700-LPI half-tone printed matter ($a = 50\%$) using the $a^* - b^*$ plot, as shown in Fig. 11. The metric chroma C^*ab of the **C** and **M** printed matters increased with increasing the screen ruling, although the metric hue angles $[\tan^{-1}(b^*/a^*)]$ are nearly constant. These shifts of the plots could be approximated roughly to the linear relations. Moreover, these slopes agreed with those obtained in the **C** and **M** solid printed matter, as shown in Fig. 4. The plots of the **Y** half-tone printed matter were nearly constant independent of the screen ruling.

For the **C-M** multi-color printed matter, C^*ab increased with increasing the screen ruling. Although the screen ruling affected the **C** and **M** printed matters, the metric hue angle of the **C-M** multi-color sample was independent of the screen ruling. Although the reflectance of the muddiness wavelength range of the **C** area (**G**) in improved by the optical dot gain, the **M** ink absorbed the **G** light. For the **C-Y** and **M-Y** multi-colors, C^*ab also increased with increasing the screen ruling. By contrast, the metric hue angles of them shifted in the **G** and **R** directions, respectively. Since the **Y** ink absorbs the **B** light effectively, the **G** and **R** colors of the **C-Y** and **M-Y** multi-printed matters, respectively, appeared better with increasing screen ruling. Therefore, the metric hue angles shifted to better color, as the screen ruling increased.

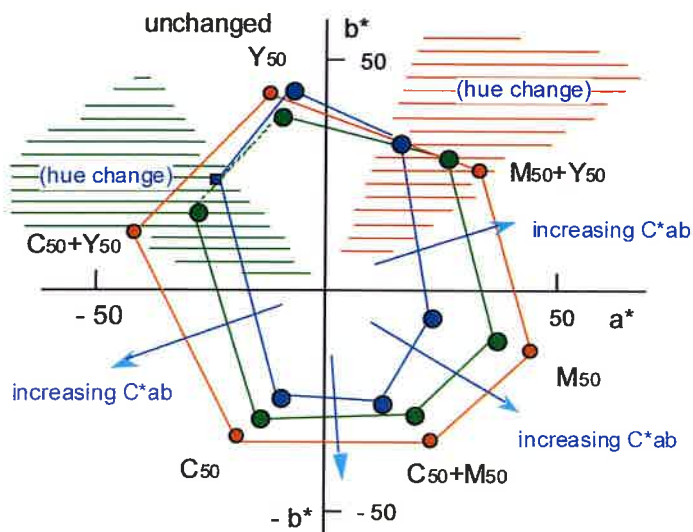


Figure 11:
CIE- a^*-b^* plots of half-tone printed matter
($a = 50\%$). Screen ruling: 175(●), 330
(●) and 700 LPI(●)

3.5 Relation between color specification values and reflectance

The results of screen ruling on the micro reflection spectra were summarized in Table II. How dose the reflectance change affect the color specification values for increasing the screen ruling? In the **C** printed matter, the a^* value increases with increasing **G** reflectance of the dot area and decreasing **R** reflectance of the non-dot area for increasing the screen ruling. Table III is listed dominant effects of the reflectance change on the color specification values. The b^* value seems to decreased with increasing **G** reflectance of dot area and decreasing **R** reflectance of the non-dot area. In the **M** printed matter, the b^* value decreases chiefly with increasing **B** reflectance of the dot area for increasing the screen ruling. Comparing with b^* value, the change in a^* value is large, as increases both with decreasing **G** reflectance of the non-dot area and with increasing **R** reflectance of the dot area. On the other hand, since the decreasing **B** reflectance of **Y** non-dot area is small, we cannot detect the change in the color specification values, a^* and b^* .

For $y > 0.8 \text{ g m}^{-2}$, there are good linear relations held on the a^* - b^* plots. For $y < 0.8 \text{ g m}^{-2}$, the relations of the **C** and **M** printed matter curved to **B** and **R** direction, respectively, drastically for the muddy absorption of ink, which is reflected the narrow color gamut. Increasing the screen ruling, the difference between the maximum reflectance and minimum value becomes small, as like as a thin ink film on the whole paper surface, as shown in Fig. 8. It is caused by the optical dot gain. The effect of the screen ruling is obviously in the multi-color printed matter and its color specification values, a^* and b^* , are sum of each specification value, as shown in Fig. 12.

Table III: Effects of reflectance change on b^* and b^* values in incresing screen ruling ($a = \text{ca. } 50\%$)

patch	a^*	area	remarks	b^*	area	remarks
C	decrease	dot non-dot	increase of G decrease of R	decrease	dot non-dot	increase of G ? decrease of R ?
M	increase	dot non-dot	increase of R decrease of G	decrease	dot non-dot	increase of B
Y	unchange	dot non-dot		unchange	dot non-dot	decrease of B

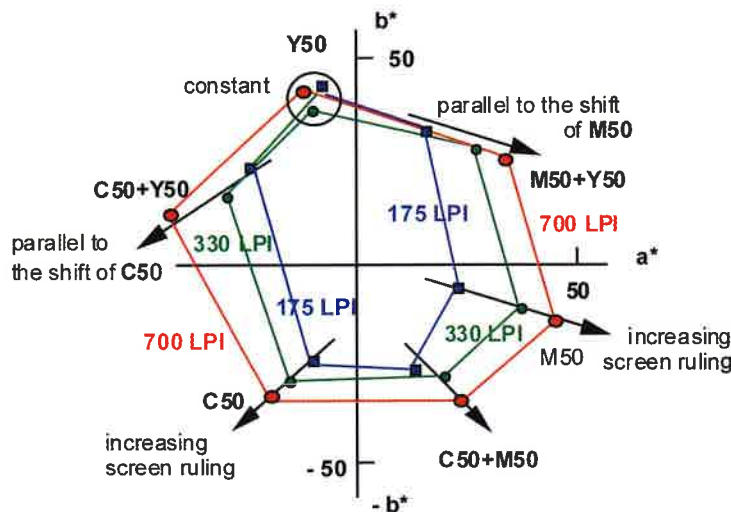


Figure 12: CIE- a^*b^* plots of half-tone printed matter 2. Arrows show the changes of a^* and b^* in increasing screen ruling

4. Conclusion

The color gamut of normal half-tone printed matters is narrow for low reflectance in the muddiness wavelength range of the ink, i.e., the **G** wavelength range of the **C** printed matter and the **B** range of the **M** printed matter. We studied the effects of the screen ruling on the color gamut for the half-tone printed matters. With increasing the screen ruling, the reflectance of the dot area in the muddiness range increases, and the non-dot area takes a pale dot color. This is caused by the optical dot gain. Conversely, the color appearance of the **Y** printed matter is unchangeable, since its color appears close to the ideal color.

For the **C-Y** and **M-Y** multi-colors, because both the dot and the non-dot areas of the **Y** printed matter decrease the **B** reflectance, the **G** and **R** reflectance improve as the screen ruling increases. Therefore, the metric hue angles change and C^*ab increases. In the **C-M** multi-color, the **B** reflectance of the **M** dot area increases. The **R** and **G** reflectance of the non-dot area (**M** and **C**, respectively) decrease. Therefore, color appearance of the half-tone printed matter becomes better according to the increase of the screen ruling. On the other hand, these changes in the color specification values were clarified by means of the micro reflection spectra only except for b^* value of the **C** half-tone printed matter.

Acknowledgements

We are grateful to Mr. M. Okamura of Okamura Printing Co. Ltd. for donating the high screen ruling printed matters and Mr. K. Shimabukuro for assistancies of the measurements of color specification values (a part of them).

Reference

- 1) S. Watanabe, J. Aoyama, T. Kikuta and I. Ikeda, Bull. Jpn. Soc. Printing Sci. Technol., 28, 49-56 (1991)
- 2) J. Isono, Bull. Jpn. Soc. Printing Sci. Tech., 30, 169-173 (1993)
- 3) S. Miyano, Bull. Jpn. Soc. Printing Sci. Tech., 31, 254-261 (1994)
- 4) M. Yamazaki, Bull. Jpn. Soc. Printing Sci. Tech., 31, 263-268 (1994)
- 5) J. Isono, Bull. Jpn. Tech. Assoc. Paper and Pulp Industry., 48, 667-676 (1994)
- 6) I. Naito, Kyushu Sangyo Univ. Res. Report Fac. Arts, 23, 105-112 (1992)
- 7) Y. Shirouzu and I. Naito, Bull. Jpn. Soc. Printing Sci. Technol., 40, 109-114 (2003)
- 8) P.G. Engeldrum, J. Imag. Sci. Tech., 38, 545-551 (1994)



Halftones characterisation by image processing

Jean-Pierre Gervasoni, Raphaël Passas, Sébastien Lebris

EFPG

BP 65, 461, rue de la Papeterie

F-38402 Saint Martin d'Hères CEDEX, France

E-mail: Raphael.Passas@efpg.inpg.fr; jgervasoni@9online.fr

1. Introduction

A user friendly image processing software has been developed that can help to characterize printed halftones with common processes such as offset or inkjet. For the sake of simplicity, we only dealt with black halftones in this study, even if all image processing is in large part colour independent.



Figure 1

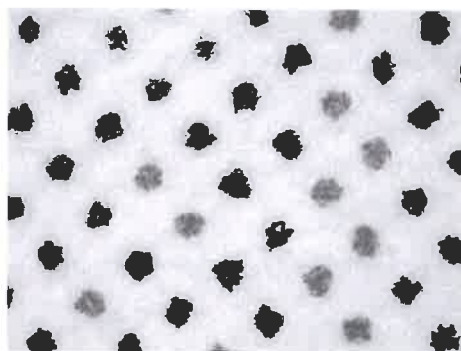


Figure 2

The software transforms a colour image (RGB) into a set of objects, which are in fact the inked areas if the dot area percentage is not too high (typically from 0% to 40%): it can't split overlapping dots. The objects touching the borders of the image are not taken into account. For each object in the image, the software gives the equivalent ellipse parameters (semi major and semi minor axis, orientation), the **Feret** rectangle (width and height), the perimeter and area, and finally the barycentre coordinates. All the results are expressed in pixels, except the angle given in degrees. A detailed description of the printed dots is made available for further exploitation. Studying the barycentres repartition inside the picture is a way to check if the halftone is stochastic or regular. In this last case, the orientation (relative to a border of the picture) and the step (measured in pixels) can be computed.

2. Methods

2.1 Experimental device

All the pictures used for this study were acquired with a tri-ccd camera CV-M90 (Jai, 2004) coupled with an Olympus BH2 microscope (Olympus, 2004) equipped with a x2.5 eye-piece. The objective mounted on the microscope is a Neo DPLAN x5. The frame grabber (meteor from Matrox) was driven through the Optimas® software (version 6.51) from Media Cybernetics (Optimas, 2004). All the pictures were saved as Tiff image file, 768x574, RGB and 8 bits per pixel. In order to measure with the best accuracy possible the pixel size (in $\mu\text{m}/\text{pixel}$) we took two pictures of a fine printed scale (see fig. 3 and fig. 4). Under the current measurement conditions a pixel represents 0.82 μm in both directions.

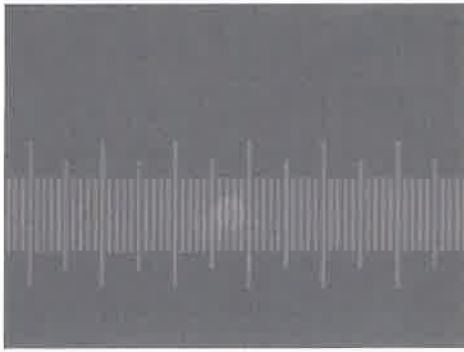


Figure 3



Figure 4

2.2 Research approach

The main difficulty was to find convenient algorithms to retrieve all the objects inside a picture. We first used Optimas® software to test many algorithms before choosing the right ones:

1. Colour to greyscale
2. Greyscale to black-and-white
3. Distance transform
4. Watershed

Optimas® has been involved only to identify step 1 to 4. We must add two other steps, dealing with object processing:

5. Labelization
6. Object properties computation

2.2.1 Colour to greyscale (fig. 5)

Our software reads TIFF pictures (RGB, 8 bits per channel). To compute the greyscale conversion, we choose to keep only one of the three RGB channels. In practice, we empirically choose to keep only the Red channel. The contrast of the resulting image is enhanced using the following formula (eq 1) where **p** is the current grey level, **min** and **max** are the minimum and maximum grey values.

$$(eq\ 1)\ p \leftarrow 255 * (p - \min) / (p - \max)$$

As it wasn't possible to include colour images in this publication, we only put a grey picture example (fig. 5).

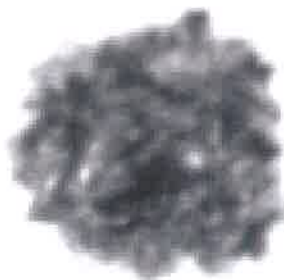


Figure 5

2.2.2 Greyscale to black-and-white (fig. 6)

There are many algorithms that can be employed to compute threshold (Trier, 1994) and (Xu, 2002). We choose a *fixed* threshold algorithm called Otsu (Otsu, 1979). The binarization of the picture is based on histogram analysis: the chosen threshold is the lowest point between two classes (peaks), and involves the computation of a between class variance.



Figure 6

Let T be the threshold. All the pixels with level varying from 0 to $T-1$ define the class called 0 , the others defining the class called 1 . Let ω_0 and ω_1 be the means of class 0 and 1 , μ_0 and μ_1 the frequencies. The between classes variance δ^2 is then defined by equation 2:

$$(eq\ 2) \ \delta^2(T) = \omega_0(T) * \omega_1(T) * \{ \mu_1(T) - \mu_0(T) \}$$

δ^2 is computed for each value of T (0 to 255). The threshold is the value maximizing δ^2 . In (fig. 7), we have drawn the histogram (thin continuous line) of a grey level picture and the corresponding curve δ^2 (T) (thicker dashed line).

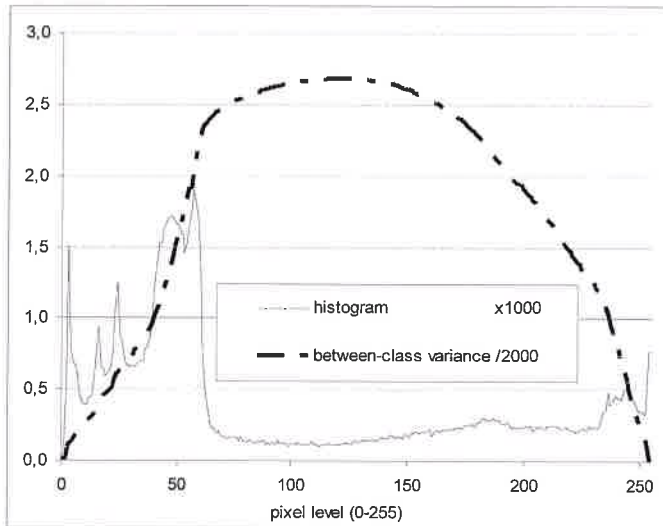


Figure 7

2.2.3 Distance transform (fig. 8)

The result of the transform is a grey level image that looks similar to the input image except that the grey level intensity of points inside foreground regions are changed to show the distance to the closest boundary from each point. We used a *Euclidean* distance metric, and the algorithm described in (Borgefors, 1986). Please refer to (fig. 8) for the distance transform of (fig. 6) (these figures are cropped parts of larger ones).

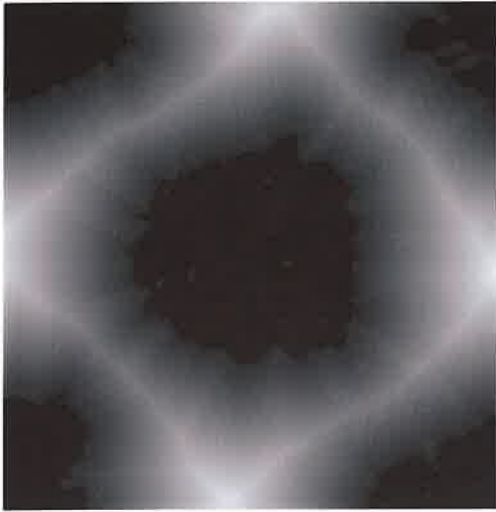


Figure 8

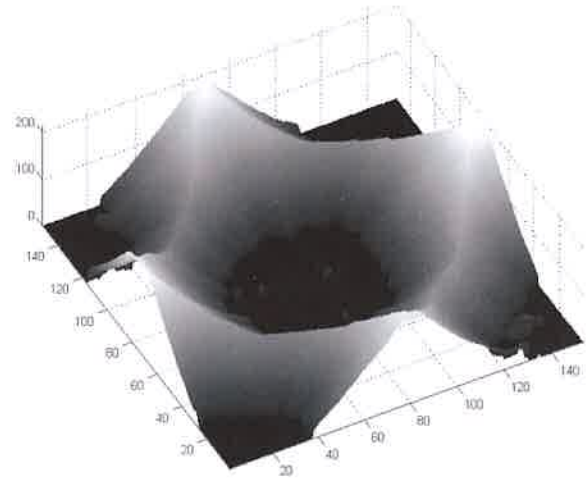


Figure 9

2.2.3 Watershed (fig. 10)

The distance transform step creates borders (in light grey) as one can see in (fig. 8) and its topographic representation in (fig. 9). The watershed algorithm is employed to separate all the regions in the picture, each region containing only one object. To understand how it works, take a look at (fig. 9) and imagine that the surface is flooded from its minima, preventing the merging of water coming from different sources (= minima) define *catchment basins* and *watershed lines*. Each basin corresponds to a region, and watershed lines to region borders. The result of this step is a grey level picture (fig. 10), a pixel level of 0 (black) does mean that the pixel belongs to the border. All pixels sharing the same level belong to the same region. We choose to implement the algorithm described in (Soille, 1991).

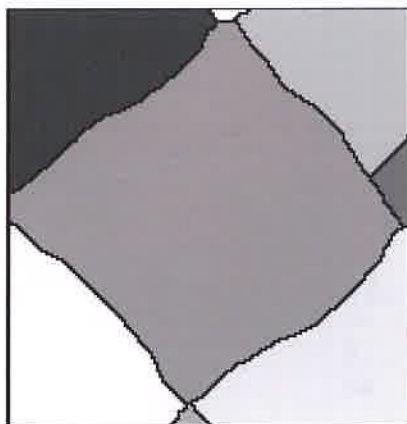


Figure 10

2.2.4 Labelization

Using the watershed transform and the black and white representations, it's very easy to obtain a complete list of objects. But image processing could have made very small objects appear. These artefacts are automatically eliminated (by comparing object area to mean object area). We can define contour pixels as object pixels (in black, corresponding to the value 0) next to the background (in white, corresponding to the value 255).

2.2.5 Object properties computation

In this step, we have stored for each object a grey level image and a black and white one, whose size corresponds to the **Feret** rectangle (materialized by a grey line in fig. 11). Computing the area can easily be done by counting black pixels (level 0) in the object, and the perimeter by counting contour pixels.

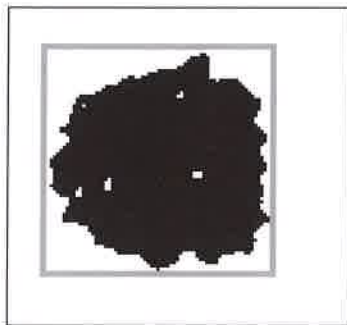


Figure 11

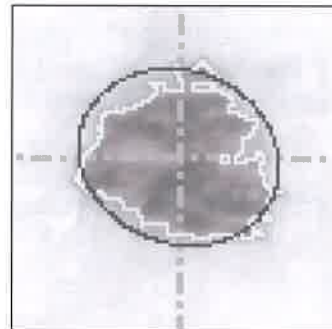


Figure 12

The main difficulty was to define an equivalent ellipse for any object. We finally chose to use independent components analysis (ICA), based upon statistical analysis of the greyscale representation of the object (Crowley, 2002). Thanks to ICA we directly obtained model axis (semi major axis **a**, semi minor axis **b**, in pixels) and orientation **theta** (in degrees). We have validated the ICA approach using a set of synthetic ellipses: the error is less than one pixel for **a** and **b**, and less than one degree for **theta**. In (fig.12) the dashed cross indicates barycentre position, the black curve is the equivalent ellipse and the light grey curve the object contour.

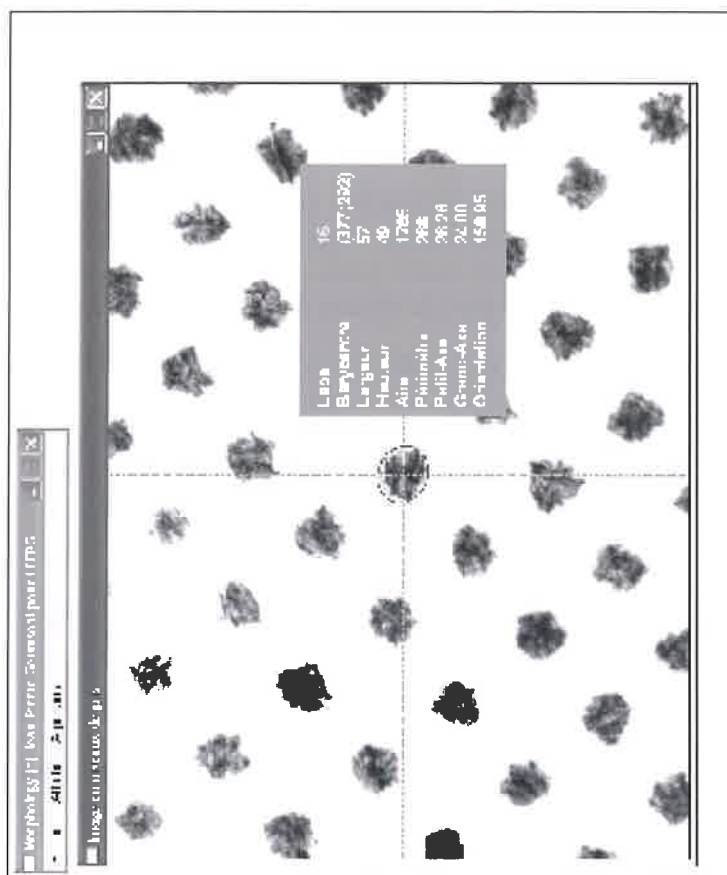


Figure 13:
(French only user interface)

2.2.6 Graphical user interface (fig. 13)

The software is driven through a graphical user interface (see fig. 13). Loading a picture triggers all the previously described computations. Once computation has finished, the software creates an Excel spreadsheet gathering all the results, and opens a window allowing the user to navigate from one object to another by simply using the left mouse button. The equivalent ellipse is drawn in blue (black on fig 13), the dot contours in green (light grey in fig. 13). The position of the barycentre is given by the crossing dotted lines. A window gives the object properties. It is possible to display in place of the RGB picture, the greyscale, the black and white, the distance transform or the watershed transform.

3. Results: dot area percentage measurement on single colour halftones

3.1 Repeatability

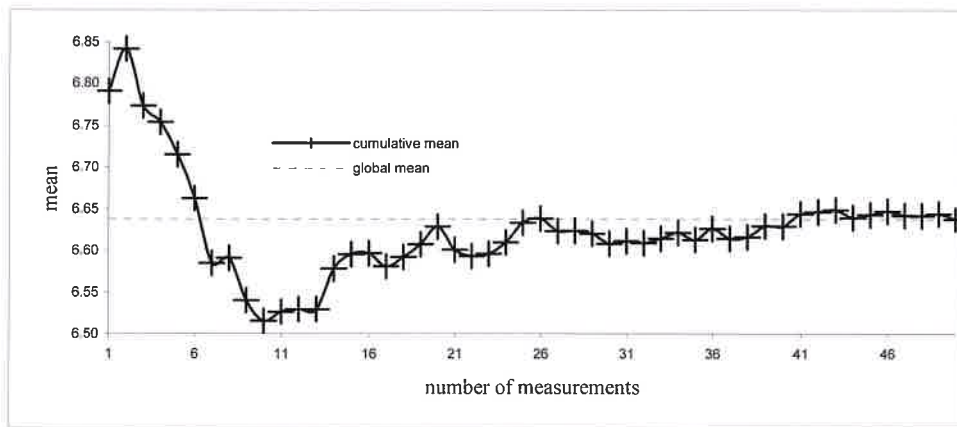


Figure 14

In order to probe the dot area percentage measure, we acquired 50 pictures of the same halftone print (a 10% black halftone Matchprint). We then computed the cumulative mean and compared it to the global mean (fig. 14). Even if the curve stabilisation doesn't occur before the $\sim 30^{\text{th}}$ measure, the amplitude is lower than 0,5%. That's why we choose to take only one picture per print.

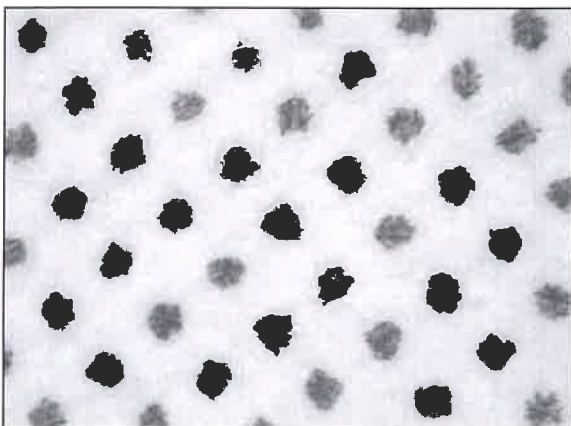


Figure 15: Offset 10%

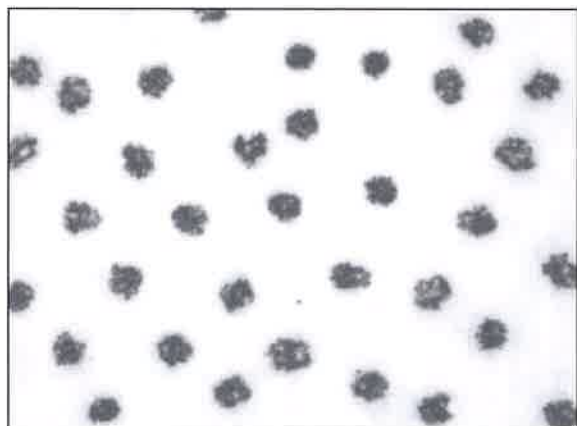


Figure 16: Inkjet 10%

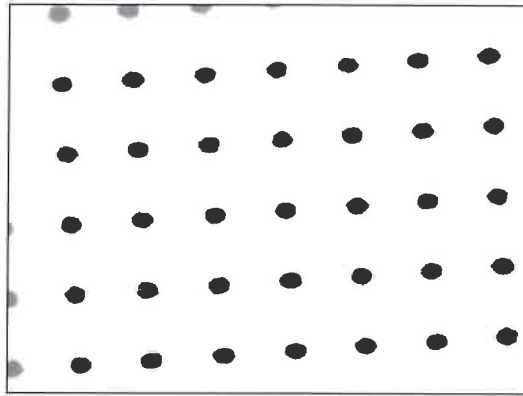


Figure 17: Matchprint 10%

3.2 Comparison between image analysis and optical densitometry methods

Black halftones with a dot area percentage range from 3% to 90% were printed using three different processes: Offset (fig. 15), Inkjet (fig. 16) and Matchprint (fig. 17). The results achieved by image analysis (using our software) were compared (fig. 19, fig. 20 and fig. 21) to those determined by optical densitometry (Techkon R420), by means of the Murray-Davies formula (Murray, 1936). We have plotted the dot area percentage measured using the two methods versus the reference dot area percentage. In the case of the image analysis method we have also plotted the correlation between the reference and the data measured. This correlation is very good for the three printing processes (R^2 is close to 1). The image analysis method of dot area percentage measure doesn't take into account grey level variations inside each object. This is certainly the reason for the difference between the two methods.

5. Conclusions

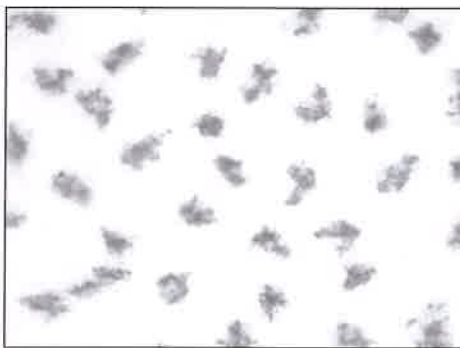


Figure A

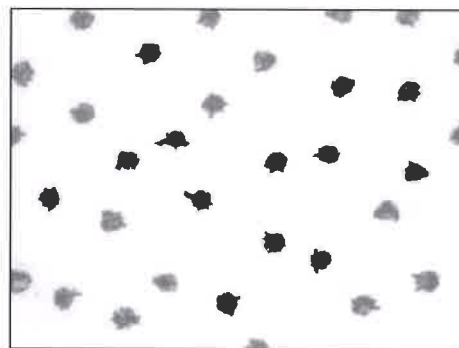


Figure B

Our tool is able to recognize non wrapping objects in an image and to give the parameters of an equivalent ellipse for each object. It has been validated on a set of synthetic pictures and successfully used for low dot area percentage prints analysis. It could be greatly improved by automatically detecting and cutting wrapped objects (fig. 18). The repartition of barycentres inside the picture could be used to check if the halftone is stochastic or regular (giving orientation and step in this case). Moreover we do believe that a statistical analysis of object contours could give pertinent information about the papers properties, especially using the inkjet printing process: (fig.A) and (fig.B) represent the same print on a lower quality paper (fig.A) and on a photo quality paper (fig.B).

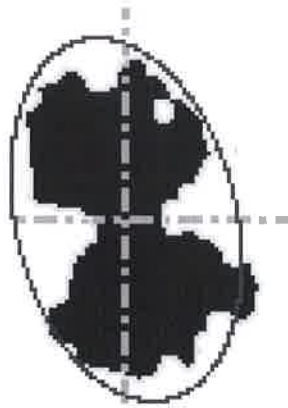


Figure 18

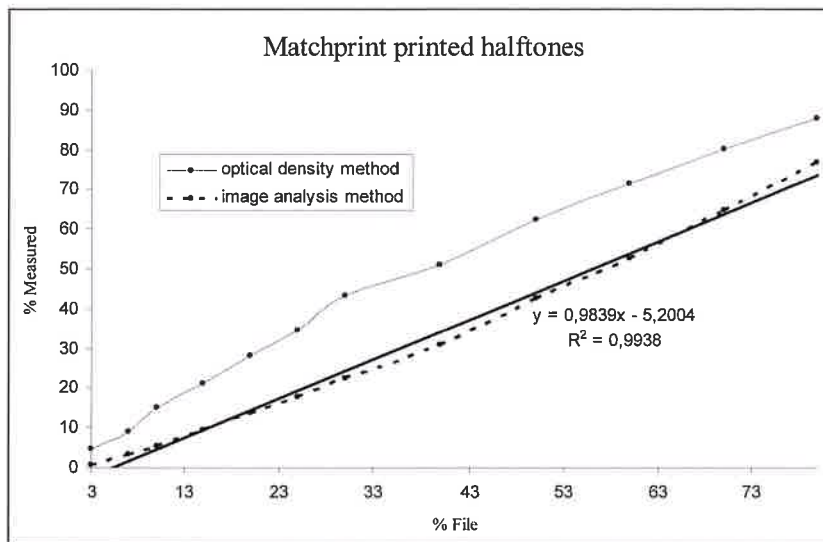


Figure 19

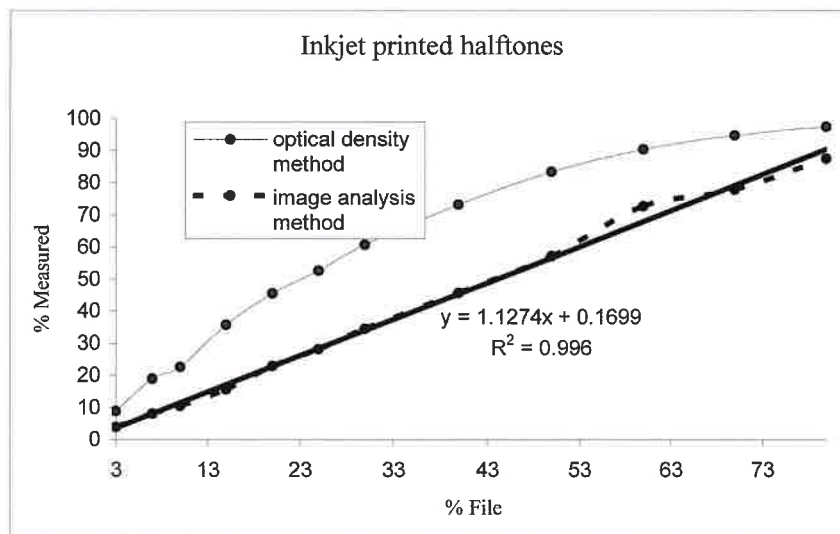


Figure 20

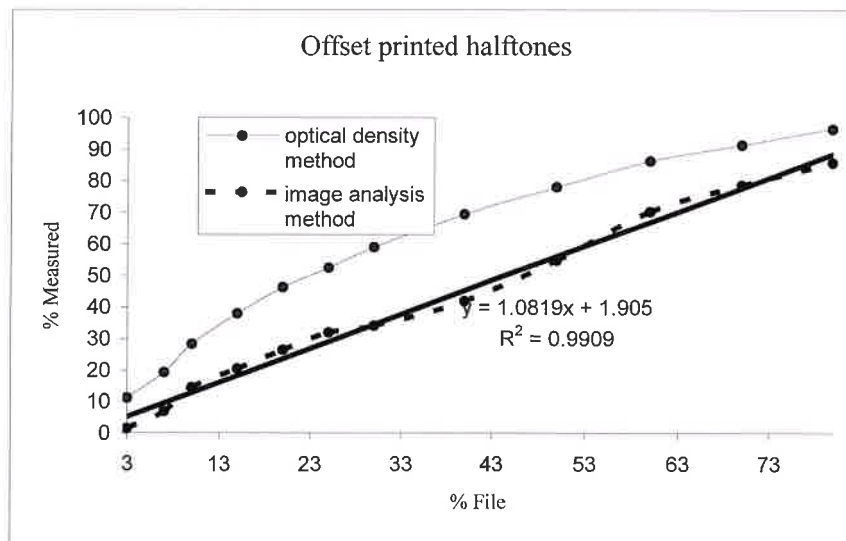


Figure 21

Literature references

- (Borgefors, 1986), G. Borgefors.: *Distance transformation in digital images*. Computers Vision, Graphics, and Image Processing, vol 34, 1986, 344-371
- (Crowley, 2002), Crowley, J. L. 2002, Notes du cours DEA-Vision par Ordinateur, ENSIMAG, Vision par Ordinateur, Link to the document (French)
<http://www-prima.imag.fr/Prima/jlc/Courses/2002/DEA-IVR.VO/DEA-IVR.VO.S4.pdf>
- (Jai, 2004), Link to the official website <http://www.jai.com/index.asp/sprog=uk>, Link to the camera description http://www.jai.com/camera/products_show.asp?id=33&sprog=uk#73
- (Murray, 1936), A.Murray 1936, Technical report 221, J.Franklin Institute
- (Olympus, 2004), Link to the official website <http://www.olympusmicro.com/>, Link to the microscope description <http://www.olympusmicro.com/primer/anatomy/bh2cutaway.html>
- (Optimas, 2004), Link to the official website <http://www.optimas.com/>
- (Otsu, 1979), Otsu, N., 1979, *A threshold selection method from gray-level histograms*, IEEE Trans. Systems, Man, and Cybernetics, 9(1), pp. 62-66
- (Soille, 1991), L.Vincent and P.Soille, June 1991, *Watersheds in digital space: an efficient algorithm based on immersion simulations histograms*, IEEE Transactions On Pattern Analysis and Machine Intelligence vol 13 n 6
- (Trier, 1994), Oivind Due Trier and Anil K.Jain, 1994, *Goal-directed evaluation of binarization methods*, Proceedings of NSF/ARPA Workshop on Performance versus methodology in computer vision, p206-217, Seattle, Washington
- (Xu, 2002), Lixu Gu, July 10, 2002, *Robarts Research Institute* London, Ontario, Canada, Link to PowerPoint presentation: <http://www.imaging.robarts.ca/coders/content/seminars/amip/amip-2.ppt>



Colorimetric description of tolerances in newspaper production

Jürgen Gemeinhardt

FOGRA Forschungsgesellschaft Druck e.V.
Streitfeldstr. 19, D-81673 München, Germany
E-mail: gemeinhardt@fogra.org

1. Introduction

In order to prepare digital data for newspaper printing the colorimetric properties of the printing process must be known. They are also required for making contract proofs, which simulate the colorimetric appearance of the production print.

The international standard ISO 12647-3 [1] shows the conditions of standardized newspaper printing. It describes the colour of the substrate to be used and the nominal values and tolerances for the solid tones of the primary inks cyan, magenta, yellow and black on newsprint. One must distinguish between the so-called deviation tolerance and the variation tolerance. The deviation tolerance shows the allowed colour difference between the ok print at the printing machine and the nominal values of the standardization or a contract proof, if available. It considers slight differences inherent to various inks and papers used for production. On the other hand the variation tolerance describes fluctuations of the production print compared with the ok print.

For the two-coloured overprints cyan and yellow, cyan and magenta as well as magenta and yellow nominal values and tolerances are defined likewise. As the colour of overprints essentially depends on the printing conditions, tolerances are wider compared to those of the primary inks.

Nominal values and tolerances also exist for the tonal increase of several tint patches. Furthermore the tone value increase of the coloured inks cyan, magenta and yellow is restricted by the so-called spread. It says that the difference between the coloured inks must be less than 6%, in order to avoid stains. But there are no colorimetric values that would be important for the calibration of digital proofing systems.

Print tests were carried out with a newspaper press. Thereby the parameters of application were varied systematically within the limits of standardization, in order to describe the effects on different colours. Moreover a mathematical model was established to evaluate the colorimetric values of tint patches of the primary inks. Because the agreement of colour measurements with the visual perception is very important for the judgement of colour differences, the visual equality of the colour difference formulas CIELAB and CIEDE2000 was investigated.

2. Print Tests

First of all four papers with different content of waste paper (0%, 50%, 70% and 100%) and one set of newspaper inks were chosen. They all met the requirements of ISO 12647-3 and were used for specimen prints with varying quantities of ink to obtain nominal values for the solid tone densities. Furthermore the specimen prints could be used to estimate the ink densities that correspond to the variation tolerance in ISO 12647-3. It turned out, that the standardization allows density variations of about $\pm 17\%$ in the production run. These are quite high compared to the $\pm 8\%$ for offset printing, but realistic for newspaper presses.

In ISO 12647-3 are recommended two sequences of colours. This is CMYK, which is mostly employed in practice, and KCMY. Despite other colour sequences are observed, too. They can be configured spontaneously, depending on the need and availability of the printing units. In order to compare different colour sequences in one print run, subdivided ducts were used for the tests with a newspaper press. They could be filled with different inks, so that CMYK, KCMY and MCMY were realized.

Two printing formes (Fig. 1) were applied to the printing machine. Testforme 1 was used for the evaluation of the colorimetric behaviour when changing the printing conditions. It consists of 99 different colour patches that are equally distributed on the edge and within the representable colour space. Each patch could be found eight times on the forme, in order to provide reliable mean values. Testforme 2 provides a choice of colour patches necessary for the performance test of the colour difference formulas.

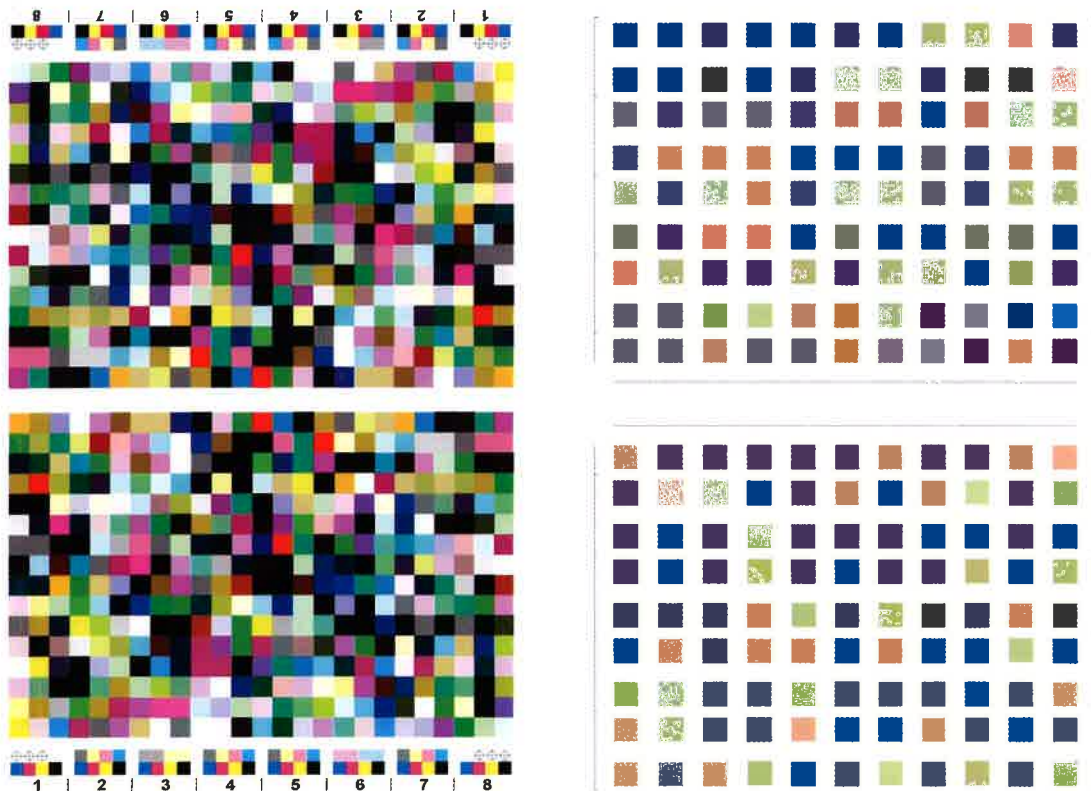


Fig. 1: Testforme 1 (left) for colorimetric description of production tolerances and testforme 2 (right) for investigation of colour difference formulas

The programme of the test print was the same for each of the chosen papers. First the machine was adjusted to reach the nominal values of the solid tone densities with 3 m/s printing speed. Then the speed was increased to 6 m/s and the densities were checked again. Afterwards systematic density variations of ± 0.1 were performed with the help of the duct rollers. Finally the speed was increased to 9 m/s.

Densities were checked in a print control strip with a scanning densitometer. With appropriately prepared Excel sheets it was possible to reach the aim values by less than ± 0.03 . Fluctuations across the printing direction could be minimized below ± 0.08 .

In order to investigate the drying behaviour of the inks Testforme 1 was measured colorimetrically after approximately five minutes, two hours, one day and two days. During the first hours after the print run the colour of many patches changes significantly, although the densities remain quite constant. This must

be taken into consideration, because the newspaper usually is read several hours after being printed. The change of the primary colours lies between $\Delta E^*_{ab} = 1$ and $\Delta E^*_{ab} = 2$ (Fig. 2a) while secondary colours can change up to $\Delta E^*_{ab} = 4$ (Fig. 2b).

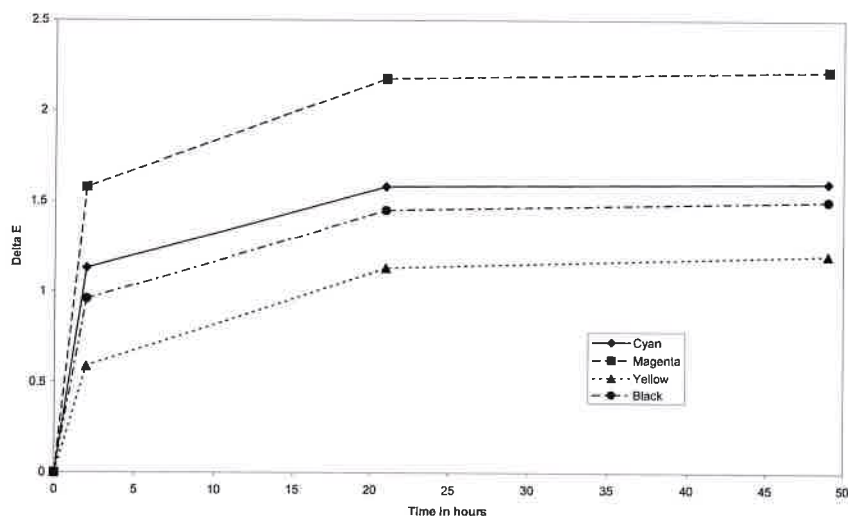


Fig. 2a: Drying behaviour of the primary colours

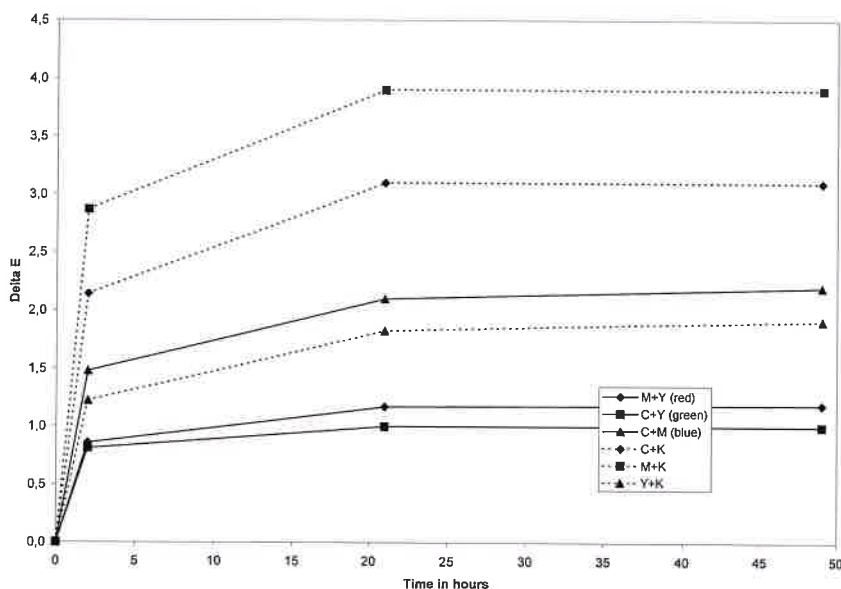


Fig. 2b: Drying behaviour of the secondary colours

Colorimetric appearance of Testforme 1 was almost identical at different printing speeds up to 9 m/s. However, there might be changes for the overprints at higher speeds, because the acceptance of the secondary printed ink depends on the state of drying of the primary printed ink.

The evaluation of different colour sequences already showed visible differences between certain colour patches. The change of sequence from CMYK to KCMY only affects overprints with the participation of black. The corresponding secondary colours (C+K, M+K and Y+K) change colour by an amount of $\Delta E^*_{ab} = 5 \pm 1$ (Fig. 3a). Changing the sequence to MCMYK only concerns overprints with cyan and magenta. The colour difference of blue (C+M) even is $\Delta E^*_{ab} = 10 \pm 1$ (Fig. 3b).

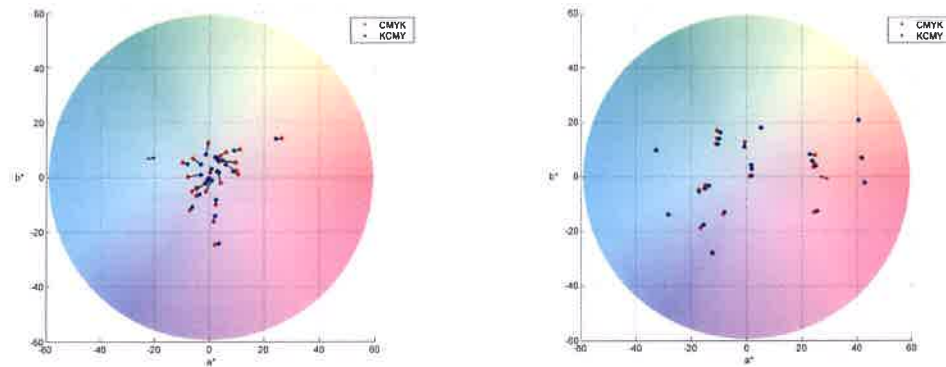


Fig. 3a: Colour shifts in the a^*b^* level for $L^* = 40$ (left) and $L^* = 50$ (right) when changing the colour sequence from CMYK to KCMY

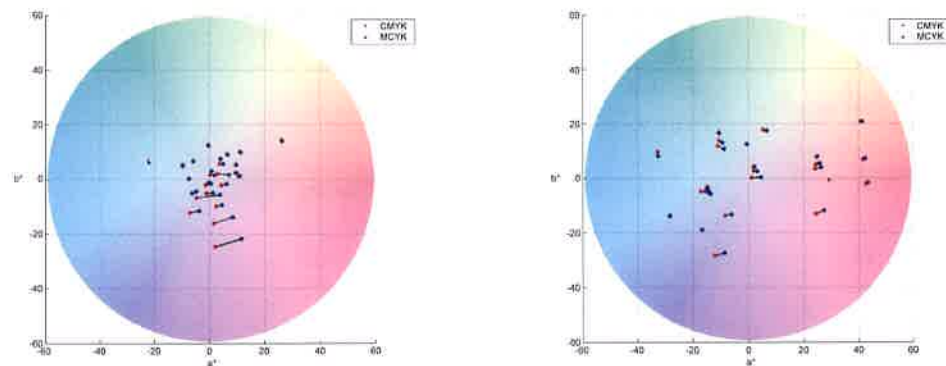


Fig. 3b: Colour shifts in the a^*b^* level for $L^* = 40$ (left) and $L^* = 50$ (right) when changing the colour sequence from CMYK to MCMY

Colour changes of the primary colours due to density variations transfer in about the same amount to the corresponding secondary colours. But density variations of the coloured inks CMY hardly affect overprints with black. When changing all densities in the same direction only differences in brightness are observable. They are approximately half as much as the sum of the participating primaries. The colour change of the tint patches increases linearly with tone value.

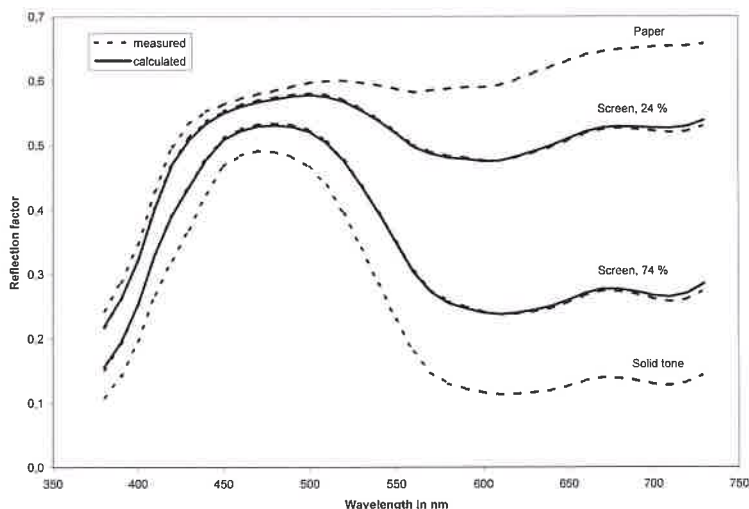


Fig. 4a: Comparison of the measured and the calculated reflection spectra of two different cyan tint patches with tone values of 24 % and 74 %

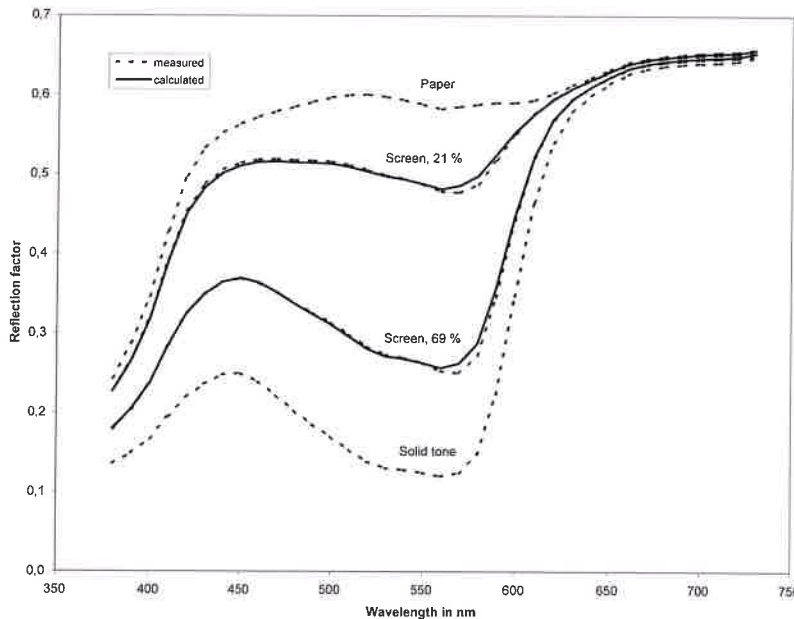


Fig. 4b: Comparison of the measured and the calculated reflection spectra of two different magenta tint patches with tone values of 21% and 69%

3. Calculations

As defined tonal variations are difficult to realize in practice, a mathematical model for calculating the colorimetric values for tint patches was established. Starting point was the well-known Yule-Nielsen-Theory [2]. Because light is scattered many times between the ink-air-paper interface, Yule and Nielsen employed a factor n (Yule-Nielsen-Factor) to be fitted. Setting this factor to infinity yields for the reflection factor R of the screen:

$$R(\lambda) = R_p(\lambda) \cdot \left[\frac{R_s(\lambda)}{R_p(\lambda)} \right]^F \tag{1}$$

R_p and R_s are the reflection spectra of the paper and the corresponding solid tone. F is the geometrical area coverage that can be calculated with the help of Murray-Davis-Formula:

$$F = \frac{\lg[A(R_s - R_p) + R_p] - \lg R_p}{\lg R_v - \lg R_p} \tag{2}$$

A is the optical area coverage, which is measured with a usual densitometer. As R_p and R_s can be obtained with a spectral photometer it is possible to evaluate the reflection spectrum of a tint patch. Measured and calculated spectra agree very well (Fig. 4). The differences are below $\Delta E^*_{ab} = 1$.

This method was used to calculate the colorimetric change of tint patches caused by variations of the tone value. ISO 12647-3 allows variations of up to 5% in the midtones. They yield to colour differences of $\Delta E^*_{ab} = 3$.

According to this model the tone value increase is mainly produced by the so-called light-catch. That is the difference between the optical and the geometric area coverage. It increases with the density of the corresponding solid tone patch.

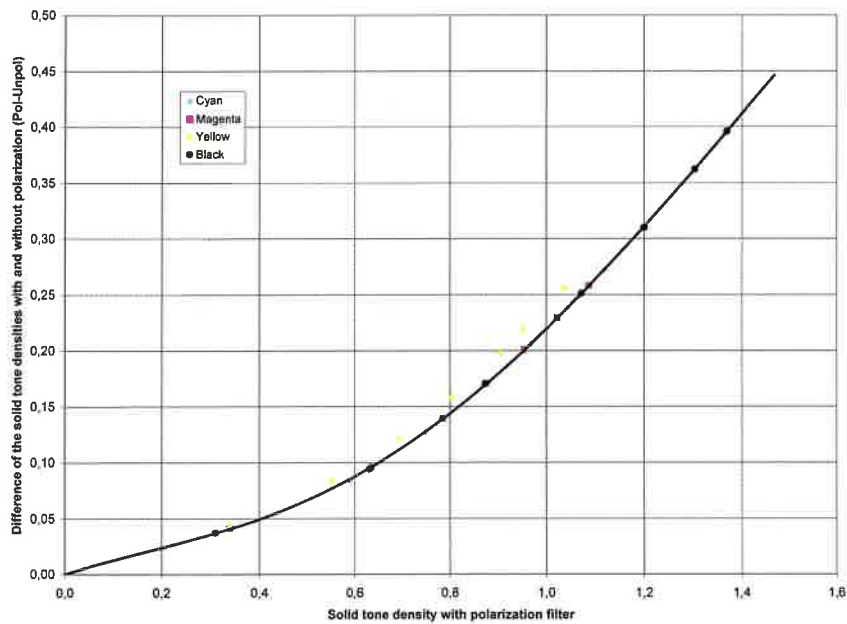


Fig. 5: Difference of solid tone densities measured with and without polarization filter

While colour measurements must be performed without a polarisation filter, it is compulsory for density and tone value measurements to minimize disturbing effects of gloss. Measurements with and without polarisation filter were performed, in order to evaluate its effect on the results.

It turned out, that densities are generally higher when measured with polarisation filters (Fig. 5). The differences increase with density and are equal for cyan, magenta and black. Furthermore a relation between the reflection factors with and without polarisation filter was found (Fig. 6). The lower the reflection factor is the higher is the amount of diminishing by the polarisation filter. The effects on tone value measurements are negligible.

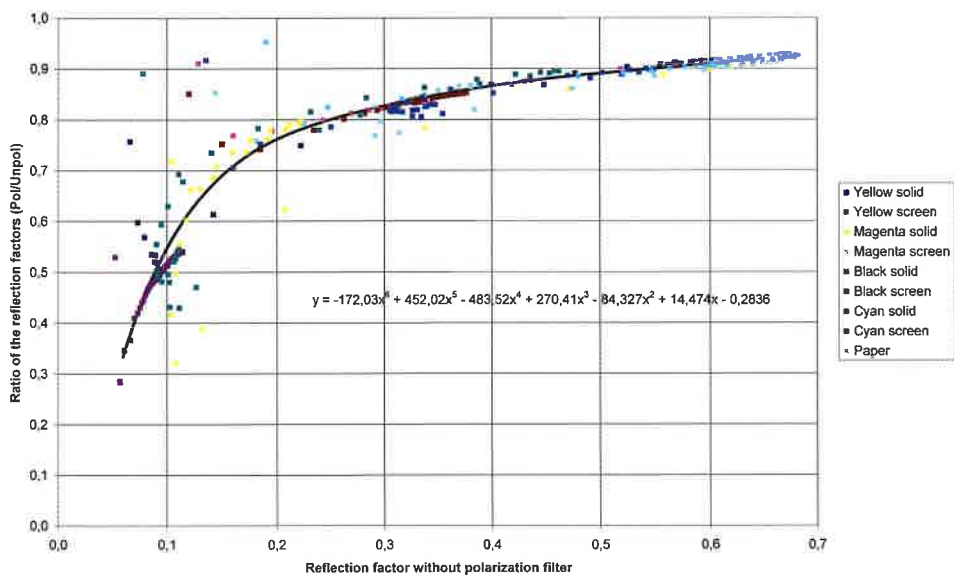


Fig. 6: Weakenig of the reflection factor due to the use of a polarization filter

4. Performance test of colour difference formulas

The patches of testforme 2 were cut out and configured in pairs. The pairs showed colour differences around five points in colour space. These were violet, blue, grey, orange and a greenish yellow. The colour differences were all along the L*, a* and b* axis in CIELAB space with amounts of about $\Delta E^*_{ab} = 2, 4, 6, 8$ and 10 (Fig. 7). The difference pairs were arranged in 15 rows, so that one row showed variations around one of the five points and along one axis. Each row was presented to 43 test persons who compared them with a reference difference pair of approximately $\Delta E^*_{ab} = 4$ (Fig. 8). The objective was to find out, which colour difference pair visually corresponds to the reference.

The usual CIELAB colour difference formula showed deficits mainly in the grey and yellow-green regions, where colour differences are judged different depending on their direction. The new CIEDE 2000 formula [3] did a slight improvement, but had weaknesses in the blue region.

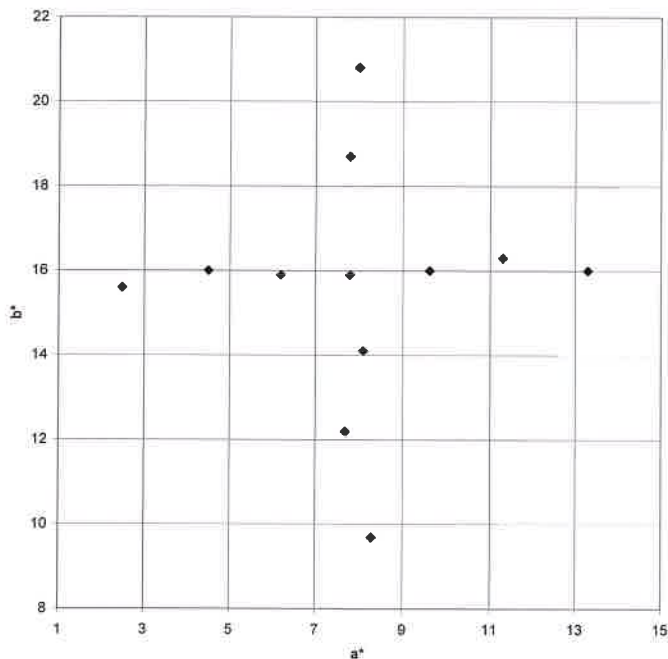


Fig. 7:
Arrangement of the colour patches of testforme 2. This example shows variations along the a* and b* axis of the CIELAB colour space

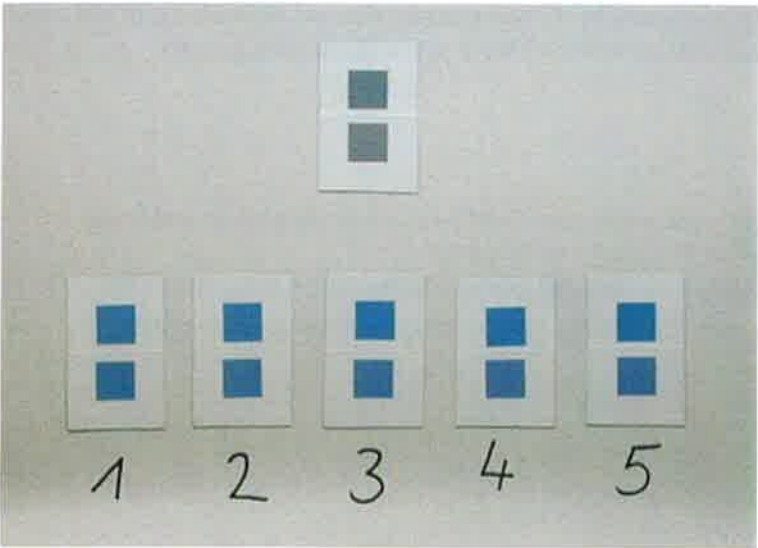


Fig. 8:
Presentation of the test charts. The picture shows the reference difference pair (above) with variations of blue along the a* axis

Tab. 1: Results of the performance test. The mean values show the colour differences for CIELAB and CIEDE2000, which visually correspond to the reference difference. A perfect colour difference system would have equal numbers in all parts and directions of colour space. The agreement of the test persons in judging the colour differences can be estimated with the standard deviation

		CIELAB		CIEDE2000	
		Reference: 4,0		Reference: 4,8	
Colour	Axis	Mean	Deviation	Mean	Deviation
Blue	L* axis	6,6	1,7	5,8	1,6
	a* axis	7,0	1,5	4,8	0,9
	b* axis	6,3	1,5	3,5	0,8
Yellow-green	L* axis	5,3	1,2	4,0	0,9
Yellow-green	a* axis	5,5	1,6	4,5	1,4
Yellow-green	b* axis	7,3	1,3	4,2	0,7
Grey	L* axis	6,9	2,1	6,1	1,9
	a* axis	3,9	1,3	5,0	1,7
	b* axis	5,1	1,6	4,8	1,4
Orange	L* axis	5,2	1,3	4,3	1,2
	a* axis	4,9	1,3	4,9	1,3
	b* axis	6,4	1,5	4,1	1,1
Violet	L* axis	6,7	1,4	6,2	1,5
	a* axis	6,1	1,6	5,2	1,3
	b* axis	6,2	1,1	4,5	0,8

5. Summary

Although ISO 12647-3 describes the conditions of standardized newspaper printing, variations within the given tolerances can lead to recognizable colour shifts. The most important parameter for the colorimetric behaviour is the colour sequence, which shows deviations up to $\Delta E^*_{ab} = 10$ for certain colour patches. Ink drying is another underestimated effect that must be considered.

In order to calculate the colorimetric values for tint patches, a mathematical model based on the Yule-Nielsen-Theory was established. It supplies accurate results that differ less than $\Delta E^*_{ab} = 1$ from the measurements.

Agreement of colour measurements with visual perception is very important for judging colour differences. The investigation of selected colour difference pairs by 43 test persons showed weaknesses of the usual CIELAB colour difference formula that could be corrected with the new CIEDE2000 formula.

6. Literature

[1] ISO 12647-3: 2004. Process control for the production of half-tone colour separations, proofs and production prints, Part 3: Coldset offset lithography on newsprint

[2] KANG, H. R.: Color Technology for Electronic Imaging Devices. Bellingham (USA): SPIE, 1997

[3] WITT, K.: Farbabstandsbewertung nach CIEDE2000. Berlin: Deutsche farbwissenschaftliche Gesellschaft, 2000

RGB colour spaces for optimal print reproduction

Manfred Werfel (ifra)¹, Beat Münch (Empa)², Walter Steiger (Ugra)³

¹ IFRA
Washintonplatz 1, D-64387 Darmstadt, Germany
E-mail: werfel@ifra.com

² Empa
Lechenfeldstrasse 5, CH-9014 St. Gallen, Switzerland

³ Ugra
Lerothen feldstr. 5, CH-9014 ST. Gallen, Switzerland

Absrtact

Since long ago a standard for monitors, prevailing incontestably for digital cameras and scanners, a dogma in the whole computer business: that is the data presentation of RGB colour images. It sets the colour coding basis for the common kind of users, just with the primary colours red, green and blue.

On the other hand, hardly anybody knows that dozens of RGB definitions are being used with varied shades of these primary colours. Even not really existing RGB basis colours are occasionally applied, even those which *cannot* exist theoretically. Straightaway, it might appear disconcerting, but let's call to mind that certain highly saturated colours would, otherwise, not be additionally re-mixable by using the above mentioned primary colours.

1. RGB since 1931

Already standardised in 1931 by CIE (Commission Internationale de l'Eclairage), the RGB Concept founded on the XYZ Standard Colour Stimulation System works indeed by superposition of positive colour components from three primary colours, so-called additive colour mixtures, according to findings from optical physiology. Due to the wide spreading of colour photography and colour display technology, colour representation with RGB data was given tremendous impetus. In this relation, an absoluteness status is often being attached to primary colours R, G, B, although primary colours might vary considerably in shade, saturation and brightness, and also basis colours of a digital picture eventually deviate massively from those of a reproduction device. As a consequence, an image can be presented, depending on RGB, in any wrong shades.

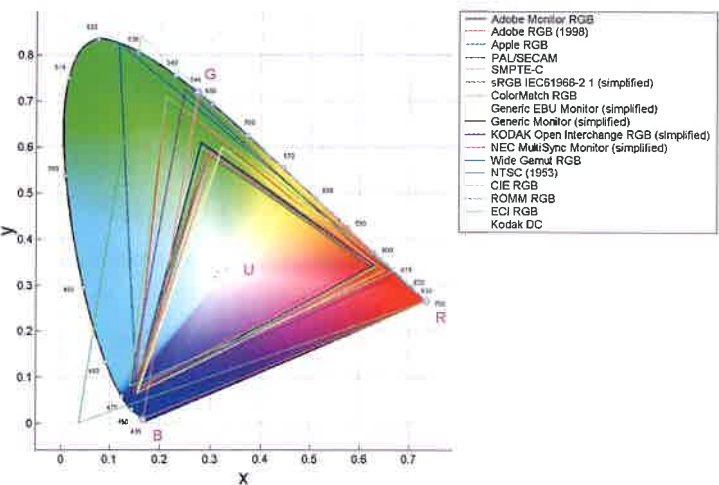


Figure 1:
Well-known RGB colours spaces
coming up with digital cameras,
scanners, displays or merely being
used as work colour spaces.
The figure shows the famous colour
space presentation in the horseshoe
shape as xy colour chart

2. From RGB to RGB -> Looking for a standard

Thus, using RGB data is problematic if true colour image rendering is needed. The correct interpretation of RGB can be granted only if together with every image, the accurate RGB specifications are available. On principle, corresponding indications should be expected in the image header, but worldwide most spread image data formats such as JPEG or TIFF have no standard specifically designed input in this regard. Diverse standardizing tests, for example by Exif header for digital camera pictures are in course, but these specifications were mostly ignored previous to Photoshop Version 7. Although the present Photoshop Version takes Exif into account, certain discrepancies were not remedied. So, only a corresponding software application will allow a correct RGB interpretation with Nikon D1X, for instance, as without this correction, the user can, without noticing, misinterpret the RGB. In spite of Exif, some software and camera manufacturers are still go their own ways.

A specific discrepancy arises from the fact that prominent colour scaling systems like Lab, Luv, XYZ, xyY, etc. have their worldwide recognised standard definitions, but unfortunately, none of the manufacturers observes the initial RGB definition, that is CIE 1931.



Figure 2: The erroneous interpretation of images with unknown RGB causes colour distortion

Four RGB types show how much the colour of the skin, to which the human eye is especially sensitive, can change under a different RGB. Each line contains an image with a defined RGB type - 1st line sRGB, 2nd line Colour Match, 3rd line Adobe98, 4th line ECI, while each column displays the interpretation by a different RGB - on the left sRGB, in the 2nd column Colour Match, in the 3rd Adobe98 and to the right ECI. Consequently the images in the diagonal line are showing the correct colour correction.

In the final analysis, the main responsible for this deplorable situation are the computer industries with their colour displays. Actually, their luminescent phosphors have strictly material based emission spectra and up to now, no phosphors with CIE radiation characteristics are known. In the software sector, it's obvious to refer to the basis colours of the display phosphors, particularly as without taking the long way over CIE RGB, a calculation intensive transformation can be avoided. For reasons of logarithmic radiation characteristics, which again, for fluorescent tubes, depend on the voltage, this initially linear matrix transformation was, additionally, linked with an exponential function laid down by means of the Gamma value. The so obtained radiation processes correlate well with the sensitivity characteristics of the human eye.

Problems occur mainly there where different RGB data are to be reproduced by printing in true colour. Graphic arts industries (pre-press and press) are therefore looking for a reliable standard, adapted to their needs.

For Internet application, the problem with lacking standard display colours seems to be resolved through the already very popular sRGB colour space, and also some digital camera manufacturers are using sRGB. Yet, this sRGB triangle is much too small for sophisticated printer applications.

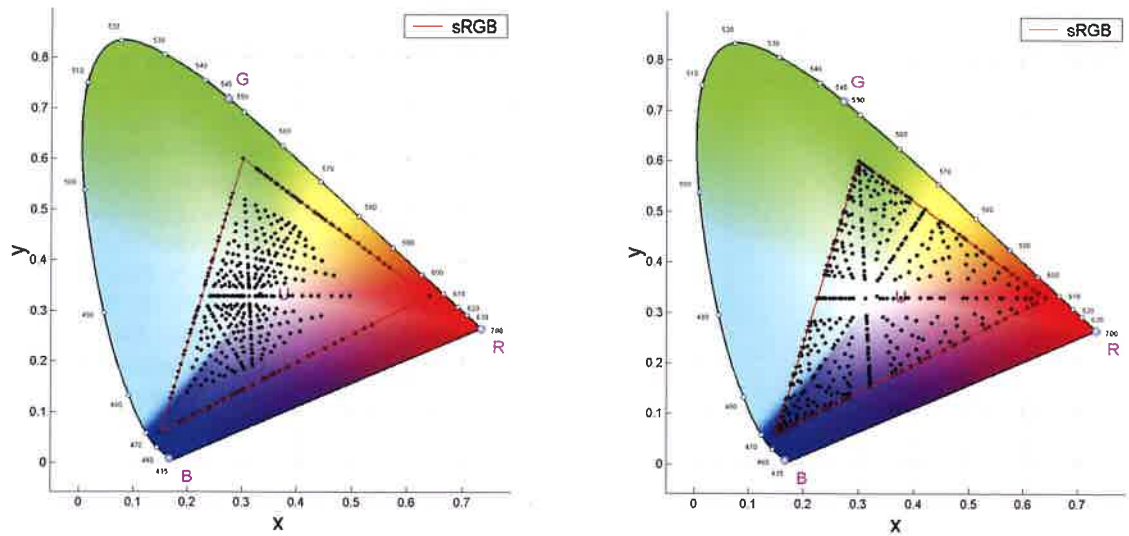


Figure 3 A and 3 B:

Additionally to size and shape of the attainable RGB colour space, the RGB data specifications also determine the distribution of the addressable colour. The Gamma value, which is responsible for the exponential progression form of brightness, plays a highly important role. The two colour charts illustrate the distribution of the colour values for sRGB under two different Gamma values. By using a Gamma value of 1 (without an exponential function) in colour chart A, the colour dots are mainly concentrated in the area of unsaturated colours, while their density decreases with increasing colour saturation. Gamma value 2.4 (colour chart B), specific to sRGB, allows a more homogeneous distribution of the encodable RGB colours

3. Looking for an "optimal RGB"

Science and industries are both discussing about an optimal RGB, and new RGB's are continually called into being. Optimisation occurs almost all the time relating to criteria with are specifically significant for the reproduction of colour images in printing and photography. Grey axis or optimised harmony of the RGB primary colours with those in colour photography, resp. with the secondary colours from sheet-fed and newspaper printing belong to this category. And so, when storing digital camera data, characteristics only needed when reproducing the picture on photo paper, on the display

or by printing, are already optimised. But they have no significance for the optimal storing of image data. Although allowing the presentation of an unchanged colour picture with its original data on the display - quite useful indeed as it is most simple - it is however an inconvenient process for true colour rendering. As a matter of fact, no image reproduction method has, on the one hand, a colour system resembling or, even lesser, corresponding to a RGM in colour space geometry or in colour difference - excepting the CRT display with a close approximation - and on the other hand, input RGB colour spaces as indicated technically for CCD cameras or scanners have quite different RGB characteristics, compared with output RGB colour spaces of displays. Furthermore, the sRGB display standard is in use since quite a while, but we are of course far from the calibration of all the displays on the market.

There are rather little chances therefore that RGB digital images will appear in true colour on a display or even on a printer, without going through a colorimetric adaptation. True colour in image reproduction has become an increasingly demanded criterion. And in this case, colour transformations are anyway indispensable. But the RGB data in raw state should be available and the transformation not occur until getting an accurate definition of the output device.

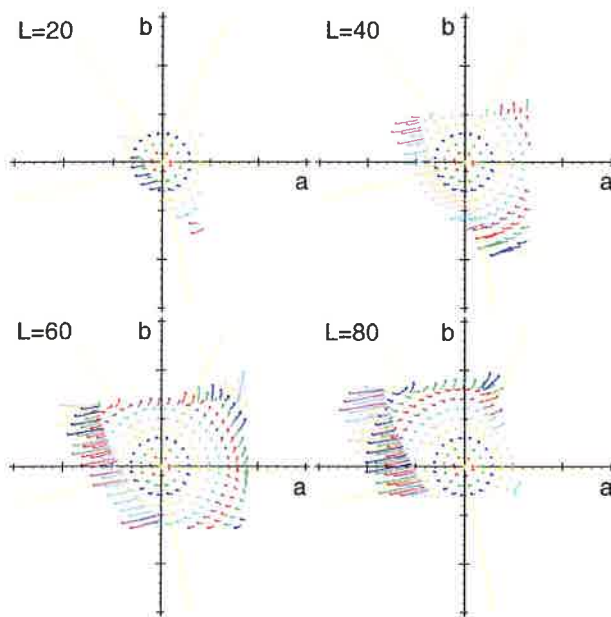


Figure 4:

A transformation from an RGB colour space into another causes two types of losses: those due to the spatial limitation to the RGB colour triangle and those by the discretization errors due to the restricted resolution of 8 bits. The figure illustrates the colour losses occurring when transforming from ECI-RGB to sRGB. They are displayed in the visually equidistant Lab colour space. Vectors from the original to the transformed colour locations display the colour shifts. Four intersections at the brightness $L=20, 40, 60, 80$ represent the three-dimensional Lab volume. The largest colour errors occur at high saturations close to the border of the colour space, since the ECI-RGB must be cut back when transforming to sRGB, mainly in green and blue areas. Discretization errors dominant at lower saturated colours

4. Treating RGB optimisation as a coding problem

Mathematically, RGB transformations are simple matrix operations linked with an exponential function. With present-day computers, there is hardly a chance to make out whether such a transformation can be managed additionally to loading the image data from the hard disk, when taking into account the time involved. For the rest, this transformation may occur without any loss, as far as the intermediary RGB results are not buffered. From a theoretical point of view, it is wrong to suppose that colour saturations would, in general, be limited to the RGB triangle in RGB colour conversions. A limitation of the RGB values exists though, but it is rather founded on encoding restrictions. In this relation, 8 bits are reserved for each of the three RGB channels in true colouring for the presently conventional 32 bit data used on computers. Then the remaining 8 bits are normally used for transparency information. For this coding, the colour definition area is, on the one hand, merely restricted to the triangle defined by the three primary colours. Thus, eventual colours beyond this limit cannot be coded and are cut back, in practice, to the triangle limits. On the other hand, 8 bits merely allow 256 value steps per RGB channel, hence the resulting discretization losses which, following RGB specifications and colour value, may be situated already beyond the perception limit of the eye. These two restrictions for colour codifiability, the

limitation to the surface of the RGB colour triangle and the too low resolution, are the cause of considerable data losses in every RGB transformation with subsequent storage of the results on the data volume. These data losses are expressed by trimmings on the colour saturation and are most troublesome for photographers and printing houses. Selecting the data RGB leads therefore to a conflict as on the one hand, primary colours should be chosen as much as possible far apart, so as to cover the greatest possible part of the really existing colours, but without taking the risk that basing on the 8 bit discretization, the colour steps become visible to the naked eye. This contradiction fuels since years the discussion about the optimal RGB standard. Following the previous consideration, it is easy to conclude that seeking for the optimal RGB is, basically, not the correct question to find the very solution to the RGB problem. All things considered, it means that mathematically, no RGB transformation is subject to any losses and that alone coding problems are causing losses.

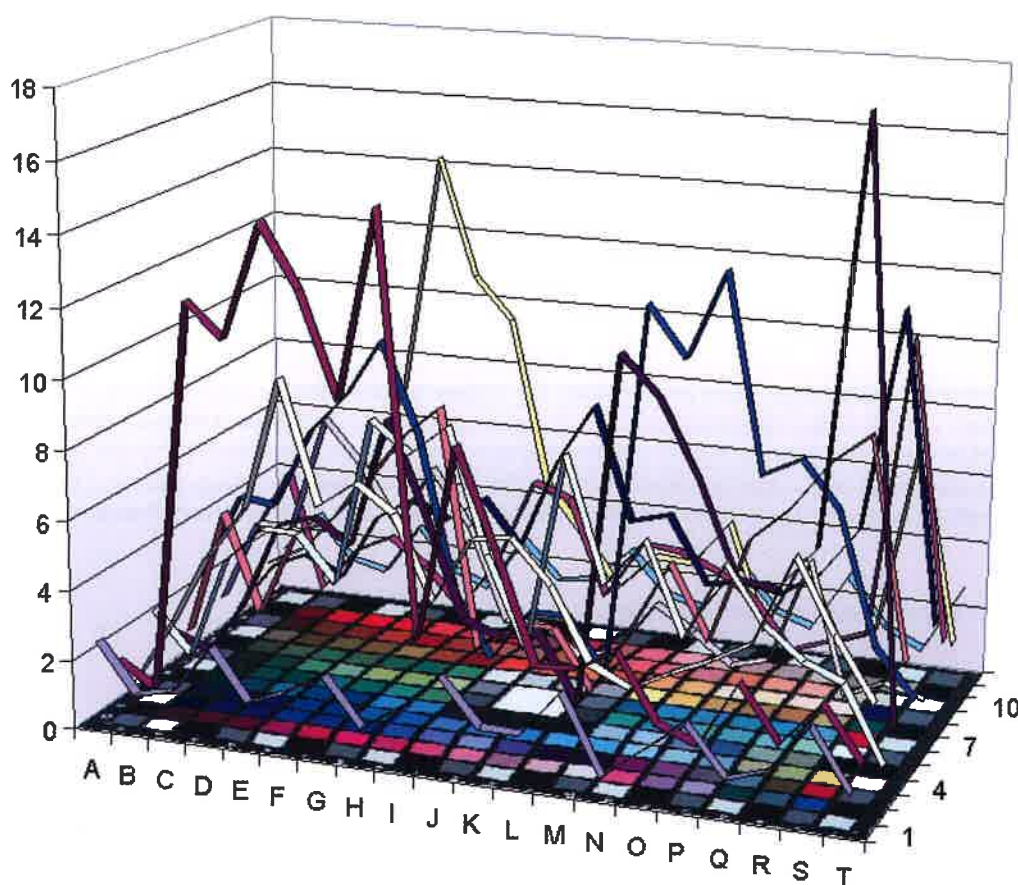


Figure 5:

The limitation of RGB spaces yields colour errors on image capturing and reproduction systems:

When capturing a Gretag Macbeth Colour Checker with a digital camera (Nikon D1X), the image data is usually mapped to a current RGB standard such as sRGB or Adobe98 RGB.

Consequently the colour may suffer considerable shifts compared to the original colours.

The figure shows the colour errors in Delta E94 of the digital image compared to the original. A standard illumination of D50 has been used. Depending on the colour errors of up to 20 Delta E94 occurred

Furthermore, due to the multitude of different, technically generated limitations of input and output colour spaces for every colorimetrically correct colour reproduction, a colour space transformation becomes imperative anyway. Thus, the research for the ideal RGB primary colours will not be good for solving the problem, and it is rather a matter of sticking to the optimisation of coding criteria.

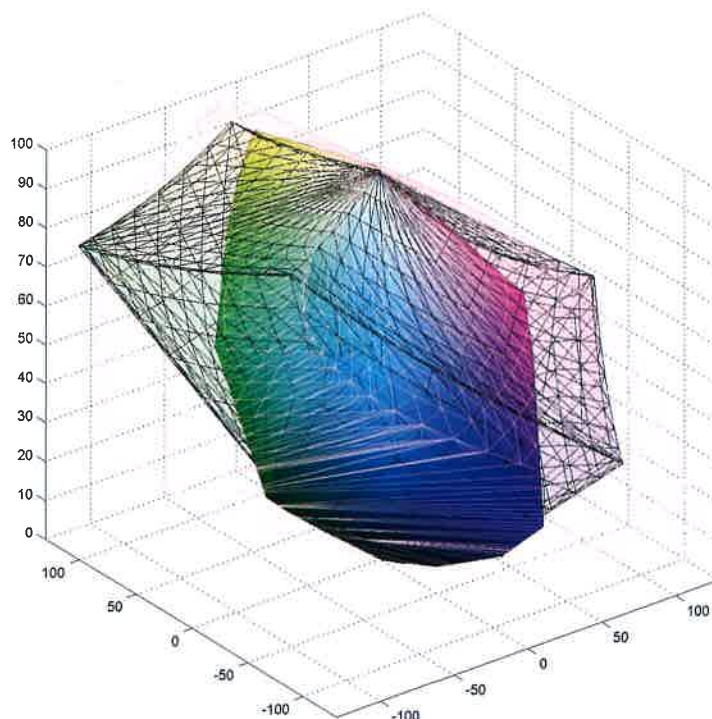


Figure 6:

Illustration of the RGB colour space problematic: the volume of all pigment colours existing in nature and technology - the so-called maximum colours - is represented in the present at D50 as a coloured body. Adobe98 RGB - sketched as a black grid - considered as a large colour space, however it still lacks of many colour areas and its geometry does not match with the geometry of the really existing colours. For comparison the so-called „optimal colour space“ of all the theoretically possible colours is sketched as a pink grid

5. Proposal for optimising the coding

The essential criteria to optimise the coding may be formulated as follows:

1. For most of today's conventional RGB codings, exclusively additive colour mixtures are admitted. That means that the RGB primary colour parts for mixing a desired colour cannot but adopt exclusively positive values. If the primary colours are not selected far from the theoretically possible colour saturation range as seen with the XYZ Standard Colour Stimulation System with its virtual primary colours, the theoretically existing colours can merely be re-mixed totally, provided that also subtractive colour mixtures with negative parts are allowed. By using adequately the available coding intervals, this effective requirement can be met with. That conditions simply a suitable transformation from the available data space into the RGB. By the way, this transformation is also needed with the conventional RGB coding and realised by the simple multiplication with factor $2^8 = 256$ which, on first sight, appears quite logical. In certain cases, however, the smallest defined difference between two colours is inadmissibly too wide.
2. The depth of colour data used for coding must be selected in a size to have the maximum differences in colour discretization situated under Delta E 1. In this connection, Delta E is understood as the smallest, colour difference perceptible to the human eye. Should the depth of colour data be chosen smaller, the eye will perceive disturbing colour gradations in continuous tones.
3. Basically, the situation of primary colours is absolutely unimportant. Those having reached a certain signification in practice will of course be preferred, but that is for purely data esthetic reasons and has

no consequences at all in practice. Presently, a certain importance is attached to a few RGB codings only, which meet with all the above mentioned coding conditions.

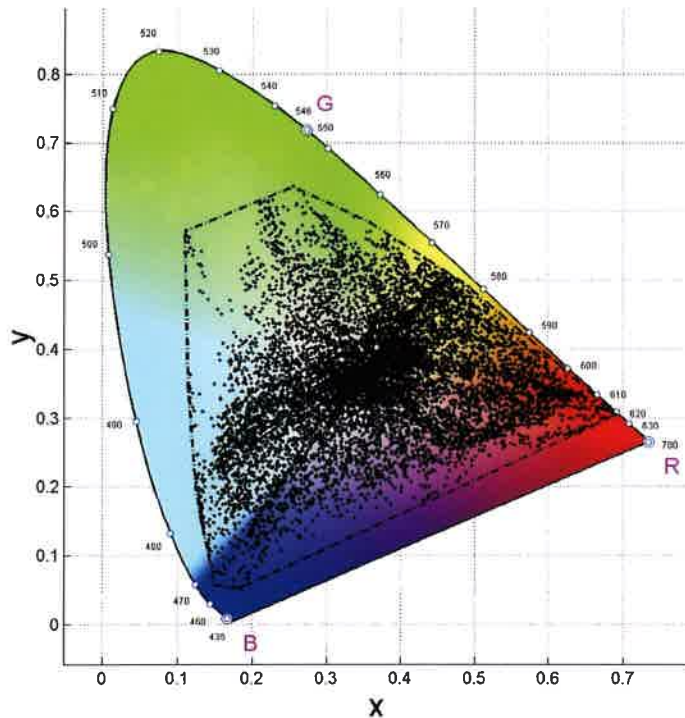


Figure 7:

The pigment colours known in nature and technology are merely filling about half of the theoretically existing colour space (according to E. Schrödinger). All the remaining colours require frequency spectra, which, presently, are not feasible. The figure shows the horseshoe shaped boundary for the theoretically possible pigment colours together with a series of highly saturated colours, whose envelope forms the limiting hull of all surface colours (maximum colours). Most of the current RGB types include only a part of these practically relevant colours. All higher saturated colours must be skipped to the respective RGB boundary

6. Positioning of e-sRGB and scRGB

The “extended sRGB” or “e-sRGB” elaborated around 2001 as ISO Standard is important. This standard uses the same primary colours like the conventional sRGB but is able to define colour shares/parts of - 53% to 168% instead of 0% to 100% and, thus, allows also subtractive colour mixtures. Hence, the whole theoretically existing colour space becomes displayable.

The e-sRGB colour data format functions with 10, 12 or 16 bits following the choice. Even with 10 bits only, the resolution is sufficiently high to keep the colour spaces between two data values in all the colour areas under the critical threshold of 1 Delta E.

An alternative comparable with e-sRGB is “scRGB” which functions with 16 bits. Up to now however, none of the two formats has gained real market acceptance; till today, leading software manufacturers are ignoring them, and they are, for instance, not available in Adobe Photoshop 7.0.

What is sure: if ISO Standard “e-sRGB” has its way among digital camera and scanner manufacturers, the discussions about the optimal RGB will stop.



Print quality evaluation for governmental purchase decisions

Peter Nussbaum¹, Jon Y. Hardeberg², Sven Erik Skarsbø³

The Norwegian Color Research Laboratory
Dept of Computer Science and Media Technology
Gjøvik University College
Box 191, N-2802 Gjøvik, Norway
E-mail: ¹ peter.nussbaum@hig.no
² jon.hardeberg@hig.no
³ sven.skarsbo@hig.no

Abstract

Potential costumers within the digital printer market have various demands considering their requirements with regards to desired print quality. This paper aims to investigate the print quality according to predefined quality factors to determine the appropriate printing equipment. In particular the study describes the methods and results of a research project conducted by researchers at the Norwegian Color Research Laboratory for the Norwegian Government Administration Service. The objective of the project was to develop methods and procedures to perform test prints from digital printers including the evaluation and assessment of the print quality according to predefined quality factors. The results of the study indicate the performance of various digital printers in terms of their obtained print quality, which will be useful for the governmental purchase decisions.

1. Introduction

In 1997 the design program for the Norwegian Ministries was established, and a design handbook was produced (Kulturdepartementet, 2000). The Ministry for Culture and Church Affairs is responsible for the design program and the ministry has delegated the responsibility for the administration, the daily running and the development of the design program to the Norwegian Government Administration Service (NGAS). NGAS is also technical editor for governmental publications, and supports all of the ministries in the printing of publications. Amongst other things, the design handbook describes and defines the colours used in the ministries logos (National Coat-of-Arms). In order to maintain control over colour reproduction of these logos it was decided to use pre-printed letterheads; letterheads produced by offset printing.

Originally, the three colours of the national logo have been specified with regard to PMS (Pantone Matching System). Although this printing technique ensures the colour accuracy of the colour logo, it is an expensive and time consuming process. On the other hand, after several years of market hesitation, digital presses have now become common and in today's printing market, where flexibility, variable content, shorter lead times, and on demand publishing, are being demanded, digital presses represent an attractive supplement to conventional offset presses (Hardeberg and Skarsbø, 2002). Consequently, the Ministry for Transport and Communications has decided to embrace this new technology and replace the conventional offset process by digital printing systems. In order to maintain the colour reproduction demands, as outlined in the design handbook, the Norwegian Color Research Laboratory at Gjøvik University College in collaboration with NGAS has carried out a project to develop methods to evaluate digital printers.

Consequently, the aim of the presented work has been to develop methods and quality factors to evaluate digital printers in terms of their potential impact on print quality, in accordance with the

quality requirements of the NGAS. Furthermore, the development of digital test documents and test procedures to obtain the evaluation results is an important part of this study. Although other aspects, such as the commercial and the technical point of view, might be considered for the acquisition of the appropriate equipment, the results of the printer evaluation will be used by the NGAS to determine the final purchase decisions. We also believe that not only the results but also the methodology will be of interest to other target groups and who are considering the replacement of conventional printing by digital printing.

NGAS, as the costumer of this project, nationally announced a printer quality competition and printer manufactures were invited to participate in the test. However, due to the current purchase process by the NGAS, the names of the participating printer manufactures and their printing systems cannot be published in this work.

In the reminder of this work the next section gives a short overview in the field of colour image quality. Then section three introduces the experimental method used for evaluating the print quality in terms of the predefined quality factors. Then in section four the data analysis performed on the experimental data is described, followed by a presentation of the results. Finally the implications of the results will be discussed and ideas will be suggested for future work.

2. Colour Image Quality

Various studies and research have been done in the field of print quality and repeatedly it has been concluded as a very complex issue. The subject has been discussed at various conferences (see e.g. Stokes, 1998; Hardeberg and Skarsbø, 2002). In another study by Marcu (2000) addresses various quality factors that determine the print quality such as printing technology, colorant/media interaction, geometric resolution, halftoning, separation, black generation, UCR, GCR and tone reproduction.

Principally there are two different methods to assess image quality. The first method is by measurement, using instruments to determine values for the various quality factors. Considering the evaluation of relative colorimetric colour reproduction of printing devices Microsoft has proposed a quality assurance system (Microsoft Corporation, 2001).

The second method is based on observation, using psychophysical experiments to gather the judgement of human observers. For instance, the pair comparison method is a robust approach where observers are asked to compare the perceptual magnitude between two stimuli (or pairs of stimuli). This method is based on Thurstone's "law of comparative judgement" (Handley, 2001; Gescheider, 1985).

To produce an accurate assessment of image quality the values obtained by measurement and observation metrics can be calculated. The term metric is generally applied to any physical and psychophysical measure of image quality. Image quality metrics can be defined as numbers, derived from physical measurements that can be related to the perceptions of image quality (Jacobson, 1995).

Compared to a number of other studies, whose aim is the comparison of colour image quality of digital presses concentrating in the field of rendering complex images, the main focus in this work is printer evaluation according to reproduction requirements of the Norwegian ministries logo (National Coat-of-Arms). Hence, considering the printer evaluation in this work, NGAS has most emphasis the colour logo reproduction (Figure 1).



Figure 1: The design handbook describes and defines the colours used in the Norwegian ministries logo (National Coat-of-Arms)

3. Experimental Method

Considering the methods to assess the digital print quality in this study we have proposed a number of quality factors. According to the presented list of appropriate quality factors NGAS has determined the most significant quality factors including their weighting rate. Then the selected quality factors have been divided into three assessment categories, namely, “visual logo assessments” (Section 3.1), “general print quality assessments” (Section 3.2) and finally the “copy quality assessments” (Section 3.3).

To complete the final ranking the results of the three categories have been weighted once again. According to the priorities of the quality requirements defined by NGAS the category “visual logo assessments has been weighted by 50%, the category “general print quality assessments” by 30% and finally the third category “copy quality assessments” by 20%.

The quality evaluation and the final ranking were done at the Color Research Laboratory at Gjøvik University College, using psychophysical experiments (expert panel) and quantitative analyses based on measurements. The psychophysical evaluations were performed to determine the colour logo reproduction in terms of colour match, visual resolution, surface texture, logo alignment and artefacts. The quantitative analyses included text quality, colour gamut, repeatability and register. The next three sections are describing the assessment categories including the defined quality factors.

3.1 Visual logo assessments

As mentioned in the previous section, the Color Research Laboratory has proposed a number of quality factors to determine the colour reproduction performance of digital printers. In the first category, which is considering the visual assessment of the colour logo reproduction, Table I lists the selected quality factors and the corresponding weighting rate defined by the NGAS. It can be seen that the quality factor “Colour match” has absolute highest priority.

Table I:
Quality factors within the
category visual logo assessments
and the corresponding weight

Quality factors	Weight %
Colour match	50
Visual resolution	20
Surface texture	10
Logo alignment	10
Artefacts	10

The next paragraph explains the quality factors in more detail.

- Colour match: The aim of this factor is to obtain, as close as possible, a colour match between the logo colours defined by the three Pantone colours and the test prints. The competitors have been

- asked to adjust the source file with the three logo colours according to the supplied Pantone colour patches to achieve a closest possible colour match between the test print and the Pantone target.
- Visual resolution: Detail reproduction in the colour logo such as the “tongue in the lions head” (Figure 1), sharp lines and smooth edges has an impact in the quality of the logo reproduction.
 - Surface texture: Observation of graininess, texture of the colours, smoothness of the image, banding.
 - Logo alignment: Positioning of the colour logo according to the requirements. The colour logo placed on the A4 document has to be aligned centre and 10mm from the top.
 - Artefacts: Observation of unwanted effects on the print such as stripes, scratches and marks.

A psychophysical experiment was carried out to evaluate the visual quality of the colour logo reproduction that the printers can obtain. The test prints have been visually assessed according to standardised illumination and viewing conditions (ISO 3664 P1). Before performing the visual assessment the expert panel, including three members from the NGAS and one member from the Color Research Laboratory, have conducted the ISHIHARA Test for Colour Deficiency to confirm their appropriate colour vision.

The magnitude estimation method was employed to judge each quality factor. The four observers gave individual ratings on a scale from excellent (6) to very poor (0). The individual marks obtained by the four experts have been collected and the average result listed by ranking.

3.2 General print quality assessments

Within this category, four quality factors have been proposed to assess the print quality independently of the Norwegian ministries logo. Table II presents the selected quality factors and the corresponding weighting rates. Note that NGAS has weighted all factors equal.

Table II:
Quality factors within the
category general print
quality assessments and the
corresponding weight

Quality factors	Weight %
Text quality	25
Colour gamut	25
Repeatability	25
Register	25

- Text quality: This quality factor analyses the performance of the text reproduction including negative text in various text sizes (3 pica point up). In addition the rendering of text on coloured background, bitmap and bitmap illustrations are further assessed. The assessment method used is based on observation from the expert panel rating on a scale from excellent (6) to very poor (0).
- Colour gamut: The colour gamut defines the range of colours achievable on a certain substrate under the predefined viewing conditions. Colour difference in terms of ΔE^*_{ab} between the logo colours (Pantone 280M, Pantone 185M and Pantone 116M) and the corresponding logo colours printed by the competitors is part of the assessment. A printer with a larger colour gamut than another is typically able to reproduce more saturated colours. However considering the predefined Pantone colours in the colour logo, it is not expected that a larger colour gamut necessarily include the target colours because the match will be determined due to the location of the Pantone colour and the device colour gamut within the entire colour space. The data used in this task are based on colorimetric measurements, which have been analysed and visualised by the icc3d application (Farup *et al.*, 2002).
- Repeatability: To determine the variation in terms of colour stability over time the quality factor repeatability is required (Morovic and Nussbaum, 2003). Essential, a Microsoft Word document (102 pages), representing an ordinary file including text, images, graphs, illustrations and two colour test charts (inserted on page 6 and page 99) was the source. To quantify the short-term repeatability of the printer, the Word document was printed five times in sequence. This results in ten

- measurements of the colour test chart with an interval of 93 pages and 9 pages respectively. The variations between the measurements are given in ΔE^*_{ab} units.
- Register: The register between individual colour image layers influences the print quality of the colour reproduction (Field, 1999). Variations in register can result in loss of resolution and sharpness. Figure 2 illustrates a sample of nonius register marks (Ifra, 2002) to determine the register deviations in the print. The evaluation to determine the register performance was carried out by the use of a microscope according to ISO 12647-2.

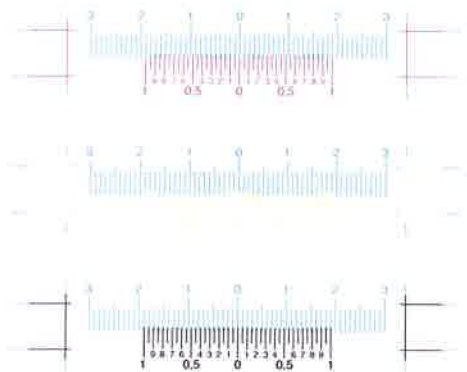


Figure 2:
Variations in register can be determined by the aid of nonius register marks (Ifra, 2002)

As mentioned in the previous section NGAS is responsible for the design program (design handbook), which describes and defines the colours used in the ministry logo (Figure 1). The three colours of the national logo, accepted by NGAS as «the optimised logo colours», refer to Pantone 280M, Pantone 185M and Pantone 116M. Table III shows the CIELAB-values of the three logo colours obtained by colour measurement at the Norwegian Color Research Laboratory using a spectrophotometer, SpectroLino (2°, D50). These obtained CIELAB-values for “optimised logo colours” are registered in the design program.

Table III: CIELAB-values (2°, D50) for “optimised logo colours” registered in the design program

Logo colours			
	L*	a*	b*
Pantone 280M	20.70	11.50	-51.10
Pantone 185M	52.70	71.90	34.00
Pantone 116M	84.70	6.90	83.20

Although this category combines visual observations and the method using instruments to determine values for some of the quality factors, a scaling from excellent (6) to very poor (0) has been employed.

3.3 Copy quality assessments

Finally in the last category, three quality factors have been analysed determining the quality performance of the copy function of the printers. The evaluation method used is based on visual assessment with individual marks given by the expert panel rating on a scale from excellent (6) to very poor (0). The quality factors in this test and the corresponding weightings are listed in table IV.

Table IV:
Quality factors within the category copy quality assessments and the corresponding weight

Quality factors	Weight %
Colour match between original print and copy	40
Copy accuracy	40
Artefacts	20

- Colour match between original print and copy: The original print for this task is the Word document with 102 pages printed from the supplied digital file. Subsequently a copy has been produced, by using the copy function of the printer.
- Copy accuracy: The rendering ability in the copy reproduction of text and illustrations has been assessed.
- Artefacts: Undesirable print artefacts, which appear on the copy print such as dust, stripes, scratches and marks have been evaluated.

3.4 Test targets

As mentioned previously, NGAS, as the costumer of this project, nationally announced a printer quality competition and printer manufacturers were invited to participate in the test. Consequently methods had to be designed, including the development of digital test documents and test procedures, for the competitors that have applied to conduct the test. The requirements for conducting the test were defined in four tasks. Included on a CD-ROM each competitor has been asked to print four test documents.

The first test document, defined in pdf-format, sRGB colour space and in size A3, contains test images, colour charts and elements for the register control. The second target, shown in Figure 3, was specified in pdf-format, CMYK for offset (coated paper) and in size A3. It consists of test images, colour charts and other control elements according to the CMYK colour space. The third document is a Microsoft Word file, A4 in size, containing 102 pages with text, illustrations and colour test charts. This test file should simulate a customised text document completed by the NGAS. The fourth document is an eps-file consisting of the three Pantone colours, which represent the national colour logo (National Coat-of-arms). The participants have been asked to adjust the Pantone colours in the file to obtain a closest possible match between the print and the «original Pantone patches». NGAS has provided the three Pantone colour patches Pantone 280M, Pantone 185M and Pantone 116M. Finally, the last task in the test, the competitors have been asked to copy the test prints from the Microsoft Word file on the same equipment as the test prints have been made. Note that the presented test documents contains test elements such as complex images, which are not taken into consideration within the test. However, these elements could be used in further image quality assessments.



Figure 3: The CMYK test target designed for the printer test

The competitors were allowed to choose their customized printing parameters such as driver settings and RIP software, with the goal of achieving their best colour image quality. Considering the substrate, NGAS has supplied all the participants with the appropriate paper, which has been required conducting the print test. The scanning function of the printers has not been part of the evaluation.

4. Results

In this section the results of the printer evaluation will be presented. To recap the aim of this work is to develop methods including quality factors to the evaluation of digital printers in terms of their potential impact on print quality, in accordance with the quality requirements of the NGAS.

The Color Research Laboratory received test prints from a total of six participants to evaluate their print quality. To avoid any prejudices throughout the evaluation process NGAS anonymised the test prints by identifying the competitors with **A, B...F**.

Firstly the results of the three categories individually will be presented before the final ranking will be shown. Table V presents the results according to the visual evaluation of the six test prints. Considering the “visual logo assessments” the experimental results identify competitor **A** as the candidate that scored best in all the quality criteria in this category.

Table V:
Results of the
category visual logo
assessments of six
test prints

Part 1: Visual logo assessments							
Quality factors	Weight	A	B	C	D	E	F
Colour match	50%	5.3	4.5	4.5	3.5	3.3	3.5
Visual resolution	20%	5	4.8	4.8	3.8	1.8	3.8
Surface texture	10%	4.8	4.8	3.8	3.8	3.3	2.8
Logo alignment	10%	5	5	4	4	3	5
Artefacts	10%	6	6	6	6	6	6
Total		26	25	23	21	17	21
Weighted mean		5.2	4.8	4.6	3.9	3.2	3.9
Ranking		1	2	3	4	6	4

Especially for the quality factor “colour match”, which the NGAS has prioritised highest, competitor **A** showed excellent performance. By presenting the results of the other competitors, only **B** and **C** could match the minimal requirements of the expert panel. Although the competitors **D, E** and **F** have shown reasonable results for the quality factors «surface texture», «register» and «artefacts» the performance regarding «colour match» was rather poor. In fact, the expert panel has decided that competitor **D, E** and **F** will be excluded in the further evaluation process because they couldn’t match the requirements of this category at all.

Table VI presents the results of the second category, namely, the evaluation of quality factors, which are not direct related to the colour logo. Nevertheless these quality factors contribute to the entire image quality and may affect the rendering of the colour logo.

Table VI:
Results of the
category general
print quality
assessments of the
competitors **A, B**
and **C**

Part 2: General print quality assessments				
Quality factors	Weight	A	B	C
Text quality	25%	3	5	4
Colour gamut	25%	6	4	3
Repeatability	25%	1	6	5
Register	25%	6	6	5
Total		16	21	17
Weighted mean		4	5.3	4.3
Ranking		3	1	2

It can be seen, that competitor **B** performs best in this category followed by competitors **C** and **A**. Due to the imperfect repeatability performance obtained by competitor **A** the total score within this category is rather poor. However, considering the quality factor “colour gamut” competitor **A** has shown the largest range of colours achievable compared to the two other competitors.

Table VII:
Results of the
category copy
quality
assessments of the
competitors **A**, **B**
and **C**

Part 3: Copy quality assessments				
Quality factors	Weight	A	B	C
Colour match between original print and copy	40%	5	2.8	4
Copy accuracy	40%	3.3	3.8	3.3
Artefacts	20%	4.3	4.5	4
Total		13	11	11
Weighted mean		4.2	3.5	3.7
Ranking		1	3	2

Table VII presents the results of the category copy quality assessment. Considering the quality factor “colour match between original and copy” competitor **A** performs best, whereas competitor **B** shows some obvious limitations. Although competitor **B** performs best regarding the quality factor “copy accuracy” all three competitors achieve a reasonable result.

Table VIII:
Final evaluation
results including
the three categories
and their corre-
sponding weights
from competitor **A**,
B and **C**

Final ranking: part 1, part 2 and part 3	Weight	A	B	C
Weighted mean part 1	50%	5.2	4.8	4.6
Weighted mean part 2	30%	4	5.3	4.3
Weighted mean part 3	20%	4.2	3.5	3.7
Total		8.2	8.8	8
Weighted mean		4.6	4.7	4.3
Final ranking		2	1	3

To obtain the final ranking the results of all three categories has been weighted according to the priorities of the quality requirements defined by NGAS. Although Table VIII shows an insignificant difference between competitor **A** and competitor **B** in terms of weighted mean, competitor **B** has scored best considering the final ranking.

5. Discussions

Although the results of our evaluation presented in the previous section are interesting, and the methods are valid themselves, it is appropriate to proceed to a critical discussion.

Even if all three competitors showed an acceptable result in the category “general print quality assessment” competitor **B** demonstrated the overall best performance in this category. Considering the quality factor “text quality” all competitors have shown an acceptable performance in terms of legibility for the font size of 3 pica. However, considering the quality factor “colour gamut” Figure 3 shows that competitor **A** can represent the biggest range of colours achievable on this substrate whereas competitor **C** has a significantly smaller colour gamut.

In terms of matching the Pantone colours of the national colour logo the results from competitor **A** show a strong correlation between the results of the quality factor «colour match» in the category

“visual logo assessments” and the quality factor “colour gamut” in the category “general print quality assessments”.

Considering the colorimetric measurements of the test print comparing with the target colours Pantone 280M, Pantone 185M and Pantone 116M, non of the three competitors are able to perform an absolute colour match, as seen in Figure 4. However, for the target colour Pantone 280M competitor A shows a colour difference of $\Delta E^*_{ab} < 5$ units whereas competitor B and competitor C show a colour difference of $\Delta E^*_{ab} > 10$. Regarding the target colour Pantone 185M it can be seen that all three competitors have their limitations in terms of colour match accuracy.

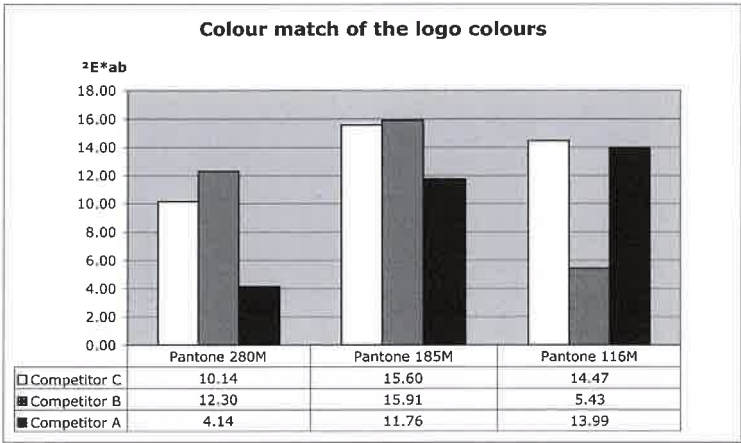


Figure 4: Colour difference in terms of mean error between the Pantone colours and the test print

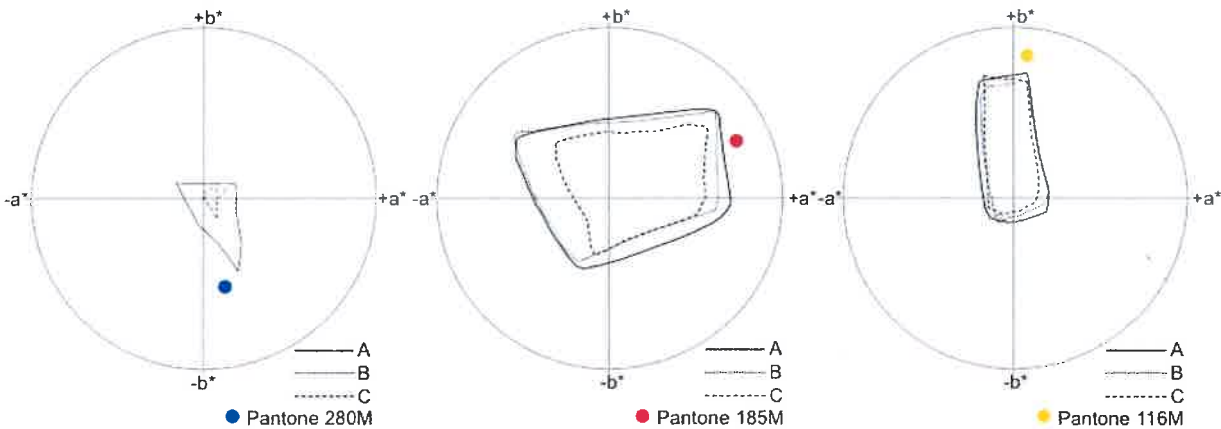


Figure 5: Colour gamut projection of the competitors A, B and C onto the a^*b^* -plane according to the level of lightness (L^*) of the three colours of the national logo

Figure 5 shows the colour gamut projection of the three competitors onto the a^*b^* -plane according to the level of lightness (L^*) of the three “optimized logo colours” (Table III). Furthermore it illustrates the distance from the nearest possible point in the colour space achieved from the print medium and the target colour. Except for Pantone 116M, competitor A shows the best performance in terms of colour difference between the Pantone colours and the test print. The Pantone 185M was in general the most difficult colour to reproduce.

Table IX: Size of colour gamuts, quantified as the volume of the convex hull of the gamut in CIELAB colour space derived to the test prints of the three competitors A, B and C

Competitor:	CIELAB volume	Relative volume
A	385000 unit	100%
B	295000 unit	77%
C	220000 unit	57%

Another way of looking at the size of colour gamuts is by considering the gamut volume. The size of colour gamuts, quantified as the volume of the convex hull of the gamut in CIELAB colour space was derived from the test prints of the three competitors A, B and C. It can be seen in Table 9 that competitor A provides the largest gamut volume, whereas the volume given by competitor C is only 57% of that given by competitor A.

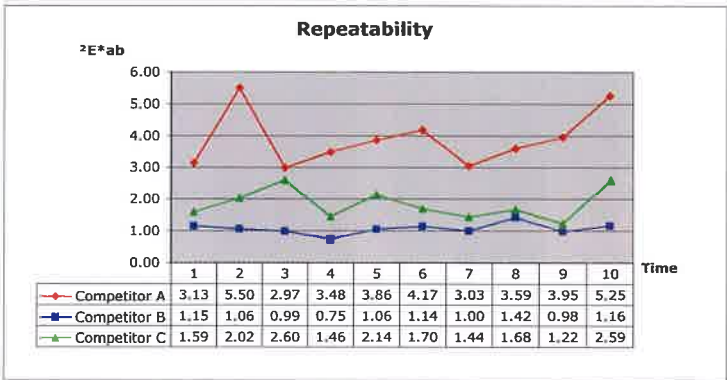


Figure 6: Repeatability variations over time in terms of ΔE^*_{ab} of the three competitors A, B and C

To quantify the effect of the printer’s repeatability, a digital test chart including 288 colour patches, which representing the achievable colour gamut on a certain substrate, was printed ten times at short-time interval. Figure 6 shows the repeatability variations according to ten measurements in sequence. Apparently competitor B performs best compare to the other two competitors with very small variations. Competitor C presents a larger variations but the result is still within an acceptable tolerance. However it is worth pointing out that competitor A has shown an unexpectedly poor repeatability performance. Currently the exact cause of this could not be determined, although the most likely cause is human error of the operator.

Finally, in Figure 7, the results of the last category “copy quality assessments” indicate the best characteristics for competitor A in terms of “colour match between original print and copy”. Nevertheless all three candidates have performed acceptably in terms of the quality factors “copy accuracy” and “artefacts”.

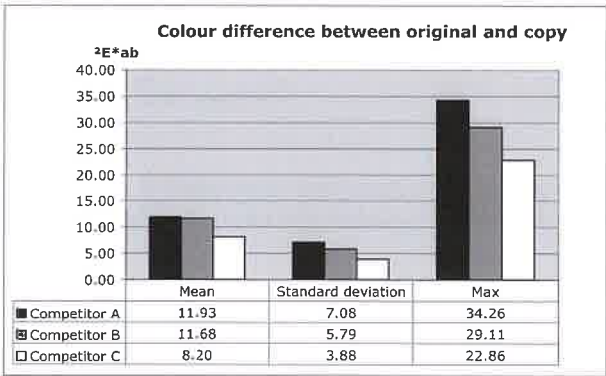


Figure 7: Colour difference between original and copy in terms of ΔE^*_{ab} of the three competitors A, B and C

Although the final ranking list shows an insignificant difference between candidate **A** and candidate **B**, competitor **B** has demonstrated the best performance. It is obvious that competitor **A** would have achieved the overall best result by performing an acceptable repeatability performance.

As seen in Table V, competitor **A** has performed best regarding the visual evaluation of the copy test. However the results of the colorimetric measurements between the original and the copy do not match the visual evaluation in terms of colour difference. Figure 7 illustrates that competitor **A** shows the highest value according to the ΔE^*_{ab} colour difference (Mean ΔE^*_{ab} 11.9 units) whereas competitor **C** shows the best performance. The fact that there is no strong correlation between the visual evaluation and the colorimetric measurement might be due to the different number of colours, which have been used for the two methods of quality assessment. For the visual evaluation, the three logo colours only have been considered whereas for the colorimetric measurement a large number of colours which represent the entire reproducible colour space have been the target.

Suppose the weight of the chosen categories and defined quality factors had been changed, the final result may have been different. Moreover it is worth pointing out that we have proposed further quality factors, which could have been applied to this study to evaluate the print quality (e.g. visual image quality, colorimetric reproduction, uniformity and addressability). However, commercial and political circumstances of NGAS have affected the consideration of the applied factors in this study.

6. Conclusions and Perspectives

The evaluation method including the selection of the quality factors used in this particular project has been unique in terms of print quality. Although various factors have been chosen and applied in the evaluation process the main target to assess the competitors has been the accuracy of the colour reproduction of the three colours of the national logo. The outcomes in this study demonstrate a strong correlation between the performances of the competitors in terms of the obtained results of the various quality factors. The competitors, which have shown good results considering the size of the colour gamut and the accuracy of the colour match, have obtained reasonably good results in other quality factors too. Except for one competitor, which has shown a very poor performance regarding repeatability. However, the result of the printer evaluation can be used by the NGAS to determine the final purchase decision in terms of image quality.

A similar approach might be adopted for other printer evaluation to justify the appropriate equipment to match the desired print quality and requirements. The proposed categories and quality factors are adjustable according to the quality requirements. After the NGAS has decided which type of equipment shall be purchased and implemented further measurement can be conducted on this new machine to confirm the results from the prior tests. Nevertheless, the similarity between the purchased printers themselves in terms of colour accuracy and stability over time would be a possibility for further studies.

There might be several potential directions for further work on this topic. The acceptability threshold considering print quality assessment is defined as a vague concept and one that depends strongly on application and industry. Moreover, a further quality metric, which could be considered more suitable for the printer market is a tolerance threshold.

Acknowledgements

The authors thank NGAS for their kind permission to use this material. Furthermore the authors wish to extend their thanks to the participating members of the NGAS for their grateful collaboration.

References

- Farup I., Hardeberg J. Y., Bakke A. M., Kopperud S. and Rindal A. (2002). Visualization and interactive manipulation of color gamuts. In *Proceedings of IS&T and SID's 10th Color Imaging Conference: Color Science and Engineering: Systems, Technologies, Applications*, pages 250–255, Scottsdale, Arizona
- Field G. (1999). *Color and Its Reproduction*. Second Edition, GATFPRESS, Pittsburgh US
- Gescheider G. A. (1985). *Psychophysics, Method, Theory, and Application*, Second Edition, Lawrence Erlbaum Associates, ISBN 0–89859–375–1, 152
- Handley J. (2001). Comparative Analysis of Bradley-Terry and Thurstone-Mosteller Paired Comparison Models for Image Quality Assessment, *PICS 2001*, 108-112
- Hardeberg J. Y. and Skarsbø S. E. (2002). Comparing color images quality of four digital presses. *Proceedings of the 11th International Printing and Graphic Arts Conference*, Bordeaux, France
- Ifra (2002). Colour quality audit in reproduction and print, Ifra Consulting Module
- ISO 12647-1 (1996). *Graphic technology - Process control for the manufacture of half-tone colour separations, proof and production prints – Part 1: Parameters and measurement methods*, First edition
- ISO 12647-2 (1996). *Graphic technology - Process control for the manufacture of half-tone colour separations, proof and production prints – Part 2: Offset lithographic processes*, First edition
- ISO 3664 (2000). *Viewing conditions – Graphic technology and photography – Second edition*
- Kulturdepartementet (2000). *Grafisk designprogram for departementene, Håndbok, annen utgave*, Statens forvaltningstjeneste
- Jacobson R. E. (1995). An Evaluation of Image Quality Metrics, *The Journal of Photographic Science*, Vol.43 1995
- Marcu G. (2000). Color Quality in Desktop Printing. *Tutorial Notes, IS&T's PICS Conference*, Portland, Oregon.
- Microsoft Corporation (2001). Windows Color Quality Specifications for Printer OEMs. Part of Microsoft Hardware Quality Labs (WHQL)'s Windows Color Quality Test Kit. <http://www.microsoft.com/hwdev/tech/color/ColorTest.asp>
- Morovic J. and Nussbaum P. (2003). Factors Affecting The Appearance Of Print On Opaque and Transparent Substrates, *Journal of Imaging Science and Technology, JIST* 47 #6
- Stokes, M. (1998). The impact of color management terminology on image quality. In *Proc. IS&T's 1998 PICS Conference*, pages 174–178, Portland, Oregon



6

Packaging and labeling



Grooving quality research on packaging cardboard

Darko Babić, Vesna Kropar-Vančina, Branka Lajić

Faculty of Graphic Arts
Getaldićeva 2, HR-10000 Zagreb, Croatia
E-mail: darko.babic4@zg.htnet.hr

1. Introduction

Packaging, as many other products of highly automated industry, has become an integral part of modern life. Manufacturers' position is not an easy one: competition is getting fiercer every day, product quality is becoming better and better, and systems of production and product quality control are becoming more and more sophisticated. As a result, all other components of a product, such as packaging, must meet higher standards as well.

As far as boxes are concerned, a straight and clear edge is one of the most important aesthetic demands. This primarily concerns cardboard packaging used in the food and cosmetic industry, since buyers frequently have a direct contact with it. Such an edge can be obtained only if the folding point has been well prepared during the production process (punching).

The research described in this paper has been carried out in order to prove that groove quality largely depends on the quality of the cardboard used, as well as, on relative humidity of conditioning, the quality of grooving channels, and tools used in the grooving process.

Since the parameters that influence groove quality are numerous, this research was restricted and focused on testing the quality of grooves moulded on channels made by CITO creasing matrixes System GmbH, Germany, VIKING iron grooving bands from Austria and KRAUSSE punching machine System GALLY, Germany. Researched material was cardboard of BELPAK - BEL/GT 1 quality of various grammage (between 280 and 450 g/m²) produced by KOLIČEVO, Slovenia. Cardboards were conditioned prior to grooving (ISO 187).

2. Methods

We have tested 4 commercial cardboards BELPAK - BEL/GT 1 quality produced by KOLIČEVO from Slovenia. Tested boards were coated and, nominally, of the same quality but of the various grammage i. e. 280, 320, 350 and 450 g/m². In Table I general properties of tested cardboards are presented.

Table I: Tested cardboards

Cardboard number	Grammage [g/m ²]	Thickness [mm]	Specific volume [cm ³ /g]	Producer/Quality
1	280	0.35	1.25	KOLIČEVO BEL/GT 1
2	320	0.41	1.28	KOLIČEVO BEL/GT 1
3	350	0.44	1.26	KOLIČEVO BEL/GT 1
4	450	0.57	1.27	KOLIČEVO BEL/GT 1

Bending stiffness of tested cardboards was determined by Taber tester (15°, ISO 2493) at $23 \pm 1\text{ }^{\circ}\text{C}$ and $50 \pm 2\%$ RH (ISO 187). Tested boards were cut into 100x210 mm samples and grooved all along the shorter side in order to observe the groove quality sideways. Twenty samples were prepared of each tested cardboard ten in MD i. e. parallel to the grain direction and ten in CD i. e. perpendicular to the grain direction altogether 240 samples and the grooving quality was examined in both directions. In Figure 1 preparing of cardboard for grooving is presented. Before grooving samples of cardboards were conditioned in a climate cabinet at 20 °C and 35, 50 and 75% of RH (TAPPIUM 549).

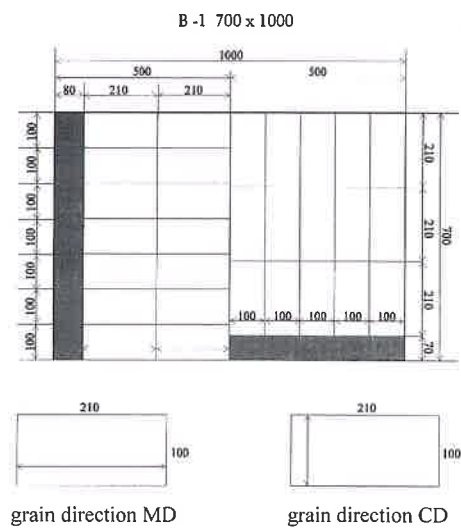


Figure 1: Preparing of cardboard for grooving

CITO creasing matrixes System GmbH, Germany (Fig. 2) and VIKING iron grooving bands from Austria (dimensions: 23.30 mm high, 0.70 mm wide and 120 mm long) were used for grooving in this work, as well as KRAUSSE punching machine System GALLY, Germany (Fig. 3).

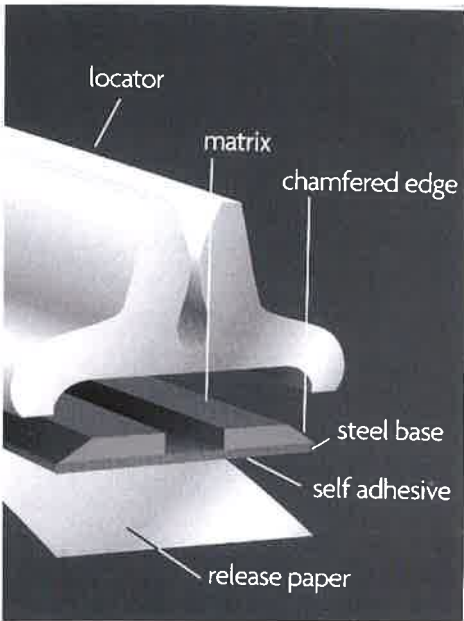


Figure 2: CITO creasing matrix

Figure 3: KRAUSSE punching machine
System GALLY, Germany



Table II: Channel groove dimensions

Cardboard number	Grammage [g/m ²]	Thickness [mm]	Channel groove dimensions [mm]	
			height	width
1	280	0.35	0.40	1.30
2	320	0.41	0.40	1.30
3	350	0.44	0.40	1.30
4	450	0.57	0.50	1.50

3. Results

In Table III results of Taber stiffness are presented.

Table III: Results of Taber stiffness of tested boards













Cardboard number	Grammage [g/m ²]	Taber stiffness [mNm]			
		Grain direction			
		MD		CD	
		\bar{x}	σ	\bar{x}	σ
1	280	84.9	9.59	45.9	18,08
2	320	126.7	7.94	61.6	10.04
3	350	133.5	3.43	115.2	2.48
4	450	159.2	6.27	124.5	3.05

Obtained results given in Table IV and Table V show the comparison between the results from Table IV and the suggested evaluation system from Table V.

Table IV: Test results

Grammage [g/m ²]	Grain direction	Relative humidity [%]	Evaluation (number of occurrences in a sample)					
			0	1	2	3	4	5
280	MD	35	5	4	1	0	0	0
		50	0	7	3	0	0	0
		75	0	6	3	1	0	0
	CD	35	5	4	1	0	0	0
		50	2	7	1	0	0	0
		75	7	3	0	0	0	0
320	MD	35	0	7	3	0	0	0
		50	1	4	5	0	0	0
		75	5	5	0	0	0	0
	CD	35	0	6	3	1	0	0
		50	1	9	0	0	0	0
		75	7	3	0	0	0	0
350	MD	35	1	3	4	2	0	0
		50	1	6	3	0	0	0
		75	2	6	2	0	0	0
	CD	35	0	6	3	1	0	0
		50	1	9	0	0	0	0
		75	7	3	0	0	0	0
480	MD	35	0	0	0	3	2	5
		50	0	0	0	9	1	0
		75	0	0	3	4	3	0
	CD	35	0	0	0	6	2	2
		50	0	0	1	5	4	0
		75	0	2	6	2	0	0

Table V:
Grooving evulation model

Fibre direction		Attributive value expressed numerically	Description of grooves	Suggested steps
CD	MD			
		0	Grooves indistinguishable. Avoid using the box at all costs.	Not to be used.
		1	Grooves almost indistinguishable, edges unclear. We do not suggest using such a box.	
		2	Grooves can be distinguished, but edges are unclear. Groove depth and width blurred. The use is impossible.	
		3	Grooves can be distinguished, but edges are unclear. Groove depth and width inexpressive. It could be used for less demanding boxes and manual production, but we do not recommend it.	Limited use.
		4	Grooves and edges of a good quality, depth and width clearly visible. Can be used for smaller editions.	To be used for smaller and less demanding editions.
		5	High-quality grooves, clear edges of optimum depth and width. Fibres rounded from the inside and outside. Grooves recommended for larger and high-quality editions.	To be used for all editions and most demanding box types.

4. Discussion and conclusions

As far as boxes are concerned, a straight and clear edge is one of the most important aesthetic demands. This primarily concerns cardboard packaging used in the food and cosmetic industry, since buyers frequently have a direct contact with it. Such an edge can be obtained only if the folding point has been well prepared during the production process (punching).

The research described in this paper has been carried out in order to prove that groove quality largely depends on the quality and climate conditioning of the cardboard used, as well as on the quality of grooving channels and tools used in the grooving process. Since the slightest change of the mentioned parameters causes a change in the quality of grooves, it is impossible to give simple instructions on how to make box blanks and/or grooves.

After having analysed the research results we can, claim with certainty that cardboard humidity as a function of relative air humidity greatly influences the quality of grooves. Since the parameters that influence groove quality are numerous, this research was restricted and focused on testing the quality of grooves moulded on channels made by CITO creasing matrixes System GmbH, Germany, VIKING iron grooving bands from Austria (dimensions: 23.30 mm high, 0.70 mm wide and 120 mm long) and KRAUSSE punching machine System GALLY, Germany (Fig. 2 and 3). The varying parameters were the grammage of tested cardboards (Table I), the conditioning of cardboards and height and width of grooving channels (Table II). Grooving channels were adjusted to cardboard thickness (Table II).

Since the aim was to define cardboard properties as precisely as possible and to compare the grooving quality by observing the channels, we examined cardboard stiffness using a Taber tester (Table III). The results of stiffness were given in mNm. Stiffness is naturally influenced by cardboard thickness, which was also tested. As was the case with other parameters, several measurements were performed, each of which was recorded as the average value expressed according to the ISO standards. For instance, cardboard samples weighing 280, 320, 350, and 450 g/m² were 0.35, 0.41, 0.44, and 0.57 mm thick, respectively. When all the measurements had been performed, we compared the results, drew up tables and charts, and tried to establish the connection between the results obtained and the grooving quality. The results included additional commentaries, which aimed at explaining each value and conclusion as clearly and logically as possible.

A proposed evaluation system based on the research results (240 measurements and 480 photos) was designed: grooving channel quality was assessed according to a model table where attributive qualities were expressed through marks. The system was developed because every cardboard grooving quality research that had previously been conducted warned us about the need to transform the researcher's subjective impression regarding the box design or grooving quality into a more quantifiable assessment. It was, naturally, much of a challenge but we tried to produce an acceptable grooving quality evaluation model that might provide comparative material for any further research. Our experience and a great number of box blanks collected over the years and a substantial number of photographs proved to be great help in the process. Each category is accompanied by a photography, a descriptive assessment, and an explanation, which we hope will help avoid any mistakes that might be made when comparing grooving quality and the chosen evaluation model.

The project represents a solid base for all further researches, which might take the optimum value of the examined parameters as a starting point and vary other product features. Our contribution to industrial production is an especially practical evaluation model, which will allow a quick quality assessment of grooves formed in cardboards. We would also like to point out once again that the most urgent and the most important future research should aim at establishing the connection between grooving quality and relative air humidity by conditioning cardboards through gradual increase of RH (by 5%) during the grooving process.

Literature

- Babić D., Kropar Vančina V., Černič Letnar M. (2002) Investigation of the Relation Strength/Grain Direction of the Board Folding Box, Proceedings of the 29th International Annual Symposium, Bled, November 13-15, 2002, Slovenia, pp 92-97
- Babić D., Vančina Kropar V., Lajić B. (2003) Relation of Board Box Strength and Grain Direction, Conference Proceedings, MATRIB 2003, Vela Luka, Island Korčula, June 26-28, 2002, Croatia, ISBN 953-7040-01-1, Croatian Society for Materials and Tribology, Zagreb, pp 1-6
- Bureau H. W., (1989), What the Printer Should Know about Paper, Graphic Arts Technical Foundation, Pittsburgh

Černič Letnar M., Kropar Vančina V., Hladnik A., (2002), Effect of Accelerated Ageing on Degradation of Unprinted and Printed Graphic Paperboards, Proceedings of the 29th International IARIGAI Research Conference, Lake of Lucerne, September 8-11, 2002, Switzerland, ISBN 3-9520403-2-0, EMPA/Ugra, St. Gallen, pp 216-233

Černič Letnar M., Kropar Vančina V., (2002) The Effect of Accelerated Ageing on Graphic Paperboards Degradation; Restaurator, 23, pp 118-132

Černič Letnar M., Scheicher L., Kropar Vančina V., (2000), Optical and Colour Durability of Graphic Board and Laboratory Prints, Proceedings of the 27th International Annual Symposium, Bled, November 15-17, 2000, Slovenia, pp 133-139

Eldred N. R., (1990), Changes in Temperature and Relative Humidity directly Affect Paper, GATFWORLD, 2, 3, pp 1-4

Kropar Vančina V., Černič Letnar M., (2001) Durability of Coated and Uncoated Boards, in Bristow A. J. (Ed), Advances in Printing Science and Technology, ISBN 1 85802 438 2, Pira International, Leatherhead, pp 43-55

Setter V. C. and Gundergon D. E. (1983) in Mark R. E. (Ed): Handbook of Physical and mechanical Testing of paper and Paperboard, Marcel Dekker, New York

Vančina V., Mikota M., Golubović A., (1992): The Effect of Humidity on the flexural Stiffness of Some Coated Boards, Acta Graph. 4, 4, pp 199-203

Holography on packaging material and an estimate on the rising trend of its application

Ivana Žiljak

Faculty of Graphic Arts, University of Zagreb
Getaldićeva 2, HR-10000 Zagreb, Croatia

Keywords:

Colors in holography, Consumer, Hologram, Hologram application, Hologram design, Hologram types, Holography in Croatia, Packaging material holography, Producer, Protection, Raster elements in holography, Statistics and databases on holography in Croatia

1. Introduction

The motive for this research is the sudden interest of the producers and the growing implementation of holography in areas that are different if compared to one another. At the same time this paper is a report on the follow-up of the success in holograph application and efforts to forge them. It is an analysis of the existing designer solutions, a comparison of their efficiency, and the relationship of holography as a marketing element in respect to the end user. My opinion is that in modern graphic product protection it is necessary to develop, use and coordinate the latest design and technological achievements, especially holograms. Holography has the tendency to develop in the direction of mass application with the goal being to protect both the producer and the consumer; applied on food and pharmaceutical products, on documents, financial stamps, banknotes and all kinds of graphic products and products for the media. Holography is used in the control of financial flows, tax control and transactions on state level basis.

Together with my co-workers I carried out the testing of various holographic foils and various techniques of foil application. Samples made by various world wide holographic product makers were researched, most of all those coming from the Optaglio hologram producers, designed for printing in various temperature areas. The application of holograms is expanding in the area of documents and they are later complemented with laser print. The behaviour of various holographic foil was observed in the temperature area ranging from 110°C to 190 °C. Cold application (self-adhesive type) and thermal application were compared. As to the design, comparison was made between the continuing form design and the application with single and double registers.

The paper gives an analysis of all the goods produced in our market with hologram application, determines which firms are applying holograms, which type of holograms are used, how they were applied. A database has been made for this work containing data on the hologram types, types of hologram application, hologram complexity, hologram size, the type of products holograms were applied to, holograms as a designer and marketing element, holography as the final authenticity control, on hologram suppliers and hologram prices in Croatia. This is a report on the state of the system in Croatia with a projection of the trend of hologram application alterations and hologram development. The research gives data on hologram application in recent years and the up-to-date situation.

This paper gives the experience of hologram application and the problem of applying holograms on transportation tickets (tram, bus, railway). The graphic industry has found itself completely unprepared as to the technique of hologram application, so that there are cases of purchasing finished holographic stickers, holographic paper or blank paper with printed holograms (because printing works are not prepared

to use technologies for good-quality application of holograms). Contemporary printing works are not equipped with special units for hologram application. They have machines equipped for foil printing.

This paper also contains measurements necessary for making financial stamps (holograms on stamps for cigarettes, alcoholic beverages). The problems linked with automatic implementation of such stamps in the market are discussed. As these fall into the group of a certain kind of securities, the proposals for having the stamps returned to financial services is being discussed.

2. Hologram application on packaging material for protection purposes

The risk in product protection is increasing, as for instance, in the pharmaceutical industry. According to the World Health Organization (Erik Swain, Trends in Security Packaging, [/www.devicelink.com/pmpn/index.html](http://www.devicelink.com/pmpn/index.html)) 10% of all medicaments are falsely labeled, and 60% of these have dangerous active ingredients. According to the same source, as many as 40% of all medicaments are faked. This issue is becoming more significant in connection with product sale through the Internet. The pharmaceutical industries are developing a specific strategy of determining the risk type for each product.

A multi-level approach to protection techniques should be applied in protecting products with the help of packaging material. The first step in a product's packaging material protection is by using holograms in printing, a technique that may not be reproduced or copied by any other graphic technique.

The most frequent protecting supplements are those that are determined by machine reading. Furthermore, there are procedures of application with optically varying numbers, invisible and electronic colors, micro-texts, animated images, morphol images (changes from text to log, for example), and oncoming new generations of materials. Let's add colors that change under different kinds of illumination, or colors that change if they are touched, colors that change depending on the temperature. Not all the listed elements against forging are available to all, and they are poorly readable or not readable at all, nor can they be reproduced with the usual scanning equipment and other forging procedures.

The most important element in protection techniques is to bear in mind the necessity of quick recognition and differentiation of forged products from the original ones. The best thing to do is to study all kinds of methods; for instance, the security measures against forging the Euro. Nevertheless, forged money is implemented, more or less successfully. Software designs for banknote protection are not easily available, but this also goes to say that experts should be consulted when planning and designing packaging material.

Mere protective elements will not contribute to general success if there is no training organized in order to educate on the existence and importance of these graphic designs, and in being able to tell the difference between the originals and the possible forgeries. In the protection strategy there should be continuous development of new patents in order to stop the progress of forging and various alternative-forging methods. There should be no set standards in the protection procedure used in printing, but constant improvements through technology and science should be implemented as well as through new types of physical and chemical protection systems. The best protection method is top coding in image and colour recognition, but such protection is possible to determine only on basis of laser reading systems, and this does not make it possible for a regular consumer to verify anything. It is necessary to alter protection strategies, and this brings new expenditures. But on the other hand, if this matter is not treated with due respect, there may be significant damages.

Although holograms have not been in use for a long period of time, the first designs have been forged with the help of foil printing, by addition of blank silver foil (with no holograms).

This is a warning that great care will be needed in expanding hologram application in the role of a protective element and in hologram designing. There should be a maximum number of clearly evident colourings and larger - more noticeable colourings and greater - more observable contrasts in design.

The paper contains the analysis of a new trend in hologram application for special emergency cases. For instance in sports' games and mass quantities of tickets for big open shows (where there are no numerated seats).

3. The advantages of holograms in comparison to other protection techniques in printing

- ◇ Holograms cannot be reproduced or copied with the help other graphic techniques;
- ◇ Hologram have a unique optical effect, recognizable with the bare eye;
- ◇ When holograms are moved under certain angles the colour and tone of the graphic elements are altered;
- ◇ Holograms may be created with the help of a computer, simulating the appearance of the hologram, as well as the changes when observed under different angles;
- ◇ Holograms may have a multi-level approach, for instance the MULTIMATRIX® hologram - a multi-level authenticity and several levels of visual safety characteristics;
- ◇ Holograms can go through postpress intervention under various temperatures;
- ◇ Holograms may be cut with various clichés with difficulty that may be applied afterwards as one cliché on top of the other;
- ◇ There is possibility of applying optically varying colours, invisible and electronic colours;
- ◇ There is possibility of applying micro-texts, animated images, and the on-coming new generations of material;
- ◇ There is possibility of numbering, and having a date on the holograms;
- ◇ A holographic ribbon may be cut in such a way that the stamp form is right only after opening the packaging material.

4. Special multi-level protection in holography (Multimatrix holograms)

There are holograms with multi-level protection level (Multimatrix holograms). These holograms have as many as three levels of reading:

1. Recognition with the bare eye - no tools are necessary

Holograms are observed under a light, by rotating the image - horizontally, vertically, rotation. A kinetic effect is observed (linear, spreading, rotation, counter-rotation). Dynamic holographic micro-texts may be read, 2D/3D and 3D (stereographic) display.

2. Professional control

Micro-texts and micro-graphics are controlled. Special lasers are used in case the cryptogram (covered image that may be seen with the help of a laser beam) or dyinagram (dynamic cryptogram) should be observed.

The best types of protection are top sorts of coding for image and colour recognition, but such protection may be read only with the help of machines with various laser systems, so that the customer cannot check anything without having tools.

3. Forensic laboratory

Nano-texts and nanographics (05 microns+), coded nanostructures, coded nanobarcodes are observed.

Other hologram types that are analysed in this paper and the observed characteristics:

- a) The 2D hologram consists of two-dimensional images. Different colours and positions in each layer are preset. Each layer stands for itself and there is no feeling of depth nor three dimensions.
- b) The 2D/3D hologram consists of multiple two-dimensional layers where hologram images are positioned next to one another with visual depth in order to create the effect of a three-dimensional hologram structure. There is a good visual depth between various layers and brilliance on the first layer.
- c) The micro-text on the hologram is observed by the bare eye with difficulty or is invisible. It may be seen clearly with a magnifying glass.
- d) A Flip-Flop hologram is designed in such a way that two different images may be seen when looking from different angles. When the angle of observation changes horizontally (from left to right) or vertically (moving up and down).
- e) The kinetic hologram contains “moving pictures” and is analysed from various angles. A logo or graphic image may be incorporated into holographic patterns with the help of special digital hologram technologies and 2d/3d technologies. Animated and 3D holograms may be created with the help of animation computer programs.
- f) Transparent holograms on transparent foil or bag are applied on documents. The text and image under the hologram may be seen and read under the hologram label even though it also has an image.
- g) Holograms with printed serial numbers. A serial number/numbering is a special protective element on holograms. It has a wide field of application against forging.
- h) Dot-Matrix Holograms allow putting an unlimited number of computer-generated dots onto the hologram. The Dot-Matrix Hologram is the result of a design consisting of many tiny dots where each dot has its colour contouring. They create the impression of changing images.
- i) 3D holograms where the created depth is real. Each image part moves independently in respect to the other image and the images overlap. Each layer is scanned with exactness with the 3D scanner (object observing angle), the color and blending, and is later computer prepared for producing the master. Certain layers are computer simulated before they go into production in order to diminish the expenses.

5. Program solutions and hologram simulation with special raster elements

Holograms that contain vector and pixel graphics with especially designed raster forms are a completely new method of protection in printing. This paper gives a proposal how to solve the question of programming and applying such raster and authentic PostScript programming code.

Each function may be proven and repeated by introducing the function into the image record. The application of specially designed rasters may be very wide. Special forms of raster elements, various lines and angles may be designed on holograms because they reach a resolution of 250,000 dpi, in several levels. When observing from various angles, an image with various rasters may be seen, high and low lines, with special stress on selection of details. This is seen when the angle of observation changes horizontally (from left to right) or vertically (moving up and down).

Each hologram element may be given separate rasters. Therefore rasters themselves may have a design role and be carriers of the visual message because they themselves have special forms. The hologram form may become the same as the form of the raster dot in the hologram. It is necessary to design the raster type, frequency, and angle of progress.

6. Hologram application procedures with modified printers

In our research we used a printer, foil (without holograms) and a hologram cliché. The printer burned the foil onto the document and embossed the hologram cliché onto the foil. Thus the foil obtained a high-resolution hologram in the designed spot and only part of the foil was embossed onto the document, the one with the hologram. Non-transparent golden based and silver based foils were used as well as transparent ones. Transparent foils were especially interesting because various graphic designs were printed below the holograms - linear or pixel. Thus each hologram became individualized because a special graphic design/unit matrix number, a human face portrait was planted into its structure. This graphic design was additionally protected with special raster and colors. Some 30 prints per minute were printed with this modified printer. This procedure turned out to be more cost-efficient than buying holographic tape. This procedure allowed changing various holographic clichés, various forms and structures. The same hologram was cut out into various shapes. For instance, the logotype of the sports federation was carried out as a flip-flop hologram, and special clichés of different form were applied onto tickets, diplomas for different sport fields such as soccer, athletics, tennis, swimming, etc. Thus smaller editions of diplomas, certificates, entrance tickets, medals, labels for special occasions proved to be cost-efficient, as well as the additional printing of the same hologram onto various types of material.

7. Holograms in the function of anti-information systems on packaging material

We were confronted with the problem of packaging material design and packaging material hologram design that are implemented into the production line. This was quite a task from the designer's point of view: it was necessary to bring into accordance new graphic and printing protective elements and make a conceptually clear and recognizable graphic design of the product. The larger part of any packaging material surface is reserved for obligatory information, therefore, it was necessary to bring into accordance the legal, designer and safety points of a product's protection.

The basic idea on anti-information systems came due to the large amount of obligatory data and regulations bringing actual damage to the product's advertising and leave little room for a designer's ideas. The goal was to divert the consumer's attention from the obligatory graphic product legal elements onto the product's advertising elements.

The advantage of holograms in this case is in their being noticeable, interesting, of strong color, animated images, and 3D images. Holograms were added to the packaging material in the production line, and this was no additional financial cost in case of million-copy- editions. In such cases the hologram's size does not influence the cost - a hologram may be as large as the space on the packaging material allows it to be. In this respect we design holograms with the producer's logotype and additional elements that carry a direct marketing message. Holograms are applied where the slogan changes into the logotype ... In such cases holograms prove to be an advantage, as an unusually interesting element diverting attention from legally set elements such as - *Bad for one's health*, *Alcohol contents*, and they are also an excellent protection against copying and placing counterfeit contents into packaging material.

Because they allow individualization and larger space for the very hologram, transparent holograms are the ones more and more frequently used for such purposes. Transparent holograms are designed in this respect with strong contrast colors underneath of which pastel colors are applied as a completely contrasting spectrum, or metallic silver colors, or blue ones. Transparent holograms proved to be extraordinary protection for ink jet colors that are not UV and do not fade in daylight. This piece of knowledge allowed us to implement very significant individualization and various special effects, such as moare of transparent hologram and base, or application of hologram over hologram.

The application of holograms on packaging material is very slowly implemented into our market because many consider holograms as an unnecessary luxury. We have succeeded in realizing only 15% of our ideas in the market, and the remaining 85% remained on the level of a project in our headquarters. But the said 15% proved to be a top marketing and protection step forward in the market packaging material design.

8. Commercial hologram individualization

Holograms on packaging material are cut/embossed with the help of clichés of most different forms. There are many examples of cutting out holograms in case the customer does not wish to invest into an original hologram design due to very small editions. In such cases holographic strips are used with commercial slogans such as *Security*, *Authentic Genuine* or *Valid*. These slogans are embossed in a certain cliché - form during hot printing onto a certain document. This type of hologram may not be counterfeited, copied or torn off the document and represents a very noticeable, authentic and safe protective element. The very product gains in value - the psychological one and the material one. In case the very logotype is applicable for such purposes (when it is planographic), excellent effects may be the result. An example: the psychological chamber holograms: Numbering, relevant texts and graphic design were printed onto these same holograms.

9. Marking Hologram Labels on Packaging Material

We have developed software designs for additional printing of numbers on hologram labels aimed at product marking and individualization. Together with the bar code system that is automatically linked with the XML database, the numbered hologram has proved to be an excellent protection for goods entrance and exit. We have designed a special hologram for certain limited editions. Such a viewpoint as to protection and distribution problems gives less room for counterfeiting, and counterfeiters are aware of the fact that the producer is in full control of the market situation.

In this respect we have developed special labels for exterior application, labels with additional printed data, dissolvable labels (they may be used in food product labeling), especially “edible” holograms on hard products (candy with embossed high-resolution clichés, tamper evident labels - labels protected against counterfeiting that are destroyed or leave a mark in the form of a certain message (for instance: opened) if moved from their surface base. We recommend sticking such labels onto places where products are opened.

We have designed a hologram for museum tickets or tickets for fun fairs that produce the words “single use” when torn, and the words “non-refundable” on transportation tickets and financial stamps. The use of tamper evident labels has proved to be excellent for organizing chance games in respect to packaging material. For instance, there is a lucky winner only under one hologram placed on drinking water packaging material.

10. Holography monitoring working groups in Croatia and abroad

In order to apply holographic design onto packaging material in a systematic manner, we organized several groups in our institute: a group for hologram application monitoring with the goal being to encourage and direct mass protection of the very product as well as financial control, the group for original idea implementation with follow-up of a database containing holograms designed in Croatia and abroad, the group for organizing and educating in respect to holography application and product protection techniques. We have taken part in this important struggle in order for hologram application to be systematic and to be treated in an adequate manner.

11. Conclusion

When marking a product there must be a top designer and marketing appearance. A hologram is a unique form for product protection and gives the product additional value as a marketing element. Holograms open many possibilities in developing multi-layer visual messages, messages in motion and a 3D presentation. It is possible to postpress them on packaging material in modified series and forms, for each production series separately. Small editions may be produced with digital printing, reaching top-quality results with modest production expenses. Such small editions are especially suited for: celebrations, business gifts. Even one single copy may be produced for some special occasion.

Certain groups of business entities are ready for the implementation of holography and this means specialization and implementation of holography in general. This paper covers the situation in respect to holography in our country, and makes comparisons with the use of holograms in the world. The report points to the trend of protecting all products with the help of holography, especially food products where holography would be applied even in cases when the packaging material is not only a graphic product. Such products are, for instance: fresh food products. A hologram is an important way to prove that a product is authentic, that it is not genetically modified, and it guarantees that the package contains what is written on the packaging material.

Links related to holography:

Optaglio; www.optaglio.com (Security Holograms, Holographic Products)

Nova Vision; www.novavisioninc.com/index.html (Security Hologram Labels and Stickers)

American Holography; www.americanholography.com (Security Holograms, Holographic Products)

Holoworld; www.holoworld.com (kits and books)

Holoshape; www.holoshape.com (offers film labels which can be affixed to fabric using a heat-activated adhesive. The labels are durable for machine washing)

Impala Industries; www.impalaindustries.com (produces synthetic fabrics in variety of holographic patterns)

Lightvision; www.lightvision.com (special - Edible Candy with Laser Etched Holograms)

Laser Magic; www.laser-magic.com (projected Holographic Images on a large scale)



Activity-based costing of on demand package production

Panu Lahtinen

VTT Information Technology
Metallimiehenkuja 10, P. O. Box 1204
FIN-02044 VTT, Finland
E-mail: panu.lahtinen@vtt.fi

Abstract

This study focuses on product costing of on-demand package production. The objective of the research was to analyse factors affecting the product costs of packaging throughout the predefined part of the supply chain. The objective was to divide the supply chain into activities and to estimate and simulate resource consumption for each activity. Also the aim was to construct more accurate costing model for the packaging production applying the principles of Activity-based costing.

Activity-based costing is especially powerful when combined with practical capacity approach. When practical capacity is used, only the cost of resources actually needed in activities will be included in product costs and the cost of unused capacity can be disclosed separately. Paying attention to the batch-level costs is particularly important in the case of on-demand production because the order sizes are relatively small and products are diverse.

1. Introduction

Production of items and packaging is moving more and more from make-for-stock to make-to-order. This causes a need to develop packaging production and packaging logistics. Demands are also set by other common trends such as shorter delivery times, broader product selections and smaller series to be packed and delivered, such as Internet-based consumer trade. By gaining accurate costing information from the current production processes and supply chain, one could estimate if the cost level, the potential for creating value and the profitability of an alternative method of producing packages are satisfactory. However, if one wants to make strategic and economically more accurate and better decisions, the information coming from internal accounting practices and used for the financial statements and profitability comparisons has to be reliable, relevant and informative.

As already since 1980's business experts have shown that standard costing or traditional budgeted hourly rate (BHR) cost systems have several shortcomings, which reduce their usefulness in today's manufacturing industry. Other costing approach has to be taken. Widely used bookkeeping centred method of cost behaviour determination diminishes the costing accuracy of costing models. If production processes and supply chain cost structures are compared, the resource consumption should be based on process thinking. It means that products consume activities that form processes. And activities consume resources, which means that activities are the primary source of product costs and product costs are based on actual resource consumption.

2. Methods

The analysis of the case products began with mapping out the current processes and activities. That was supported by interviews with production personnel and other people responsible for the production. Interviews were essential for understanding the current production processes and business logic. In different

cases the supply chain was defined so that it would be possible to gain enough information from activities that were included and that would be of interest. In the next stage the main factors affecting resource consumption and behaviour were defined and resource costs were divided according to four-stage activity hierarchy:

- unit-level activities
- batch-level activities
- product-level activities
- facility-level activities

In this research only unit-level, batch-level and product-level activities were considered important because they contain costs that can be allocated directly to individual products. Facility-level costs were left outside in this study because they can only be allocated to products arbitrarily and the cost information was hard to access. Also the costs of marketing and administration were not included in these calculations because relevant data was missing. However, they can account a very high proportion of the total product costs because they are not volume-related costs.

When the basic data collection, analysis and structural model were done cost model building was conducted. The models were built on commercially available Activity-based costing software and data handling and pre-calculation were done using standard spreadsheet application. During the model building the most important product properties that affect resource consumption were defined. And according the principles of Activity-based costing different cost drivers for different resource groups were selected carefully. The throughput rate was considered the essential factor determining resource consumption in different process stages. Also in this stage an analytical approach was used to determine practical capacity levels for different activities. Even though practical capacity is not easy to determine, it would allow the classification of resources to used and unused capacity.



Figure 1: Activity-based cost model measures the cost of resources used for products, services or customers. Practical capacity is defined on the left-hand side of the equation

After cost model building appropriate case products were selected for closer examination and production data collection was started. In order to achieve accuracy of final product costs information gathering is essential. Here three different methods were used to support modelling: educated guess, systematic appraisal, and collection of real process data. The collected data was used to analyse the cost behaviour of selected products and current supply chain that was considered as reference. When enough information and knowledge was gained from the reference line the design of alternative package production models was started. In the first step a study of the technical state of the on-demand production equipment was conducted. In this case digital printing was considered to be the production method suitable for true on-demand package production. For different case products possible solutions were mapped and after closer examination the best solution for on-demand production was selected.

After selecting the right technical solution for on-demand production, the creation of structural model for alternative supply chain was started. Also print trials were carried out to gain information for the preliminary costing and simulation. After technical studies and discussions with production engineers and machine suppliers a framework for on-demand package production was created. Cost models for alternative supply chain structures were built as for the conventional supply chain and production data collection was carried out during pilot runs.

When the cost models for the conventional supply chain and the alternative supply chain structure were establish and analysed separately the final phase included comparative analysis. An analysis of the supply chain cost structure by the most important segment makes it possible to focus efforts to reduce costs and prevent waste at the appropriate process levels.

3. Results and discussion

The model used for describing on-demand production is presented in figure 2. The primary activities are found in the boxes and the part of the supply chain modelled is outlined in the figure. In the model prepress activities are handled through digital prepress workflow, which was also tested in practice. When different activities are combined so that printing, converting, and filling can be done in the same facility, some activities can be eliminated. When digital printing is used for on-demand production these structural changes should lead to cost savings, which compensate for the higher production costs of digital printing.

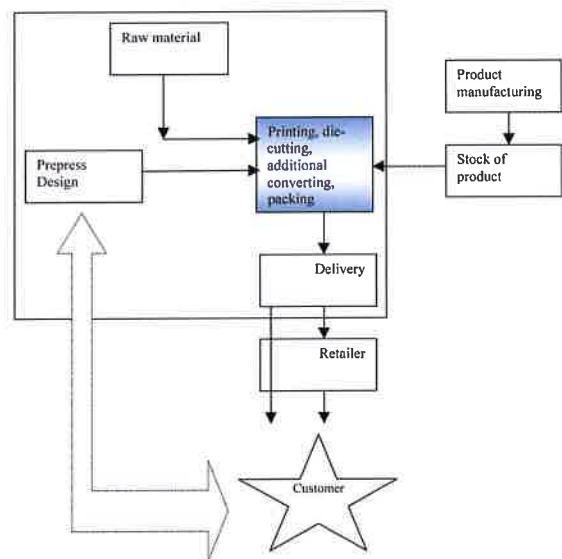


Figure 2:
Schematic illustration of on-demand package production modelled

Simulation results of the cost modelling can be presented as in figure 3. This cumulative cost curve can be constructed to show how different production stages and the consumption of activities lead to product cost accumulation. Figure 3 represents the situation in the conventional supply chain for one case product.

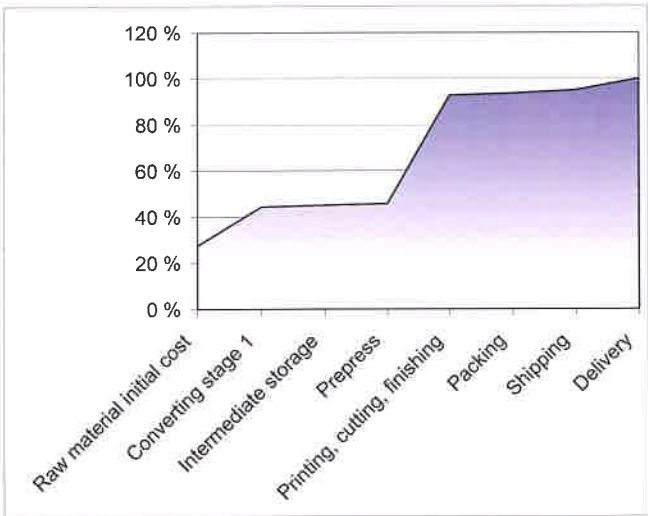


Figure 3:
Cumulative costs of the case product (4 colours + varnish) in conventional supply chain

This is an example of high-volume product. It can be seen that approximately 45% of total costs are coming from resource consumption related to printing, cutting and finishing activities. Substrate cost account for another 30% of total costs.

When more detailed cost classification is desired, different cost items can also be presented in a bar chart. Figure 4 presents the comparison of product cost structure for one case product. In this case two different printing methods have been used for the production of two different order sizes.

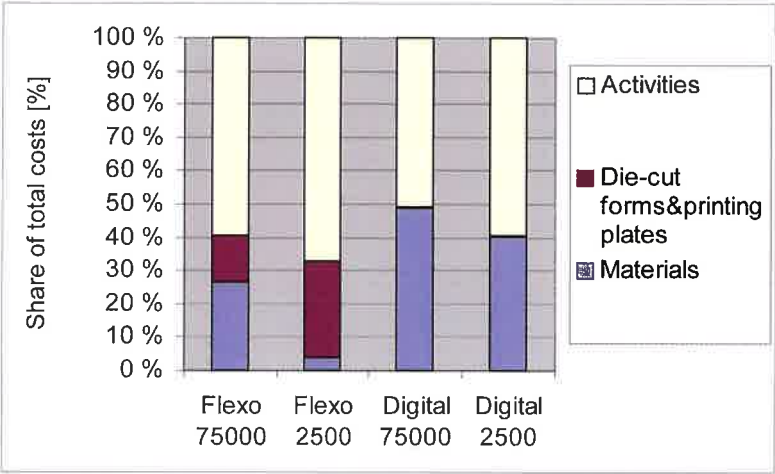


Figure 4: Comparative product cost structure. Modelling has been done for two different order sizes (2500 and 75000) when flexo and digital printing has been used

When conventional printing method is used the share of batch- and product-level costs will increase. Figure 4 shows that material costs account less that 5% of total costs when 2500 pieces have been produced using flexo printing. When the same amount has been produced using digital printing, the share of material costs will increase because of high colour price and lower total costs. As can be seen in figure 4, activity costs become more significant when the order size decreases. Activity costs will be presented more in detail in figures 5-8. In these figures y-axis on the left-hand side is being scaled so that all the figures are comparable. The figures next to the axis present scaled unit costs.

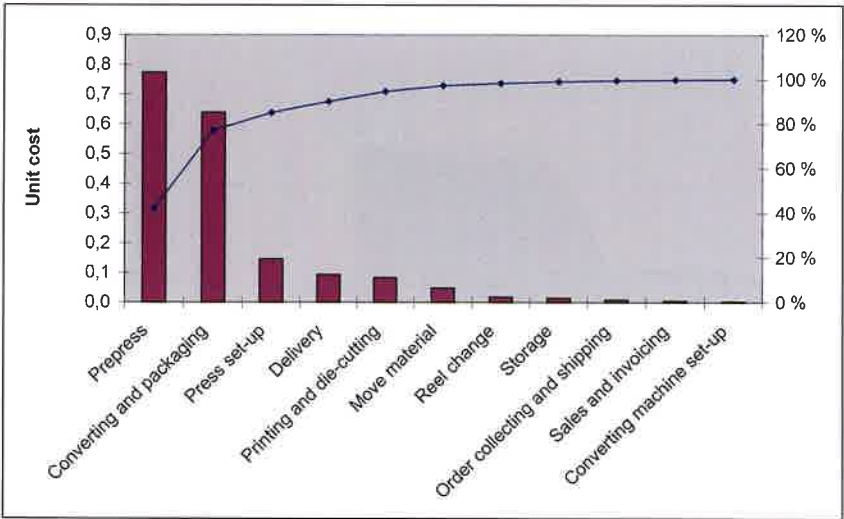


Figure 5: Cumulative activity cost structure when the order size is 75 000 and flexo printing has been used

In Activity-based costing it is very common to notice that 20% of the activities consume 80% of the costs (80/20 rule). That can be seen also in figures 5 and 6 where two most expensive activities consume around 80% of the activity costs. In both cases that is approximately 45% of the total costs.

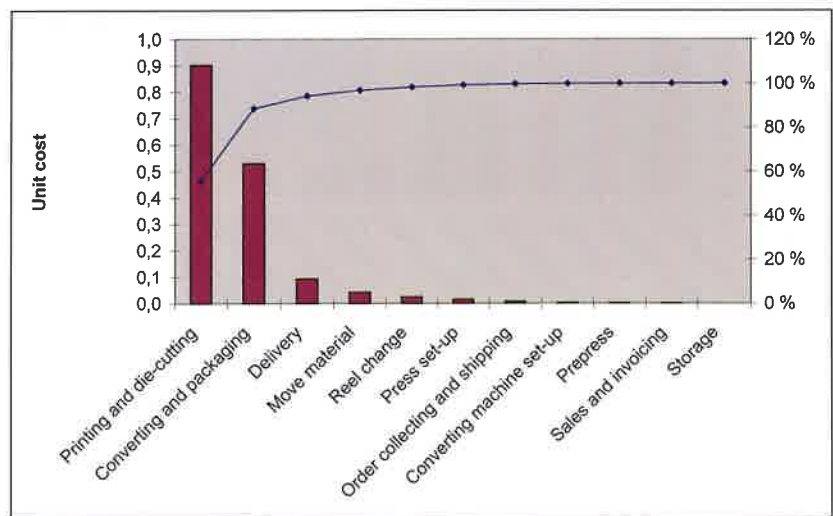


Figure 6: Cumulative activity cost structure when the order size is 75 000 and digital printing has been used

The 80/20 rule is especially common in the production where volumes are high and product costs are dominated by volume related (unit-level) activities. When the order sizes are smaller and product diversity increases, complexity in the supply chain will also increase. That will lead to higher cost structure if process improvements are not carried out accordingly. As can be seen in figures 7 and 8 batch-level activities will have stronger effect on product costs if order size is small. According to the results obtained from cost modelling the 80/20 rule does not apply in on-demand production. E.g. in figure 8 three most expensive activities consume only around 60% of the activity costs.

Also the different nature of conventional (flexo) and digital printing methods can be seen in figures 7 and 8. In figure 7 prepress work and press set-up dominate costs and when volumes increase unit costs decline. When digital printing is used total costs are more stable regardless of volume.

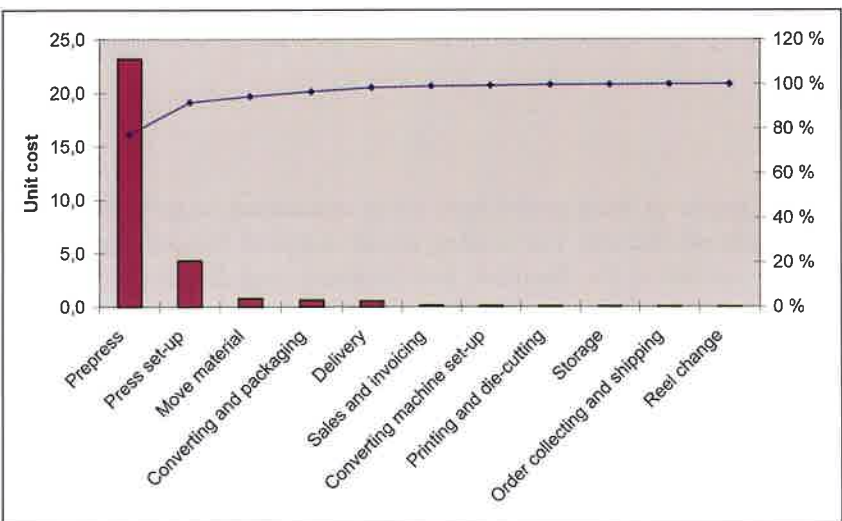


Figure 7: Cumulative activity cost structure when the order size is 2 500 and flexo printing has been used

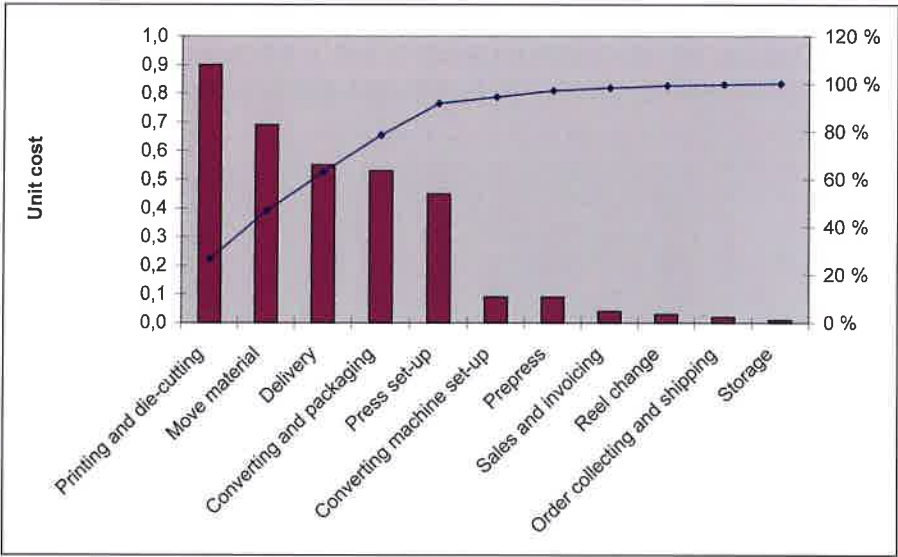


Figure 8: Cumulative activity cost structure when the order size is 2 500 and digital printing has been used

When Activity-based costing has been applied it has resulted in improved costing accuracy compared to traditional costing models. Although Activity-based costing has already been used for several years, only few studies have been published dealing with the percentage changes in product costs between Activity-based costing and Standard costing, which allocate all the overheads as a percentage of direct costs. In the packaging industry this kind of information has not been widely available, but results obtained from paper and IT industry show that the percentage change has normally been between 5-20%.

Also when calculation is done with care activity drivers for each product should be quantified separately. If the same average driver quantity is used for all products in the same product group, the accuracy and usefulness of the results diminishes. However, an accurate cost model requires more work and it is also more complex. If the tools used for calculation and analysis are not easy to use, many companies are not willing to change their costing practices.

For the packaging manufacturers with a large number of customers, who have their special demands and thus need for customising their orders, this kind of accurate cost model is more useful than for companies producing cheap and standardised products for permanent customers.

4. Conclusions

Activity-based costing prove to be a useful tool when evaluating supply chain cost structures and different types of package production. The costing model supplies the activity-based cost information needed to manage the activities for business improvement and for decisions concerning pricing. Activity-based costing is especially powerful when combined with practical capacity approach. When practical capacity is used, only the cost of resources actually needed in activities will be included in product costs and the cost of unused capacity can be disclosed separately.

Also a big difference between Standard costing and Activity-based costing is found in the management of batch-level costs. Standard cost systems based on hourly rate force all expenses to be allocated to the products produced and hence distort the product costs. Paying attention to the batch-level costs is particularly important in the case of on-demand production because the order sizes are relatively small and products are diverse.

5. Literature

- Cooper, R., (1990), *Cost Classification in Unit-Based and Activity-Based Manufacturing Cost Systems*. *J. Cost Manage.* Vol. 4, No 3, p. 5-6
- Cooper, R., (1991), *The design of cost management systems: text, cases, and readings*. Prentice-Hall, Englewood Cliffs, NJ, 580 p
- DeBruine, M. & Sopariwala, P.R., (1996), *The Use of Practical Capacity for Better Management Decisions*. *Emerging Practices in Cost Management*, 1996 Edition. Ed. Brinker, B., J., Publ. Warren, Gotham & Lamont, Boston, MA, p. H2-1-H2-7
- Dilton-Hill, K.G. & Glad, E., (1996), *Managing Capacity*. *Emerging Practices in Cost Management* 5. edition, Ed. Brinker, B., J., Publ. Warren, Gotham & Lamont, Boston, MA, p. H3-1-H3-8
- Fogelholm, J., (1997), *Accurate product costing models for the paper industry (in Finnish)*. *Paper and Timber*, Vol. 79, No 3, p. 164-169
- Fogelholm, J., (2000), *Cost Function Modelling in the Paper Industries*. Helsinki University of Technology, Laboratory of Industrial Management, Report No 11, 102 p
- Fogelholm, J., (1999), *Pricing models for the packaging industry (in Finnish)*. *Pakkaus*, Vol. 34, No 6, p. 42-44
- Kaplan, R.S., (1998), *Cost & effect: using integrated cost systems to drive profitability and performance*. Harvard Business School, Boston, MA, 357 p
- Lawson, R. A., (1996) *Beyond ABC: Process-Based Costing*. *Emerging Practices in Cost Management*, 1996 Edition. Ed. Brinker, B., J., Publ. Warren, Gotham & Lamont, Boston, MA, p. E13-1-E13-11
- O'Brien, K., (2002), *Less complaining and more changing, please*. *American Printer*, Vol. 229, No 5, p. 8
- Roztock, N. & Needy, K.L., (1998), *An Integrated Activity-Based Costing And Economic Value Added System As An Engineering Management Tool For Manufacturers*. 1998 ASEM National Conference Proceedings, Virginia Beach, October 1-3, 1998, p. 77-84





7

Current topics



Environmental data on gravure and offset printing

Maria Enroth¹, Martin Johansson²

¹STFI-Packforsk (Pulp, Paper, Print and Packaging Research) and

Media Technology and Graphic Arts, Royal Institute of Technology (KTH)

²STFI-Packforsk (Pulp, Paper, Print and Packaging Research)

STFI-Packforsk

Box 5604, SE-114 86 Stockholm, SWEDEN

E-mail: maria.enroth@stfi.se

Abstract

The paper presents environmental data relating to gravure and offset printing. The paper focuses on the printing steps in the production chain of publication printed products. The other steps in the life cycle of printed products have also been studied, but they are not the subjects of this paper.

The study is based on case studies where almost twenty gravure printers and ten offset printers spread over Europe and the United States have been involved.

The general, significant environmental aspects of publication printed products have been identified as the following; use of paper, use of energy, consumption (loss) of volatile organic compounds (VOC) including toluene, hazardous waste and environmental management. Transport has also been identified as a significant environmental aspect for printed products but its magnitude depends to a great extent on the specific product. The data collected from printers in different parts of the world are compared with environmental data representing offset printers in Sweden, which are mainly taken from coldset printers.

The paper presents significant environmental data for a fairly large number of companies representing a considerable part of the printing capacity not only in Europe but also worldwide. These data can provide guidance for both printers and buyers of printed products working to achieve continual improvements and striving towards more environmentally adapted printed products. To some extent, the data can also be used as reference values, since there are few compilations of data providing a general coverage of printers in different parts of the world.

1. Introduction

In order to develop their products from an environmental point of view, companies have to work on the approach of supply chain management. This approach is very important when the main environmental aspects of the product can be identified in parts of the product life cycle that cannot be directly influenced by the company itself.

In the case of printed products, environmental studies including life cycle studies show that the production steps including material and resource usage, the production of pulp and paper, printing and transport are of great importance for the total environmental impact of the products throughout their life cycle. The major impact, at least for some typical printed products, has been identified as arising from the use of paper, although neither the printing process with its use of non-renewable and hazardous materials nor transport can be neglected (Axel Springer Verlag, 1998; Drivsholm, 1997; Enroth 2001; Enroth 2003a; Johansson, 2002; Larsen, 2004). The user phase of the products is, in the case of printed products, not of great importance, which is of course different from those products, which are energy - or fuel - demanding during use. The phases of waste treatment, recovery and the reuse of materials in

relation to printed products have not yet been covered comprehensively in life cycle studies. Most life cycle studies performed so far describe offset printed products.

The main environmental impacts of the gravure process, apart from the general environmental impact of the product chain of printed products, have been reported to be the emissions of chemicals and metal particles from the cylinder-making with engraving and copper and chromium plating and the emissions of VOC from the printing ink (Fleck, 1999; Silfverberg, 1998). The emissions from cylinder-making end up as hazardous waste, generated mostly in the treatment facilities for effluents to water. In the offset process, the main environmental issues, apart from the general concerns of printed products, are often said to be the emissions of VOC from alcohol in the fountain solution and solvent-based cleaning agents and inks (Fleck, 1999; Silfverberg, 1998).

2. Methods

The study is based on case studies where publication printed products are described from an environmental point of view. The study is part of an extensive work embracing all the different production steps of printed products. The overall aim of the work is to strive for a reduction in the environmental impact of printed products and for the use of resources as efficiently as possible in a sustainable manner. This paper comprises the part of the work that deals with the printing processes in the production chain. The study involves approximately twenty gravure printers and ten offset printers spread over Europe and the United States.

By sending questionnaires to suppliers involved in the production of printed products and through literature studies, the significant environmental aspects of each specific supplier group were identified. In addition, indicators reflecting the environmental aspects have been defined and quantified where possible.

Each supplier group has received its specific questionnaires, covering the years 2000 and 2002. The first questionnaires, for the year 2000, were very extensive and had the character of providing the basis for an environmental review. Together with literature studies, the answers to these extensive questionnaires were used to identify the significant environmental aspects of the specific supplier groups. The second questionnaire for the various supplier groups for the year 2002 reflected mainly the parameters relevant to the identified environmental aspects. All the questionnaires asked for both qualitative and quantitative information.

When the printers were asked for environmental data related to the production of printed products, we asked for data representing the whole yearly production. Although product specific data would in principle be more relevant, we have taken into account practical aspects in order to make the inventory process at each printer reasonable.

The collected data have been analysed, compiled and reported back to the printers in order to verify the data. To make it possible to compare the quantifiable environmental data between different years and also, to some extent, between different printing companies, we have considered the environmental data in relation to the annual production of the companies, in metric tonnes. The annual production has been defined as “Consumed quantity of printing paper minus Paper waste”. (For the definition of Paper waste, see *Table I*.)

The indicators describing the significant environmental impacts that it has been possible to quantify are defined in *Table I*.

The updated model of industry specific environmental indicators for the graphic arts industry is mainly applicable to companies printing with offset. Collected data and calculated mean and median values in this study are industry specific for the Newspaper companies.

Table 1: Definitions of quantifiable environmental indicators for gravure and offset printing. The indicators reflect general significant environmental aspects of the two printing methods

Environmental indicator	Unit	Definition Gravure printing	Definition Offset printing
Use of paper	tonne/year	All paper used for the production. Data are balanced with regard to storage.	See Gravure printing.
Paper waste	tonne/year tonne/tonne product	All paper rejected in connection with printing and finishing, e.g., paper wrapping, paper used for adjusting the press, waste from cutting, etc.	See Gravure printing.
Use of energy	kWh/tonne product	The use of energy, process energy (i.e. the use of energy by presses, dryers and toluene-recycling units) and energy used for heating the print shop. All types of energy are added together.	~The use of energy, process energy (i.e. the use of energy by presses and gas for heatset drying) and energy used for heating the print shop. All types of energy are added together.
Consumption (loss) of volatile organic compounds (VOC) including toluene	kg/tonne product	The amount of toluene is calculated as the amount purchased toluene (in ink, etc) minus sold recovered toluene minus the amount of toluene in ink and rags sent for destruction. (Data are balanced with regard to storage.)This calculation gives the emission of toluene after passing adsorbers, the emission of toluene via the general ventilation system (not led via a recovery unit) and the loss of toluene with the product.	Volatile organic compounds (VOC) are organic compounds that at a temperature of 20°C (293.15K) have a vapour pressure of at least 0.01 kPa (according to EU Directive 1999/13/EG).The amount of VOC is calculated as purchased quantity, balanced with regard to stock keeping minus the amount of VOC destroyed in the heatset dryer.
Hazardous waste	kg/tonne product	The waste fractions that are handled as hazardous waste in any specific company. Excludes electronic waste.	See Gravure printing.

3. Results

This paper focuses on the printing steps in the production chain of publication printed products. The other steps in the life cycle of the printed products have also been studied, but they are not the subjects of this paper. The paper presents environmental data for gravure and offset printing.

We have been able to obtain data from fourteen gravure printers for the year 2000 and from nineteen gravure printers for year 2002. Corresponding figures for offset are eight printers for the year 2000 and nine printers for the year 2002. All the offset printers studied use traditional offset with a fountain solution and most of them have a heatset dryer, i.e. a forced drying process.

The average production at the gravure printers studied was 160,000 tonnes/year in 2000 and 140,000 tonnes/year in 2002. Of the nineteen gravure printers in 2002, thirteen were situated in different parts of Europe and six in the United States. The overall publication gravure print capacity in Europe expressed as actual paper consumption per annum was calculated to be 5,900,000 tonnes/year in 2002 (ERA 2004). The companies studied in Europe in 2002 represented a total production of 1,900,000 tonnes/year in 2002, which corresponded to 32% of the actual print capacity in Europe.

The average production at the offset printers studied was 25,000 tonnes/year in 2000 and 54,000 tonnes/year in 2002. Of the nine offset printers in 2002, seven were situated in different parts of Europe and two in the United States. The overall offset print capacity, excluding the coldset offset print capacity, in Europe expressed as actual paper consumption per annum was estimated to be 20,000,000 tonnes/year

in 2002 based on data published by CEPI (Confederation of European Paper Industries) and Intergraf (Intergraf, 2003). The companies studied in Europe in 2002 represented a total production of 320,000 tonnes/year in 2002, which approximately corresponded to 2% of the actual print capacity in Europe.

The significant environmental aspects of publication printed products have been identified as the following; the use of paper, the use of energy, the consumption (loss) of volatile organic compounds (VOC) including toluene, and hazardous waste. Transport and environmental management have also been identified as significant environmental aspects for printing activities. Data for all the identified significant environmental aspects with the exception of transport are presented in this paper.

Using the defined indicators, the main environmental impacts from both gravure and offset printed publication products have been illustrated.

The data describe the average situation in 2000 and in 2002 for the significant environmental aspects identified. For 2002, the range of values among the different companies is also illustrated.

The indicator Paper waste has been used to illustrate the use of paper. This is shown in *Figure 1* for gravure printers and in *Figure 2* for offset printers.

For gravure printers, the range of values in 2002 was 0.044-0.19 tonne/tonne product. There is a 77% difference between the maximum and minimum values. The range of values was about the same in both years. The mean value is fairly stable, which indicates that the companies are well aware of this parameter. However, the different companies seem to handle these figures in different ways. The mean paper waste value in 2002 was 0.13 tonne/tonne product or 12% (paper waste in relation to the total amount of paper used). For offset printers, the range of values for 2002 was 0.02-0.37 tonne/tonne product, where the lowest value was unrealistic low. The mean paper waste value in 2002 was 0.21 tonne/tonne product or 17% (paper waste in relation to the total amount of paper used).

The mean values are comparable to the data from fourteen coldset offset printers (newspaper printers) in Sweden; 0.14 tonne/tonne product or 12% (paper waste in relation to the total amount of paper used) and five commercial offset printers in Sweden; 0.25 tonne/tonne product or 20% (paper waste in relation to the total amount of paper used). The commercial offset printers are comparatively small companies with small print runs (Enroth, 2003a).

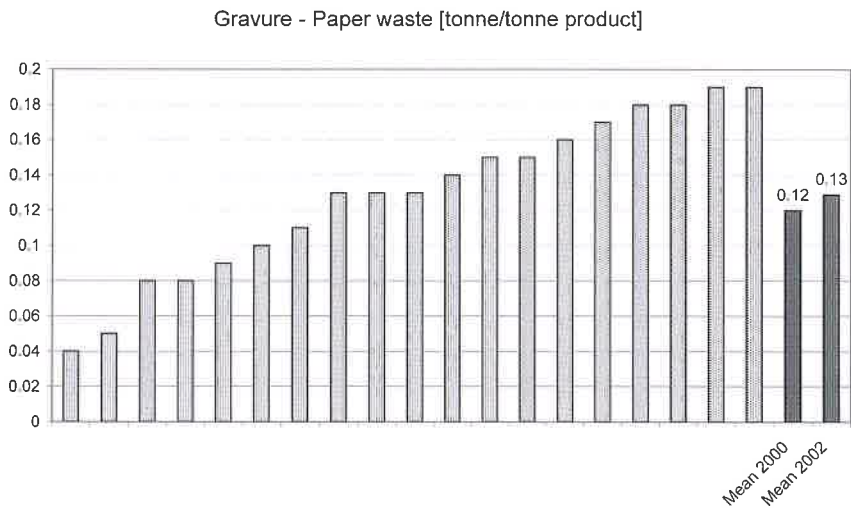


Figure 1: Paper waste in tonne/tonne product for 19 gravure printers during 2002. The mean values for both 2000 (14 companies) and 2002 (19 companies) are shown in the diagram

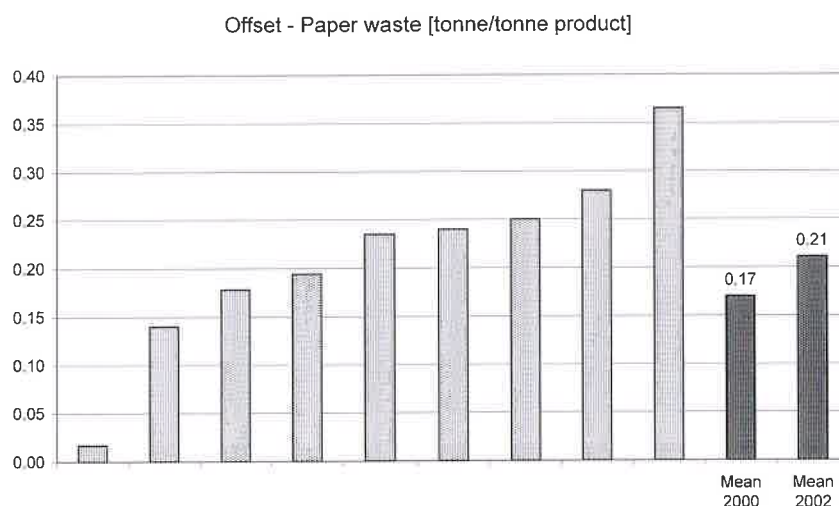


Figure 2: Paper waste in tonne/tonne product for 9 offset printers during 2002. The mean values for both 2000 (8 companies) and 2002 (9 companies) are shown in the diagram

The indicator Use of energy is shown in Figure 3 for gravure printers and in Figure 4 for offset printers. For gravure printers, the range of values in 2002 was 210-1900 kWh/tonne product. There is an 89% difference between the maximum and minimum values. The range of values was about the same in both years. The individual values have converged since the year 2000 which indicates that the companies are slowly achieving a common way of handling energy data. This process has led to an increase in the mean value from 590 to 890 kWh/tonne product. For offset printers, the range of values in 2002 was 140-1000 kWh/tonne product. There is an 86% difference between the maximum and minimum values. Except for one company, the individual values have converged since the year 2000, which indicates that the companies are slowly achieving a more common way of handling energy data. The mean value has been stable and was 610 kWh/tonne product in 2002.

The mean values can be compared to data from fourteen coldset offset printers (newspaper printers) in Sweden; 730 kWh/tonne product, and five commercial offset printers in Sweden; 1400 kWh/tonne product (Enroth, 2003a).

The indicator Consumption (loss) of volatile organic compounds (VOC) is shown in Figure 5 for gravure printers and in Figure 6 for offset printers. For the gravure printers, VOC are measured as toluene.

For gravure printers, the range of values in 2002 was 0.003-6.4 kg/tonne product, which is an immense spread and indicates that the different companies handle figures describing the balance of toluene in different ways. The mean value in 2002 was 1.9 kg/tonne product. The mean value was fairly stable between the two years studied.

For offset printers, the range of values in 2002 was 0.05-6.4 kg/tonne product. The mean value based on eight companies (one is missing) was 3.0 kg/tonne product in 2002. No mean value for 2000 is available. For most of the companies, products such as alcohol in fountain solution and cleaning agents can contribute to the emission of VOC. Two of the nine offset companies in 2002 used no alcohol in the fountain solution.

No corresponding data to compare the values for the loss of toluene from gravure printing have been found. The values for offset printing can be compared with data from fourteen coldset offset printers (newspaper printers) in Sweden; 0.34 kg/tonne product (Enroth, 2003a) and the mean value of 3.8 kg/tonne product representing five commercial offset printers in Sweden (Enroth, 2003b). These companies, the newspaper printers in particular, work actively on the substitution of products to reduce their VOC emissions.

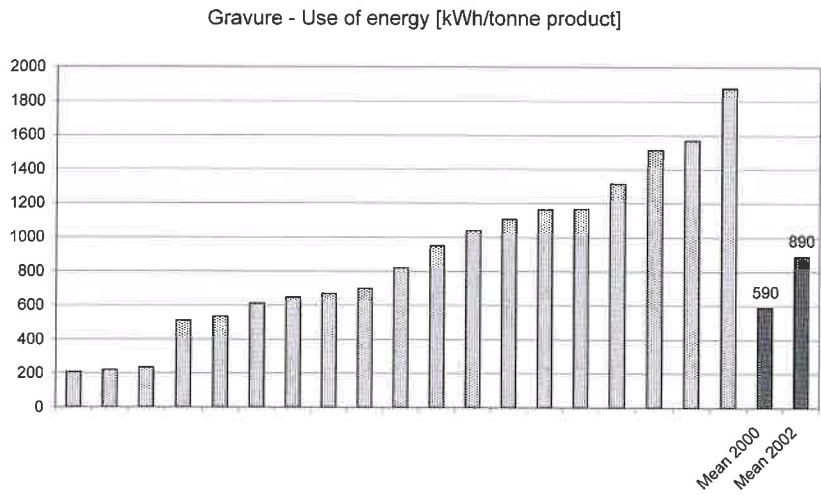


Figure 3:
Use of energy in kWh/tonne product for 19 gravure printers during 2002. The mean values for both 2000 (14 companies) and 2002 (19 companies) are given in the diagram

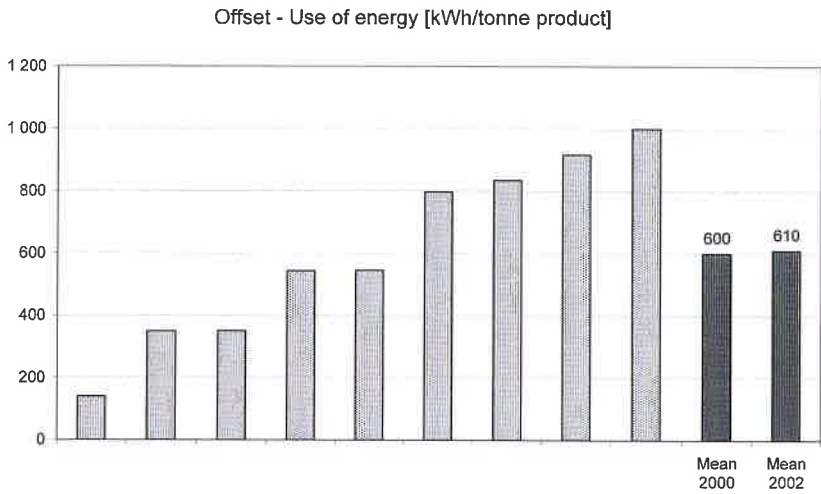


Figure 4:
Use of energy in kWh/tonne product for 9 offset printers during 2002. The mean values for both 2000 (8 companies) and 2002 (9 companies) are given in the diagram

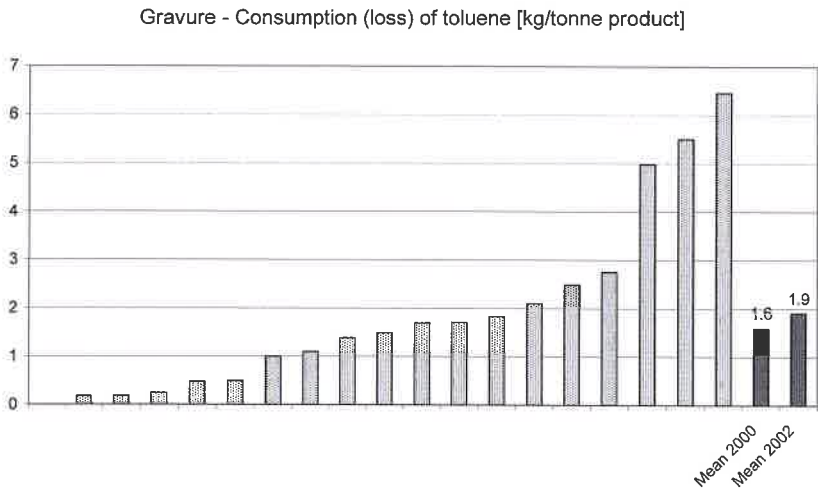


Figure 5:
The consumption (loss) of toluene in kg/tonne for 19 gravure printers during 2002. The mean values for both 2000 (14 companies) and 2002 (19 companies) are given in the diagram

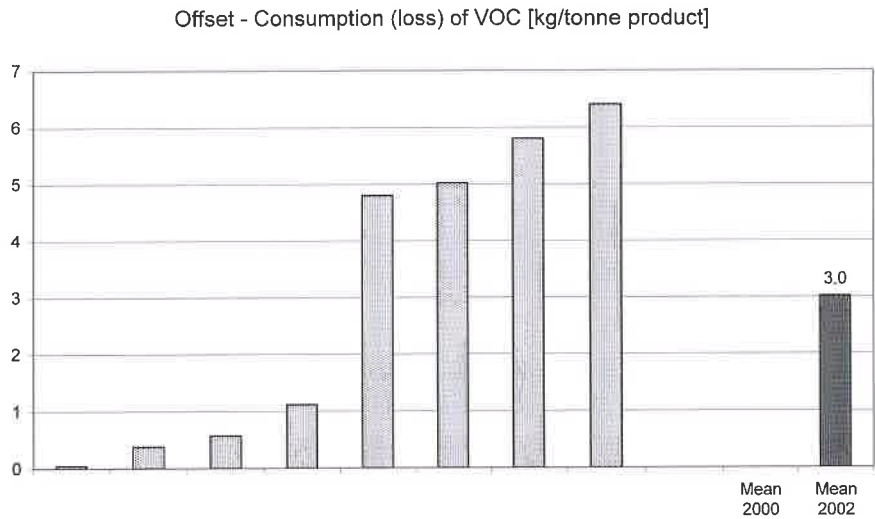


Figure 6: The consumption (loss) of volatile organic compounds (VOC) in kg/tonne product for 8 offset printers (one missing) during 2002. The mean value for 2000 is missing.
The mean value for 2002 (8 companies) is given in the diagram

The indicator Hazardous waste is shown in Figure 7 for gravure printers and in Figure 8 for offset printers. Waste fractions handled as hazardous waste have, for example, been metal hydroxide sludge, sewage concentrates, used and contaminated solvents/ink/oil.

For gravure printers, the range of values in 2002 was 0.26-3.0 kg/tonne product. The mean value was 1.1 kg/tonne product in 2002 and is missing for the year of 2000. The definition of hazardous waste is different in different parts of the world, and this makes it difficult to relate the values to each other. High values can have many causes e.g., strict legislation in the actual country with many types of waste fractions classified as hazardous, a high level of consciousness and well quantified waste fractions at a company, and insufficient work with waste handling.

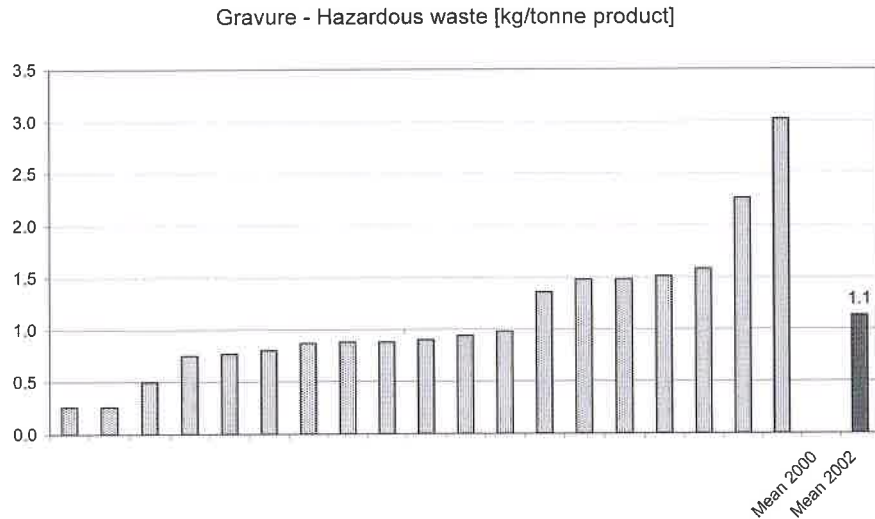


Figure 7: Hazardous waste in kg/tonne product for 19 gravure printers during 2002. The mean value for 2002 (19 companies) is shown in the diagram. The mean value for 2000 is missing

No corresponding data have been found to enable the values on hazardous waste generated from gravure printing to be compared. The values for offset printing can be compared with data from fourteen coldset offset printers (newspaper printers) in Sweden; 4.6 kg/tonne product (Enroth, 2003a) and the mean value 15 kg/tonne product representing five commercial offset printers in Sweden (Enroth, 2003b).

Environmental management

In 2002, six of the nineteen studied gravure printers (32%) and four of the nine studied offset printers (44%) had a certified environmental management system. The management systems were certified according to either ISO 14001 (International Standardization Organization) or EMAS (the European Management and Audit Scheme).

For offset printers, the range of values in 2002 was 0.08-17 kg/tonne product, which is an immense spread. The mean value in 2002 was 3.5 kg/tonne product. A preliminary mean value was 2.1 kg/tonne product for 2000.

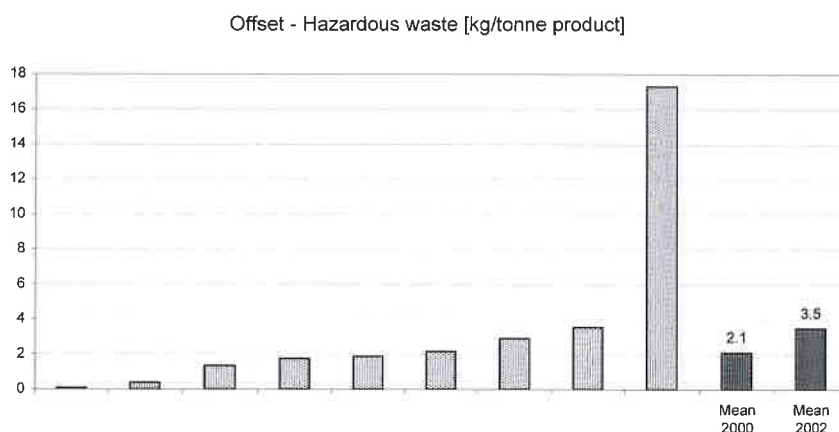


Figure 8: Hazardous waste in kg/tonne product for 9 offset printers during 2002. The mean values for both 2000 (8 companies) and 2002 (9 companies) are shown in the diagram

4. Discussion

The identification of significant environmental aspects and corresponding environmental indicators is based mainly on aspects which have been shown to be important from an environmental point of view. Other important prerequisites have been that the indicators should not be too many, they should be measurable and they should also preferably be quantifiable in a manner which is reasonable for the companies. The chosen indicators could also be used for both gravure and offset printing, and this was seen to be advantageous for the study.

We have chosen to present data for significant environmental aspects that are general for publication printed products, which means that data for transport are not presented in this paper. The environmental impact of transport related to printed products depends greatly on the location of the various facilities used in the whole product chain and on the type of product, including the manner of distribution to the readers.

The range of values among different companies is wide for all the studied indicators. This has probably many explanations. From the development between the years 2000 and 2002, we can see a tendency for the data to converge among the companies, which is probably an effect of starting to use the same definitions of indicators and of measuring and calculating in a similar way.

As a consequence of this learning process for all the parties involved, the mean values for the different indicators have had a tendency to increase, which is a phenomenon that has been reported before (Enroth, 2003b).

The differences between gravure and offset printers in the indicator Paper waste, with a higher average value for offset printers, can be explained by the fact that offset printers generally print smaller editions than gravure printers. A similar situation has been reported in previous studies where values from newspaper printers have been related to values from comparatively small commercial printers.

This study comprises companies with different prerequisites such as for example different legislation, different printing capacities, different experiences from environmental work and different experiences of quantifying the environmental impact from printed products. Generally data on e.g., volatile organic compounds (including toluene) and hazardous waste are uncertain, due to the different legislation in different countries and to the different handling procedures within specific companies. This is indicated by a wide scatter of values.

5. Conclusions

The paper presents data for significant environmental aspects in a fairly large amount of companies representing a considerable part of the printing capacity not only in Europe but also worldwide. Among other things, the study shows that the paper waste has been 0.13 tonne/tonne product for gravure printers and about 0.2 tonne/tonne product for offset printers. The use of energy has varied around 900 kWh/tonne product for gravure printers and 600 kWh/tonne product for offset printers.

The data presented can be used as guidance for both printers and buyers of printed products who are striving for continual improvements towards more environmentally adapted printed products. To some extent, the data can also be used as reference values since there are few general compilations of data covering many printers in different parts of the world.

Acknowledgements

The authors would like to thank Inter IKEA Systems B.V. Catalogue Procurement and especially Ingemar Stedt and Lars Carlson for making this study possible and for a most challenging co-operation.

The authors would also like to thank all the companies involved in the case studies for their time and for the valuable information provided.

Among the companies participating in the study were Broschek Rollenoffset, Frank-Druck, Gruner+Jahr, Mondadori Printing, Ruter Media Group and Tiefdruck Schwann-Bagel.

Literature

- Axel Springer Verlag, Stora, Canfor, Infrac (1998), *LCA Graphic Paper and Print Products*
- Drivsholm, T., et al. (1997), *Miljøeffekter og ressourceforbrug for 3 grafiske produkter i et livscyklusperspektiv*, Miljøprojekt nr 341, Miljø- och Energiministeriet. Miljøstyrelsen
- Enroth, M., (2001), *Tools for Eco-efficiency in the Printing Industry*, Licentiate Thesis, Royal Institute of Technology (KTH), Stockholm, TRITA-NA-0142
- Enroth, M., M. Johansson, Å. Moberg, (2003a), *Environmental indicators in the newspaper industry*, *Advances in Printing Science and Technology*, *Proceedings of the 30th International Icarigai Research Conference*, Dubrovnik September 2003, Conference edition, ISBN 953-96276-6-4, Acta Graphica Publishers, pp. 237-248

- Enroth, M., Å. Moberg, M. Johansson (2003b), *Miljönyckeltal för tidningsföretag - utveckling av en branschgemensam databas*. STFI Report, PUB 15, December 2003
- ERA (2004), *Publication gravure printing/Market situation in Europe*, European Rotogravure Association, www.era.eu.org. 21st of June 2004
- Fleck, W., et al. (1999), *Printing and the Environment, Guidance on Best Available Techniques (BAT) in Printing Industries*, Intergraf/EGF
- Intergraf (2003), *The Evolution of the Graphic Industry, Period 1999-2002, Multilingual Statistical Report (English-French-German)*, www.intergraf.org
- Johansson, M. (2002), *Livscykelanalys av arkoffsettryckning. Jämförande analys av vattenfri och konventionell offsettryckning samt computer-to-plate och konventionell prepress*. Framkom Rapport 2002:09
- Larsen, H.F., M.S. Hansen, M. Hauschild (2004), *Ecolabelling of printed matter. Part II: Life cycle assessment of model sheet fed offset printed matter*. Ministry of Environment and Energy, Denmark, Danish Environmental Protection Agency, To be published
- Silfverberg, E., et al (1998), *Best available techniques (BAT) for the printing industry*, Nordic Council of Ministers. Tema Nord 1998:593

Printing process simulation based on data for standards taken from actual production

Vilko Žiljak, Klaudio Pap, Zoran Nježić, Ivana Žiljak

Faculty of Graphic Arts, University of Zagreb
Getaldiceva 2, HR-10000 Zagreb, Croatia
E-mail: vilko.ziljak@zg.htnet.hr

Abstract

The paper shows the created tools that enable a description of virtual printing machines with all the belonging parameters and material necessary for the printing process. Real-life characteristics are built into the virtual machines and the measured time periods for individual machines in the printing process. Thus the cost-efficiency order of each machine for certain types of jobs was obtained, and the digital job order system was determined.

The results obtained are the ones improving and raising production planning and control on a higher level, as well as allowing additional building-in of JDF. The set goal is to create as many production situations as possible, archive the gained results into databases, aiming at getting a complete computer science description of graphic production units and situations.

Keyword

Estimation, Normative provisions, Printing, Simulations, XML

1. Introduction

Computer simulation of printing processes enables the research and study of the smallest workflow structures and interconnected dependencies of multi-linked variables from prepress to postpress. A field is created with an enormous number of possible solutions for preset jobs with instructions on the best choices for a certain printing works and for the given types of business management. Computer simulation means carrying out many experiments in the environment that is close to what we might consider as the best solution. It is possible to make many different versions if data generators are prepared in advance in order to initiate carrying out new experiments with algorithms. Only a base of initial data describing certain variables or algorithm data generating enables multiple simulation experiments. The actual questions might be: test a continuous edition of 10 to 50 thousand copies, for Poliman or Litoman machines, for pages from ... to ..., etc. regardless of the data from the concrete offer request. Many variables are given in the graphic product description comprising: printing machines for the given printing works, manpower, material, time period necessary for the completion of certain phases - all in differently defined value ranges. The “graphic space” for possible initiators of printing process simulation experiments may be through norm regulation tables or mathematically with the help of related algorithms. Simulation processes are based on printing press norms and take place twice. The first simulations are in the part where answers are given in respect to the client's offer request. This is the part where the situation in the graphic production market is taken into account, as well as the competition, and the monopoly over the product. The second phase of simulation takes place after the job is granted, i.e. after the order has been placed. Both of these simulations systems are based on production norm data, but with different goals. The working out of concrete estimates for the first as well as the second phase is vital for the printing organization administration. Computers and new programs for estimating “good production” enable the simulation of a great number of combinations and automatic

search for quality situations that becoming better and better. New production paths are the goal of simulation as well as stepping away from standard behavior in making decisions that are characteristic for printing business calculation specialists.

2. Defining production entity norms

The necessity to implement digital job orders and to monitor the production process requires a detail and complete graphic production plant description. Computer science description requires real and actual values that have been acquired on basis of measuring and testing certain units. This paper describes the tools that enable norm setting and storing individual machine parameters in databases. Through XML a relation and data visualization have been determined between: the database - the user - the digital job order. Solutions are given for organizing and using of the relative and native databases with the goal being to have a final and complete operating cycle simulation. Thus a new approach to production planning is given including the following: prepress, press and postpress.

The basic condition is to provide a systematic approach to norm setting for all the elements that are part of the graphic production. It has been determined that the defining of graphic postpress requires the most thorough and most complex computer science descriptions of machines because each machine is specific in its own way in respect to the functions it performs. Description of certain postpress machines requires the setting of a functional dependence of parameters that are specific for that certain machine. There are several hundred different types of machines used in postpress. The norm setting system is based on the measured periods of time that are defined by the influence of various types of material used, edition quantity and the respective prepress prices and prices for machine/per hour use.

A database construction is based on the belonging tables definition for each single postpress machine. The database contains values needed for initial calculations and production control. These are numerical and concrete machine production norms. From each table there is an XML description created for each machine separately, with defined and described specific characteristics. On basis of given schemes it is possible to alter norm values, and to reach them. The estimated values are stored in temporary DOMs (Document Object Model) in which they “travel” for further production activities. If there is necessity, it is possible to save these values as well, not on the norm level however, but on the level of production control. Thus the link in respect to organization, production control and postpress production control level is defined.

A system describing individual graphic products is proposed for the process of setting norms for the prepress production. The descriptive parameters define the graphic design, page-break, scanning, and specific accessory jobs. The price and belonging time period are linked to each of these parameters. The categorization of norm descriptive parameters that are subject to adaptation in respect to certain prepress plants is proposed in the database.

Norm setting for the printing process includes the definition of parameters describing individual printing machines. A system is proposed that stores parameters such as the number of colors, preparation time, machine price, speed and format into the database. A model is also proposed that includes linking the printing machine with the printing material. Thus it will be possible to make calculations that are also the elements for digital job orders.

3. Virtual printing production supported by simulation methods

By defining prepress, press and postpress norms, the area for simulating a virtual printing works is determined. It is necessary to determine the maximum production capacity of individual plants, and at

what points it is necessary to engage outside printing works. Furthermore, it is possible to plan and design virtual production equipment that would be realized only in the future. This enables simulation with norm values that had been previously stored in the databases.

With the described approach we are entering an area where it is possible to open new work posts in planning and organizing graphic production, and improving and expanding the complete level of knowledge and skill. The purpose of doing simulation is evident in several large segments, namely: firstly in determining optimal workflows preceding the start-up of printing, secondly - in determining the production bottlenecks, thirdly - in investment planning, and fourthly by simulators enabling the experience of physical printing and postpress control without having any material costs. Thus it is possible to make the best solutions for certain production situations, and to have remote control of production flows.

Due to the major share of the electronic and computer parts in the digital machine value, as well as to the speedy development of electronics on the other hand, it is evident that this modern production equipment will be altered in a rather small space of time to follow. These alterations will be the reason to implement new skills and knowledge, new organization and new parameters in order to optimize the production. It is possible to implement successfully new education, new training, and new optimizing by the mere use of simulators and simulation programs on computers that we have in everyday use. Thus it will be possible to determine at once the reason of discrepancies in respect to determined values by inspection of the proposed simulated environment. With the help of simulation it is possible to design various production versions in several different printing editions. The accumulated experience in simulation and application of this method in the graphic production is evident and shown during operation.

4. Normative structure description linked with newspaper production table description

The whole model has been developed on related base norms where all operations are described as well as the graphic production recourses. Information forming the graphic production norm structure was stored in two ways. The first was by using the related database as the main information storage. We used the Microsoft SQLServer related base together with the SQLXML module. The second way was storing data in a pure XML record. The decision what to store into the usual related base records and what to store into the XML element and attribute structure depended on the requirements and the manner in which data was used. For fast query over the keys, in respect to large amounts of data, variable keys were placed into separate related base fields. Variables for calculation processes used by the application, and data that was not used for extensive research were stored inside the XML technology. It has been made possible to alter norm data during time periods. This is possible by using the advantages of related data base technologies and XML technology. They do not exclude each other but complement one another.

An XML interface was made over the related base through XMLSchema where the desired communication dictionary not equal to the names and definitions in the related database tables was determined. Thus the heterogeneous written norms were changed into an XML record over which program modules were built for processing production nodes. The XMLSchema enabled us to determine the XML document view, making the links with the related database tables and fields as well as determining related relations on the level of XML elements and attributes. This manner of realization enabled all transactions to be in the form of XML records regardless of the data source: related base tables or self-standing XML record. Figure 1 shows the norm structure of a printing production.

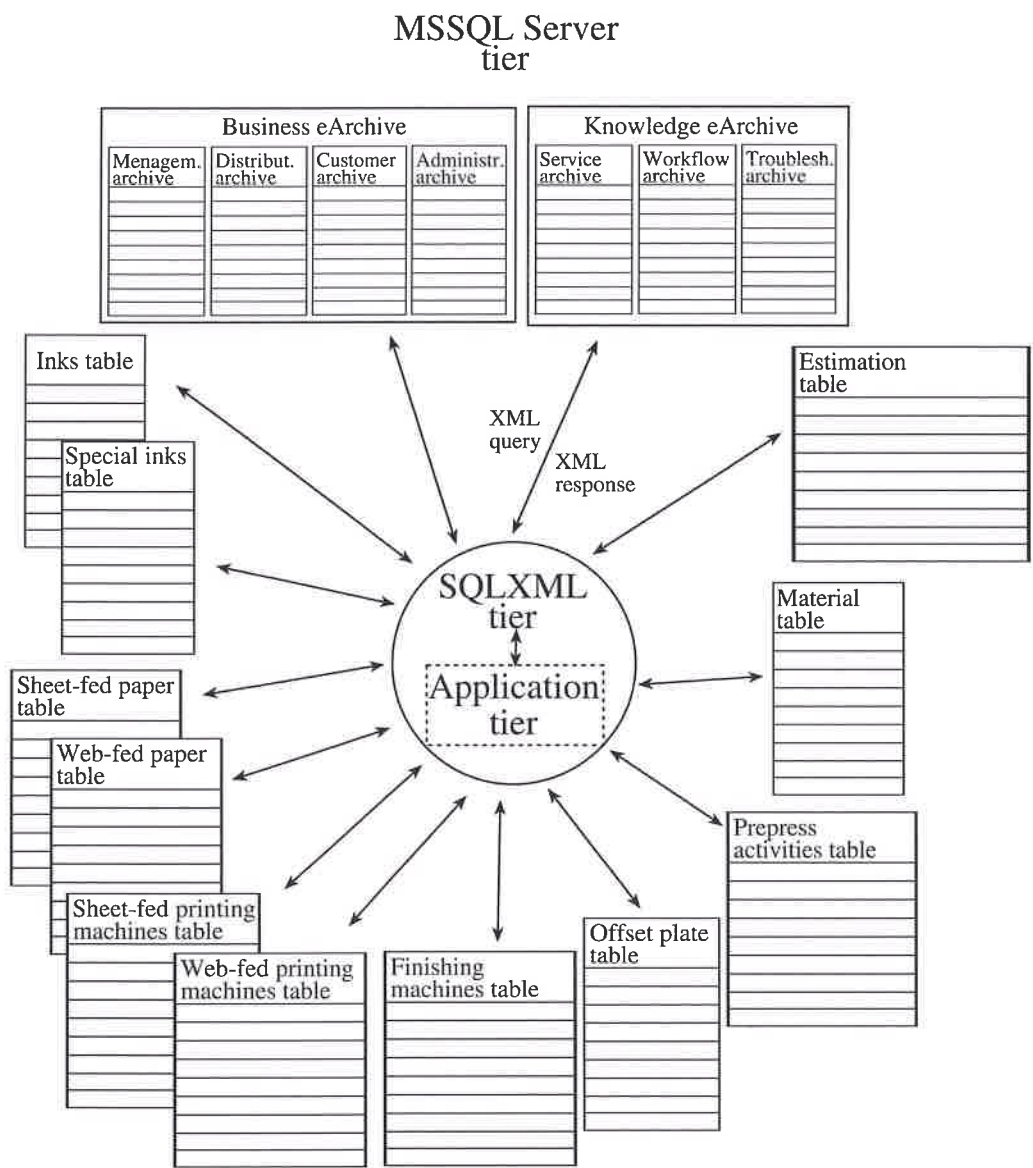


Figure 1

5. Experimental testing of the virtual edition

Simulation was performed in respect to a review magazine in such a manner that besides the number of printed copies, the edition scope was also taken into account and printing was performed on virtual equipment on sheets and rolls. The results are seen in the profitability order sequence of the machines that are part of the individual graphic production equipment in respect to individual jobs.

In the role printing experiment the virtual magazine review issue had 16, 32, 48, 64, 72, 86 and 112 pages. Lythoman and Polyman virtual rotation machines had been created for the experiment. The number of published copies amounted to 100, 500, 1000, 5000, 10000, 50000, 100000, 200000 and 500000. All the editions were defined in the A4 format. The cost and time period ratio (prepress, press) for both of the machines had been taken from actual production. Printing speed time and the price of the edition in all scopes and numbers of printed copies were taken for comparison purposes. In

the 16-sheet scope the printing time curve shows insignificant discrepancies in the 500 copy and 1000 copy editions. The greater speed of the Lythoman in respect to Polyman is evident only when the number of copies printed amounts to 5000 and more.

Analysis of the price curve shows that the Polyman machine is cheaper when printing up to 50000 copies, and over this figure Lythoman is more favorable. For all other ranges (32, 48, 64, 72, 86 and 112 pages) the necessary printing time was shorter on the Lythoman machine than on the Polyman. The price for the 32-page range was lower on the Lythoman for all the various editions. The following, 48-page scope proved to be cheaper on the Lythoman for the number of printed copies amounting to less than 5000, and Polyman proved to be cheaper when the number of printed copies was over 5000. For the 64-page edition Lythoman proved to be cheaper for all printed copy scopes, and the curves met only when the number of printed copies amounted to 500000. The assumption is that the Polyman is cheaper if the number of copies is higher than 500000.

For a 72-page magazine the Polyman is more expensive for the quantity up to 10000 printed copies, and the Lythoman when exceeding this number. The following, 86-page magazine showed the greatest difference in price when the number of printed copies amounted up to 50000 (Polyman is more expensive), and beyond this figure the price curves were significantly closer to each other, but in all cases Lythoman was still cheaper. The last, 112-page issue was more profitable printed on the Lythoman in cases of up to 50000 printed copies, and above this figure - on the Polyman machine.

A virtual book edition printing was simulated from sheets in the experimental printing part in identical circulation and number of printed copies, as was the case for the review magazine printing. Three printing machines were created for the experiment, four-color ones, two-color ones and a single-color printing machine. The price and time period ratio were taken from actual production (prepress, press). For the scope of 16 pages in the 100-copy issue the time curves of the one-color and four-color machines had been identical, while the two-color one was the slowest. The same order sequence was shown in the 1000 copy edition, whereas the single-color machine was the slowest in the 5000 copy edition. In the edition amounting to 10000 copies, the fastest was the four-color machine, followed by the two-color machine, and the single-color machine proved to be the slowest one. The same order sequence remained up to the end of the experiment (Figure 2).

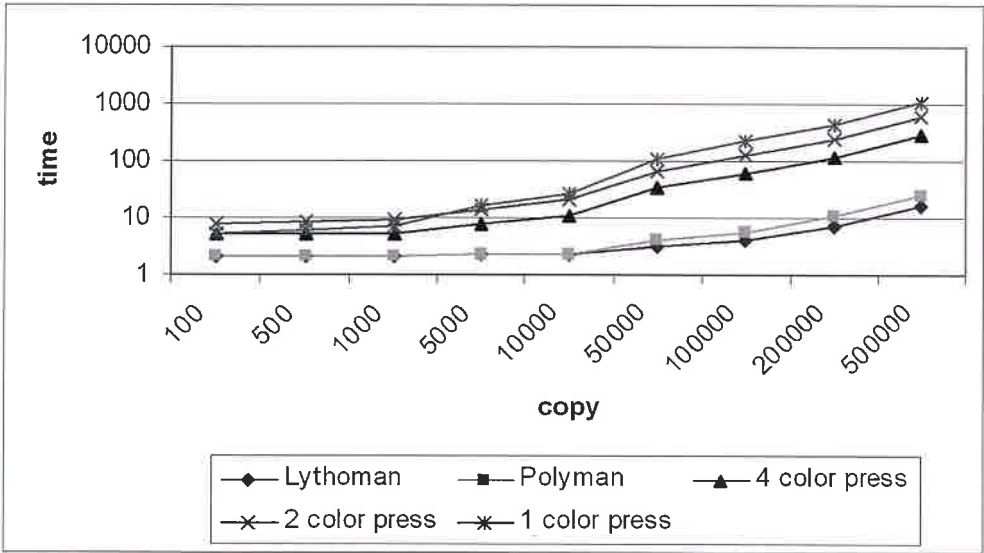


Figure 2

The same time period was needed for 32-page and 48-page scopes. The 64-page edition in 100 printed copies proved to be the fastest on the single-color machine, followed by the four-color machine and the slowest was the two-color machine. In the 500-copy edition the two-color machine remained the slowest one, followed by the single-color machine, whereas the four-color machine proved to be the fastest one. The same order sequence was for the 1000 printed copy edition, whereas the single-color machine was the slowest in the 5000-copy edition, followed by the two-color and then the four-color machines.

The above order sequence remained the same in all the experiments for 10000, 50000, 100000, 200000 and 500000 copies. The following, 72-page edition showed identical results for the single-color machine, and so was the case with the 64-page edition, whereas the time ratio in respect to the speeds of the single-color and four-color machines proved to be constantly in favor of the four-color machine. In the case of the 86-page-100 printed copy edition the single-color machine was once again the fastest one, followed by the four-color machine, whereas the two-color machine was the slowest one.

The same order sequence remained for the 500 printed copy edition, whereas the four-color machine became the fastest one in the case of the 1000 copy edition, followed by the single-color, and then the two-color one. After 5000 printed copies the order remained the same till the very end; the slowest was the single-color machine, then the two-color machine, and the four-color machine was the fastest. The order sequence for the 112-page edition was the same as for the 86-page edition (Figure 3).

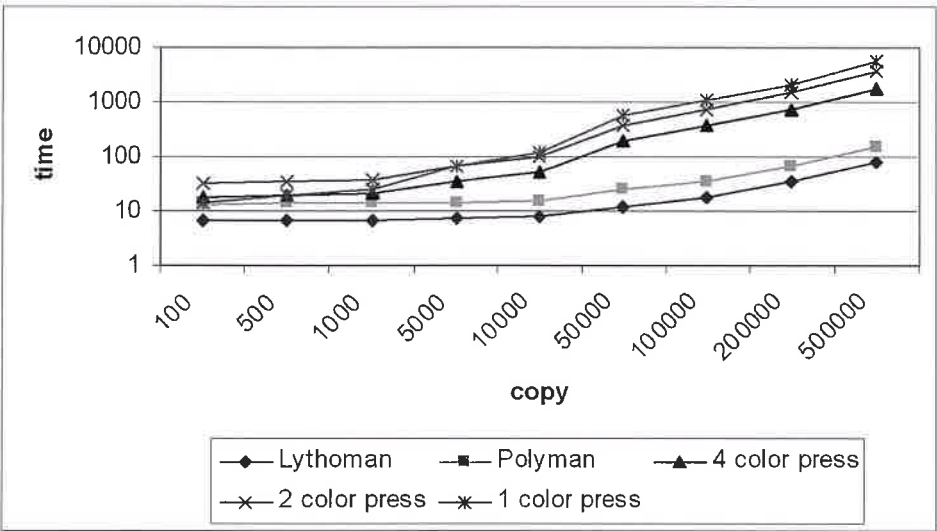


Figure 3

When observing the price through all the scope combinations and numbers of printed copies, the conclusion is that the most expensive printing is always on the single-color machine. The two-color machine has proved to be more profitable as to the price only in issues up to 1000 printed copies and in the scopes of 16, 32 and 48 pages. In all the other situations the four-color machine proved to be more profitable.

In this manner the virtual printing machine giving the optimal ratio between the price and the time necessary to print individual editions was determined. This paves the way for the recommended manner of planning and determining actual jobs. There is opportunity to investigate and create one's own operation plan without unpleasant consequences, without material expenses and without actual wastages. First the benefits of the proposed configuration are proven on basis of computer simulation, and then they are realized in actual time for real.

6. Conclusion

The results obtained improve and enhance the level of production control and planning, and enable additional JDF build up. The final results are the comparative relations of condition interdependence for individual experiments. Only integrated databases supported by XML can raise communication on the highest level of openness and transparency in the adequate and interactive manner. A supplement to the work is the used group of norm settings enabling simulation to be performed. The paper compares the structure of relations between the above given variables. The goal is to create as many as possible real production situations, to store the obtained data into databases and in this manner to aim at obtaining detailed computer science descriptions of graphic production units.

Operations have shown that the simulation method gives results that raise printing processes on a new and higher computer science level. Thus it was proven that restructuring of existing plants could be carried out with a new type of graphic production organizing and planning. On basis of the obtained results supported by simulation, it is possible to predict the direction production will take, and use this information for immediate and dynamic transforming of the production to comply with new market requirements.

Literature references

1. K. Pap, (2003), Standardizacija i automatizacija grafičke proizvodnje u XML-u, *Znanstveno stručni skup o pravcima razvoja grafičke industrije I tiskarstva, Stubičke toplice, Croatia*
2. M. Žagar, V. Žiljak, Z. Sabati, K. Pap, (2003), Proposal for XML Technology Programming Solutions in the Printing Business Informix database, *IIS 2003 Proceedings, Varaždin, Croatia*
3. V. Žiljak, K. Pap, D. Agić, I. Žiljak, (2002), Modelling and Simulation of Integration of Web system, Digital and Conventional Printing, *29th International Research Conference of IARIGAI, Lake of Lucerne, Switzerland*
4. V. Žiljak, (2003), Managing the graphic production with xml technology, *Međunarodni simpozij "Ofsetni tisak", Zagreb, Croatia*
5. V. Žiljak, (2003), Digital Printing and XML Technology in Graphic Production Planning, *International Conference on innovative educational content management and Digital Printing: Proceedings, Athens, Greece*
6. V. Žiljak, A. Koren, (2003), Modelling and Simulation as a Planning Method for Printing Houses Modernization with JDF, *IIS 2003 Proceedings, Varaždin, Croatia*
7. Z. Nježić, V. Žiljak, K. Pap, B. Sviličić, (2003), The stochastic model of simulation of a virtual printing-house, *30th International Research Conference of IARIGAI, Dubrovnik, Croatia*



Electronic business processes in book production - - Applicability of JDF/PrintTalk and Papinet/XBITS

Hannele Antikainen, Asta Bäck

VTT Information Technology
Tekniikantie 4B, P. O. Box 12041
FIN-02044 VTT, Finland
E-mail: hannele.antikainen@vtt.fi

Keywords

Electronic procurement, Finnish book industry, JDF/PrintTalk, Papinet/XBITS

1. Introduction

Book publishing processes need good communication between the publisher and the printer. Some books find their way quickly from the idea to the published book, but more often than not, book publishing is a project with considerable length, even up to some years. During the process, the parties need to keep each other up-to-date of the timetable and product details in order to make sure that the book production can be carried out efficiently and without errors.

The communication between the parties is typically carried out in conventional ways - e-mail, fax, mail and phone - and after receiving information through these channels, the data is manually entered into the recipient's computer systems. These kinds of processes take time and are error prone. The errors can be avoided, if the communication takes place between computer systems. Electronic data interchange also makes the processes much quicker to react to changes, and improves their overall efficiency. However, to introduce electronic data interchange between computers, electronic processes and common vocabularies supporting these processes need to be established.

Several vocabularies have been proposed to support electronic data exchange between processes and system, also within the graphic arts industry. The most interesting vocabulary in relation to print production is JDF (Job Definition Format) and its extension: PrintTalk. JDF defines the structure of the printed product, and PrintTalk is used to complement it to define the business transactions. Another relevant vocabulary is Papinet/XBITS, which is a US based initiative, developed on the paper industry's Papinet. It is currently being extended to meet the requirements of the US book industry.

The objective of the project was to analyse the current book production processes in Finland to see the potential for improving the efficiency of the whole production chain with the help of electronic data interchange. The objective was also to propose the vocabularies needed to adopt electronic business processes.

2. Research methods and materials

When developing business processes and to introduce new electronic ways to operate between partners, two things are of prime importance. First, to understand, why these processes are being carried out and how they add value, and second, to find out, how to utilise electronic commerce and communication in an optimal way.

Business process modelling is the tool to tackle these challenges. We chose to utilise UN/CEFACT Unified Modelling Methodology (UMM) for describing the current processes. The information for modelling was collected by interviewing publishers and printers. Gummerus Oy, Kustannusosakeyhtiö Tammi, WSOY, Yliopistopaino were interviewed in the role of a publisher, and Gummerus Oy, Otavan Kirjapaino Oy, WS Bookwell Oy, Yliopistopaino in the role of a printer

The interviews were complemented with examples of current business documents, which include the necessary data content of business transactions. Our analysis covered request for quote (RFQ), quote, purchase order (PO), order confirmation (OC) and note on transferring shipping addresses from the publisher to the printer

Available versions of JDF and Papinet/XBITS vocabularies were analysed and their expressive capabilities were compared with the requirements of the chosen Finnish business processes. This analysis covered both the business process and data content

We also built a software application to encourage the further development of electronic processes between publishers and printers. This demonstration also tested implementing JDF - mapping data collected via an HTML form to the JDF structure

3. Results

3.1 Process models

UMM is a modelling method utilised by ebXML initiative (Anon. 2000). It shows a way of how to proceed from the top level to the actual processes. The UMM uses the following hierarchical levels: Business reference model, Business area, Process area and Business processes.

Business reference model defines the industry. Business areas are used to divide each industry into sectors. Each business area has several process areas, which consist of the actual business processes. In general, we can state that process areas are usually important value adding functions in the industry. If and when electronic business processes are introduced, the process area as a whole remains, but the actual business processes within the process area may change, and even be eliminated.

In our case, the UMM Business Reference Model is "Book publishing and printing". It can further be divided into two main business areas: "Book publishing" and "Book production (printing and binding)". There are several players within book publishing and printing, and an overview picture was made to chart their main role and information requirements. (Fig. 1)

The UMM method includes a set of tables that describe the different levels of the model (Anon. 2001). The UMM methodology provides a set of tables that can be used to collect and report the processes. Table I shows an example of such a process area model. Altogether, nine process area tables covering the transaction between book publishers and book printers were produced

The classification of the processes was added to describe the characteristics of each of the business processes. The classes were: processes between persons, processes requiring expertise, query/response process, transaction process, information transmission process (information to be stored in a data system), payment process, workflow process, internal process, and material (including digital material) transmission process. Transaction processes, query/response processes as well as information transmission processes have the highest potential for electronic implementation.

This wide choice of process types shows that these process have a wide array of operations that deal with production knowledge, making business deals and preparing and transmitting digital files and

Business Area: Book publishing

Process Area: Managing book production (publisher)

The goal of the process area: To ensure that the production has the right files for production and also otherwise correct and up to date information on schedule and book structure.

Important input: Original files for dust jacket, cover, decorations and block, working instructions, shipping instructions including shipping addresses

Important output: Correct books at correct delivery addresses

Owner of the process: Publisher

3.2 Vocabularies

The electronic business processes need vocabularies for data exchange. The options are to utilise an existing vocabulary, to adopt and modify an existing one, or to make a new vocabulary. Starting from scratch is usually not recommended, because it requires a lot of work, and it obviously means that there is not any kind of existing software support for it. Existing vocabularies may support different ways to modify them, all with their pros and cons.

Of the existing vocabularies, JDF version 1.1 A (Anon, 2002) along with PrintTalk version 1.1 A (Anon, 2003) and Papinet/XBITS were analysed and mapped against the Finnish requirements for book structure. The result was a detailed gap analysis that explains what is missing from them from the Finnish book industry's point of view. The use cases of these messages were analysed in a similar way. Table II introduces the business transactions or messages covered by Papinet/XBITS and PrintTalk. JDF version 1.2 was published in May 2004 (Anon, 2004-a).

The main problem with JDF is that it lacks the support for book related information, such as author and ISBN-number and also more complex book structures. This is understandable from JDF's historical background with a strong focus on the actual print production. PrintTalk seems to have only few practical implementations, none of which are in the book industry.

Papinet/XBITS is being developed in the US. It supports the common practices in the American book industry. So far (spring 2004) Papinet/XBITS has finished messages on Book Specification (Anon, 2004-b), Delivery Message (Anon, 2004-c), Inventory Disposition Instructions (Anon, 2004-d), Order Confirmation (Anon, 2004-e), Order Status (Anon, 2004-f), Purchase Order (Anon, 2004-g) and Shipping Instructions (Anon, 2004-h). However, it is a very new vocabulary, and some relevant messages, such as RFQ, are still missing from its set of messages. The first implementations of Papinet/XBITS are expected in early 2004.

The differences between the Finnish and American books industries are evident in the order of the developed messages. In America, the publisher often organises the whole production process from buying the paper, organising the production of the different components and having them put together into complete books. There, the publishers find it very important to get various types of production data.

In Finland, the production is typically bought from one company who takes care of the whole production. Therefore, from the publisher's point of view the most important thing is the information flow between the publisher and the production unit prior to the production.

Table II: Business transactions covered by XBITS and PrintTalk

Message	Conventional Process	XBITS	PrintTalk
Request for Quote (RFQ)	eMail, fax, mail, phone	Papinet message *)	Yes
RFQ Response or Quote	eMail, fax, mail, phone	Papinet message *)	Yes
Purchase Order (PO)	eMail, fax, mail	Yes	Yes
Order Confirmation	eMail, fax, mail, phone	Yes	Yes
Book Specifications	Communicated within messages	Yes *), is used to define book specifications within other messages (RFQ, RFQ Response, PO, Order Confirmation)	JDF is used within PrintTalk messages to define book structure
Cancellation	eMail, fax, mail, phone, negotiation	Yes, but there is no separate Cancellation Message. Cancellation is expressed by setting message status Cancellation (applied within RFQ, RFQ Response, PO, Order Confirmation, Shipping Instructions)	Yes
Refusal	eMail, fax, mail, phone, letting a message expire	Yes, but there is no separate Refusal Message. Refusal is expressed by setting message status Reject (applied within RFQ, RFQ Response, PO, Order Confirmation, Shipping Instructions). Also by letting a message expire means refusal.	Yes Also by letting a message expire means refusal.
Order Status	Phone, email	Yes	Yes
Proof Approval Request	eMail, fax, mail, phone	No	Yes
Proof Approval Response	eMail, fax, mail, phone	No	Yes
Shipping Instructions	Yes, especially for shipping addresses	Yes	No separate message, Shipping Instructions are included in Purchase Order
Delivery Message	Yes, printed on paper	Yes	No
Invoice	Mail	Papinet message *)	Yes
Complaint	eMail, fax, mail, phone	Papinet message *)	No
Complaint Response	eMail, fax, mail, phone	Papinet message *)	No
Inventory Disposition Instructions	Not commonly used eMail, phone	Yes	No

*) a corresponding Papinet message for paper, pulp and recovered paper industry is available

3.3 Software demonstration

During the project, a software application that enables exchanging RFQs and quotes between book publishers and book printers was build. By means of the software and its WWW user interface, the user can - in the role of a book publisher - send RFQs to printers. The user chooses between a hard cover and perfect bound book, and gives other book structure specifications including format and desired book materials. The software application transforms the defined book structure into JDF. In the role of a book printer, the user can open the RFQ and complement it into a quote. Similarly, the quote is transformed into JDF and sent back to the publisher. The software demonstration was implemented using Java servlet technology.

Basic information

start page | finish

basic information | block | hard covers | dust jacket | delivery | price

indicates publisher usually fills | indicates printer usually fills | both parties CAN fill

Required fields are marked *

Book's name	Isari Hermanni	* Pub
Author (comma separated if more than one)	Kalle Päätalo	* Pub
ISBN	951-20-6407-3	* Pub
RFQ expires	10 October 2003	* Pub
Quota expires	[day] [month] [year]	* Pub
Print run	40000 number of copies	* Pub
Format (w*h) (block)	135 * 205 mm	* Pub
Page count	608 pages in block	* Pub
Spine thickness	mm	* Pub
Volume of one book	mm	* Pub

Discussions * | Subscribe... | Discussions not available on http://customdp.vtt.fi/

Hard covers

start page | finish

basic information | block | hard covers | dust jacket | delivery | price

indicates publisher usually fills | indicates printer usually fills | both parties CAN fill

Required fields are marked *

Specifications of cover material	Other -> Galtex	* Pub
Material details		* Pub
Cover material colour	musta	* Pub
Thickness of cover board	2.0 mm	* Pub
Decorations	<input type="radio"/> Debossing <input type="radio"/> Embossing <input checked="" type="radio"/> None	* Pub
Foil stamping	<input checked="" type="radio"/> Yes <input type="radio"/> No	* Pub
Specifications of foil material	puolikiiltävä folio	* Pub
Colour	kulta	* Pub
Original files (for decorations)	PDF	* Pub

Discussions * | Subscribe... | Discussions not available on http://customdp.vtt.fi/

Figure 2: Examples on the user interface of the software demonstration. Left are basic information of the book such as the name of the book, ISBN number and the format is given. The picture on the right shows how the specifications of hard covers can be defined using the software

4. Conclusions and discussion

In order to make the book production chain more efficient, it is important to find ways to make it possible for the parties to communicate about the job and send, receive and manage the relevant content files efficiently. The point when the files arrive into print production is the critical one.

The process has become more streamlined with electronic originals and proofs. What is missing is the transfer of product and production information. This requires that management information systems are used by both parties.

JDF aims at including all product and production information into the JDF description of a print job, and this would seem to be the ideal way. This is also a very ambitious goal, which requires JDF capabilities from all programs and production steps that are used to design and make the product. It also has the biggest potential, if we can combine the digital content and business information together.

The Papinet/XBITS approach focuses on the information interchange at a level that covers only product information and it does not offer compatibility with the production systems. On the other hand, it focuses on the information interchange between the book publishers and book printers including the use cases for the messages. The XBITS counterpart in JDF approach, the PrintTalk, has not been developed specially for the book industry.

The key requirement in developing a vocabulary is that a wide community can accept it. Even though much of book publishing and production is carried out within one country, there is also import and export, and the same production systems are used in many countries. This motivates using and developing vocabularies at international level, even though at short range, it might be the quickest way to develop a national solution, which strictly meets the criteria of the application. On a longer term this is often not a viable solution. Utilising existing vocabularies, it is possible to take advantage of existing material and knowledge that has already been put into them.

The reality is that we will have to learn to live with several vocabularies, or at least with several versions of some vocabulary. The different organisations should put emphasis on ensuring the interoperability of the different vocabularies. Good data vocabularies with explanations of the meaning of the different terms and concepts are needed to make mapping between the different vocabularies possible.

Acknowledgements

The project was made possible by the grant from Graafisen Tekniikan Tutkimussäätiö (Graphic Arts Technology Research Foundation) and financing by the participating companies Flowman Oy, Gummerus Oy, Kustannusosakeyhtiö Tammi, Otavan Kirjapaino Oy, Prosys PMS Oy, WM-data, WS Bookwell Oy, WSOY, Yliopistopaino.

In addition to the authors of this paper, Giorgos Pachoulis and Magnus Melin at VTT participated in the project.

Literature

- Anon, 2000. UNCEFACT/TMWG/N097. The UN/CEFACT Unified Modelling Methodology. An Overview. 28th March 2000. www.unece.org/cefact/docum/download/00bp030.doc
- Anon, 2001. Business Process Analysis Worksheets & Guidelines v1.0. Business Process Team 10 May 2001. www.ebxml.org/specs/bpWS.pdf
- Anon, 2002. JDF Specification Version 1.1 Revision A, CIP4 organisation 5 September 2002. www.cip4.org
- Anon, 2003. PrintTalk Version 1.1 A. PrintTalk organisation 27 January 2003. www.printtalk.org/implementation1-1a.pdf
- Anon, 2004-a. JDF Specification Version 1.2, CIP4 organisation 9 May 2004. www.cip4.org
- Anon, 2004-b. BookSpecification Documentation. Papinet Standard version 2.20. Papinet/XBITS January 2004. www.papinet.org/V2R20/200401/documents/BookSpecificationV2R20.pdf
- Anon, 2004-c. DeliveryMessageBook Documentation. Papinet Standard version 2.20. Papinet/XBITS January 2004. www.papinet.org/V2R20/200401/documents/DeliveryMessageBookV2R20.pdf
- Anon, 2004-d. InventoryDispositionInstructions Documentation. Papinet Standard Version 2.20. Papinet/XBITS January 2004. www.papinet.org/V2R20/200401/documents/InventoryDispositionInstructionsV2R20.pdf
- Anon, 2004-e. OrderConfirmation Documentation Book Manufacturing. Papinet Standard Version 2.20. Papinet/XBITS January 2004. www.papinet.org/V2R20/200401/documents/OrderConfirmationBookV2R20.pdf
- Anon, 2004-f. Book OrderStatus Documentation. Papinet Standard Version 2.20. Papinet/XBITS January 2004. www.papinet.org/V2R20/200401/documents/OrderStatusBookV2R20.pdf
- Anon, 2004-g. Book PurchaseOrder Documentation. Papinet Standard Version 2.20. Papinet/XBITS January 2004. www.papinet.org/V2R20/200401/documents/PurchaseOrderBookV2R20.pdf
- Anon, 2004-h. ShippingInstructions Documentation. Papinet Standard Version 2.20. Papinet/XBITS January 2004. www.papinet.org/V2R20/200401/documents/ShippingInstructionsV2R20.pdf



Index of authors

- Agić, Darko 43
 AL-Rubaiey, Hussain 13
 Antikainen, Hannele 245
 Antoine, Christine 123

 Babić, Darko 203
 Bäck, Asta 245
 Beier, Wolfgang 61
 Elisabeth Berli 123
 Blayo, Anne 105
 Bohan, Mark F.J. 83
 Bould, David C. 83

 Canet, Christine 145
 Catusse, Robert 49
 Claypole, Timothy C. 75, 83

 Davies, Glyn R. 75
 Diserud, Ola H. 123

 Enroth, Maria 227

 Fujiki, Satoshi 113

 Gemeinhardt, Jürgen 173
 Gervasoni, Jean-Pierre 49, 163
 Gethin, D. T. 83

 Hakola, Liisa 3
 Hardeberg, Jon Y. 189
 Hägglund, Åsa 27
 Hübler, Arved Carl 61

 Johansson, Martin 227
 Johansson, Per-Åke 27

 Kinoshita, Akihiro 151
 Klamann, Marianne 27
 Klinger, C. 61
 Koga, Keiko 113
 Kropar-Vančina, Vesna 203

 Lahtinen, Panu 217
 Lajić, Branka 203
 Lebris, Sébastien 163
 Lee, Syon 151
 Lindqvist, Ulf 3

 Mandić, Lidija 43
 Marx, Günter 61
 Meyer, N. 61
 Münch, Beat 181

 Naito, Ikuo 113, 151
 Nitta, Yoshiaki 113
 Nussbaum, Peter 189
 Nježić, Zoran 237

 Oittinen, Pirkko 13

 Pap, Klaudio 237
 Passas, Raphaël 163

 Räsänen, Pia 13
 Rodríguez Giles, Jorge M. 97

 Saad, Ashraf A. El Rhman 97
 Shibata, Kazuyuki 113
 Skarsbø, Sven Erik 189
 Solheim, Olav 123
 Steiger, Walter 181

 Wallström, Eva 3
 Werfel, Manfred 181

 Zhmud, Boris 3
 Žiljak, Ivana 209, 237
 Žiljak, Vilko 237
 Žvorc, Dean 43

This book is printed on 115 gr Biomat paper, generously supplied by

B&B

P A P I R N I C A V E V Č E

Papirnica Vevče d. o. o.

Papirniška pot 25

SI-1261 Ljubljana Dobrunje

Phone: +386-1-5877-200

Fax: +386-1-5285-450

Email: info@papir-vevce.si

Web: www.papir-vevce.si

Printing arranged with the kind support of



NARODNE NOVINE d.d.

CROATIA · HR · 10020 · Zagreb · Ivana Šibla 1

phone +385 1 66 52 777 · telefax +385 1 66 52 770

www.nn.hr · e-mail: nn@nn.hr

Binding by courtesy of



printing productions and
commerce Ltd.

HR-10410 Velika Gorica

Hrvatske bratske zajednice 41

tel.: ++385 (0)1 6221-163, 6221-173

fax: ++385 (0)1 6225-074, 6256-437

e-mail: pasanec@zg.htnet.hr

www.pasanec.hr